The Dissertation Committee for Anthony David Battistini certifies that this is the approved version of the following dissertation:

Stiffness and Fatigue Behavior of Cross Frames for Steel Bridge Applications

Committee:

Todd A. Helwig, Supervisor

Michael D. Engelhardt, Co-Supervisor

Karl H. Frank

John L. Tassoulas

Krishnaswamy Ravi-Chandar

Stiffness and Fatigue Behavior of Cross Frames for Steel Bridge Applications

by

Anthony David Battistini, B.S.C.E.; M.S.E.

Dissertation

Presented to the Faculty of the Graduate School of

The University of Texas at Austin

in Partial Fulfillment

of the Requirements

for the Degree of

Doctor of Philosophy

The University of Texas at Austin

August 2014

Dedication

To the love of my life Liz, for always being there to support me in good times and bad.

To my Mom, Dad, and Sister for supporting all my dreams and ambitions.

To my family that has left this world, may I continue to make you proud and one day see you again.

Acknowledgements

I would like to thank the Texas Department of Transportation for providing the funding for my research and my education. It has been very rewarding to partner with engineers focused on incorporating the research into practice. I especially thank Michelle Romage, for her input and assistance to make the project a success.

I also want to thank the faculty on my Dissertation Committee for all of their assistance. In particular, I thank my co-supervisors Todd Helwig and Michael Engelhardt. Working with these gentlemen day-to-day taught me that becoming a professor was hard work but very enjoyable and rewarding. I look forward to becoming their colleagues in our field. I also thank Karl Frank, whose knowledge on steel bridges and fatigue never ceases to amaze me. Finally, I thank John Tassoulas and K. Ravi-Chandar for their occasional input on our research and helping provide clarity in my dissertation.

The staff at the Ferguson Structural Engineering Laboratory was amazing, in particular Blake Stasney, Dennis Fillip, David Braley, Andrew Valentine, Mike Wason, and Eric Schell who helped me countless times setting up my lab tests. Additionally, I thank Barbara Howard and Michelle Damvar for making sure everything was properly billed and accounted for.

I also acknowledge my coworker Weihua Wang for all his help and ideas as well as all my workout partners, particularly Garber and Andy for all their emotional support outside of work. Lastly, I am completely indebted to my research partner Sean. You attacked the lab work like a true wolf and you made every day at the lab a howl!

Thanks!!

August 15, 2014

Stiffness and Fatigue Behavior of Cross Frames for Steel Bridge Applications

Publication No. _____

Anthony David Battistini, Ph.D.
The University of Texas at Austin, 2014

Supervisor: Todd A. Helwig
Co-Supervisor: Michael D. Engelhardt

Cross frames are critical for the stability of straight and curved steel bridges. Conventional cross frames are often fabricated from steel angles which are welded to gusset plates through one leg only. Due to this eccentric connection, these angles have substantial bending at the connection that can reduce the member stiffness and can potentially decrease fatigue performance. Because of the low buckling strength, cross frames with angle diagonals are often designed as tension-only systems, therefore increasing the necessary steel to be an effective brace.

Improved behavior may result if concentric members are utilized. The increased buckling strength of tubes and double angles results in effective members in both compression and tension, and a single diagonal cross frame can provide effective bracing;

however, a suitable connection must be developed. Tubes are often connected by slotting the tube in the center and welding to a gusset plate, which requires precise fabrication. Two proposed solutions that would connect easily to the ends of the member and seal the end of the tube include a steel casting and a T-stem connection. The dissertation studies the development of a steel casting for use in cross frame design and evaluates the performance of the various details described herein in regards to stiffness, strength, and fatigue.

Additionally, the dissertation covers the behavior of single angle X and K frame configurations. To date, the determination of the single angle fatigue detail has been largely based on component tests only. The project incorporated full-scale cross frame fatigue tests to fully examine the interaction of the cross frame members with the overall structure. Results from currently used details and proposed connections provide insight to the live load behavior of these braces and multiple recommendations are made to improve the fatigue life. The project examined the stiffness behavior of current and proposed cross frame layouts with large-scale laboratory tests and computational modeling. From these results, a case study compares the fatigue analysis of a commercial structural software package to the stress ranges obtained in a three-dimensional finite element model. Suggestions on how to properly model the cross frames are given.

Table of Contents

List of Tables

List of Figures

CHAPTER 1
Introduction

1.1 PROBLEM STATEMENT

Cross frames are critical bracing elements for the stability of straight and curved steel bridges. The cross frames provide stability to the girders by restraining twist and increase the capacity and stiffness of the overall bridge system. Effective stability bracing must satisfy both strength and stiffness requirements [Winter 1958]. The cross frames are usually designed as torsional braces, which increase the overall strength and stiffness of the individual girders by creating a girder system that translates and rotates as a unit along the bracing lines.

Conventional cross frames are often fabricated using steel angles, consisting of two diagonal members and two horizontal struts to create an X-type brace, as shown in Figure 1.1.

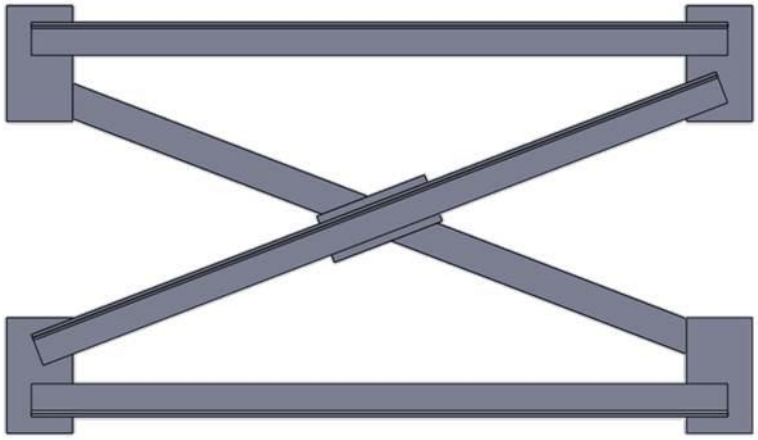

Figure 1.1: Typical X-type Cross Frame with Steel Angles

Another common form that is frequently utilized consists of a K-type brace in which the single angle members are arranged as shown in Figure 1.2.

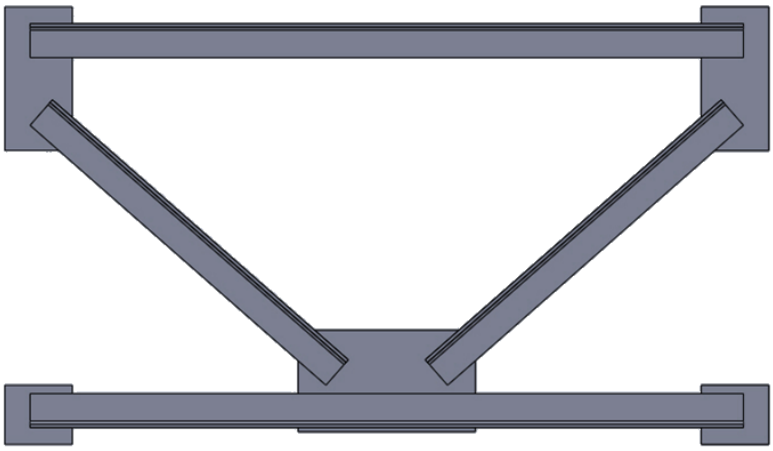

Figure 1.2: Typical K-type Cross Frame with Steel Angles

Although the X-type and K-type cross frames are very widely used in steel bridges, there are a number of potential concerns with these cross frames. Significant material handling is required in the fabrication of cross frames due to the number of pieces comprising a single brace, as well as the multiple welds necessary to connect the various pieces. These handling requirements for cross frames can substantially increase the cost of fabrication, making cross frames one of the most expensive components per unit weight on a steel bridge. The fabrication costs are dependent on the member sizes and the connection requirements for the cross frames as well as some of the design decisions. Due to the relatively poor buckling resistance of angle members, X-type cross frames are often modeled as a "tension-only-diagonal" system. In a tension-only-diagonal system, the compression diagonal is conservatively neglected in strength and stiffness calculations. However, neglecting the contribution of the compression diagonal to cross frame stiffness and strength can lead to heavier diagonals and potentially higher cost for the cross frame. In addition, the angles are connected to the end plates along only one leg of the member, resulting in an eccentric connection. Results from laboratory tests and three-dimensional finite element studies have demonstrated that the eccentricity causes out-of-plane bending of the members resulting in a reduction in the stiffness of the cross frame [Wang 2013]. The eccentric connection also may have an impact on the fatigue performance, which is part of the focus of the results reported in this dissertation.

The fabrication difficulties as well as connection eccentricities create uncertainties in the behavior of existing cross frames that require deeper study including the following:

- the impact of the connection eccentricity for angle members on the strength and stiffness of the cross frames;
- the potential for improvements in cross frame behavior with the use of other structural shapes besides angles;
- a measure of the fatigue performance of the different cross frames both at the member and system level.

Although single angle members are attractive from a fabrication perspective due to the ease of connections, improved structural behavior may result by using concentric members to construct the cross frame. HSS tubular members and double angle members have significant buckling strength, allowing the diagonal to be utilized in both tension and compression. Furthermore, these members allow for concentric connections, thereby reducing potential problems that may arise due to member bending that occurs with eccentric connections. Thus, a single diagonal cross frame with concentric members may lead to improved structural efficiency for the steel bridge system.

The use of four steel angles in the X configuration shown in Figure 1.1 requires the fabricator to turn the cross frame over in order to weld the connections on both sides of the cross frame. By reducing the number of cross frame members, handling requirements in the fabrication shop should be reduced. Figure 1.3 shows an example of a single diagonal tubular cross frame.

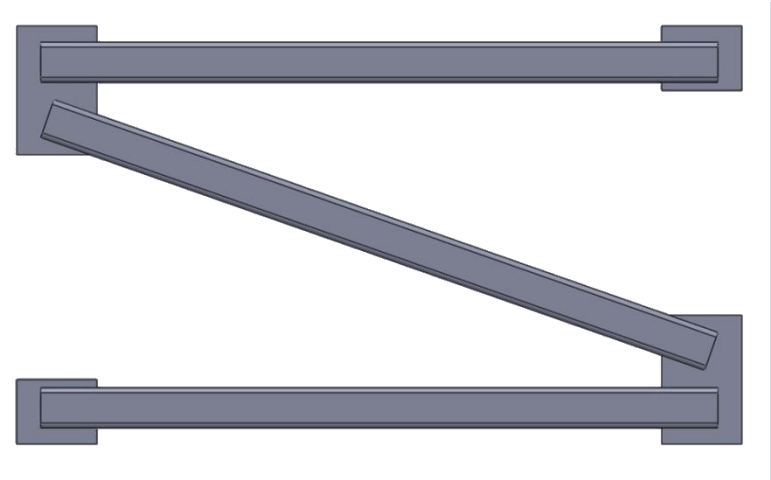

Figure 1.3: Single Diagonal Tubular Cross Frame

Although there are several structural advantages of utilizing tubular members, one drawback is designing a simple means of connecting the circular cross section to a flat plate. Frequently, tubes are slotted to produce a concentric joint. However, previous tests on the slotted-tube detail have reported relatively poor fatigue behavior [Liu et al. 2006]. In addition, the detail requires additional fabrication time and produces and opened tube to the atmosphere that may compromise the corrosion resistance of the member.

A potential connection for tubular members that may alleviate some of these problems is the use of a steel casting that provides a more uniform transfer of the forces into the tube and seals the end of the tube. The steel casting can be engineered to account for the complex geometry of the connection, and once produced, would be relatively easy to use in cross frame fabrication.

As part of this research a number of cross frames comprised of traditional and newly proposed details were tested. The traditional details consisted of single angle members, while the newly proposed details consisted of double angle members and tubular members with both cast and slotted connections.

1.2 RESEARCH OBJECTIVES

The research presented in this dissertation was performed in conjunction with TxDOT Project 0-6564 to investigate the behavior of cross frames from both a stiffness and strength perspective. The strength of the cross frames include both the static strength and the fatigue strength. The prevailing design methodology for cross frame design was assessed to understand the current performance of both the X-type and K-type cross frame configurations.

Furthermore, the use of tubular members in steel bridge cross frames was explored to verify the structural adequacy of utilizing a single diagonal cross frame configuration and to quantify the fatigue performance of the connection. The behavior of cross frames comprised of angles was also a major focus of the study. The research included experimental tests on individual components of the cross frame as well as full scale cross frames. Finite element analyses were carried out to improve the understanding of the behavior of the cross frames. The computational studies focused on the behavior of an individual cross frame as well as studying the behavior of straight, skewed and horizontally curved steel girder systems. The research was carried out at Ferguson Structural Engineering Laboratory at the University of Texas at Austin.

This dissertation will focus on the following tasks, which comprise a subset of the research conducted within TxDOT Project 0-6564:

- Survey existing TxDOT bridge designs to understand applicable bridge geometries to determine typical ranges of cross frame dimensions.
- Review the available technical literature concerning previous studies on the strength, stiffness, and fatigue behavior of steel members and connections, particularly as applied to cross frame systems.
- Review the available technical literature on the use of steel castings in structural applications and determine the feasibility of designing a cast steel connection for cross frame design.

- Develop FEA models of tubular members and the connection region for use in developing optimized prototype connections for laboratory testing.
- Develop FEA models of a cast connection to analyze its strength and work with steel foundry engineers to optimize the design for production.
- Conduct axial tension and compression tests on tubular members to validate connection behavior.
- Conduct fatigue tests on the proposed cross frame members to develop a fatigue rating for the connection and the member.
- Conduct stiffness tests on full cross frame systems to fully understand the elastic behavior for design applications.
- Conduct fatigue tests on full scale cross frame systems.
- Conduct a case study to compare cross frame design software used at TxDOT with three dimensional FEA models.
- Make design recommendations based upon laboratory and computational results and provide recommended connection details.

1.3 DISSERTATION OUTLINE

The dissertation consists of nine chapters. Chapter 2 provides background information on the stability of steel bridges, as well as the previous use of tubular members in bracing applications. A summary of TxDOT bridge practice and current details is also included in Chapter 2.

Chapter 3 outlines the current AASHTO provisions for the fatigue classification of cross frames. An overview of fatigue behavior, analysis methods, and testing is provided.

An introduction to steel castings is provided in Chapter 4, including important terminology and a detailed discussion of the process required to create steel castings. Attention is also given to potential defects in the cast steel material and the variety of measures that can be conducted to detect these flaws.

A summary of the connection design process is provided in Chapter 5. This chapter contains the proposed connections under investigation, including laboratory test results involving a number of different members and corresponding connections. For tubular members, three connections were evaluated: 1) cast steel connections, 2) T-stem connections, and 3) slotted-tube connection. In addition to tubular members, double angle members and single angle members and the resulting gusset plate connections were also studied. Finite element analysis is provided in conjunction with the test data.

Test results from the large scale cross frame stiffness and ultimate strength tests are presented in Chapter 6. Brief information on the test setup for the stiffness tests is provided, followed by the results for several cross frame layouts both currently in use and proposed. For complete details on this aspect of the testing phase, see Wang [2013].

Chapter 7 provides details on the full scale cross frame fatigue tests, as well as comparison data to FEA models. Key observations are identified, and suggestions for improved behavior based on test data are provided.

Chapter 8 provides information on an FEA model of a horizontally curved bridge that was developed to directly compare the cross frame fatigue forces obtained in commercial software to those obtained by a three dimensional finite element program.

Finally, a summary of the research and conclusions are given in Chapter 9.

CHAPTER 2
Background: Bridge Stability

2.1 INTRODUCTION

I-shaped plate girders are often utilized for steel bridge superstructures since the I-shaped sections are very efficient at resisting in-plane bending. By placing a large area of steel away from the neutral axis, the moment of inertia about the major axis for the compound shape greatly increases, which in turn increases the stiffness of the beam or its resistance to vertical deflections.

However, while I-shaped sections have a large in-plane stiffness, the sections are often susceptible in instabilities about the weak axis of the section. Similar to Euler buckling in columns, the compression flange of the section can reach a critical limit and will buckle in a mode involving flexure about the minor axis of the beam. At this stage, the tension portion of the beam is still stable, and does not tend to buckle leading to a twist of the cross section. The resulting mode of failure is referred to as lateral torsional buckling, and is a primary concern in the design of steel I-girder sections, particularly before the deck is cast, which provides lateral support to the top flange after it cures.

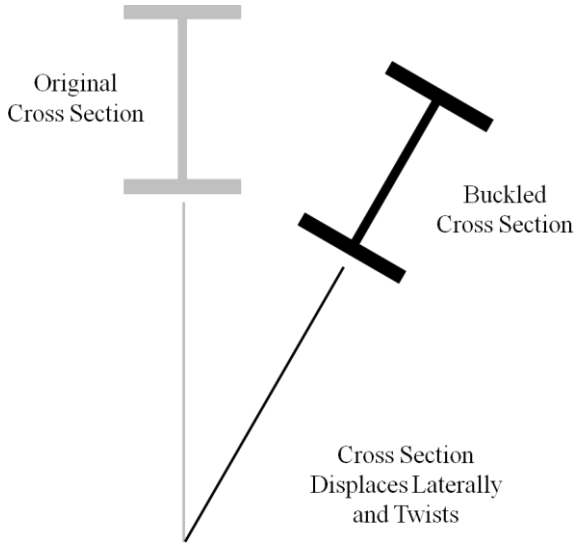

Figure 2.1: Lateral Torsional Buckling of Steel I-Beam

This chapter outlines background information for the stability design aspects of cross frames for I-girder bridges, specifically the determination of cross frame stiffness. The common detailing practices for cross frames that often utilize single angle members are discussed. Finally, the potential benefits of utilizing tubular members in steel bridge systems are addressed.

2.2 STABILITY OF BRIDGES

Stability is a crucial consideration when designing large, steel girder bridges. To prevent the onset of buckling in the beams, cross frames are used to interconnect adjacent girders and improve the system stiffness. The critical stage for cross frames is during construction, when the full weight of the wet concrete slab acts on the non-composite steel girder section. The cutting, fitting, and welding required to construct cross frames can be a labor-intensive process. Consequently, cross frames are generally the most expensive component per unit weight on a steel bridge.

2.2.1 Lateral Torsional Buckling

The classical solution for lateral torsional buckling of doubly-symmetric beam sections subjected to uniform moment was derived by Timoshenko [Timoshenko and Gere 1961]:

$$M_{cr} = \frac{\pi}{L_b}\sqrt{EI_y GJ + \frac{\pi^2 E^2 C_w I_y}{L_b^2}} \tag{2.1}$$

where:

M_{cr} = *critical buckling moment*
L_b = *unbraced length*
I_y = *weak-axis moment of inertia*
E = *elastic modulus*
G = *shear modulus of elasticity*
J = *torsional constant*
C_w = *torsional warping constant*

In general, the solution given above is divided into two parts: the first term under the radical is referred to as the uniform torsional stiffness of the beam, or the St. Venant stiffness, and tends to dominate the expression for long unbraced lengths; the second term under the radical is the non-uniform torsional stiffness of the beam, or the warping stiffness. Since $1/L_b$ appears in both terms, the critical moment of the overall system can be increased if the unbraced length is reduced.

Within Timoshenko's solution for the lateral torsional buckling equation of the beam is the assumption that the ends of the unbraced length are restrained from twist [Timoshenko and Gere 1961]. Thus, if some means of torsional restraint is provided along the length of a beam, the unbraced length can be reduced and the critical buckling moment of the girder in that region will be increased. In the completed bridge, the concrete deck provides continuous torsional bracing along the length of the beam; however, during construction, the non-composite steel section must sustain the majority of the dead weight of the superstructure and any construction loads. Therefore, cross frames are used to increase the buckling strength of the girders during this critical stage.

2.2.2 Fundamentals of Beam Bracing

In order to reduce the unbraced length of the girder, the cross frame must provide a minimum amount of torsional restraint. Taylor and Ojalvo [1966] developed the following expression for doubly symmetric beams subject to uniform moment loading and continuous torsional bracing along the length:

$$M_{cr} = \sqrt{M_0^2 + \overline{\beta_b} E I_y} \tag{2.2}$$

where:

M_{cr} *= critical buckling moment*
M_0 *= buckling capacity of the unbraced beam*
$\bar{\beta}_b$ *= torsional brace stiffness per unit length*

Yura [2001] provides the following equation for the critical buckling moment, which accounts for various loading conditions as well as discrete torsional braces:

$$M_{cr} = \sqrt{C_{bu}^2 M_0^2 + \frac{C_{bb}^2 \bar{\beta}_T E I_{eff}}{C_T}} \leq M_y \text{ or } M_{bp} \tag{2.3}$$

where:

C_{bu} = *C_b factor corresponding to an beam with no intermediate braces (C_b accounts for moment gradient, see AISC Chapter F [2010] or SSRC [2010] for additional guidance)*
C_{bb} = *C_b factor corresponding to beam fully brace at location of intermediate cross frames*
C_T = *top flange loading modification factor; C_T = 1.2 for top flange loading and C_T = 1.0 for centroidal loading*
$\bar{\beta}_T$ = *equivalent effective continuous torsional brace stiffness, determined by:*

$$\overline{\beta_T} = \frac{\beta_T n}{L} \tag{2.4}$$

where:
β_T = *torsional brace stiffness provided by single cross frame.*
n = *number of intermediate braces*
L = *length of entire span*

Finally, an expression for the torsional brace stiffness provided by a single cross frame is given by [Battistini 2009]:

$$\frac{1}{\beta_T} = \frac{1}{\beta_b} + \frac{1}{\beta_{\text{sec}}} + \frac{1}{\beta_g} + \frac{1}{\beta_{conn}} \tag{2.5}$$

where:

β_b = *torsional brace stiffness provided by the in-plane stiffness of the brace*
β_{sec} = *torsional brace stiffness provided by the web cross section including stiffeners*
β_g = *torsional brace stiffness provided by the girder*
β_{conn} = *torsional brace stiffness provided by the cross frame connections*

Expressions for β_b, β_{sec}, and β_g are given by Yura [2001] and the determination of β_{conn} is covered by Quadrato [2010]. In particular, the research focus of this dissertation will center on the accuracy of the derived expressions for the individual torsional brace stiffness β_b. More details are given in Section 2.4.

2.3 CROSS FRAME TERMINOLOGY

Before discussing the design and fabrication of cross frames, it is prudent to describe terminology which will be used throughout the dissertation in relation to cross frames. In the cross frames studied, the *cross frame members* will refer to any of the steel structural shapes which comprise the system. The term *struts* refer to either the top or bottom horizontal members, and *diagonals* refer to members which are inclined from the horizontal.

Gusset plates refer to the steel plates to which the cross frame members are welded. The members are welded to the gusset plates in the fabrication shop, and the cross frame is complete. In the case of an X frame, a *spacer plate* is also welded between the crossing diagonals.

Lastly, the cross frame gusset plates are welded to the *connection plates* in the field to attach the completed cross frame to the steel superstructure. In this dissertation, the term *stiffeners* may be used when referring to the *connection plates*. In general, stiffeners refer to the vertical plates welded to the webs of steel beams to increase the shear capacity of the section; stiffeners are not required to be welded to the flanges. A connection plate on the other hand, is a vertical plate welded to both the web and the flanges, and has a cross frame is attached to it. By welding to the flanges, connection plates help to minimize distortion-induced fatigue caused by the forces introduced by the cross frame members.

Figure 2.2 graphically depicts the various terminology described.

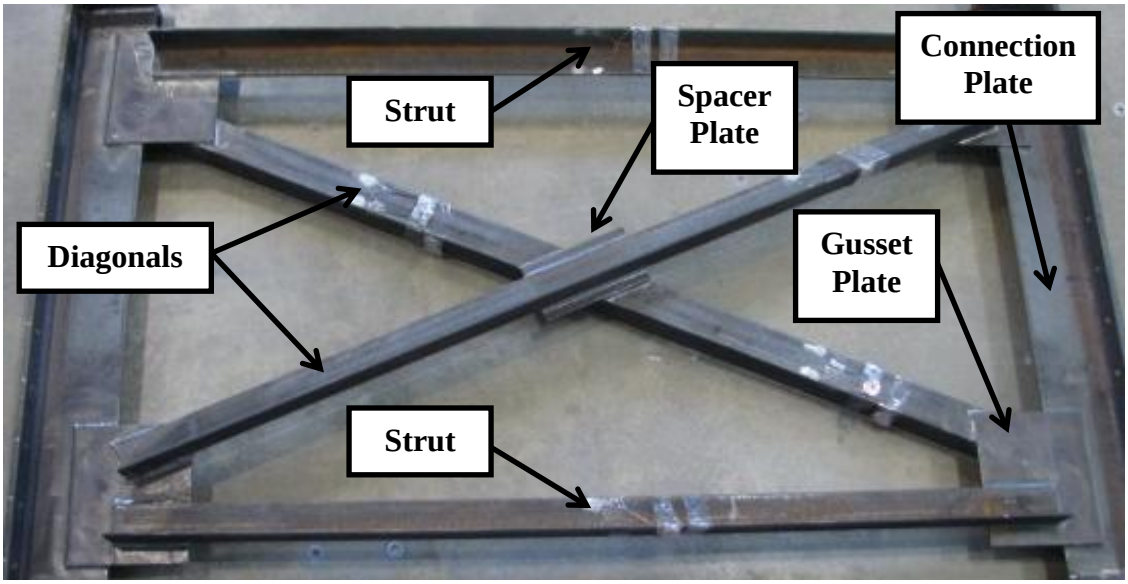

Figure 2.2: Cross Frame Terminology

2.4 CROSS FRAME DESIGN

To provide an effective brace, the cross frame must satisfy both strength and stiffness requirements [Winter 1958]. As previously mentioned, steel bridge cross frames are usually designed to restrain the twist of the girders, which forces the girders to rotate as a unit. Therefore, if one girder wants to rotate, it needs to twist all the girders in the system. Since the force required to rotate the system is much larger than for an individual girder, effective cross frames help to increase the buckling strength of each girder.

Conventional cross frames are often fabricated using two diagonal members and two horizontal struts to form an X-type brace, as depicted in Figure 2.3. The diagonals are typically formed from steel angles, while the struts are either angles, WT, or W-sections. The X-type braces studied in this research focused on cross frames constructed entirely from angle members.

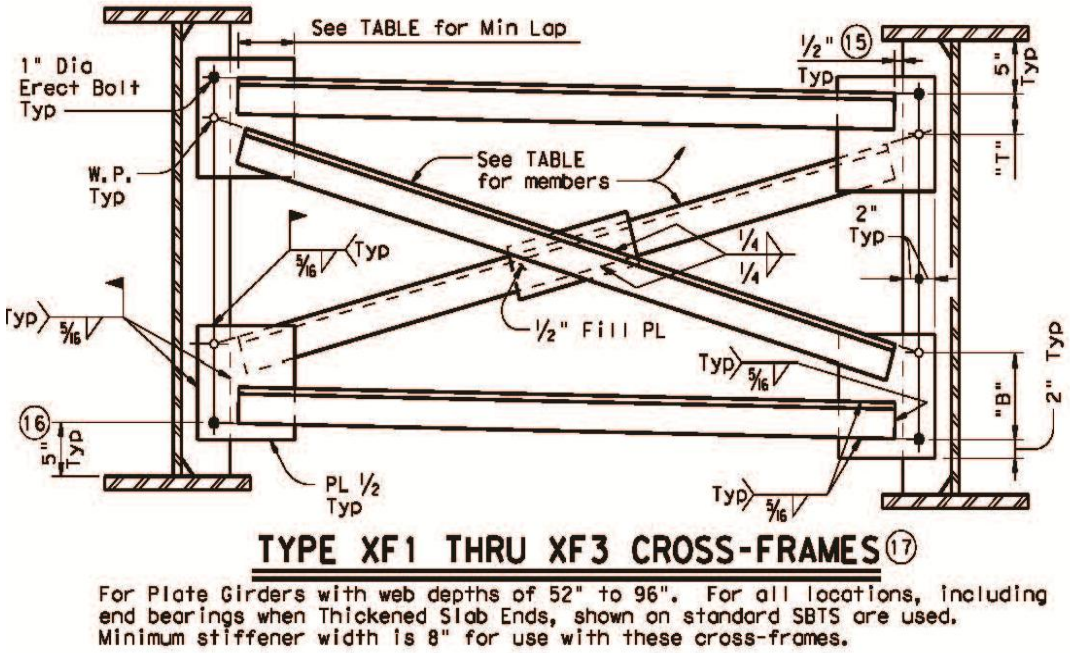

Figure 2.3: Typical X-Type Cross Frame Detail [TxDOT 2006]

In the X-type configuration, the angles used for the diagonals are welded at the ends to the connection plates, as well as at the center where they overlap. Furthermore, geometric constraints require one angle to be positioned on the backside of the connection plates. The layout of the welding details necessitates the cross frames to be turned over during fabrication, increasing the amount of required fabrication time and resources for handling since the cross frames often weigh several hundred pounds.

In addition to fabrication complexities, the angles are connected through one leg only, creating eccentric connections that lead to bending of the angle and relatively poor structural behavior. The lack of bending stiffness in the angles also results in low buckling strength. Considering the forces on the cross frame when the girder system twists, one diagonal of the cross frame experiences compression while the other goes into tension. Because of the low buckling strength of single angle members, the diagonals are often modeled as a tension-only system, which conservatively ignores the relatively low compression resistance provided by the compression diagonal.

The use of concentric members in place of the angles may result in significant improvements in the structural performance. Since concentric members, like tubes and double angles, have a substantial buckling strength, cross frames with only one diagonal can effectively satisfy the strength and stiffness requirements with the diagonal in either tension or compression. In horizontally curved girders, the direction of the torque is usually well known and the diagonal can be oriented to be in tension. With only one diagonal member, handling requirements for the cross frame during fabrication may be reduced. Lastly, connections in the cross frame can be made concentric with the centroid of the tubular member, eliminating the out-of-plane bending experienced by the single-leg angle connection.

2.4.1 Cross Frame Stiffness

The concept of using a single diagonal cross frame stems from the tension-only system that is commonly used to model these braces in bridges. In all brace configurations, girder twist induces a torsional restraining moment from the cross frame, Fh_b. The torsional moment is represented by a force couple applied at the top and bottom of the brace (see Figure 2.4).

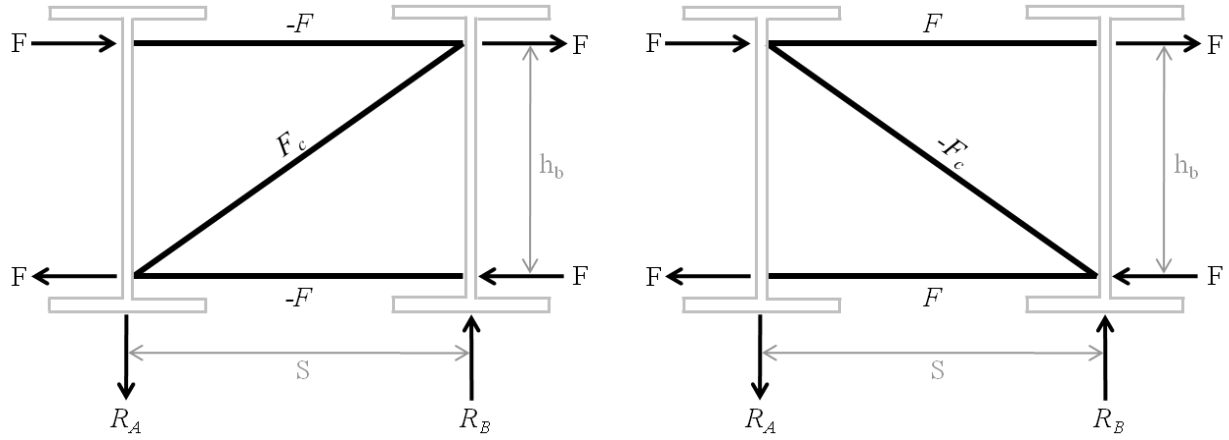

Figure 2.4: (a) Tension Diagonal System and (b) Compression Diagonal System

Considering the cross frame as a truss member system, the forces induced on the cross frame as a result of girder twist are depicted in Figure 2.4 along with the

corresponding internal forces. Static equilibrium on the cross frame system produce the following expressions for the resulting shears on the cross frame (R_A and R_B) and force in the diagonal, F_c:

$$R_A = R_B = \frac{2Fh_b}{S} \tag{2.6}$$

$$F_c = \frac{2FL_c}{S} \tag{2.7}$$

where:

h_b = *brace height*
S = *girder spacing*
L_c = *length of the diagonal*

Following the derivation provided by Quadrato [2010], a deflection analysis on the tension diagonal system can be performed to determine the rotation of the cross frame, and ultimately the brace stiffness is (in accordance with the formula given by Yura [2001]):

$$\beta_b = \frac{Eh_b^2 S^2}{\frac{2L_c^3}{A_c} + \frac{S^3}{A_h}} \tag{2.8}$$

where:

β_b = *the torsional brace stiffness provided by the cross frame considering only the in-plane axial stiffness of the cross frame members,*
E = *the modulus of elasticity,*
A_c = *the area of the diagonal member*
A_h = *the area of each strut*

Eq. 2.8 assumes that the cross frame members experience only axial forces. In cross frames comprised of single angle members, the connections possess an eccentricity that leads to bending in the members. As part of this research study, Wang [2013] found

that this eccentricity greatly reduces the stiffness of the cross frame. The findings of this research are summarized in Chapter 6.

Similar deflection analyses can be conducted on a tension-compression system (Eq. 2.9) and a K-frame system (Eq. 2.10).

$$\beta_{br} = \frac{A_c E h_b^2 S^2}{L_c^3} \tag{2.9}$$

$$\beta_{br} = \frac{2 E h_b^2 S^2}{\frac{8 L_c^3}{A_c} + \frac{S^3}{A_h}} \tag{2.10}$$

2.4.2 TxDOT Design Practice

In conversations with various TxDOT bridge engineers, it seems the current TxDOT selection of cross frames utilizes conservative "rules of thumb" to initially size the cross frame members. The determination of member size is typically based on the AASHTO design requirement for member slenderness given for compression bracing members, given as $L/r \leq 140$ [AASHTO Section 6.9.3, 2012]. Based upon a known girder spacing and depth, the engineer selects an appropriate member cross section that satisfies the minimum radius of gyration requirement for the chosen cross frame layout. While, the X-type brace configuration is the most common for newly constructed steel I-girder bridges in Texas, other brace orientations may be selected by the designer with the members sized using the AASHTO slenderness requirement.

In order to determine the locations of the cross frames, TxDOT often employs the use of the former AASHTO requirement that the cross frame spacing not exceed 25 ft. This requirement was removed in the first edition of the AASHTO LRFD Specification in 1994 and replaced by the allowance of a "rational analysis"; however, many engineers still use the requirement as a guideline based on previous successful use. In this case, a uniform spacing less than 25 ft would be selected to determine the locations of the cross frames. Once the geometry has been finalized, grid-type computer models are used to

verify the cross frame layout and the cross frame member sizes are adequate for strength and fatigue demands.

When looking at the TxDOT standard plans, three typical angle sizes are preferred for cross frames [TxDOT 2006]. The angle properties are given in Table 2.1, with the tension capacity based upon ASTM A36 steel, the preferred specification for angles.

Table 2.1: Standard Angle Sizes and Properties

Angle Size	Area	Tension Capacity
L4 x 4 x 3/8	2.86 in^2	92.7 k
L5 x 5 x 1/2	4.75 in^2	154 k
L6 x 6 x 9/16	6.45 in^2	209 k

The angle sizes listed are to be used in cross frames for depths of 52 in to 96 in with varying spacing [TxDOT 2006]. For a baseline comparison between the strengths of tubes and angles, a typical brace diagonal length of 13 ft will be assumed. This would approximately correspond to the extreme case of a 96 in depth, along with a 120 in girder spacing. From various plans of recent steel bridge construction provided by TxDOT, this diagonal length seems to be a reasonable benchmark.

The comparison given in Table 2.2 indicates the approximate size of the tubes that are necessary to deliver the same performance as the angles based on tensile strength demands only. Recall, the angle systems are designed as tension-only braces. Therefore, if a one tube diagonal is to replace two angle diagonals, for an equivalent design the tension and compression strength of the tube needs to meet or exceed the tension strength of the angle. The buckling strength of the HSS sections of Table 2.2 were determined from the AISC manual [2010] assuming an effective length coefficient K = 1.0 and using LRFD values. This condition corresponds to a member with pinned ends.

Table 2.2: Angle Tensile Strength vs. Tube Buckling Strength

Angle Size	Angle Capacity (36 ksi)	Tube Size	Tube Capacity[1,2]
L4 x 4 x 3/8	92.7 k	HSS 5 x 5 x 3/16	88.6 k
		HSS 5.563 x 0.258	99.6 k
L5 x 5 x 1/2	154 k	HSS 5 x 5 x 3/8	160 k
		HSS 5.563 x 0.375	139 k
L6 x 6 x 9/16	209 k	HSS 5 x 5 x 1/2	199 k
		HSS 6.000 x 0.500	207 k

1. Tube capacity was calculated using a length of 13 ft
2. Yield stress (F_y) is assumed to be 46 ksi for square tubes and 42 ksi for round tubes [AISC 2005]

The laboratory tests, finite element analyses, and cast connection development discussed in Chapters 4-7 include the tube sizes listed above to be comparable to the currently used angle members.

2.5 TUBULAR BRACES IN LITERATURE

While tubular braces may not be commonly used in steel bridge design, there are a variety of structural applications where tubular members and braces have been used. The following sections highlight the documented use of tubular members.

2.5.1 Offshore Industry

Tubular members have long been the primary cross-section used in the construction of offshore platforms for the oil industry. Their increased strength in compression helps to resist the large overturning moments caused by waves acting on the structure. Also, because the tube is axisymmetrical, it helps to simplify the analysis as the tidal forces may act on the members from any direction. Lastly, using tubular members helps to resist torsional loads that may be applied to the structural system.

2.5.2 Concentrically Braced Frames

In addition to the offshore industry, tubular members have seen increased use in structures designed to resist earthquakes. Again, the superior strength of tubes in compression, as compared to other available structural shapes, is the motivating reason for their use.

2.5.3 European Bridges

The use of tubular members in structures has been steadily growing throughout the world and particularly in Europe. One emerging type of bridge involves a three-dimensional steel space truss structure made composite with a concrete deck. The truss consists of hollow tubular members and is usually connected with cast steel nodes [Haldimann-Sturm and Nussbaumer 2007]. Tubular members have also been used as the primary support structures of arch bridges, such as the Humboldthafen Rail Bridge in Germany shown in Figure 2.5 [FHA 2001]. Coincidentally, the steel bearing connections shown were cast specifically for this bridge.

Figure 2.5: Large Cast Steel Bearing in Tubular Arch Bridge [FHA 2001]

2.5.4 Wichita Falls, TX Bridge Retrofit

Tubular braces were also utilized in a retrofit to a curved steel I-girder bridge located in Wichita Falls, TX. Two three-span steel bridge units were constructed as part

of a direct connector ramp to take traffic from northbound US-82 to westbound US-277. Each unit consisted of 235 ft end spans and a 250 ft center span, resulting in an unfavorable span ratio approaching 1.0. Due to site restrictions, these span ratios were necessary to accommodate support placement. In addition, the bridge had an 819 ft radius of horizontal curvature further complicating design [Turco 2009].

After placement of the concrete deck, excessive rotations were observed in the superstructure. To accommodate the design ramp speed, a cross slope of 6 percent was desired in the finished deck. However, survey measurements indicated the slope was significantly less than required, approaching a minimum of 1 percent near mid-length of the end spans [Turco 2009].

The existing cross frame system consisted of the X-type braces using L4x4x3/8 members and set at approximately 17 ft spacing. When the problems were discovered, further analysis using a finite element model was conducted, revealing torsional flexibility in the system as a result of the disadvantageous span arrangement as well as high length-to-width ratio [Turco 2009].

To solve the problem, a retrofit was necessary requiring removal of the concrete deck over the end spans. Shore towers were then installed and the bridge was jacked into proper position, followed by the addition of a lateral truss connected to the bottom flange as shown in Figure 2.6. Once the concrete deck was placed and hardened, the bottom flange braces formed a quasi-closed box with significant torsional stiffness compared to the open I-girder system. Because some members of the braces may experience significant torsion, HSS 6x6x5/8 tubular braces were selected. The connection detail consisted of a split tube connection also shown in Figure 2.6. The torsional stiffness of the retrofitted bridge proved to be significantly higher than the open I-girder system [Turco 2009].

Figure 2.6: Tubular Bracing Retrofit of Curved Steel Bridge in Wichita Falls, TX with Close-up of Connections [Turco 2009]

2.5.5 Advantages of Tubular Members

Tubular members offer several advantages over the use of other readily available structural shapes. The behavior of tubes is well understood, allowing a more accurate prediction of structural forces and deflections as compared to angles, which are subject to biaxial bending. Tubular members are available in a wide array of sizes, allowing the designer to select the appropriate cross-section for a given application.

The main reason for selecting tubular members for use in steel bridge braces is to allow the use of a single diagonal cross frame layout. In order to provide an effective torsional brace, the single diagonal needs to handle both tension and compression, depending upon the buckling direction. For unbraced lengths on the order of 12-15 ft, tubular cross-sections are the most efficient way to resist these forces and provide an adequate design.

In addition, the concentric nature of the tubular connection may result in improved fatigue performance versus the eccentric single angle members. Additional information on fatigue is presented in the following chapter and results from fatigue tests are presented in Chapters 5 and 7.

CHAPTER 3
Background: Fatigue Design and Behavior in Steel Bridges

3.1 INTRODUCTION

While cross frames are important structural members for providing girder stability and improving the torsional stiffness of the bridge, the braces in the completed bridge are susceptible to fatigue crack formation from repeated stress cycles from traffic loads such as heavy truck traffic. The cross frame forces leading to fatigue issues primarily result from differential deflection of adjacent girder lines. Therefore, the impact of fatigue on the bracing behavior should be considered in the design of the bracing system.

A major aspect of the research conducted within this dissertation was the assessment of current cross frame connections and the potential development of new details for use in steel bridge applications. The following information provides a brief overview of the classification of bridge details for fatigue design, including information on the current use of single angle members and available research covering the proposed connections.

3.2 INTRODUCTION TO FATIGUE

Fatigue is the phenomenon by which localized structural damage occurs to the material due to cyclic loading. It is often grouped into two classifications: low-cycle fatigue, typically less than 10,000 cycles, and high-cycle fatigue, more than 10,000 cycles. In the determination of fatigue life, the stress range, S_R, applied to the member is related to the number of cycles, N, to failure. Low-cycle fatigue is characterized by stress ranges near the yield stress of the material, namely $S_R \approx F_y$. High-cycle fatigue involves stress ranges much lower than the yield strength of the material, or $S_R << F_{y.}$

In steel bridges, the designer is concerned with high-cycle fatigue. The members of the bridge are subjected to periodic loads due to the passing of traffic on the

superstructure. These stresses are usually much lower than the yield strength of the material, especially in cross frame members.

3.2.1 Geometrical Discontinuities

Fatigue cracks are most likely to form at geometrical discontinuities, such as that caused by the cross frame member connection to the gusset plates as well as at the attachment of the cross frame gusset plates to the connection plates. In steel bridges, the term "connection plate" generally refers to a transverse web stiffener that connects the cross frame or diaphragm to the girder. The connection plate also serves as a stiffener to increase the shear capacity of the girder web, while providing the connection to the cross frame. The local geometry causes an increase in stress to build up at a specific point, thereby exceeding the yield stress and causing permanent damage. The damage initiates on a microscopic level and often over the course of thousands of cycles, a crack will grow. Figure 3.1 shows the eccentric single angle detail studied in the research. Note how the stress transfer from the angle member to the gusset plate leads to a build-up of stress at the forward edge of the fillet weld connection. In addition, a secondary stress concentration occurs in the gusset plate at the toe of the weld at the back end of the member.

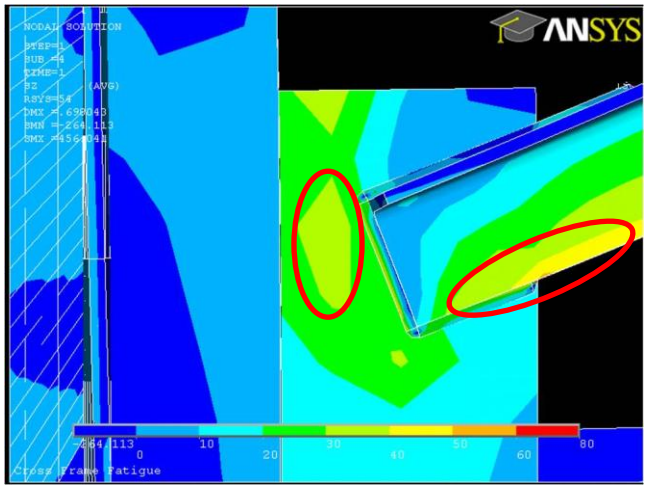

Figure 3.1: Stress Concentration due to Geometrical Discontinuities at the Cross Frame Connection

A major focus of the research is to identify the effect geometrical discontinuities can have on the formation and growth of fatigue cracks. Due to the nature of the fillet welded connections, stress concentrations arising from the changes in geometry are inevitable. The research aims to relate connection and member geometry to fatigue behavior. Cyclic testing on individual cross frame members/connections and full scale cross frames will be combined with visual inspection of crack locations to determine the AASHTO fatigue rating of the details. Using the observations from the experimental tests along with limited use of finite element analysis, recommendations will be made to improve the overall fatigue performance of the cross frames.

3.2.2 Material Defects

At the most basic level, fatigue cracks typically initiate at defects in the material. There are many possible sources of the defects, which range from the atomic level to the macroscopic level. For instance, in an ordinary plate of steel, atomic vacancies in the lattice structure of the material cause microscopic stress risers, similar to the stress concentration formed in the classic example of a uniaxially loaded plate with a hole. Although the cracks start small, they continue to grow under repeated cycling of stress.

In welded steel structures, defects in the welds are the most likely location for fatigue cracks to initiate. For fillet welds (which will be used in the cross frames studied), very small slag inclusions at the weld toes often initiate cracking. While this particular defect is inevitable, careful control of the weld geometry can help reduce the local weld toe stress. In addition, visual inspection and magnetic testing can be used to make sure the inclusions are not too large. The following subsections describe various possible defects which must be controlled to produce quality welded connections.

3.2.2.1 Undercut

Undercut is a notch-type defect occurring in the base metal at the welded connection and is related to the temperature and placement of the weld metal. If the input heat is too high, or the weld is directed into one plate more than the other, the base metal

melted at the edge of the weld is not filled, creating a divot at the weld toe (as seen in Figure 3.2 and Figure 3.3). The divot can cause localized stress concentrations, amplifying the concentration already existing at the weld toe, resulting in lower fatigue life. The permissible depth of undercut is 3/64 in or less [AWS 2012]. Any undercut experienced as part of the research program was measured using a calibrated depth gauge, and were always within permissible limits.

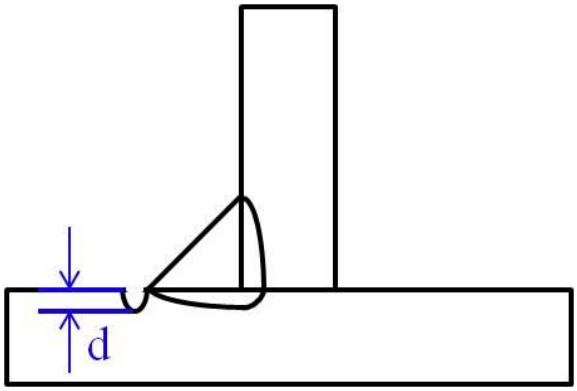

Figure 3.2: Undercut at Toe of Fillet Weld Connection (Schematic)

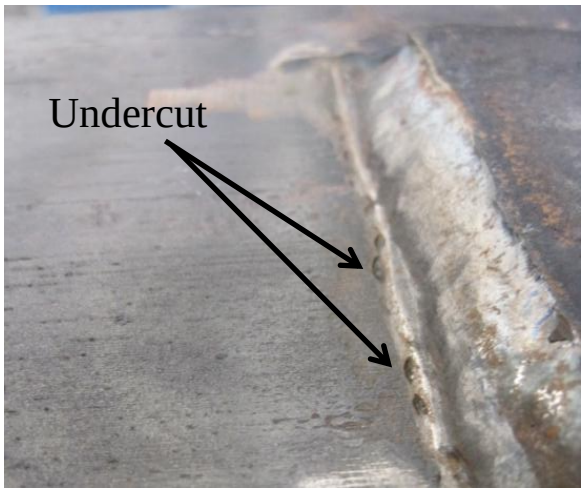

Figure 3.3: Undercut at Toe of Fillet Weld Connection (Example)

3.2.2.2 Incomplete Fusion

Incomplete fusion is the failure of the weld to fully penetrate the base metal, particularly at the root of the weld, thus reducing the strength of the weld. Insufficient welding current, lack of access to the weld, and poor pre-weld cleaning are the leading causes of incomplete fusion [Connor 1987]. In terms of fatigue, gross incomplete fusion can lead to an increase of stress at the toe of the weld reducing the fatigue life.

3.2.2.3 Slag Inclusions

Slag inclusions are nonmetallic solid materials that get trapped in the weld metal as a result of poor technique and inaccessibility of the connection [Connor 1987]. The slag is only present in the methods that use a solid material to shield the weld from the air, which includes the basic Shielded Metal Arc Welding (SMAW) and the Flux-Cored Arc Welding (FCAW) processes frequently used for cross frame fabrication.

In a properly welded connection, the slag will trap impurities within the metal and float them to the surface of the molten weld, thus removing them from the connection. If large amounts of slag get trapped in the weld, there can be a large vacancy which cannot distribute load. The vacancy can lead to fatigue crack initiation and eventually failure. In general, small slag inclusions will not be detrimental to the fatigue strength of the weld. A schematic of a slag inclusion is shown in Figure 3.4 and an example in Figure 3.5.

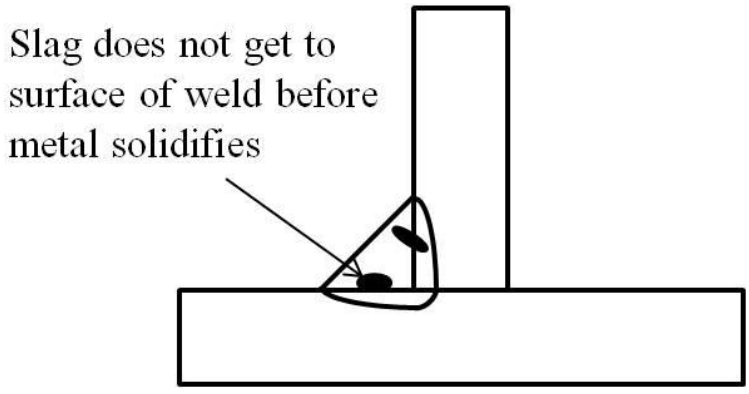

Figure 3.4: Slag Inclusion in Fillet Weld (Schematic)

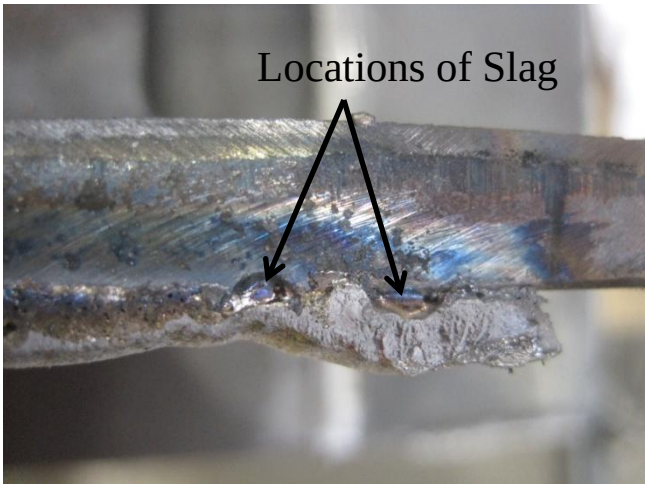

Figure 3.5: Vacancy Resulting from Slag Inclusion in Cross Section of Fillet Weld (Example)

3.2.2.4 Porosity

The last and perhaps most common defect is porosity, which involves gas trapped in the solidifying weld metal [Connor 1987]. In a weld metal, the molten weld pool could contain the following gases: hydrogen, oxygen, nitrogen, carbon monoxide, carbon dioxide, water vapor, hydrogen sulphide, argon, and helium. Of these, hydrogen, oxygen, and nitrogen are the only ones that diffuse in high concentration into the liquid metal. Hydrogen can be from several sources, including, but not limited to, the hydrogen in the atmosphere immediately surrounding the weld, the hydrogen that can form from constituents like cellulose in the flux or electrode covering, and the hydrogen from dissociation of water. Water can be from excessive humidity or rainwater in the vicinity of the weld. Oxygen can enter the molten pool through oxides on filler wire or base metal, flux and electrode covering, and from the atmosphere [Connor 1987]. Porosity leads to small vacancies that can become the initiation points for fatigue cracks in the connection. A schematic of porosity is shown in Figure 3.6 and porosity in a fillet weld is shown in Figure 3.7.

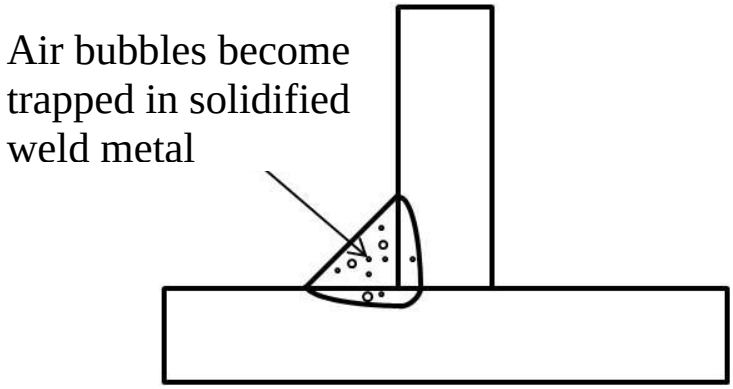

Figure 3.6: Porosity in Fillet Weld (Schematic)

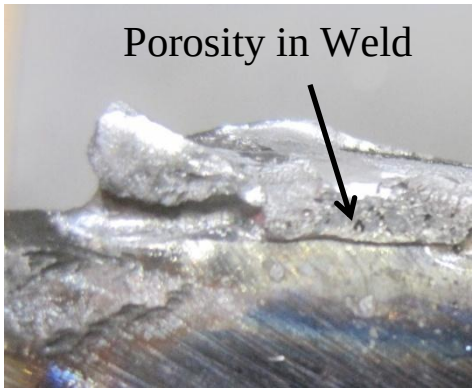

Figure 3.7: Porosity in Cross Section of Fillet Weld (Example)

3.2.3 Distortional Fatigue

Finally, fatigue cracks can initiate at the web-flange interface at the connection plate location due to local distortion of the web. To minimize cracking at this location, the connection plates should be welded to the flanges, which limits the bending of the web and improves the fatigue behavior. Web gap distortional fatigue was not specifically studied as part of this dissertation; the connection plates in the research were welded to the flanges and no fatigue cracks were observed at the web-flange interface in the large scale tests described in Chapter 7. More information is given in the following section.

3.3 AASHTO BRIDGE FATIGUE DESIGN METHODOLOGY

With the numerous potential defects present at welded connections, fatigue loading on the connection needs to be considered. In general, fatigue is often divided into distortion-induced fatigue and load-induced fatigue [Fisher et. al. 1998]. Distortion-induced fatigue is controlled by proper detailing. An example of distortion-induced fatigue is a crack that might initiate in the web of a girder around a cross frame connection plate that is not fastened to the girder flange. Prior to the 1990s, connection plates were often not fastened to the girder flanges and extensive fatigue cracking often occurred in girder webs around the cross frame locations. Fastening the connection plate to the girder flange largely eliminated the distortion-induced fatigue problem around the cross frames. The other type of fatigue cracking is categorized as load-induced fatigue. The American Association of State Highway and Transportation Officials (AASHTO) LRFD Bridge Design Specification [2012] has well-defined procedures for accounting for load-induced fatigue. The AASHTO design procedure accounts for load-induced fatigue using different categories based on the type of connections on the bridge. In conjunction with the detail category, the average daily truck traffic on the bridge is the other prevailing factor in the fatigue design of the steel bridge. The following subsections outline the methodology AASHTO uses when designing for fatigue.

3.3.1 Fatigue Design

In LRFD design, the factored resistance to fatigue cracking of the detail must exceed the factored load demand on the detail. AASHTO specifies in Article 6.6.1.2.2 that any load-induced fatigue detail needs to satisfy the following condition:

$$\gamma(\Delta f) \leq (\Delta F)_n \tag{3.1}$$

where:

γ = *Load factor specified in Table 3.4.1-1*

(Δf) = *Force effect, or the live load stress range (specified in Article 3.6.1.4)*

$(\Delta F)_n$ = *Nominal fatigue resistance (specified in Article 6.6.1.2.5)*

3.3.2 Live Load Stress Range

The fatigue loading magnitude and configuration is covered in AASHTO Article 3.6.1.4.1 and is used to determine the factored live load stress range acting on the detail, or (Δf) [2012]. The specification uses one design truck (as specified in Article 3.6.1.2.2) but with a constant spacing of 30 ft between the 32 kip axles for the truck. The AASHTO specification also includes consideration of a design tandem, which consists of two 25 kip axles spaced at 4 ft apart. Unless short spans are used, the design truck, with the much higher load, will govern the strength behavior of the bridge and often the fatigue stresses [Frank 2008]. The geometry and loading associated with the fatigue design truck and the tandem are given in Figure 3.8 and Figure 3.9.

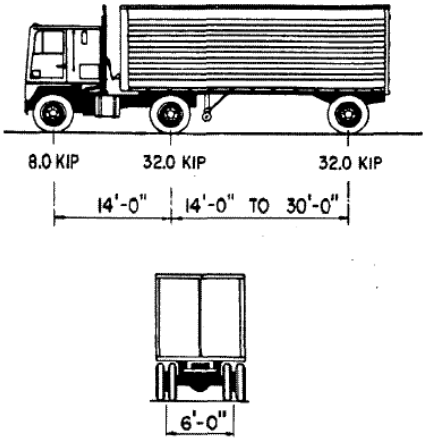

Figure 3.8: AASHTO Fatigue Design Truck [AASHTO 2012]

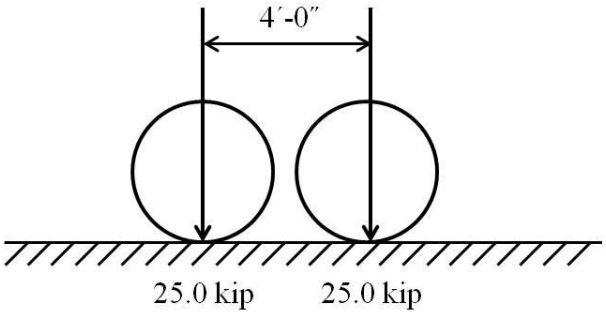

Figure 3.9: AASHTO Fatigue Design Tandem

Article 3.6.1.4.3 specifies the fatigue load distribution to determine the fatigue forces in the various bridge components. Simply stated, the fatigue truck or tandem shall be placed transversely and longitudinally to maximize the stress range at the detail under consideration, regardless of the traffic position or lane designations [AASHTO 2012]. Chapter 8 highlights the results from a fatigue design comparison between ANSYS and MDX in which the placement of the fatigue load will be discussed in more detail.

3.3.3 AASHTO Fatigue Design Categories

To simplify fatigue design, AASHTO designates categories to different connection types that account for the stress concentration resulting from geometrical discontinuities and local notch stresses. There are currently eight categories in the AASHTO specification: A, B, B′, C, C′, D, E, and E′ (pronounced ‘E prime’) [AASHTO 6.6.1.2.3 2012]. In order to be used in steel bridge design, the detail must meet one of these fatigue categories. AASHTO Table 6.6.1.2.3-1 gives an extensive list of the categories for different connection and other details typically found in steel bridges [2012].

The basic premise is that Category A pertains to the base metal of steel, that simply accounts for material defects in the base metal away from any connection details or geometric anomalies. Each category below A, B through E′, apply to increasing severity of stress concentrations or lower fatigue resistance, with E′ being the lowest category. The category method helps determine the resistance of the detail to the

development of fatigue cracks, which must be larger than the applied loads in LRFD design.

3.3.4 Nominal Fatigue Resistance

The nominal fatigue resistance is covered in Article 6.6.1.2.5 and is separated into two load combinations [AASHTO 2012]. Using the Fatigue I load combination and considering infinite life for the detail:

$$(\Delta F)_n \leq (\Delta F)_{TH} \tag{3.2}$$

where:

$(\Delta F)_n$ = *Nominal Fatigue Resistance (specified in Article 6.6.1.2.5)*

$(\Delta F)_{TH}$ = *Constant Amplitude Fatigue Threshold (specified in Table 6.6.1.2.5-3)*

Alternatively, the Fatigue II load combination is used and the designer considers a finite life for the detail as follows:

$$(\Delta F)_n \leq (A/N)^{\frac{1}{3}} \tag{3.3}$$

where:

$(\Delta F)_n$ = *Nominal Fatigue Resistance (specified in Article 6.6.1.2.5)*

A = *Constant, taken from Table 6.6.1.2.5-1 related to fatigue category*

N = *Number of stress cycles over the life of the bridge*

$$N = (365)(75)n(ADTT)_{SL} \tag{3.4}$$

where:

365 = *Days per year*

75 = *75 year design life, typical in AASHTO*

n = *Number of stress range cycles per truck passage (Table 6.6.1.2.5-2)*

$(ADTT)_{SL}$ = *Single lane average daily truck traffic (Article 3.6.1.4)*

AASHTO specifies the frequency of the fatigue loading to be taken as the single-lane average daily truck traffic $(ADTT)_{SL}$ which, without better information, is taken as a percentage of the average daily truck traffic (ADTT) of the bridge [2012]. For simple spans longer than 40 ft, *n* is taken as 1.0; for continuous spans longer than 40 ft, *n* is taken as 1.5 [AASHTO 2012].

The values for *A* and $(\Delta F)_{TH}$ in Equations 3.2 and 3.3 are given in Table 3.1 and Table 3.2, respectively.

Table 3.1: Detail Category Constant, A [AASHTO Table 6.6.1.2.5-1 2012]

Detail Category	Constant, *A* times 10^8 (ksi^3)
A	250.0
B	120.0
B′	61.0
C	44.0
C′	44.0
D	22.0
E	11.0
E′	3.9
M 164 (A325) Bolts in Axial Tension	17.1
M 253 (A490) Bolts in Axial Tension	31.5

Table 3.2: Constant-Amplitude Fatigue Thresholds [AASHTO Table 6.6.1.2.5-3 2012]

Detail Category	Threshold (ksi)
A	24.0
B	16.0
B′	12.0
C	10.0
C′	12.0
D	7.0
E	4.5
E′	2.6
M 164 (A 325) Bolts in Axial Tension	31.0
M 253 (A 490) Bolts in Axial Tension	38.0

3.3.5 AASHTO S-N Chart

When determining the associated fatigue performance of a typical detail using the AASHTO design code, it is useful to graph the results of Equations 3.2 and 3.3 on an S-N plot. The S-N plot is a log-log plot of the constant-amplitude stress range (S) versus the number of cycles to failure (N). An overview of an S-N plot with the fatigue categories of AASHTO is given in Figure 3.10 and a more detailed, refined view is given in Figure 3.11. The latter plot will be used throughout the dissertation to make comparisons between the data.

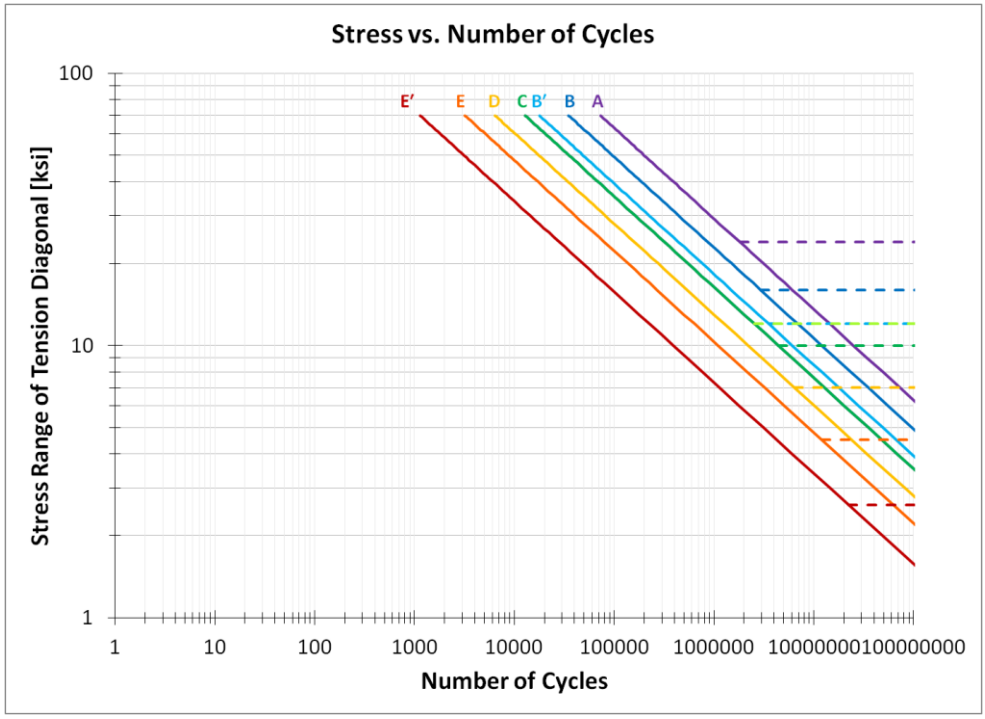

Figure 3.10: Overview of S-N Plot indicating AASHTO Fatigue Categories

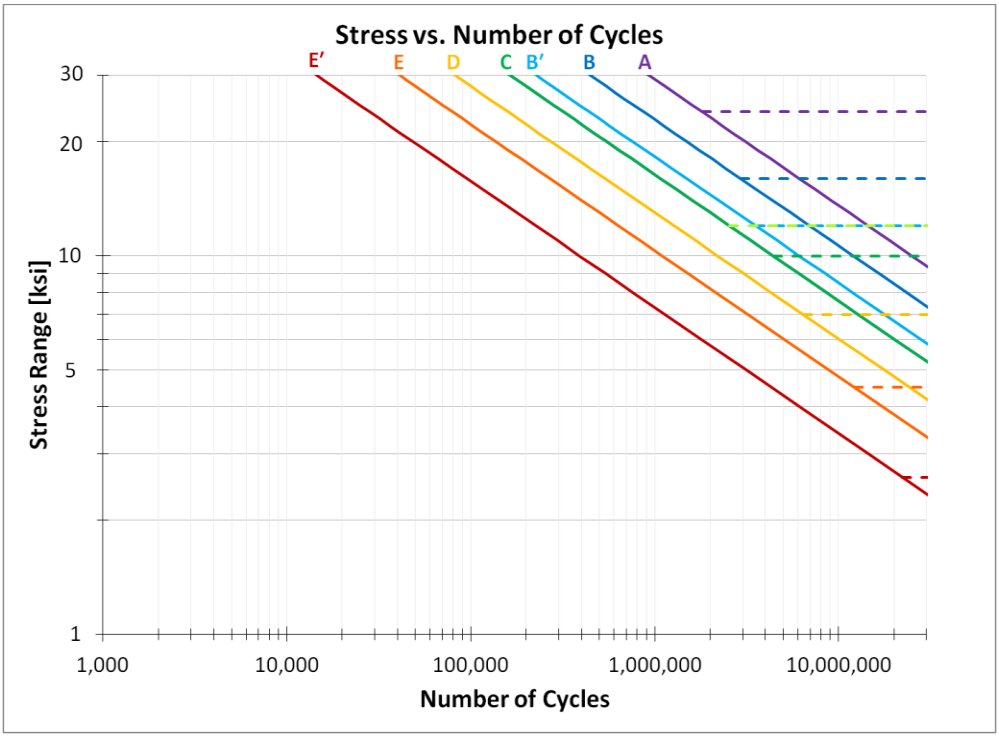

Figure 3.11: Refined View of S-N Plot indicating AASHTO Fatigue Categories

Data points that lie above and to the right of the finite life portions of the curve are considered adequate. The finite life portion is the sloped line on the graph, which on the log-log scale has a slope of 3, the generally accepted value resulting from fatigue tests performed on numerous steel details in previous research.

If it is determined the stress range acting on a detail is lower than the infinite life portion of the design curves (the dashed lines in Figure 3.10 and Figure 3.11), then the detail is considered to have infinite life according to the specification.

For ease of design, AASHTO only considers the constant-amplitude stress range, and applies different load factors to the Fatigue I and Fatigue II loadings to adjust for load variation according to a perceived stress range distribution function [AASHTO 2012]. For a more detailed analysis, advanced techniques utilizing rain flow counting methods or the Palmgren-Miner rule can account for variation in stress range, but is not carried out in the current research. Fasl [2013] provides a method for fatigue evaluation using the Palmgren-Miner rule and an index stress range that allows the direct comparison of details with different fatigue categories. The method provides a valuable means for utilizing strain data on a bridge to evaluate and compare fatigue damage to that bridge.

3.3.6 Fatigue Testing Methods and Failure Criteria

In order to assess the fatigue life of a given detail, numerous connections are tested to rate the connection according to the categories outlined in AASHTO. The connections tested can be either small scale (uniaxial tension tests) or large scale (full scale cross frame tests) in nature. The testing method employed usually consists of specimens that are tested at a constant stress range, verified and updated by external measurements of force/stress and strain. The connections are typically tested at the maximum frequency at which the test setup remains stable.

During most laboratory tests, once a stress range is selected for the test, the detail is cycled until failure. The number of cycles-to-failure are recorded and compared to the AASHTO fatigue categories to classify the behavior of the detail. Failure is usually

taken as the point at which the specified force for the stress range can no longer be sustained. The process is outlined in Figure 3.12.

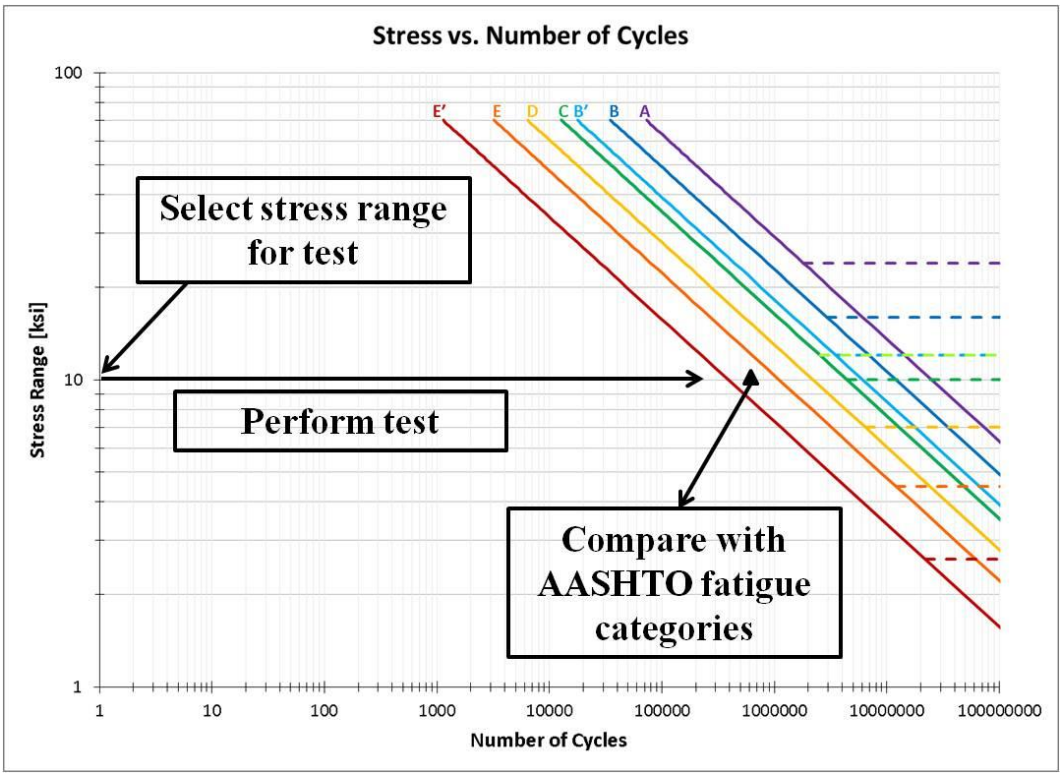

Figure 3.12: Fatigue Testing Procedure

3.4 FATIGUE BEHAVIOR OF SINGLE ANGLE MEMBERS

The majority of steel bridge cross frames constructed utilize single angle members. The angles are typically welded to the gusset plates along only one leg of the angle, resulting in an eccentric connection. While the single angle detail has been used for numerous years, there is relatively little information on the corresponding fatigue performance. Fortunately, the eccentric single angle detail has not caused widespread fatigue problems within the cross frame bridges. However, as analysis tools become more advanced and the prevailing bridge codes allow more direct analysis, designers may begin to place higher force demands on the cross frames by using smaller cross frames

with a larger spacing. It is important to therefore understand the behavior of this connection and the potential failure modes.

3.4.1 Effect of Angle Eccentricity

In a cross frame, forces are transmitted to the cross frame members from the girder via the gusset plate. Due to the eccentricity of the angle centroid from the gusset plate centroid, a moment is applied to the member in addition to the axial force. Figure 3.13 shows a typical angle to gusset plate connection alongside the associated bending that occurs when a uniaxial tension is applied to the gusset plates.

Figure 3.13: (a) Eccentric Connection of Angle and (b) Bending of Angle due to Eccentricity

The test shown in Figure 3.13(b) was performed as part of research conducted by McDonald and Frank [2009] for the American Institute for Iron and Steel. During the tests, lateral deformation of the angle was reported to be as high as approximately 1 in at mid-length of a short 4 ft specimen.

3.4.2 Fatigue Classification of Single Angle Detail

Prior to 2012, there was little guidance given in the AASHTO LRFD Bridge Design Specification regarding the fatigue classification of the single angle detail. A Category E detail was recommended by the LRFD Design Manual for Highway Bridge Superstructures [AASHTO 2007], which takes into account the fatigue performance for shear on the throat of the fillet weld, but does not consider the geometric differences provided by the angle.

The current specification recommends the detail to be Category E, as referenced in AASHTO Table 6.6.1.2.3-1 [2012]. The table goes on to specify that fatigue stress range be based on the effective net area of the member, A_e, which includes a shear lag factor, U, as given in the following equations.

$$A_e = UA_g \tag{3.5}$$

where:

A_e = *Effective area of the angle*

U = *Shear lag factor*

A_g = *Gross area of the member*

$$U = 1 - \frac{\bar{x}}{L} \tag{3.6}$$

where:

$\bar{x}$ = *Distance from the centroid of the member to the surface of the gusset or connection plate*

L = *Maximum length of the longitudinal welds*

The AASHTO code cites the research by McDonald and Frank [2009] regarding the behavior of the single angle connection, and specifies that the moment due to the

eccentricities in the connections shall be ignored when calculating the fatigue stress range [AASHTO 2012].

3.4.3 Previous Fatigue Tests of Single Angle Detail

The research conducted by McDonald and Frank [2009] was motivated by the lack of laboratory testing performed on the single angle detail in fatigue. The research program consisted of three angle cross section arrangements, the L4x4x3/8 angle, the L5x3x3/8 angle with the short leg connected to the gusset plate, and the L5x3x3/8 angle with the long leg connected to the gusset plate. The angles were connected to the gusset plates with 5/16 in fillet welds, and the specimen longitudinal weld lengths were either "equal" or "balanced". Equal means the weld lengths were the same along the outstanding leg and the horizontal leg. Balanced means the weld length along the horizontal leg was reduced so that the center of gravity of the weld resistance was in line with the center of gravity of the member.

The specimens were tested in a 550 kip MTS universal testing machine. Due to the large amount of bending resulting from the angle eccentricity (shown in Figure 3.13), there was concern the moment on the grips could cause damage to the test machine from cyclic loading during a fatigue test. Therefore, the tests were primarily performed with two specimens back-to-back. A spacer plate was positioned between the gusset plate ends to allow the angles to deform out-of-plane and to prevent the contact pressure between the plates from changing the force distribution on the angles. The gusset plate ends were also thicker than plates typically used in practice to ensure cracking occurred in the angle member. The symmetric nature of two specimens tested back to back eliminated the impact of the bending from the eccentricity, which may have improved the fatigue performance. Furthermore, the thicker end plates would have lower stresses than the gusset plates typically found in practice.

Results from the fatigue tests showed three types of failures: (i) cracking at the forward weld toe of the angle-gusset weld propagating into the toe of the horizontal leg of the angle; (ii) cracking at the forward weld toe of the angle-gusset weld propagating

into the heel of the angle; and (iii) cracking at the end weld toe propagating into the gusset plate [McDonald and Frank 2009]. A summary of the crack locations is given in Figure 3.14.

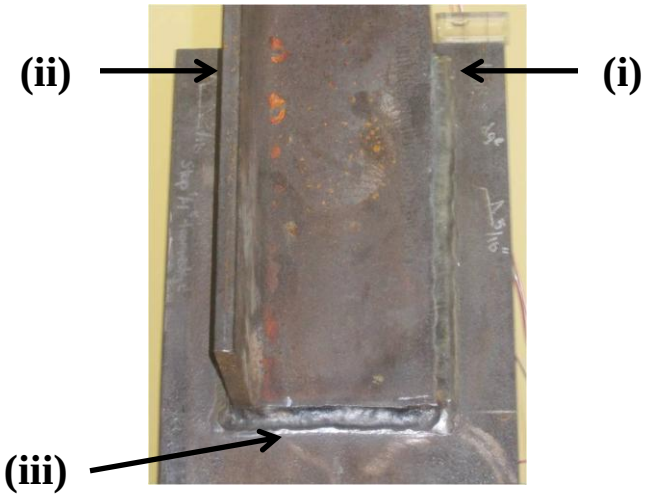

Figure 3.14: Single Angle Fatigue Crack Failure Locations

Analysis of the test data showed that calculating the fatigue stress range using the effective net area of the member, which accounts for shear lag in the connection, reduced the scatter of the results. The connections tested ranged from Category E′ to Category D, with the majority of the connections classified as Category E′ and Category E [McDonald and Frank 2009]. In particular, it is noted the specimens with "equal" weld length, which is typically seen in practice, were primarily on the lower end of performance.

Tests on angle connections were also performed by Wilbur Wilson, and reported in Munse's *Fatigue of Welded Structures* [1964]. The geometry was much different than seen in typical cross frame construction, with the horizontal leg of the angle tapering from the width of the angle to the thickness of the angle over the connection length. Although being significantly different, fatigue performance of the connection was similar to the aforementioned results (Category E′ to Category E) as discussed by McDonald and Frank [2009].

3.4.4 Discussion of Previous Fatigue Tests of Single Angle Detail

Although the tests conducted seem to indicate that Category E′ would represent an appropriate lower bound prediction of fatigue failure, the AASHTO specification still considers the detail as Category E [AASHTO 2012]. Perhaps considering the mean of the test data would justify this classification. In addition, the latest specification requires the stress range to be calculated on the smaller, effective area rather than the gross area, which is a major change from the previous requirements.

In addition, the previous tests had thicker gusset plates than typically used in cross frame construction and were tested back-to-back in the test machine to minimize the eccentric moment applied to the grips. It is theorized the stress concentration at the angle-gusset weld connection due to the increased bending that would occur as a result of thinner plates and allowing out-of-plane bending would further reduce the fatigue life of the single angle detail. In fact, the one test data point completed which allowed bending had the worst performance of all specimens tested [McDonald and Frank 2009].

Axial tests performed in the research of this project (Chapter 5) showed similar testing problems with the bending moment induced at the grips due to the single angle detail. The solution was to test the entire cross frame assembly in fatigue, using weld details and member sizes indicative of common plate girder design. The results of this test series are documented in Chapter 7.

3.4.5 Previous Finite Element Analysis (FEA) of Single Angle Detail

As part of the research conducted by McDonald and Frank [2009], an extensive parametric study was undertaken to determine the effect certain variables on the behavior of the connection. Following the DNV method for hot spot stress extrapolation, the stress concentration factor (SCF) at the forward edge of the fillet weld on both the horizontal and vertical angle legs (Locations (i) and (ii) in Figure 3.14) was determined, and the maximum value recorded. More information on finite element modeling for fatigue hot spot stress extrapolation is provided at the end of the chapter.

The results of the FEA study showed that the SCF increased as the thickness of the gusset plate decreased, following approximately linear behavior. According to the equation provided in Eq. 3.7, the SCF using a thickness of 1.5 in, corresponding to the tests performed, is 3.72. Using the typical 0.5 in gusset plates seen in construction, the SCF would be 4.21, an increase of 13%. The increase may contribute to reduced fatigue life.

$$SCF = -0.49x + 4.4542 \tag{3.7}$$

where:

SCF = Stress concentration factor

x = Gusset plate thickness

Further FEA showed the SCF to increase with increasing length of the outstanding leg of the angle. The outstanding leg increases the eccentricity, and although the stiffness of the angle is also increased, the eccentricity seems to significantly affect the behavior of the angle and heightens the effect of the stress concentration. This variable showed the greatest effect on the SCF, which is why the effective area was chosen to calculate the stress range. It is theorized the use of an unequal leg angle with the long leg attached to the gusset plate would therefore lower the SCF, and could offer the same or better performance.

Other variables had small effects on the SCF: increasing the gusset plate length slightly increased the SCF; increasing the angle length reduced the SCF; and increasing the angle thickness reduced the SCF. The gusset plate width, weld lengths, and horizontal angle leg width did not significantly change the SCF and no discernible trend was shown [McDonald and Frank 2009].

3.5 FATIGUE BEHAVIOR OF TRANSVERSE FILLET WELDS

Another aim of the research documented in this dissertation is to provide alternative details that offer similar or improved fatigue performance compared to

existing details. The cast connections and T-stem connections outlined in Chapters 4 and 5 require transversely loaded fillet welds to transfer the forces from the tubular members to the gusset plates. In addition to the advantages of the tube in compression, the concentric connection the tube provides may improve the fatigue strength of the diagonal members relative to angles. In order to make sure the fatigue behavior of the tubular members is superior, these two methods of connecting tubular members were also investigated. The details are shown in Figure 3.15.

Figure 3.15: (a) T-stem Connection and (b) Cast Connection

One shortcoming of current design rules is the fatigue strength of fillet weld connections failing through the throat of the weld are based on data obtained from simple cruciform joints tested in tension under normal stresses [Maddox 2008]. Figure 3.16 shows a typical fatigue test on a cruciform joint, with the loading direction and failure crack indicated.

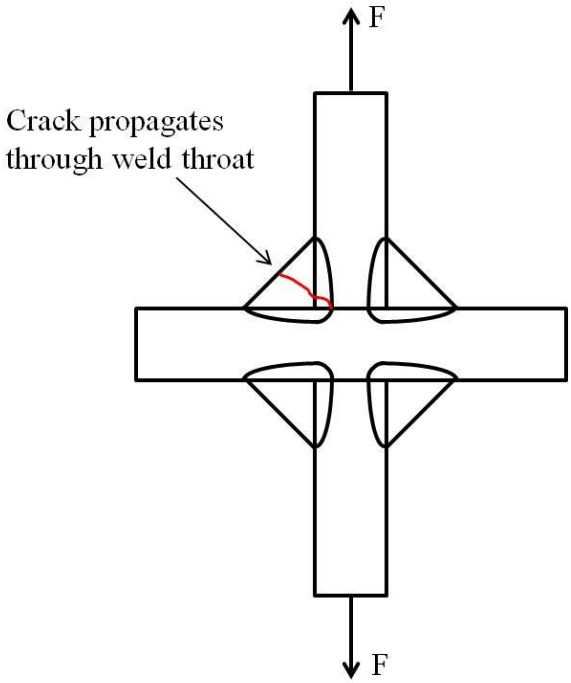

Figure 3.16: Typical Cruciform Joint with Fatigue Crack

Although useful, the cruciform joint test fails to include other factors that could affect the fatigue life of the joint, such as non-uniform stress along the length of the weld, bending/shear stresses on the weld throat, and the size of the unfused zone at the weld root [Maddox 2008]. In particular, due to the geometry of the T-stem connections, there is a stress concentration located along the weld near the stem of the WT.

Another factor is the effect of the unfused zone at the root for both the T-stem and cast steel connection. The cruciform joint can be compared to the classic fracture mechanics analysis of a uniformly loaded plate with a crack in it, with the thickness of the loaded plate being the width of the initial crack. Since the fillet welds to the tubular members will only be welded to the outside wall, the lack of connection at the weld root through the member thickness could lead to potential problems. Figure 3.17 and Figure 3.18 summarize these considerations.

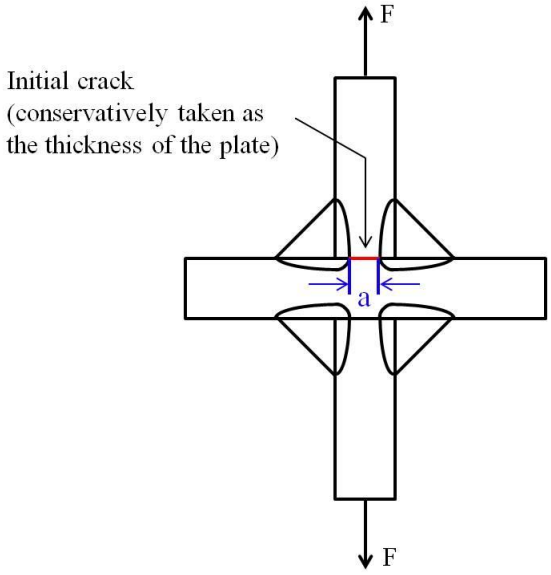

Figure 3.17: Comparison of Cruciform Joint to Uniformly Loaded Plate with Crack

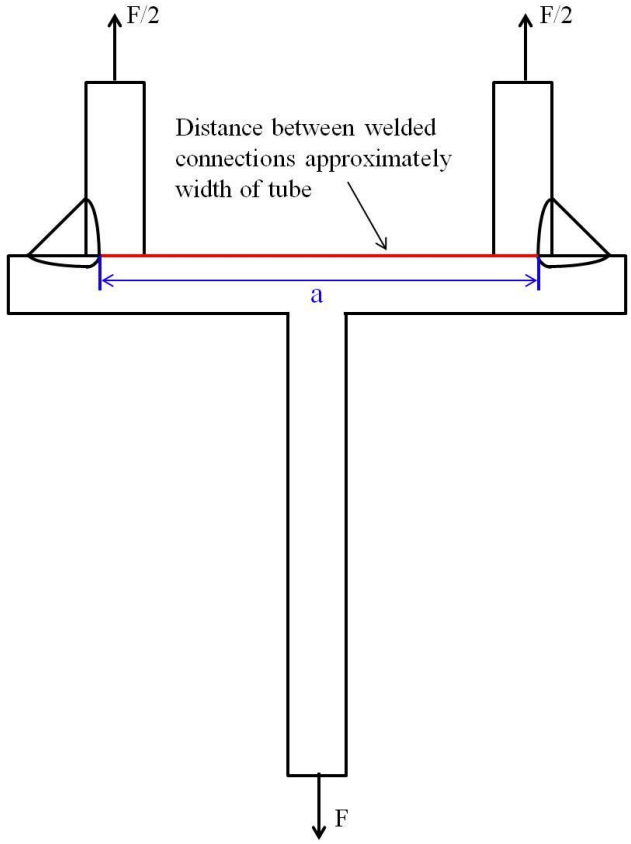

Figure 3.18: Lack of Weld Root Fusion Inherent to T-stem and Cast Steel Connections

Results from cruciform joint tests show that the fatigue strength is a function of the weld size, weld penetration, and plate thickness [Frank 1979]. Using the results of previous research in combination with fracture mechanics solutions, Frank [1979] proposes an equation to predict the stress range required to achieve a desired life in the welded joint. As the plate thickness becomes large, i.e. the distance between weld roots increases, the required stress range is reduced. The concern in a tubular connection is the distance between weld roots will not be the thickness of the tube; rather it will be the width of the tube.

Using the T-stem detail in the research, the fit-up of the connection was closely monitored. The ends of the tube were saw-cut and ground to create a flush interface between the tube and the WT flange. Previous research by Mori et al [2000] reported that gaps up to 3 mm (0.118 in) in cruciform joints did not affect the fatigue performance of the connection [Maddox 2008].

While there may be potential problems for the fatigue resistance of transversely loaded fillet welds, the ease and availability of this detail made it worthwhile to investigate. Details from the tests are given in Chapter 5.

3.6 FATIGUE BEHAVIOR OF KNIFE PLATE DETAIL

One way used to avoid eccentric connections in tubular members is to cut a slot in the tube, allowing the insertion of a gusset plate, which can then be welded in place and act as the connecting element. This procedure was selected for ease in the Wichita Falls, TX bridge retrofit (as discussed in the previous chapter). However, there is evidence that this configuration may not have good fatigue performance due to stress concentrations at the end of the slot. An example of this type of connection with the stress concentrations indicated is shown in Figure 3.19.

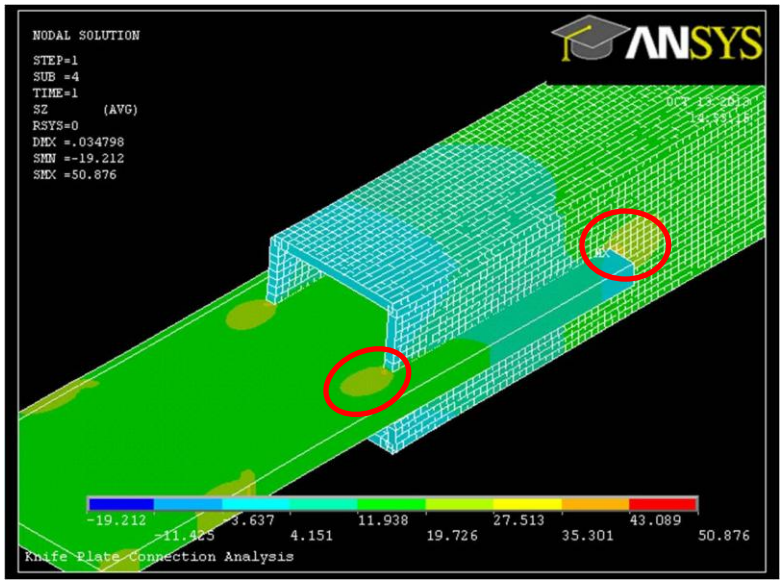

Figure 3.19: Knife Plate Connection with Stress Concentration Locations

The typical mode of tension failure in slotted end HSS connections is either circumferential tensile fracture of the HSS member or tear-out along the weld [Martinez-Saucedo and Packer 2009]. Tests have indicated that a significant shear lag exists in the detail connection type, which often makes the net section of the tube at the forward edge of the fillet connection the critical section [Martinez-Saucedo and Packer 2009, Willibald et al 2006].

Furthermore, tests presented by Liu et al [2006] showed specimens with this type of connection failed in fatigue at a relatively low number of cycles. The fatigue stress concentration cracks typically formed in the HSS walls at the forward edge of the fillet weld connecting the HSS member to the knife plate [Liu et al 2006]. The locations of these stress concentrations are given in Figure 3.19.

Due to imperfect fabrication and construction tolerances, it is difficult to obtain good fit-up between the end of the slot and the gusset plate. If the gap is large, it is often left unfilled and the knife plate is only connected by two longitudinal welds [Liu et al 2006]. In general, it is impractical to try and fill this gap with weld material due to the aforementioned tolerances [Dowswell and Barber 2005]. In some cases, the area at the

gap is drilled to reduce the stress concentration and possibly increase the fatigue life [Liu et al 2006, Soderberg 2010].

The tests performed by Liu et al [2006] involved both static and fatigue tests performed on HSS4x4x1/4 and HSS4x4x3/16 sections. The typical failure cracks originated at the forward ends of the fillet welds connecting the knife plate to the HSS member, with the cracks propagating into the HSS tube wall. The tests were performed at various stress ranges, and the effect of different knife plate thickness and slot lengths was investigated [Liu et al 2006]. The number of cycles at first crack initiation was also recorded.

The knife plate connection tends to show evidence of failure at a very early stage in the cyclic loading history. The average time of first detection was 9% of the number of cycles at ultimate failure [Liu et al 2006], showing that the connection, although cracking early, is fairly resilient and offers significant time for identification of fatigue cracks prior to failure.

The tests also showed thicker knife plates have a longer fatigue life at lower stress ranges and a shorter fatigue life at higher stress ranges when compared to a specimen that is 2/3 the thickness [Liu et al 2006]. The previous finding indicates the stress concentration at the forward edge of the fillet weld causes the specimen data to not follow a slope of 3 on the standard S-N curve.

Another important finding from the research shows the slot gap between the HSS member and knife plate does not have a significant effect on the overall fatigue life of the specimens [Liu et al 2006]. Therefore, while every effort will be made to ensure good fabrication techniques, small deviations will not affect the research results on these connections.

3.7 DNV Hot Spot Stress Analysis

3.7.1 Description

Theoretically, when a geometric discontinuity occurs in a connection, the stress at that location will increase towards infinity. However, this result is not practical as the

real material will yield in the vicinity of the stress concentration. In order to remain computationally efficient, it is useful to have a method of analysis which does not require including nonlinear material properties, but still would be able to predict the magnitude of this "hot spot stress".

The international classification society named Det Norske Veritas (DNV) has established a well-documented and frequently used method for hot spot stress analysis. The method has been summarized in their report titled "Fatigue Design of Offshore Steel Structures" [DNV 2010].

3.7.2 DNV Method

The DNV method is recommended for use with steels having a yield stress less than 960 MPa (139.2 ksi), at temperatures less than 100˚C, and subjected to high cycle fatigue. The method primarily concerns Mode I cracking (cracks opening due to transverse loads) and can be applied to cracks propagating from the discontinuity into the base metal, weld metal, or along the boundary between the two [DNV 2010].

The DNV method is an approximation of the hot spot stress using a finite element analysis. The finite element model is permitted to be comprised of shell elements or solid elements with a elements in the vicinity of the hot spot equal at a density equal to the thickness, t, of the connected parts [DNV 2010]. Once the model is meshed and the associated loads analyzed, the user is to determine the stresses away from the hot spot at distances equal to 0.5t and 1.5t. One can then linearly extrapolate these stresses to the point of interest to obtain the hot spot stress. A schematic of the process for the stress concentration at the toe of a single angle fillet weld connection is shown in Figure 3.20.

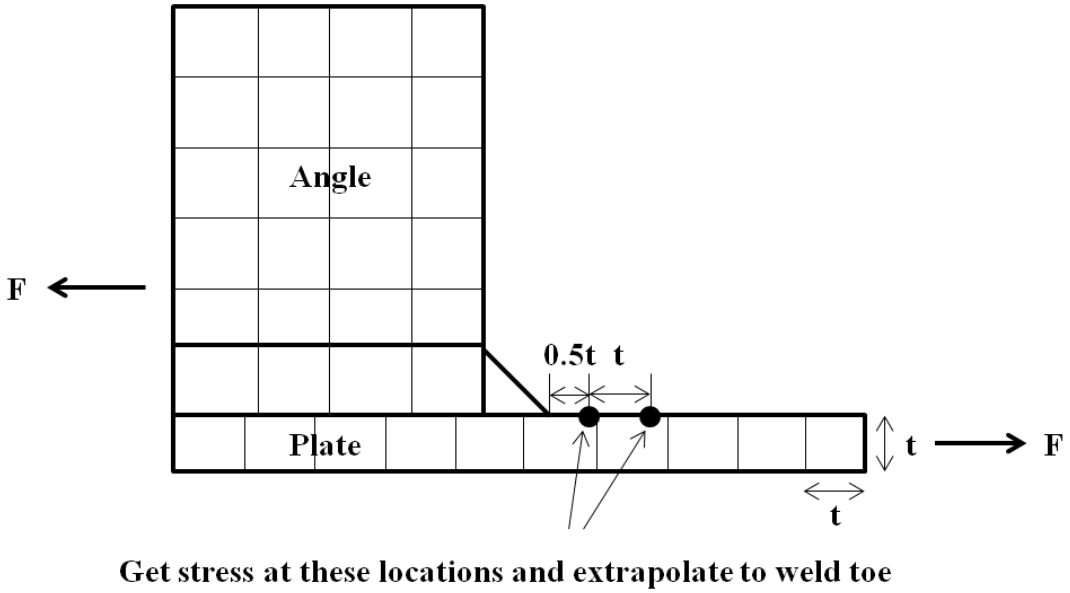

Figure 3.20: DNV Method for Hot Spot Stress Analysis

Lastly, the DNV method is sometimes used to establish a stress concentration factor (SCF). The SCF is simply the hot spot stress obtained using the method just described divided by the gross area stress applied to the connecting element. For instance, if a 10 ksi stress was applied to the plate in Figure 3.20, and the hot spot stress was extrapolated to be 25 ksi, than the SCF would be 2.5.

CHAPTER 4
Background: Steel Castings

4.1 INTRODUCTION

One of the objectives of this research project was to investigate the feasibility of using steel castings as connections for tubular members in cross frames. This chapter provides background information on steel castings and discusses the procedure for developing prototype castings for possible use in bridge cross frames.

4.2 STEEL CASTINGS IN LITERATURE

Historically, steel castings were once relatively common in structural engineering applications when complex connections were required. However, with modern welding technology, fabricated connections using wrought steel materials became more economical, significantly reducing the use of castings in structural engineering [de Oliveira 2006]. A lack of knowledge in the behavior of steel castings has caused most engineers today to be hesitant of using castings in design. The following case studies document some current uses of steel castings and the advantages cast steel can offer.

4.2.1 Greenbank Telescope

One modern application of steel castings is the Green Bank Radio Telescope shown in Figure 4.1. Due to the complex geometry and large number of connections, steel castings provided an economical solution to simplify construction of the telescope.

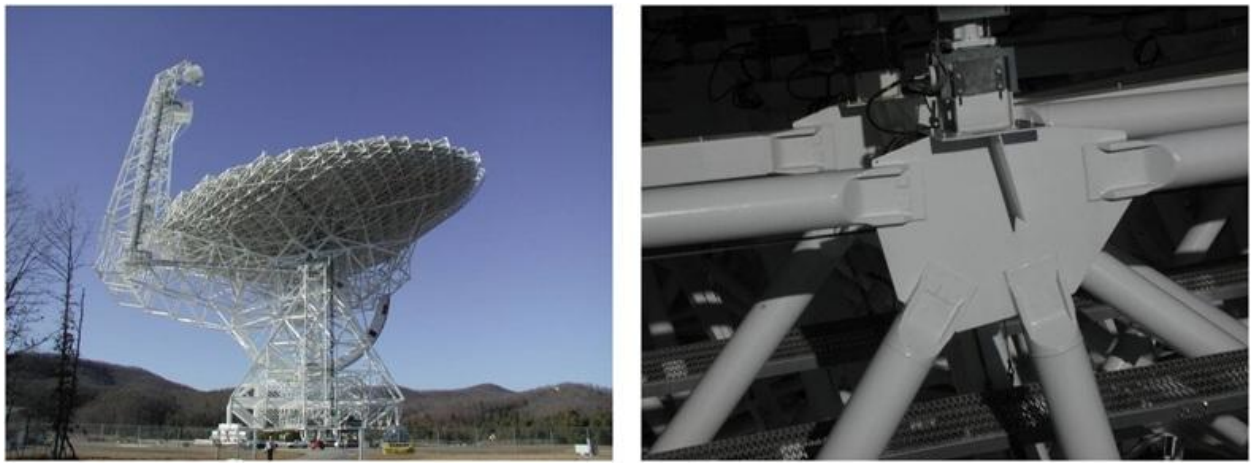

Figure 4.1: (a) Green Bank Radio Telescope and (b) Steel Casting

4.2.2 Connections for Seismic Applications

Steel cast connections have seen recent use for applications in seismic-resistant steel buildings. Castings have been developed for use in connections in braced and moment frame structures. Two examples are provided in this section.

4.2.2.1 Kaiser Bolted Bracket

The Kaiser bolted bracket, developed by Steel Cast Connections, Lehigh University, and IFC Kaiser Engineers, is a high-strength, haunched steel bracket designed to connect the flanges of a beam to a column [Adan and Gibb 2008]. The brackets, which are bolted to the column and either bolted or welded to the beam, were engineered so that yielding and plastic hinge formation occurs primarily in the beams at the tip of the bracket. The brackets come in various sizes and are proportioned to handle the probable moment required to fully yield the beam cross-section [Adan and Gibb 2008].

4.2.2.2 Cast ConneX

Similarly, Cast ConneX has developed high-strength cast steel connections for use with concentrically braced frames comprised of HSS members (Figure 4.2) [de Oliveira et al 2008]. These connectors are designed to handle the expected forces developed in the HSS brace during a seismic event. The connections are designed to

permit the brace member to yield or buckle during an earthquake without failure of the connection. This behavior is important because yielding and buckling are the primary methods concentrically braced frames dissipate energy from the earthquake [de Oliveira et al 2008].

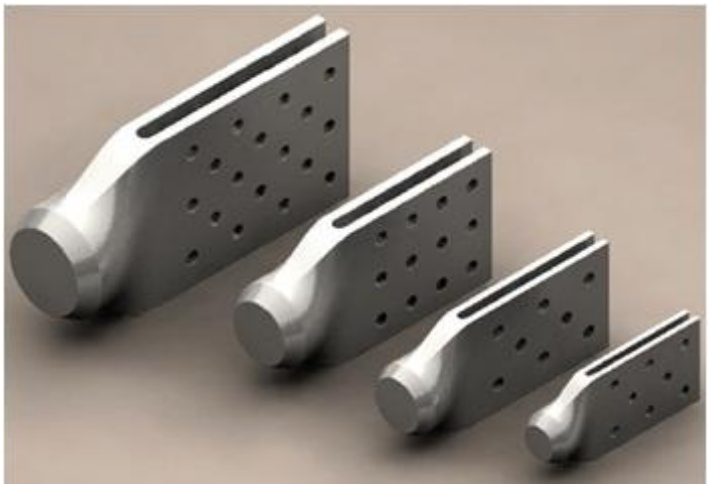

Figure 4.2: Cast ConneX Cast Steel Connections [de Oliveira and Stine 2008]

4.2.3 Crane Connections

Cast connections have been used in the assembly of large tower cranes. By using a pin-type end connector welded to the ends of steel tubular members, construction workers can quickly piece together the support structure for a large tower crane. In addition, the simplified connection helps avoid confusion on the job site [Soderberg 2010]. A sample of the connection is shown in Figure 4.3.

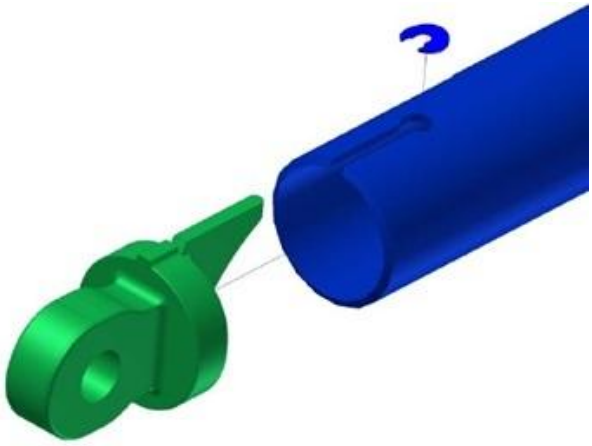

Figure 4.3: Cast Steel Connection used in Tower Crane Construction [Soderberg 2010]

4.3 ADVANTAGES OF STEEL CASTINGS

Since cast steel connections are formed from liquid metal, complex geometries can be fabricated. Moreover, steel castings can be designed to specific applications, potentially allowing the inclusion of items like holes for erection bolts or increased thicknesses to facilitate welding. This ability has the potential to greatly reduce fabrication and construction time.

The economy of steel castings will also improve as the necessary quantity increases. Typical current practice involves creating a prototype of the connection from a plastic polymer or metal. The prototype part is then placed in a mold box, where chemically treated sand is inserted and compacted. Once the sand is hardened, the pattern is removed to form a negative space, where ultimately the molten steel will be poured to create the final product [Steel Founders' Society of America 2009]. It is evident from the creation process that once an initial prototype is engineered and created that the part can be easily mass produced.

4.3.1 Fatigue Behavior

Due to the geometric flexibility of casting liquid steel, castings can be tapered to create smooth transitions, minimizing stress concentrations and improving fatigue

performance. Experimental tests conducted by Haldimann-Sturm and Nussbaumer [2008] showed the fatigue behavior of tubular members with cast nodes were governed by the fracture resistance of the butt welds used to connect the two components.

4.3.2 Efficient Use of Material

Because steel castings are designed for specific applications, the required steel material can be optimized, resulting in the most efficient use of the material. Accordingly, material can be added to lower the stress in the part, which can also aid in improving fatigue behavior.

4.3.3 Seals Tube

One of the advantages cast steel connections have when used at the end of a tubular member is sealing of the tube. If the tube is open to the atmosphere, rain, dirt, debris, animals, and insects are capable of getting inside the tube, potentially decreasing the corrosion resistance of the metal. Moreover, because the corrosion would work from the inside of the tube, a visual inspection of the member would not reveal any structural deficiency. Thus, it is important to develop a cast connection which will isolate the inside of the tube from the elements.

4.3.4 Standardization

Lastly, the use of steel castings is likely economically feasible only when large amounts of castings are required. As a case study, the direct connector linking Texas SH 71 East with Texas SH 130 North was examined. The connector consists of 10 steel spans of varying length and 4 I-girders across. The following calculations summarize the quantity of steel castings that would be required for this project.

107 cross frame lines
x 3 cross frames
321 cross frames

321 cross frames
x 6 connections
1926 Cast Connections

With such a large number of cross frame connections, steel castings could greatly reduce the time necessary to construct these braces. Furthermore, the casting can be designed to handle more than one tubular cross-section, allowing its use in potentially all cross frames in steel bridges.

4.4 STEEL CASTING TYPES

Steel castings can offer several advantages over conventional fabricated steel connections. The primary advantage, since cast steel is poured into a mold, is that it can easily accommodate complex geometries. The final shape of the casting can be engineered for its particular application, therefore allowing more efficient use of the steel material and reducing stress concentrations, which can lead to better fatigue behavior. In addition, the mechanical properties of cast steel are isotropic, which is beneficial in cases where three-dimensional states of stress could present a problem for design [de Oliveira 2006]. Finally, in situations where the casting design can be standardized, such as for the proposed cross frame connection, the casting can potentially become a cost competitive alternative to the normal fabricated connection.

4.4.1 Investment Casting

While there are a variety of methods available for casting steel, the two main types identified for possible use with creating a connection for tubular cross frame braces were investment casting and sand casting.

Investment casting, also referred to as the "lost-wax" method (Figure 4.4), begins with a pattern matching the final shape of the cast part that is created from an expendable material such as wax or plastic. The patterns are invested in a ceramic slurry, which hardens to create a shell encasing the parts. Next, the wax or plastic is melted to leave

the ceramic shell hollow. The cast steel is then poured into the shell to solidify into the final product.

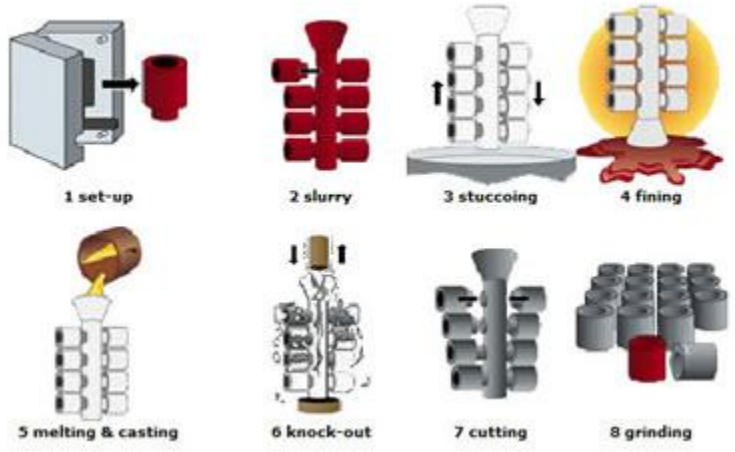

Figure 4.4: Investment Casting Process [Ningbo Yinzhou KST 2010]

One advantage to using investment castings is the ceramic shell better controls the geometry of the final part, resulting in lower geometric tolerances and better quality surface finish as compared to sand castings. However, investment castings tend to be more expensive per unit weight and are limited to overall size. Investment castings are often cast along a "tree" with the final parts branching off from the main portion. The arrangement of the parts limits the weight of each casting. While de Oliveira [2006] reports investment castings can weigh up to 154 lb (70 kg), the facilities investigated in Texas had weight limits near or below the approximate weight of the prototype connection, about 45 lbs. Furthermore, the process is more time-consuming than sand casting, which translates into increased cost. Therefore, sand casting was the process selected for the cast connection for TxDOT Project 0-6564 described within this dissertation.

4.4.2 Sand Casting

Sand casting receives its name from the green sand often used to create the molds. Sand casting begins with a pattern, typically constructed from wood, which is used to form a negative shape of the finished casting in the sand mold. The flexibility in creating

the sand molds allows the castings to weigh from only a few pounds up to several tons and to be virtually any shape. The following section further explores the steel casting process and provides detailed information on the manufacture of the cast steel connection proposed for use with tubular cross frames.

4.5 STEEL CASTING PROCESS: PATTERN CONSTRUCTION

The steel casting process begins with identifying a foundry capable of producing the desired part, in this case, the cast steel connection for use with tubular cross frame members. While many foundries specialize in bronze and aluminum castings, fewer foundries specialize in steel castings, particularly structural grades of steel. The project team identified Quality Electric Steel Castings, a foundry in Houston, TX, as suitable for the needs of the project. Their previous work on suspension bridge hanger attachments and drawbridge bearings showed they had experience with the transportation industry and were capable of producing steel grades for structural applications.

In order to better understand the creation of steel castings, multiple site visits to Quality Electric Steel Castings were conducted. During the visits, foundry engineers and sales representatives met with the project team to discuss the feasibility of using cast steel connections for cross frames and to provide more detailed information on the steel casting process. The following outline of the steel casting process represents information that was gained through tours of the foundry, including the pour of the cast connections.

4.5.1 Working with the Foundry

The first stage of creating a steel casting is to develop a good relationship with the foundry. As with any project, good communication will decrease the time required to finish the job. The engineers at the foundry know the limitations of the equipment and can provide useful knowledge towards developing an optimized design for the casting.

In addition, it is important to coordinate the design of the casting. The foundry will need to design the gating system for each particular casting. The gating system simply refers to the delivery path of the molten metal to the cavity in the mold eventually

becoming the completed part. The foundry has software which models the solidification of the casting to assist in the gating system layout. Using the software, the foundry can analyze the casting geometry and provide feedback on how to streamline the casting process to make the part more easily created.

4.5.2 Constructing the Pattern

The next stage of creating a casting is to make the pattern representing the finished part. The pattern is a three-dimensional model which contains all the features desired in the completed part. In terms of geometry, the pattern is usually slightly over-sized to offset the effects of shrinkage, which will cause the part to reduce in size as the liquid metal solidifies. Also, the patterns typically represent only half of the completed part. The halves will be used individually to create sand molds, so that when the two molds are matched together, the vacant space remaining will become the completed part. More information on the structural design and analysis of the steel casting can be found in Chapter 5.

4.5.2.1 Plastic Prototypes

Rapid prototyping is one method that can be employed to create patterns. There are various kinds of prototyping machines, but the majority will create three-dimensional plastic parts from a solid model computer file. Aside from pattern production, the plastic models can be a useful tool when discussing ideas with the foundry engineers, as it clearly indicates the design and function of the final product.

Prototypes of the cross frame connection for this research were created in conjunction with the Mechanical Engineering Department at the University of Texas at Austin. First, the solid model of the connection was created using the computer drawing software SolidWorks 2010. From the program, the solid model was exported as an .stl file type, which takes the original solid model and creates a three-dimensional representation using small triangular elements. The file was uploaded into a software associated with the prototyping machine that divided the cast connection volume into

thousands of 0.003 inch cross-sectional layers. These layers would be created sequentially by the prototyping machine to create a solid volume. The machine used was a 3D-Systems Sinterstation using selective laser sintering (SLS) technology and is shown in Figure 4.5.

Figure 4.5: Rapid Prototyping Machine

Once the computer files were input into the prototyping machine, the machine built-up the part in layers. The roller shown in Figure 4.6(a) delivers a 0.003 in thick layer of plastic powder to the center bay. Next, the laser of Figure 4.6(b) lowers, and will move around the powder layer, melting the specific portions to become the hardened prototype. The laser retracts, the center bay lowers, and another layer of powder is placed. This process repeats until the prototype is complete.

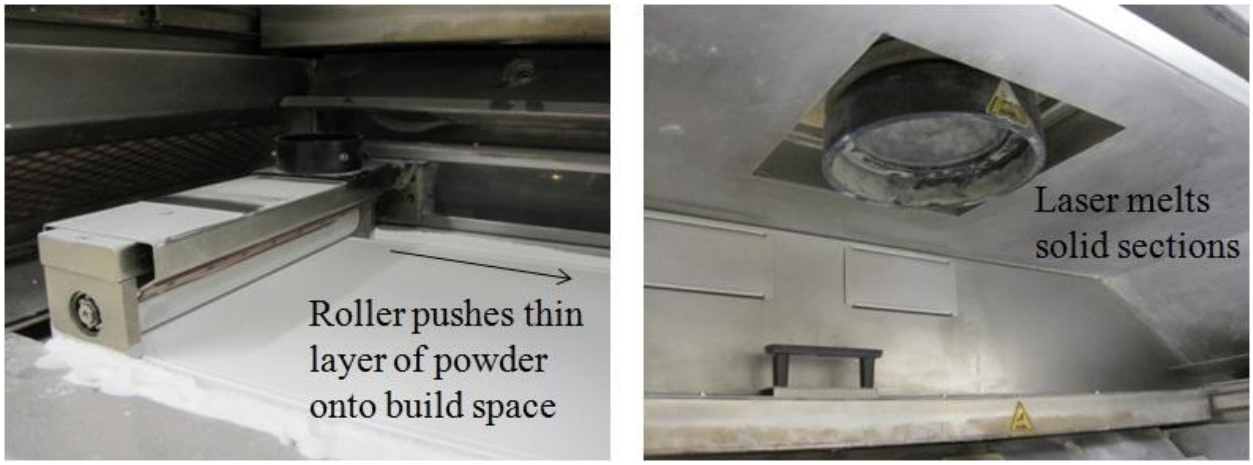

Figure 4.6: (a) Roller and (b) Laser

Upon completion, the part remains in the machine to allow it to cool to a reasonable handling temperature. When it is ready, the plastic powder block is removed from the machine and the completed prototypes can be cleaned using brushes and compressed air as seen in Figure 4.7. An example of a finished cross frame prototype is shown in Figure 4.8.

Figure 4.7: (a) Removal of Powder Block and (b) Cleaning of Prototype

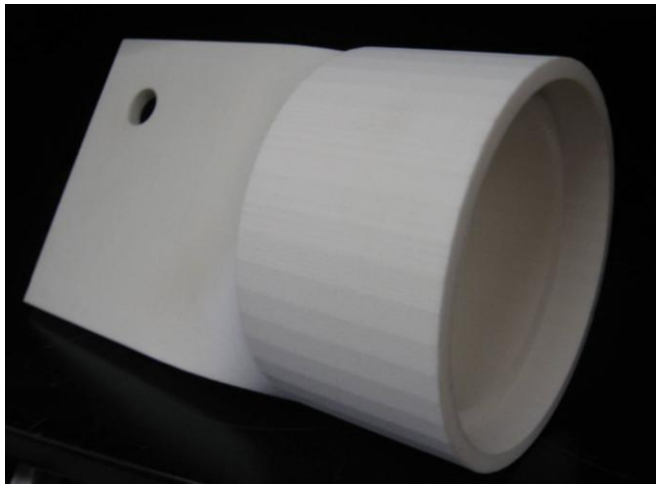

Figure 4.8: Prototype of Cross Frame Connection

While the plastic prototypes are easy to construct, the foundry did not recommend them for use in the sand casting process. Primarily, the plastic prototypes do not make a very good impression in the sand molds, which results in a relatively poor surface condition. Additionally, the means by which the sand is packed into the pattern box to create the mold would most likely damage the pattern, making it unusable for future castings.

4.5.2.2 Wooden Patterns

The most common patterns used are created from hard woods, such as pine, oak, and mahogany. Pine is the least expensive option of the woods, however, as the pattern is continually used, it is most likely to lose its original shape. On the other hand, mahogany will not degrade as quickly as pine, but it is more costly to create. At Quality Electric Steel Castings, the patterns are created by a separate vendor who works in conjunction with the foundry. Completed patterns are usually coated with a special primer to protect the surface quality. For the preliminary cast steel connection design, a wooden pattern constructed from pine was selected as most economic since the connection will be tested, and the design perhaps changed, prior to final recommendations. The wooden pattern is mounted in a pattern box for the sand mold making process, as shown in Figure 4.9.

Figure 4.9: Wooden Pattern for Use in Sand Casting

4.5.2.3 Polyurethane Patterns

The most durable type of pattern is made from polyurethane. While it is expensive to initially produce, foundry engineers indicated these patterns show almost no signs of degradation and ultimately produce the best quality castings. These patterns are most beneficial for high volume castings as the pattern would not need to be replaced frequently, if at all. An example of a polyurethane core box is shown in Figure 4.10.

Figure 4.10: Polyurethane Core Box

4.6 STEEL CASTING PROCESS: SAND MOLD FORMATION

The next major stage in the steel casting process is to create the sand mold which will be used to form the steel casting. The sand mold contains the negative image of the pattern, so that when the molten steel is poured, it will fill the cavity and harden into the desired part geometry. The procedure begins with transporting the pattern box to the sand mold assembly line, where it will be filled with sand slurry.

4.6.1 Sand Slurry Composition

The slurry used at Quality Electric Steel Castings is a combination of sand from a source in Arkansas and iron oxide, which is mixed with a binding agent, causing the sand to harden to a brick-like consistency. The foundry takes great care in selecting the sand for use in the molds as the grain size plays an important role in the surface condition of the casting.

The raw sand must be passed through a series of sieves to separate the grains according to diameter. Very fine grains are undesirable because collectively, they have a very large surface area. As the sand is mixed with the binding agent, sections with very fine grains will tend to be moister, and the binding agent may not completely burn away when preparing the casting surface. On the other hand, grains with larger diameters are likely to create an irregular geometrical profile on the surface of the sand mold, thus directly affecting the surface quality of the casting. Additionally, sections with large grains will be more porous, potentially allowing the molten liquid steel to seep into the sand. The foundry did not specifically report which grain sizes are used, as that information is considered proprietary. For good compaction and strength, it is recommended the washed and dried sand have at least 85% of the sand on four adjacent screens and an American Foundry Society grain fineness number of approximately 55 [Totten et al. 2004].

Iron oxide is mixed into the sand to provide strength. The sand molds are lifted, rotated, and transported many times prior to casting. Additionally, the sand needs to

support the weight of the casting during the pour. The iron oxide helps to distribute these forces without cracking the hardened sand.

Once the iron oxide and green sand are mixed, the binding agent, a phenolic urethane resin, is added. Phenolic urethane resins are advantageous to use because they have a low viscosity, allowing them to more efficiently coat the sand [Totten et al. 2004]. Typically, the phenolic urethane resins are a three part system: Part I is a resin comprised of approximately 45% solvents and 55% solids by weight; Part II is a polymeric isocyanate; and Part III is a catalyst [Totten et al. 2004]. Phenolic urethane resins are common in "no-bake" systems, meaning the sand molds will cure without additional heat.

4.6.2 Forming the Raw Sand Mold

After the sand slurry is mixed, it is immediately poured into the pattern boxes to make the sand molds. Various methods of consolidating the sand are employed, including the use of vibratory compactors, as well as manual force. Figure 4.11 (a) shows an example of a pattern box which is then filled with sand using the depicted machine. Figure 4.11 (b) shows the pattern box on vibratory rollers, while the worker finishes the top.

Figure 4.11: (a) Pouring Sand Slurry into Pattern Box and (b) Compacting Sand Mold

Once the sand has cured, about 3-5 minutes for the prototype cross frame connection, the pattern box is flipped onto a piece of plywood to remove the sand mold, revealing the hollow cavity which will eventually become the finished steel casting. The sand molds consist of two halves: the cope and the drag. The cope is the top portion of the completed mold, which will need to be joined to the drag prior to casting. The drag is the bottom portion of the mold, which will contain any sand cores necessary for the given cast part.

The sand molds are brushed to remove any loose sand, and air-blown to remove all loose grains. A file is used to create extra vents along the parting line to allow hot gases to escape during casting. Figure 4.12 shows the pattern removal and sand mold preparation for the cross frame connection.

Figure 4.12: (a) Removing Pattern from Sand Mold and (b) Adding Vents along Parting Line

4.6.3 Coating the Sand Mold

The next stage is to coat the sand mold to seal the surface, preventing the liquid metal from seeping into the sand. Smaller molds are suspended over a basin while workers use a low-pressured hose to flow coat the mold. Flow coatings consist of two main parts, a refractory material and a carrier. In the cast steel industry, the refractory

material is usually zircon (zirconium silicate) and the carrier is either water or alcohol based [Brannon et al. 2001]. Flow coating allows both a surface and sub-surface coating to form. The surface coating helps to improve the surface finish of the casting, while the sub-surface coating fills in the voids in the sand to prevent seepage of the molten metal [Brannon et al. 2001]. Figure 4.13 (a) shows the application of the flow coat to the sand mold.

Once coated, the sand molds continue down the assembly line to dry. If the foundry uses an alcohol-based carrier in the flow coat (such as isopropyl alcohol), the mold can be burned to eliminate the alcohol and to harden the coating. Figure 4.13 (b) shows the burning of the sand mold.

Figure 4.13: (a) Flow Coating the Sand Mold and (b) Burning the Sand Mold

4.6.4 Creating the Sand Cores

In addition to the sand molds, cores are required for castings containing hollow sections. The cores are made from sand in a similar manner to the sand molds, and are set in the completed sand mold. Large cores often contain steel rebar for reinforcement as the sand cores must be strong enough to resist the loading effect of self-weight when it is lifted and moved into place.

Smaller cores, like the ones necessary for the proposed cast steel connection, do not require reinforcement and are simply made by filling the core box with the sand slurry, and allowing the core to cure. Once completed, the cores are positioned in the main sand mold, attaching to nonessential portions of the mold. Examples of cores are shown in Figure 4.14.

Figure 4.14: (a) Cores used for Cross Frame Connection and (b) Large Sand Core

4.6.5 Completing the Sand Mold

The final stage in the preparation of the sand mold is to join the two halves of the mold. First, any cores required for the mold are placed in the drag, and glued into place, as illustrated in Figure 4.15 (a). Note the taper on the core which helps to lock it into place in the sand mold, preventing it from shifting during the pour.

Glue is also spread along the top of the drag to bond to the cope, which is flipped over and lowered on top to complete the mold, as shown in Figure 4.15 (b). Finally, clamps are inserted into the sand on either side of the parting line and tightened to create a good seal. The sand molds are then moved to the pouring line.

Figure 4.15: (a) Setting the Cores and (b) Closing the Sand Mold

For very large castings, the sand molds are coated by hand using paint brushes and rollers, rather than hosed down with the flow coat, primarily because they cannot be suspended to allow the flow coat to drain properly. Similarly, these molds are burned to remove the carrier agent, cores are set into place, and the cope and drag are united. Some large sand molds are surrounded by formwork and bound with metal straps to resist the hydrostatic force of the molten steel.

4.7 STEEL CASTING PROCESS: POURING THE STEEL

The third major stage in the steel casting process is the actual pouring of the molten steel into the sand molds to create the desired part. Due to the large amount of electricity required for this operation, Quality Electric Steel Castings pours steel overnight when the electricity demand in the surrounding area is lower.

4.7.1 Melting the Steel

Depending upon the size of the job, steel is either melted in a large electric arc furnace or a smaller induction furnace according to the desired chemistry of the completed product. The foundry adds scrap steel of known chemical content to the furnace in order to produce a steel close to the material grade specified by the customer.

The electric arc furnace operates by running a large current through three carbon electrodes. The electrodes, which can move up and down vertically, are positioned to

allow a small gap between the electrode tip and the steel, very similar to the procedure used in welding. When the current is turned on, an electric arc will connect the electrode tip and the steel. The arc is extremely hot (over 5400°F (3000°C)) and will quickly melt the steel [Lye 1971]. The electrodes are shifted up and down to melt all the steel in the furnace. As the arcs continuously jump around inside, the steel is also mixed, ideally leading to a homogenous mixture.

On the contrary, induction furnaces do not use electric arcs to melt the steel. Instead, the scrap steel is set into a crucible, which has an induction coil surrounding the perimeter. Alternating currents are passed through the coil creating alternate magnetic fields in the crucible. The result is a large amount of heat being developed in the scrap steel, enough to melt it. The alternating magnetic fields also help to mix the steel into a uniform composition [Lye 1971].

An example of an electric arc furnace and an induction furnace is shown in Figure 4.16. For the first round of castings, the small induction furnace was used since its capacity better met the needs of the project.

Figure 4.16: (a) Electric Arc Furnace and (b) Small Induction Furnace

4.7.2 Checking the Chemistry of the Steel

As the steel melts, workers monitor its chemical composition until the specified alloy of steel is achieved. Samples are taken with a small ladle, then poured into small cups made from sand, similar to the sand molds. These samples are typically submerged in water to cool and are taken to a spectrometer to perform a chemical analysis. Figure 4.17 shows a worker taking a sample from the molten steel, and what the sample looks like after it cools and is ready for analysis. More information regarding the chemical analysis is provided later in this chapter in Section 4.10.1.

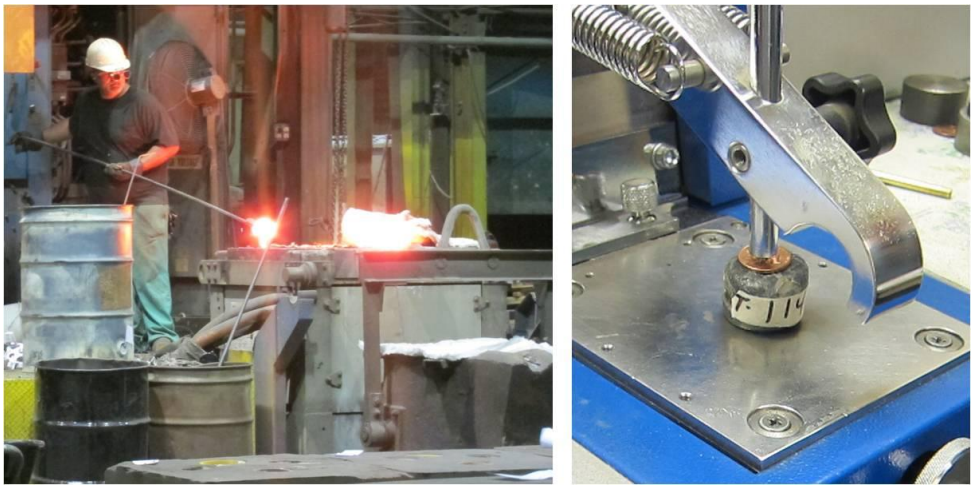

Figure 4.17: (a) Sample Taken from Furnace and (b) Cooled Sample for Chemical Analysis

4.7.3 Checking the Temperature of the Steel

The temperature of the steel plays an important role in the quality of the casting as well as in the design of the gating system. The gating system simply refers to the path the steel will take from when it is poured into the sand mold until it fills in the part cavity (more information on the gating system is given in Section 4.7.4). Using software designed for temperature and flow analysis, the foundry will design the gating system to deliver steel into the cavity at a specific velocity as well as temperature. If the flow rate is too fast, it is possible that turbulent flow will result, damaging the surface of the sand

mold and decreasing the smoothness of the finished part. Turbulence can also cause sand inclusions in the cast metal. If the steel is not at the proper temperature, it will not flow properly, possibly cooling before the entire mold is filled as shown in Figure 4.18.

Figure 4.18: Example of Steel Casting with Incomplete Run-Out

Workers will check the temperature of the steel using a large thermometer specially designed and calibrated for the high temperature of the molten steel. Typically, the steel will be between 2700°F and 3000°F when it is considered ready for pouring. The steel is poured from the furnace into large ladles, which are lined with a special refractory material that protects them from the molten steel and will allow various gases to escape. Figure 4.19 (a) shows a typical ladle used at Quality Electric Steel Casting. Figure 4.19 (b) shows the molten steel from the small induction furnace being poured into a ladle.

Figure 4.19: (a) Ladle and (b) Pouring Steel into Ladle

4.7.4 Pouring the Steel

The ladle containing the molten steel is transported by crane to the pouring line. Some ladles have an opening in the bottom through which the steel will flow, while other ladles are tilted, allowing the steel to flow over the top rim. Either way, the steel enters the gating system of the sand mold, which is set up to control the flow of the steel to the casting. The gating system is designed by the foundry for each particular casting and consists of the pouring cone, pour box, runners (sluices), gates, and risers. Using temperature and flow analysis software, the foundry determines the optimum sizes to use for the gating system to feed the casting. A schematic of the gating system is shown in Figure 4.20.

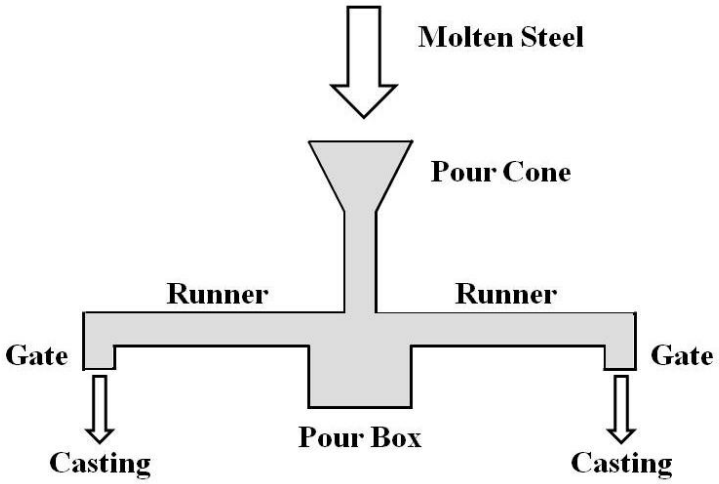

Figure 4.20: Gating System

First, the steel enters the pour cone, which helps to funnel the liquid steel into a smaller channel. The pour box helps to control the flow by reducing turbulence, and gradually fills up until the steel heads down the runners to the gates, eventually entering the casting.

Good casting designs utilize directional solidification which causes the part to cool incrementally from one side to another. Thicker sections of the casting can sometimes cause problems because they will be the last to become solid. Risers can be placed above these sections to provide a constant hydrostatic head of molten steel to the region of the casting that will cool last. The placement of the risers prevents large voids from forming in the casting due to shrinkage. Since the risers are designed to be the last section to harden, the shrinkage void will therefore lie in this region and not in the casting, and can subsequently be removed. For the first cross frame prototypes, the foundry used one riser placed as shown in Figure 4.21.

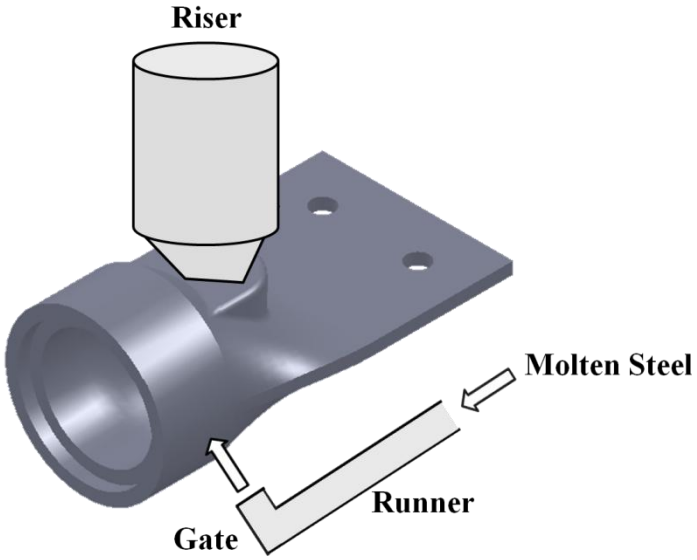

Figure 4.21: Approximate Position of Riser for Cast Connection

Figure 4.22 shows the molten steel being poured into the sand molds for the cross frame connection. Note the fire present on the surface of the previously poured molds. As the casting cools, hot gases that were diffused in the molten steel will bubble to the surface and escape through vents placed in the cope portion of the mold, as well as along the parting line. It is important for these gases to escape and not become trapped in the final product causing a defect. These gases also escape from the surface of the risers and the pour cone.

Figure 4.22: Pouring the Steel into the Sand Molds

4.7.5 Casting Steel Material Test Blocks

During the casting of the parts, the foundry will cast material test blocks for the current heat of steel. These blocks are poured at the approximate halfway point in order to provide a representative sample of the steel. The blocks are cast into standard size molds and will be used to verify the chemistry of the final product and to produce mechanical test specimens, such as tension test coupons and Charpy V-notch specimens. Figure 4.23 shows the casting of the material test blocks.

Figure 4.23: Casting Steel Material Test Blocks

4.8 STEEL CASTING PROCESS: FINISHING THE PART

4.8.1 Casting Shake-Out

Finally, the casting, along with the gating system, is removed from the sand mold once it has cooled to a handling temperature. The molds are transported to a shake table where the hardened sand is separated from the steel casting. The sand is reclaimed for future molds, and the part is removed for further finishing.

4.8.2 Shot Blast

The next step is to get the surface of the casting to a rough finish by using a shot blaster to polish the surface. Basically, steel pellets are shot at the casting to remove excess sand and clean the surface. Figure 4.24 shows the castings following blasting.

Figure 4.24: Cross Frame Connections Following Shot-Blast

4.8.3 Torching and Air Carbon Arc Gouging

The cast steel part is cut from the gating system using a high-powered oxy-acetylene torch. Due to the intensity of the torch, these cuts tend to be rougher and are not performed close to the casting profile. Subsequently, air carbon arc gouging is employed to remove the metal on the surface of the casting, creating a smooth geometrical profile.

4.8.4 Weld Repair and Grinding

Next, the casting is inspected for any surface flaws. If allowed by the customer, weld metal will be used to fill in any voids or cracks on the surface. The weld repairs, along with any remaining irregularities from cutting away the gating system, are ground flush to the part using regular metal disc grinders.

4.8.5 Heat Treatment

Lastly, the castings are subjected to a heat treatment procedure. This helps to relieve any internal stresses that were created during the pour as well as surface stresses caused by weld repairing. The heat treatment results in a steel part with isotropic material properties. Additionally, the typical heat treatment involves a tempering phase, which helps to increase the ductility and toughness of the casting. It is anticipated the

practice of weld repairing will be acceptable for the cross frame connections, so long as the heat treatment is performed to remove residual stresses.

4.9 CASTING DEFECTS

Controlling the steel casting process helps to ensure a good quality casting, free from any potential defects in the material. In order to prevent defects from compromising the behavior of the casting, a better understanding of what types of defects are possible is necessary. The following sections describe the more common defects for steel castings.

4.9.1 Shrinkage

As previously discussed, shrinkage serves a major role in the design of the casting and the layout of the gating system. There are two types of shrinkage that can occur: microshrinkage and macroshrinkage. Microshrinkage, sometimes referred to as shrinkage porosity, affects the material on the molecular level. As the steel begins to solidify, dendrites, molecules of steel creating a branched like structure, may form. Dendrite growth is related to the degree of undercooling that may occur in the casting as part of the cooling process [de Oliveira 2006]. While dendritic growth is not desirable, most castings exhibit some degree of this defect. The major problem occurs when adjacent dendrites are allowed to grow large, potentially becoming entangled and preventing liquid metal from accessing the spaces in between. As the liquid cools, thermal contraction in these spaces occurs, leaving small voids in the material. Due to the scale of this defect, it is only detectable and problematic when it affects large sections of the casting [de Oliveira 2006].

Macroshrinkage is a large-scale defect that is present in all castings that are created. The term is generally applied to the thermal contraction of the steel material as it cools from the liquid to solid phase. As the liquid begins to solidify, it begins to contract, exerting an inward pressure to those sections of the casting remaining in the liquid phase, typically regions with larger thicknesses. The pressure will expel the molten steel unless

it is balanced by another pressure, typically the hydrostatic head provided by the risers. If the risers are not present nor properly designed, large voids could form in the casting [de Oliveira 2006]. In addition, macroshrinkage also incorporates solid shrinkage, which is the volumetric shrinkage taking place once the entire casting has solidified and begins to cool. This type of macroshrinkage is accounted for by creating a pattern that is slightly larger than the desired size of the casting. Typically low carbon steels exhibit about a 2.5 to 3 percent decrease in volume [de Oliveira 2006].

4.9.2 Gas Porosity

As the temperature of the steel is increased beyond its melting point, the diffusivity of gases into the metal is also increased. However, as the casting cools, the diffusivity decreases again, causing excess gases to form bubbles in the steel, ultimately leading to the formation of voids. These voids occur on the microscopic scale of the material, and similar to microshrinkage, gas porosity is only detectable when large sections of the casting exhibit this defect [de Oliveira 2006].

4.9.3 Surface Flaws

The most obvious of casting defects are those visible on the finished surface of the casting. Surface flaws can be voids, pits, or cracks along the casting profile and can potentially significantly reduce the fatigue life of the casting by providing points for crack initiation and propagation [de Oliveira 2006]. Surface flaws are usually a result of poor mold quality, poor gating system design, or inadequate cooling conditions. Often, surface voids and cracks are repaired by welding the completed casting using an arc welding process. The weld is subsequently ground flush to the casting profile, and the entire casting is heat treated to relieve any residual stresses induced. While this can be done at the discretion of the customer, it has been shown that weld repairs can improve the high-cycle fatigue life of the casting [de Oliveira 2006].

4.9.4 Inclusions

Inclusions refer to any sort of foreign particles that may accidentally be introduced to the steel casting. Examples of inclusions consist of dirt and dust particles, refractory, slag, or sand that may be picked up by the liquid during the casting process. The major concern of having inclusions is they may create unwanted stress concentrations in the steel matrix and can therefore become an initiation site for cracking [de Oliveira 2006].

4.9.5 Segregation

The final casting defect covered in this section is segregation, which is characterized by an unequal distribution of alloying metals in the steel material. This defect can occur on the macro and micro scales, and can lead to a variation in mechanical properties at different locations throughout the casting. Adjusting the cooling rate of the casting, as well as subjecting it to a heat treatment can help mitigate the effects of segregation [de Oliveira 2006].

4.10 QUALITY ASSURANCE

In order to make sure a casting does not contain any significant defects, there are a variety of methods, both invasive and non-destructive, to assure a quality product. The following methods can be prescribed as necessary based on the final application of steel casting.

4.10.1 Chemical Analysis

Throughout the entire casting process, the foundry monitors the chemistry of the molten steel to make sure it meets the requested specification. As more scrap is added to the molten steel mix, samples of the liquid are removed and analyzed. The machine used to determine the chemical breakdown is a spectrometer, shown in Figure 4.25.

Figure 4.25: (a) Spectrometer with (b) Sample for Analysis

Basically, the steel surface is melted in a small region which emits a specific color of light. The light is passed through a series of filters to determine the specific wavelengths radiated. Based upon the wavelength, each element present in the steel can be identified, and depending upon the strength of the specific wavelength, a relative percentage can be obtained. The machine outputs the results in a tabular format shown in Figure 4.26.

No	C	Mn	Si	P	S	Cr	Ni
	%	%	%	%	%	%	%
1	0.315	0.74	0.66	0.023	0.018	0.52	0.496
2	0.309	0.76	0.65	0.024	0.020	0.54	0.51

No	Mo	V	Al	Ti	Cu	Nb	Co
	%	%	%	%	%	%	%
1	0.159	0.0082	0.128	0.0029	0.112	0.0022	0.0074
2	0.167	0.0083	0.032	0.0025	0.115	0.0023	0.0087

Figure 4.26: Sample Data from Chemical Analysis

Once the steel matches the specification, the part can be cast. Along with every heat of steel for each casting order, a sample block of metal is cast to be used both for final chemical analysis as well as for supplementary mechanical tests. The block undergoes the same cooling conditions and heat treatment as the casting to maintain uniformity. Once cooled, the sample block is again tested to verify the chemical content meets the specification. The results from this final analysis are reported to the customer,

often constituting an average of 2-4 separate tests. In order to maintain precision and accuracy, the foundry calibrates their spectrometer daily using several standardized test samples with a known chemical content.

A key advantage of using the cast steel connection is the customer can specify the grade of material to be made since it is being formed directly from molten steel. Depending upon the grade selected, the foundry can add the appropriate alloying elements to guarantee the chemistry of the specified material is satisfied. One concern for the cast connection was its compatibility with weathering steel construction, a relatively common practice in steel bridges. For the steel castings obtained, the material was specified to meet ASTM A588 Standard Specification for High-Strength Low-Alloy Structural Steel, up to 50 ksi Minimum Yield Point, with Atmospheric Corrosion Resistance [2005].

The material composition breakdown for cast steel connections is given in Table 4.1. Comparing the cast steel composition with the ASTM A588 specification, it is seen the appropriate requirements are met for all specified elements. ASTM A588 Grade C was the specified grade of material.

Table 4.1: Comparison of Cast Steel Composition with ASTM A588 Specification

Element	ASTM A588 Gr. C (%)	Cast Steel Sample Average (%)
Carbon	0.15 (max)	0.105
Manganese	0.80-1.35	0.97
Phosphorous	0.04 (max)	0.015
Sulfur	0.05 (max)	0.0058
Silicon	0.15-0.40	0.331
Nickel	0.25-0.50	0.298
Chromium	0.30-0.50	0.390
Copper	0.20-0.50	0.275
Vanadium	0.01-0.10	0.054

4.10.1.1 Weldability

One of the major concerns of using cast steel in structural applications is its ability to be used in welding details. The major concern for cast steel is the increased

carbon content which gives the casting its strength but could compromise its ability to be welded. To help determine how easily a steel can be welded, a Graville diagram can be utilized. The diagram uses the percentage of carbon equivalent versus the percentage of carbon to determine whether or not difficulties will be encountered when welding [de Oliveira 2006]. Figure 4.27 shows a Graville diagram with the steel from the first set of castings plotted.

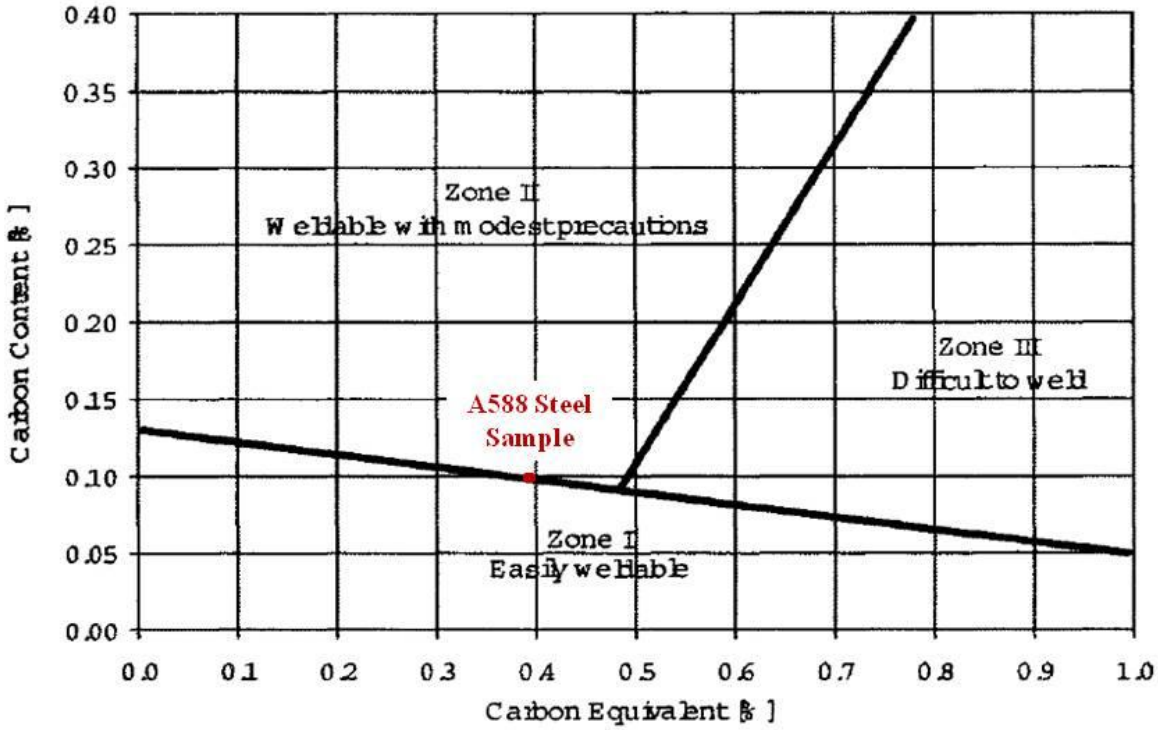

Figure 4.27: Graville Diagram for First Round of Cast Steel Connections [Kaufmann, Viscomi, Lu 1995]

4.10.2 Mechanical Testing

Mechanical testing is conducted to determine the approximate strength and toughness of the steel used to create the casting. Mechanical tests are performed on specimens, machined from the test blocks that are cast with each heat of steel for every casting order.

4.10.2.1 Tensile Tests

The tensile tests conducted are the standard direct tension test on a machined bar. The results are compared to the required specification to make sure the appropriate strength is achieved. It is important to note that while the tension specimen is machined from a sample of the same heat of steel, its properties could be somewhat different than the casting due to differences in thickness and in the relative rate of cooling.

Table 4.2 summarizes the results for the tension tests from the first set of castings and how the values satisfy the ASTM A588 specification.

Table 4.2: Comparison of Cast Steel Mechanical Properties with ASTM A588 Specification

	ASTM A588	**Cast Steel**
Tensile Strength	70 ksi (min)	85.09 ksi
Yield Point	50 ksi (min)	68.16 ksi
Elongation (2 in)	0.21 (min)	0.29

4.10.2.2 Charpy V-Notch Tests

In order to determine the toughness of the steel used to create the castings, standard Charpy V-Notch tests can be conducted. The toughness of the steel is a representation of how susceptible the steel is to brittle fracture and hence, gives insight on the fatigue life of the casting. Many of the ASTM standards for structural steels do not include Charpy impact requirements, so it is recommended the customer specify these values for the given application. One suggested Charpy V-Notch impact test value for use in steel castings in structural applications is 27 Joules at -20°C (19.9 ft-lb at -4°F) [de Oliveira 2006].

For the castings developed in the project, the Charpy test values were 112, 112, and 110 ft-lb at 40°F and 90, 72, and 90 ft-lb at -40°F, well above the steel bridge toughness requirements of ASTM A709, Grade 50W for both fracture and non-fracture critical members.

4.10.3 Visual Inspection

In terms of inspection, the easiest to perform is a visual inspection, which examines the surface of the casting to identify the presence of any major flaws or defects. This inspection would be recommended for most any casting, and can be done in accordance with the standard ASTM A802.

4.10.4 Magnetic Particle Inspection

Magnetic particle inspection uses magnetism to reveal any voids or cracks at or near the surface. The steel casting is magnetized and subjected to magnetic particles. Cracks, pits, or voids in the steel disturb the magnetic field, attracting the particles. A visual inspection is then conducted to determine the approximate location and magnitude of the defect [de Oliveira 2006]. The governing standard specification for this test is ASTM A903.

4.10.5 Liquid Dye Penetrant

Liquid dye penetrant requires the steel casting to be covered in a colored dye. Once the casting is wiped clean of excess dye, it is covered with a powder. The powder will soak up any remaining dye, revealing the location and magnitude of the surface flaws. While this method is convenient to detect surface irregularities, it will not uncover subsurface defects [de Oliveira 2006]. The ASTM A903 standard covers liquid dye penetrant examination.

4.10.6 Radiography

One way to detect flaws internal to steel castings is to pass X-rays or gamma rays through the casting and capture the image on film. The resulting pictures can provide an indication of where surface flaws might exist, usually shown as lighter shades of gray on the film [de Oliveira 2006].

Figure 4.28 and Figure 4.29 show scanned images of x-rays performed on the cast steel connection used in the research. The associated reports indicated minor porosity,

inclusions, and shrinkage cracking; however, all were within acceptable ranges according to ASTM E94.

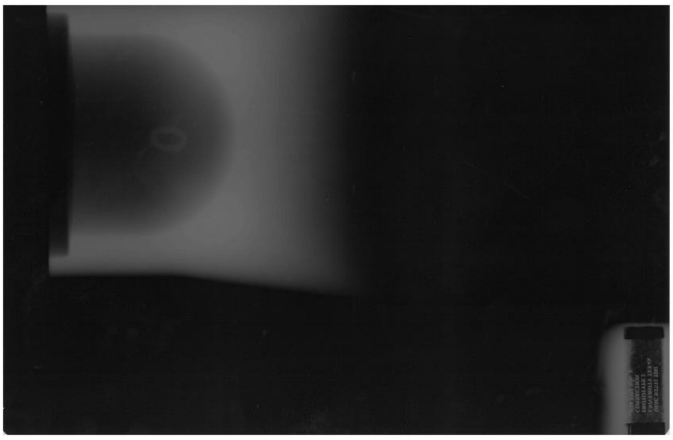

Figure 4.28: 0° X-Ray View of Cast Steel Connection

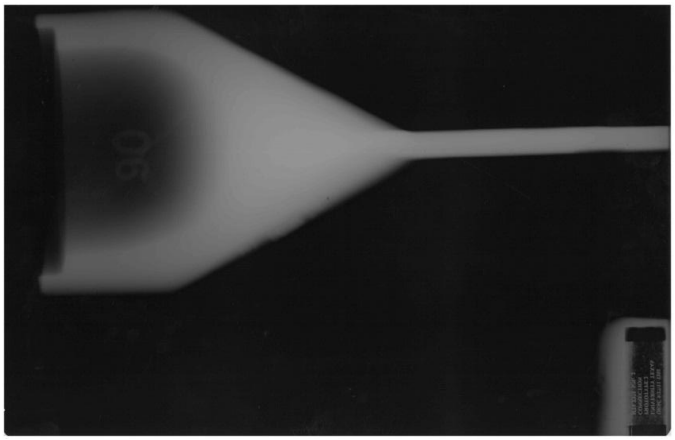

Figure 4.29: 90° X-Ray View of Cast Steel Connection

4.10.7 Ultrasonic Inspection

Another way to detect internal defects in steel castings is to use ultrasonic inspection. Ultrasonic inspection applies high-frequency sound waves to the surface of the casting. Using a calibrated measuring device, the reflection of the waves through the material are measured, indicating the approximate size, location, and depth of the flaw [de Oliveira 2006]. While ultrasonic inspection is useful, it is sometimes difficult to pick up small flaws in the material. Additionally, interpreting the results requires skilled training, and depending on how the device is oriented, it can miss some defects. The standard used for this inspection is ASTM A609.

4.11 COST ANALYSIS

There are two main factors constituting the cost of the completed part: the amount of steel required for the casting and the amount of time to create the casting. The first factor indicates the gross steel quantity necessary to cast the part. The quantity would include the final steel weight of the casting as well as the excess metal consumed during the pour (see section 4.7). The second factor refers to the processing time required to create the sand mold and the time required after the pour to finish the part. Complex molds using multiple cores and needing an intricate gating system will increase the cost of the final product. Therefore, it is important to make sure the design is well suited for both the final application and the casting operation.

For the cross frame connections produced for this research project, Quality Electric Steel Castings in Houston, TX charged a cost of $4.82 per pound of the finished casting weight. The completed prototypes weighed 44 lb, resulting in a cost $212.08 per connection.

Unfortunately, the cost of these weathering steel connections could prevent them from widespread use in steel bridge cross frames. One bridge fabricator reported the completed cost of an average X-type single angle cross frame to be on the order of $500 [Frank 2011]. If that is the case, the cost per unit weight of castings would need to be much lower to offer a competitive advantage. The foundry was not available to give the

researchers an approximation on cost for each connection should the number of connections in the order be very large.

In terms of the pattern, the foundry offered the following approximations for the cost. To generate a wooden pattern made from pine, the cost would be roughly $2,000-3,000. For the polyurethane pattern, the cost would be about $8,000-10,000. To mount either pattern, it would cost about $500. These would be only initial start-up costs to create the pattern, and subsequently, the customer would own the pattern for use in all future castings.

Initially, pine wood was used to make the prototype connection. The resulting cost was $4235, which included the cope and drag portion for two connections, as well as a core box to make the hollow portion of the casting to reduce overall weight.

4.12 TIMELINE

In terms of the required lead time for pattern construction and casting of the steel connection, the foundry provided the following approximations. To construct the pattern from pine, it would take about 4 weeks. The actual time was roughly 5-6 weeks. Once the pattern is at the foundry, they estimated it would take about 4-6 weeks, to schedule the steel castings to be poured. The actual pour took place 5 weeks from submittal of the purchase order. The purchase order indicated the castings would be delivered 10 weeks from payment. Delivery of the castings actually occurred at the 16 week mark.

4.13 SUMMARY

This chapter has provided a brief description of the process of producing cast steel connections. Castings provide the advantage of being able to accommodate a wide range of complex geometries and allow the development of an optimized design. In addition, castings can be made to a variety of different steel specifications, including weathering steels. This chapter has also described some of the specific steps involved in producing the castings for the tubular cross-frame connections being investigated in this research. The next chapter provides further details on the design of this cast connection, along with

results of static and fatigue tests on the cast connection as well as other cross frame connections investigated in this research.

CHAPTER 5
Small Scale Cross Frame Connection Tests

5.1 INTRODUCTION

The overall research project, in conjunction with TxDOT Project 0-6564, focused on improving cross frame details by investigating a variety of different cross frame geometries, member types, and connection details. Much of the research investigated the feasibility of using tubular cross frame members rather than the conventional single angle members. As previously discussed, tubular members may permit the use of single diagonal cross frames, leading to potentially simpler and more cost effective cross frames. Tubular members also allow the use of concentric connections, thereby eliminating the eccentric single angle connections. Concentric connections may lead to increased cross frame stiffness and improved fatigue performance. This research project also investigated the use of double angle diagonals, which would also allow for a concentric connection and provide improved stiffness and improved strength in compression.

In reviewing the background information provided in Chapter 2, 3, and 4, it is seen there are a variety of ways to make the connection between the cross frame members and the gusset plates or cross frame connection plates. This chapter describes analysis and tests on four types of connections studied for potential use in cross frame construction. Three connections were investigated for use with the tubular cross frame members: the cast steel connection, the T-stem connection, and the knife-plate connection. The fourth connection investigated in this chapter is the welded double angle connection. For each connection type, this chapter will describe the design of the connection, the experimental tests, and the associated finite element model analyses. The single angle connection currently used in TxDOT cross frames will also be studied to investigate the expected performance of these connections and to compare with the alternative connection details considered in this research.

5.2 CROSS FRAME CONNECTION LABORATORY EXPERIMENTS

The cross frame connection tests conducted in this research were divided into three main series of tests: stiffness tests, ultimate strength tests, and fatigue tests. The purpose of the stiffness tests was to determine the effect the connection had on the overall stiffness of the member and connection system. As previously discussed in Chapter 2, the system stiffness can be reduced by flexible connections. The stiffness tests provided data to quantify this effect.

The ultimate strength tests were used to determine the failure modes of the connections and their ultimate strength under static loading.

In addition, fatigue tests on the various connection types were performed to determine the adequacy of using these connections in cross frames from a fatigue perspective. The AASHTO LRFD Bridge Design Specification [2012] has requirements for the fatigue behavior of these connections, as outlined in Chapter 3, and the results will be discussed herein.

5.2.1 Testing Machine

The cross frame connection tests were performed in the 220 kip MTS Universal Testing Machine at the Ferguson Structural Engineering Laboratory at The University of Texas at Austin. The basic test setup is shown in Figure 5.1 and Figure 5.2.

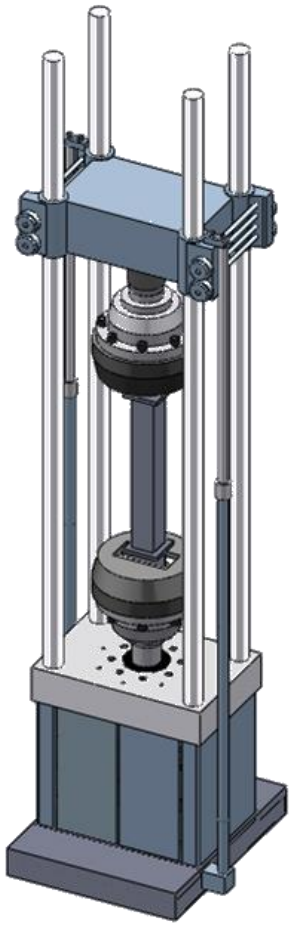

Figure 5.1: 220 kip MTS Testing Machine with Specimen

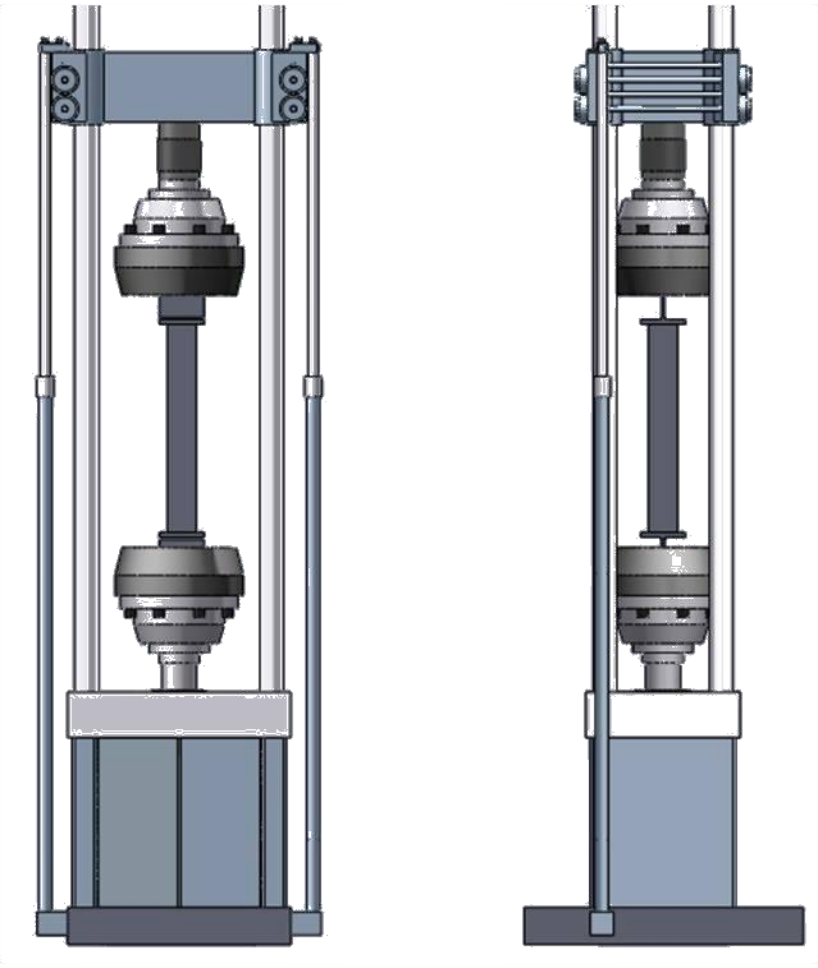

Figure 5.2: Test Setup (a) Front View and (b) Side View

5.2.2 Stiffness Tests

As previously mentioned, tests were conducted to quantify the effect of connection details on the axial stiffness of a cross frame member. Quantifying axial stiffness required measuring the axial force imposed on the member and also measuring the axial displacement of the member. Axial force was measured by the load cell in the MTS test frame. In order to measure axial displacement of the cross frame member, two dial gages were used. One gage has an accuracy of 0.001″ and the other 0.0001″. The gages are shown in Figure 5.3. Dial gages were chosen for the measurements due to their high accuracy.

Figure 5.3: Displacement Dial Gage with (a) 0.001" Accuracy and (b) 0.0001" Accuracy

The axial displacement of the cross frame member was measured between points at the member ends that were attached to the connection plates that were gripped by the test machine. The measurement points were located 2 in from the end of the actual cross frame member. The overall measurement attachments can be seen in Figure 5.4 and Figure 5.5. The gage locations were slightly modified for the cast connection.

Figure 5.4: Test Setup Front View with Dial Gages

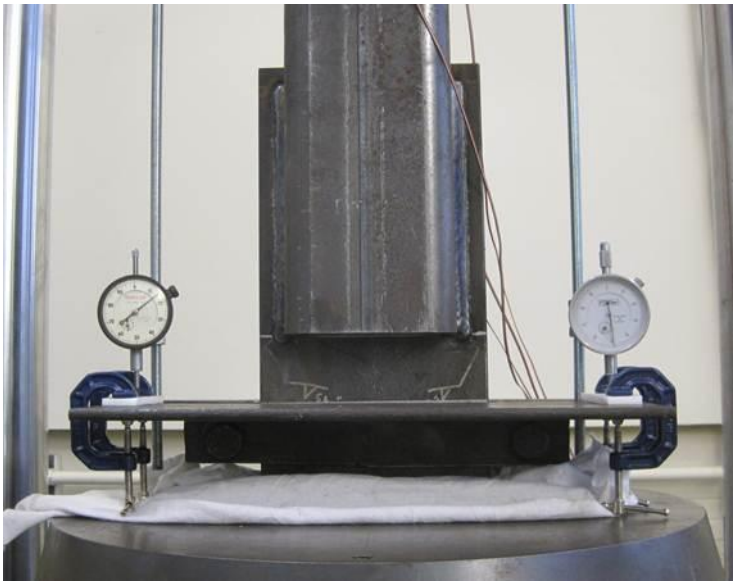

Figure 5.5: Close Up View of Dial Gages and Angle Clamps

In addition to the displacement measurements, strain data was taken to validate the results of the finite element models. The strain gages were 350-ohm general purpose strain gages produced by Micro-Measurements of the Vishay Precision Group. The gage

designation was CEA-06-250UN-350/P-2 and the gages were thermally compensated for use with mild carbon steel. The placement of these gages for each specimen will be discussed in the corresponding parts of this chapter. A close-up of the strain gages are shown in Figure 5.6.

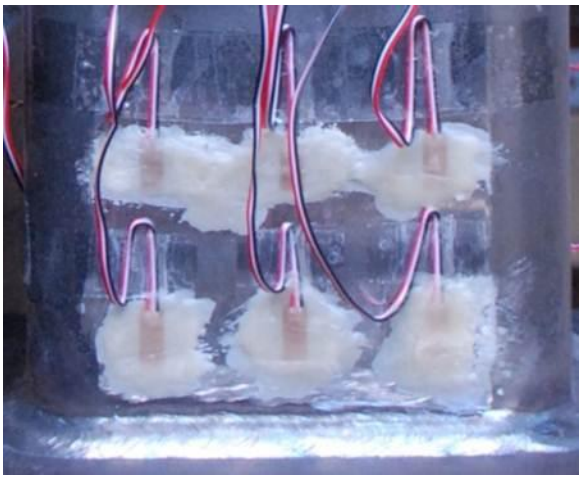

Figure 5.6: Close-Up View of Strain Gage

5.2.3 Ultimate Strength Tests

The ultimate strength tests were performed in the same setup as the stiffness tests, using the same specimens. Tests were first conducted in the elastic tension and compression range to determine the stiffness behavior. The sample was then loaded in tension to failure, or until the limits of the testing machine were reached.

5.2.4 Fatigue Tests

The fatigue tests were also performed in the 220 kip MTS Universal Testing Machine using the same basic setup as the stiffness tests, but subjecting the specimens to cyclic loads rather than tension and compression loads. The tests were conducted using close-looped force control, with the specimens exposed to sinusoidal cyclic loads and loading compensated for force errors. The specimens were initially placed under tensile stress, and then further loaded in tension to produce the desired stress range. An example setup is shown in Figure 5.7.

Figure 5.7: Basic Fatigue Setup

The results of the fatigue test were used to establish the relationship between the stress range and number of cycles to failure. The values were plotted against performance requirements from the AASHTO Bridge Design Specification to determine the fatigue category of the connection, as outlined in Chapter 3.

Part I: Cast Connection

5.3 CAST CONNECTION DESIGN

In order to design the cast steel connection, computer software was used to both generate a solid model and analyze it for a given load condition. SolidWorks 2010 was

the CAD program selected to make the three-dimensional solid model of the connection. From the program, the model geometry was exported as an .iges solid geometry file. This format basically reduced the model into small triangular elements for use in exporting to other software. The geometry was then uploaded into ANSYS® Academic Research, Release 11.0, a three-dimensional finite element analysis (FEA) program. Once uploaded, the appropriate loading and boundary conditions were applied and the connection was analyzed. Figure 5.8 summarizes the design process for an early version of the cast steel cross frame connection.

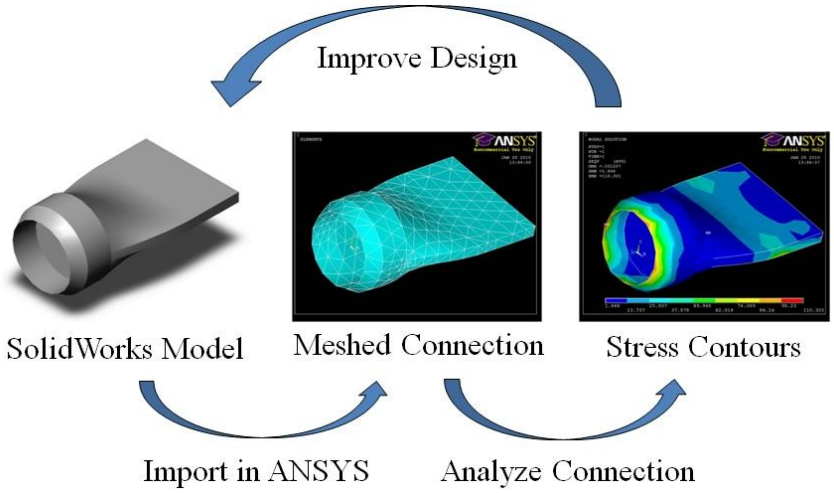

Figure 5.8: Cast Steel Connection Design Process

After iterating through the design process of Figure 5.8, a final geometry for the connection was selected.

5.3.1 Features

Initially, the prototype was designed to fit to the inside diameter of the round tube to reduce the amount of steel required for casting and improve handling of the parts. However, pipes, as well as round HSS members, are specified by the outside diameter. In order to standardize the casting geometry, which improves the economy of using the connection, a prototype that fits to the outside diameter is more beneficial. Namely, fitting to the outside diameter allows one cast connection geometry to be used with pipe

sizes of the same outside diameter but varying thicknesses. Therefore, the designer can use a thicker tube when a higher strength cross frame member is needed, and vice versa.

The prototype connection is shown in Figure 5.9. The design incorporates a ledge on the inside of the hollowed portion to facilitate fit-up with the circular tube. The hollow is provided to remove unnecessary material from the casting making it lighter and reducing the cost. Additionally, two erection bolt holes were added in the flat portion to aid in the construction of the braces. Since these steel parts were cast from molten metal, features like erection bolts could be easily added with little effect on the cost of the part.

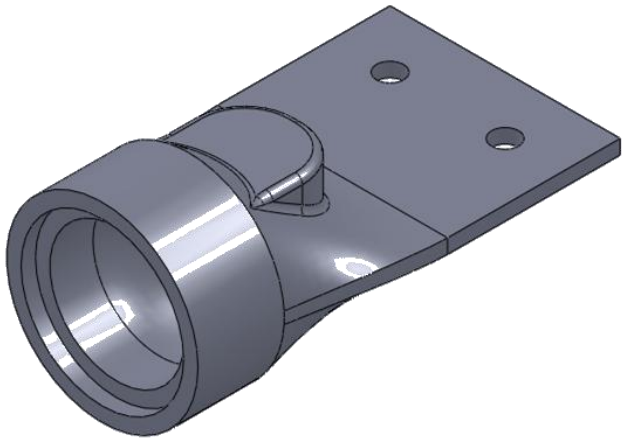

Figure 5.9: Prototype Cross Frame Connection

The prototype also featured a taper from the circular cross section to a flat plate, making it easy to weld to gusset plates or cross frame connection plates, thereby preventing large stress concentrations from forming. After corresponding with the foundry, a steel pad was placed along the taper of the casting to facilitate the finishing process of the castings. As discussed in Chapter 4, risers are used in the design of the gating system to ensure the portion of the casting that cools last has liquid steel feeding it, preventing macro shrinkage. Through temperature and flow analysis software, the foundry identified the section along the taper to be critical and placed the riser pad accordingly. Finite element analyses showed the riser pad to have little effect on the flow of forces through the part; however, the foundry ended up removing the pad during the

finishing process resulting in the connection shown in Figure 5.11 and Figure 5.12. Figure 5.10 shows the taper of the casting and the final specified geometry of the casting.

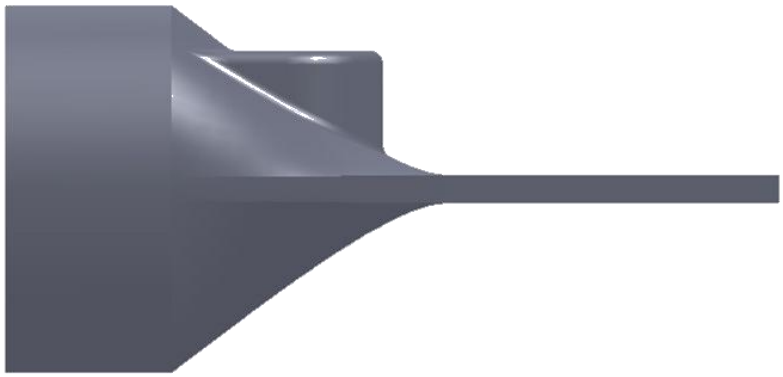

Figure 5.10: Prototype Cross Frame Connection (Side View)

It was anticipated the connection between the tubular member and the casting would be a fillet weld. Using a fillet weld was intended to simplify fabrication as well as reduce inspection requirements. Since the weld will be situated along the circumference of the tubular member, a setup involving some roller supports could be arranged in the fabrication shop so the welder could rotate the tube while fillet welding the connection.

The completed cast connections, after heat treatment and finishing processes, are shown in Figure 5.11 and Figure 5.12. The aforementioned riser pad was removed during finishing of the part.

Figure 5.11: Cast Steel Cross Frame Connection

Figure 5.12: Cast Steel Cross Frame Connection (Side View)

5.3.2 Dimensions

When determining the required size of the cross frame connections, the project team identified the tube sizes necessary for the single diagonal cross frame layout (as discussed in Chapter 2). The tube sizes are approximated from current TxDOT details using angle members, with the round and square tube sizes having similar capacity in compression at a length of 13 ft as the angles have in tension. The length of 13 ft was used as it approximately represents the diagonal length of a cross frame with an 8 ft (96 in) girder depth and 10 ft girder spacing. In actuality, the length would be less due to the addition of gusset plates and positioning of the members. Table 5.1 shows how the tubular member compression capacities compare to the yielding capacity of the angle.

The laboratory testing focused on the tube sizes corresponding to the L4 x 4 x 3/8 and the L5 x 5 x 1/2 angle members. Thus, the first prototype for the steel casting was designed to fit to the outside diameter of an HSS 5.563 tubular member. The other main dimensions calculated were the width and thickness of the flat portion of the casting, as it needs to also reach the appropriate strength for the connection to be successful. Using analytical strength equations, and the results from the FEA, a connection width of 8 in and thickness of 0.5 in was deemed adequate. The other dimensions for the casting were developed by performing multiple finite element analyses, optimizing the use of material to make an efficient connection. Figure 5.13 and Figure 5.14 show the plans submitted to the foundry for use in creating the cast steel connection patterns and cores.

Table 5.1: Angle Tensile Strength vs. Tube Buckling Strength

Angle Size	Angle Capacity (36 ksi)	Tube Size	Tube Capacity[1,2]
L4 x 4 x 3/8	92.7 k	HSS 5 x 5 x 3/16	88.6 k
		HSS 5.563 x 0.258	99.6 k
L5 x 5 x 1/2	154 k	HSS 5 x 5 x 3/8	160 k
		HSS 5.563 x 0.375	139 k
L6 x 6 x 9/16	209 k	HSS 5 x 5 x 1/2	199 k
		HSS 6.000 x 0.500	207 k

1. Tube capacity was calculated using a length of 13 ft
2. Yield stress (F_y) is assumed to be 46 ksi for square tubes and 42 ksi for round tubes [AISC 2005]

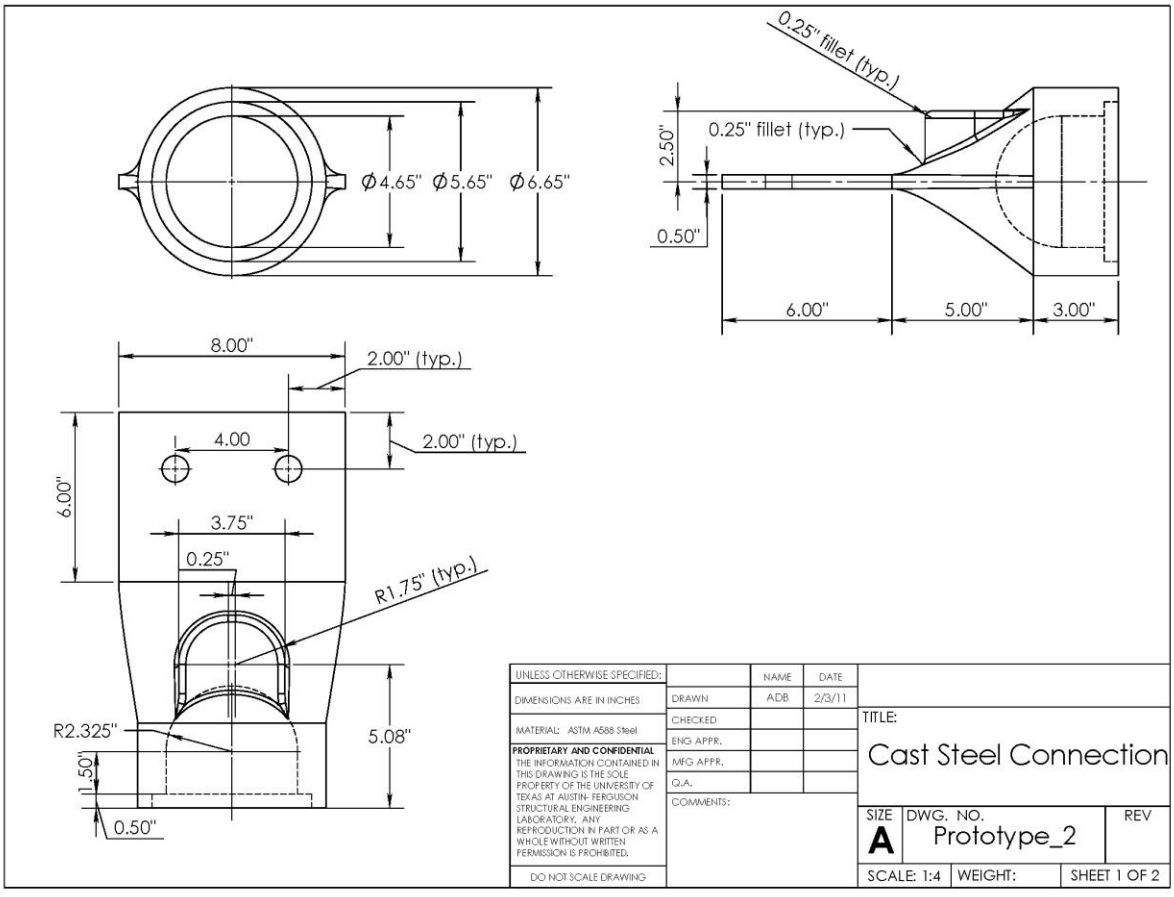

Figure 5.13: Two Dimensional Drawing of Cast Steel Connection

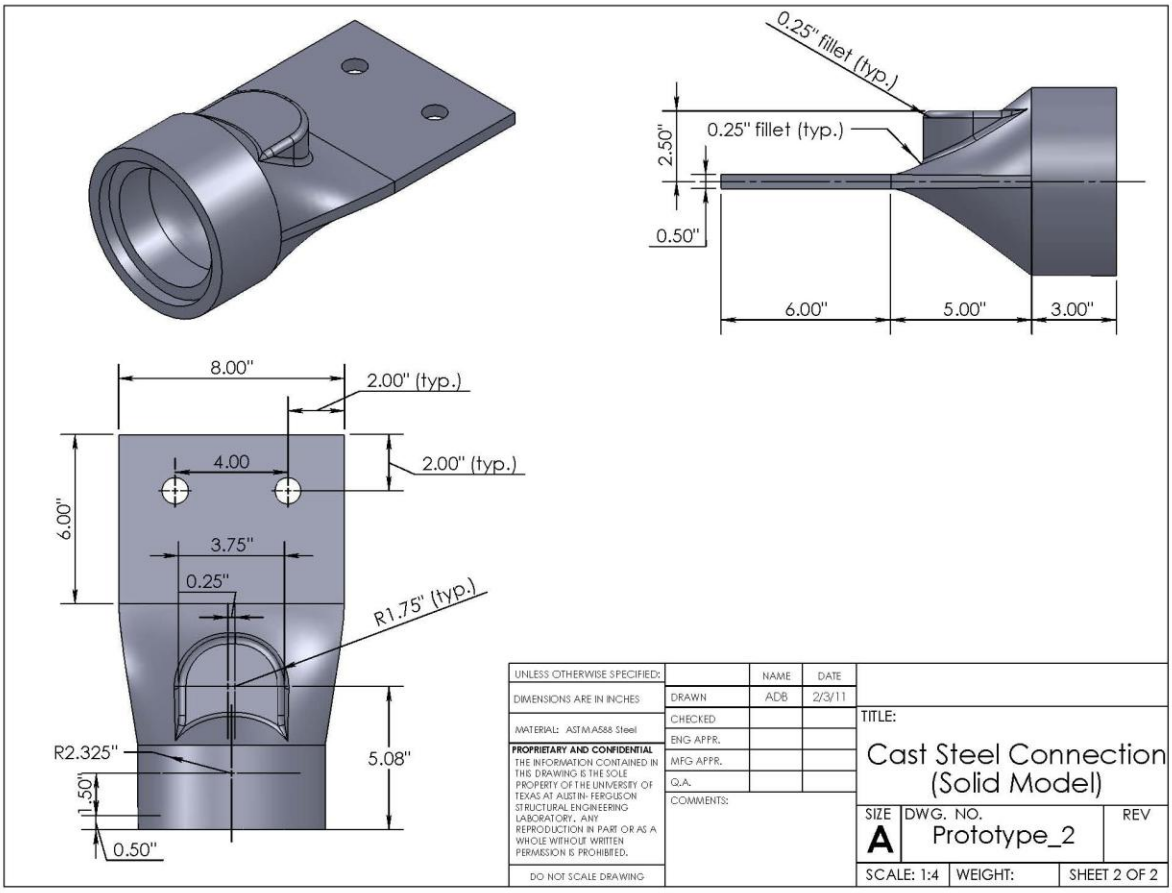

Figure 5.14: Three Dimensional Drawing of Cast Steel Connection

5.3.3 Analysis

As previously mentioned, multiple finite element analyses were performed on the cast connection geometry to determine appropriate dimensions. The primary focus of these analyses was to determine if the cast connection showed signs of any stress concentrations.

Using the FEA program ANSYS, the solid model file was uploaded and meshed using SOLID187 elements, which are 10-noded tetrahedral solid elements. Each node has three degrees of freedom, translation in the nodal x, y, and z directions. The element

can support quadratic displacements and is well-suited to model irregular meshes [ANSYS 2011].

Figure 5.15 shows the loading and boundary conditions used for the analysis of the cast steel connection. Using the program, a 100 kip load was discretized into smaller point loads and applied uniformly to the casting at the location of the tube-to-casting fillet weld. One effect of fixing nodes in an FEA model is that large stress concentrations will develop at the fixed location. To reduce this effect in the model, a gusset plate was included in the model to analyze the casting. The gusset plate was constructed of SHELL93 elements, an 8-noded plate element with six degrees of freedom at each node: three translations and three rotations. The casting was connected to the plate using MPC184 elements, multipoint constraint elements that rigidly join two nodes and are often used to model welded connections [ANSYS 2011].

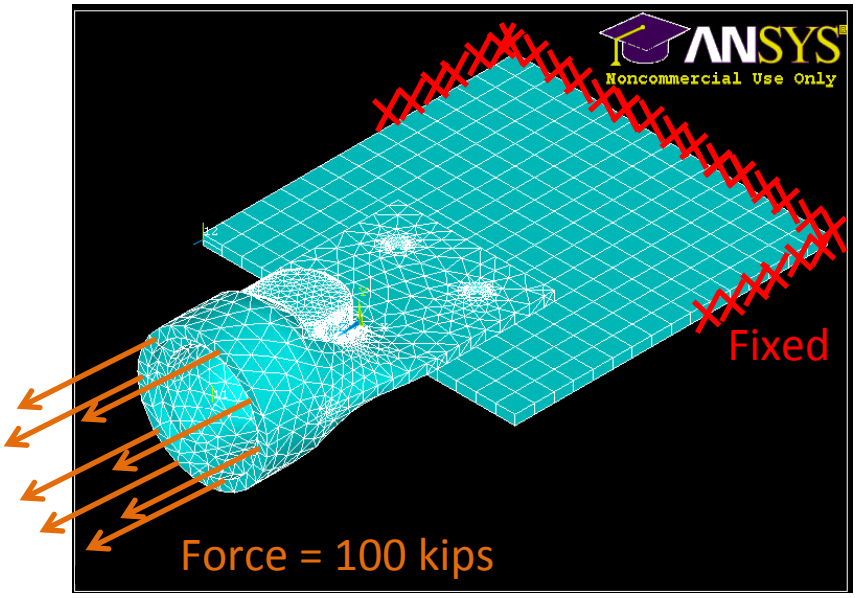

Figure 5.15: Load and Boundary Conditions for Steel Casting Analysis

Using the prescribed boundary conditions, an analysis of the cast steel connection was performed to determine if large stress concentrations in the longitudinal direction were developing in the connection and if the connection was strong enough to resist the

applied loads. Figure 5.16 shows the results of an elastic, static analysis of the connection.

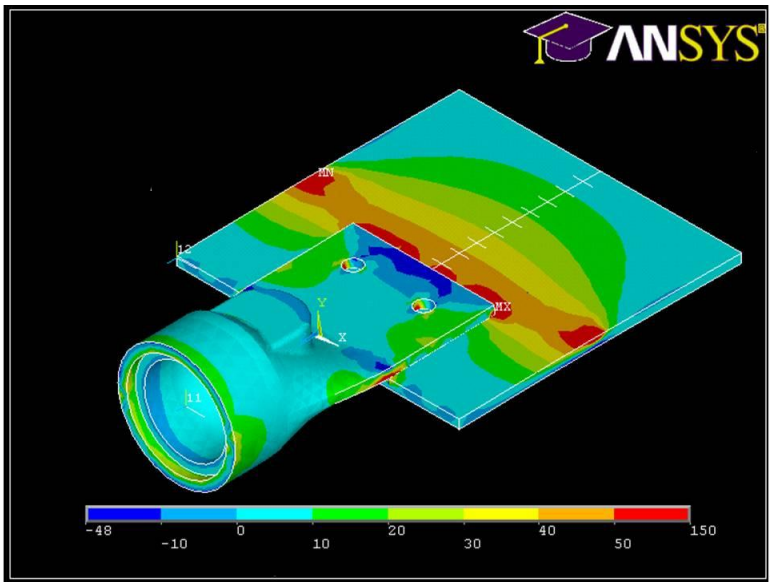

Figure 5.16: Longitudinal Stresses [ksi] Resulting from an Elastic Analysis on Steel Casting Connected to Gusset Plate

While every effort was taken to minimize the effect of stress concentrations in the FEA model, some of the high localized stresses predicted by this elastic model will be reduced due to localized yielding. A subsequent analysis was carried out using an inelastic material model. A bilinear hardening material model was used with an initial modulus of elasticity of 29000 ksi to a yield stress of 50 ksi, followed by a 580 ksi hardening modulus. Figure 5.17 shows the results of the inelastic analysis. Note the stress pattern in the casting is similar to Figure 5.16, indicating the use of the gusset plate helps to minimize the effects of stress concentration.

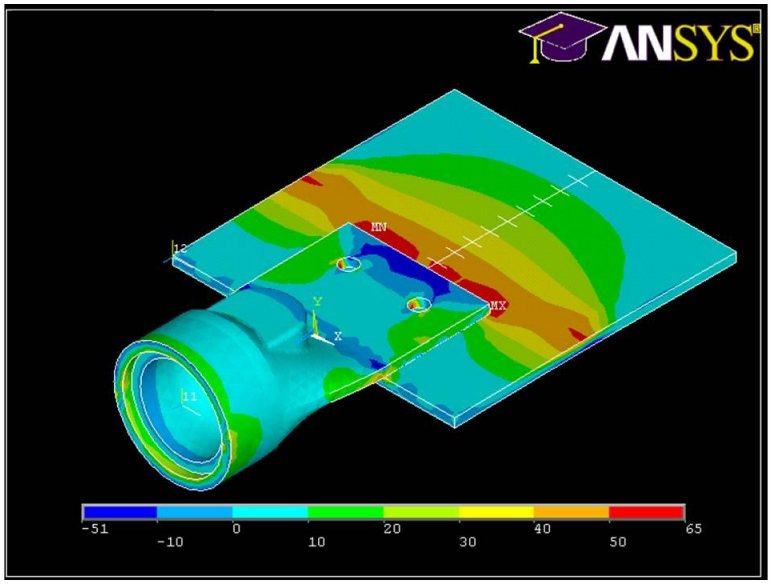

Figure 5.17: Longitudinal Stresses [ksi] Resulting from an Inelastic Analysis on Steel Casting Connected to Gusset Plate

5.4 CAST CONNECTION LABORATORY EXPERIMENTS

Once the design of the cast steel connection for tubular cross frame members was complete, the project team worked with a foundry to create a pattern for the design, and to cast the connections. Quality Electric Steel Castings in Houston, TX was selected for the task, and the connections were made following a procedure typical to the sand casting method. In-depth discussion of the procedure employed to form the castings and to assure a quality casting was provided in Chapter 4.

Upon delivery of the castings, the project team fabricated test specimens to determine the strength and stiffness of the connection to make sure it is adequate for the application of constructing cross frames.

5.4.1 Stiffness Tests

In order to determine if the castings were capable of resisting the designed tension and compression loads, specimens were created with the intent of determining the

strength of the casting. Furthermore, these tests quantified the effect the connection has on the overall stiffness of the tubular member.

The stiffness tests were conducted in the 220 kip MTS Universal Testing Machine as outlined in Section 5.2.2 and depicted in Figure 5.18. Due to geometrical constraints, the angle clamps could not be used to support the gages, so the dial gages were attached to the casting along the sides, using smaller angle sections that were epoxied to the casting.

Figure 5.18: Cast Steel Connection Stiffness Tests with Dial Gages

Using the obtained deflection measurements, the load versus displacement relationship was plotted. The slope of the elastic portion of the curve is then equal to the

stiffness. The stiffness measured is that of the combined system, meaning the stiffness of the cross frame member and the two connections at either end. Figure 5.19 depicts a plot of the displacement data. The stiffness listed was found by using a linear best fit line through the data.

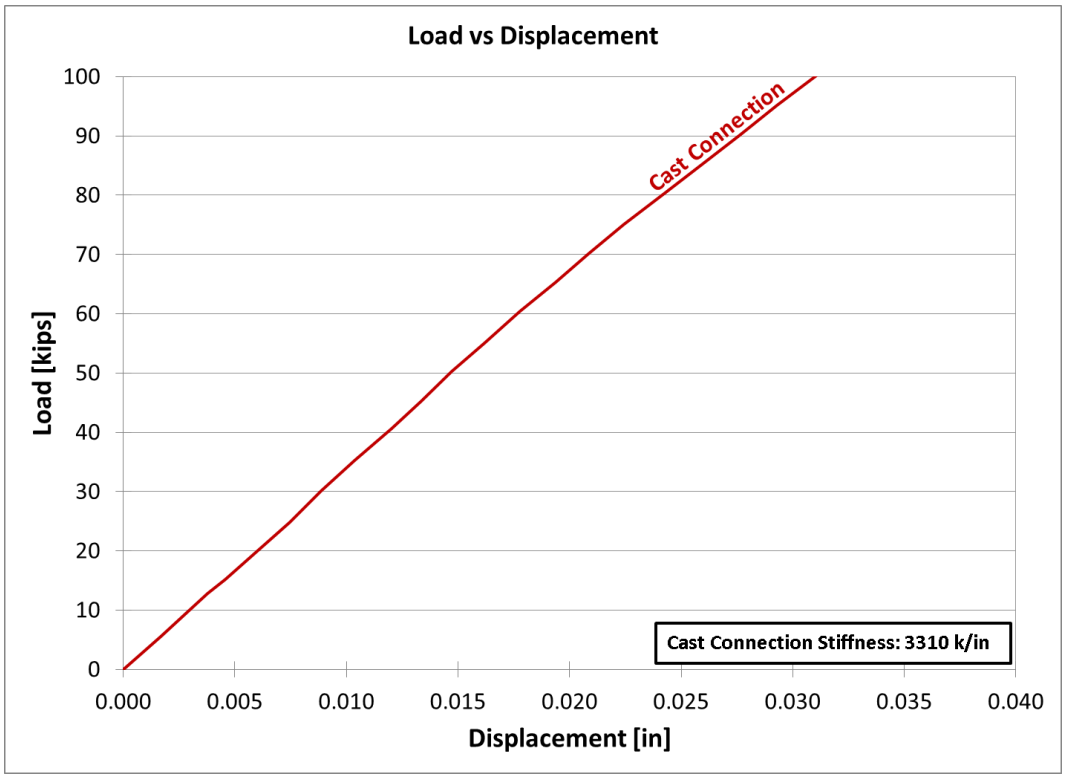

Figure 5.19: Cast Steel Connection Stiffness

5.4.2 Ultimate Strength Test

Additional tests were performed in a 550 kip MTS Universal Testing Machine to determine the ultimate strength and failure mechanism of the cast connection, and to obtain supplemental stiffness data. The specimen in the 550 kip machine is shown in Figure 5.20.

Figure 5.20: Cast Steel Connection Test in 550 kip MTS Testing Machine

Using standard steel design checks, the calculated strength of the cast steel connection was approximately 240 kips, and was controlled by fracture of the fillet weld connecting the casting to the tube. When loaded in tension, the steel casting and welded connection exceeded these strength calculations, showing that typical checks performed on the cast steel connection and tube combination can provide a safe design. The results of the ultimate strength test are shown in Figure 5.21.

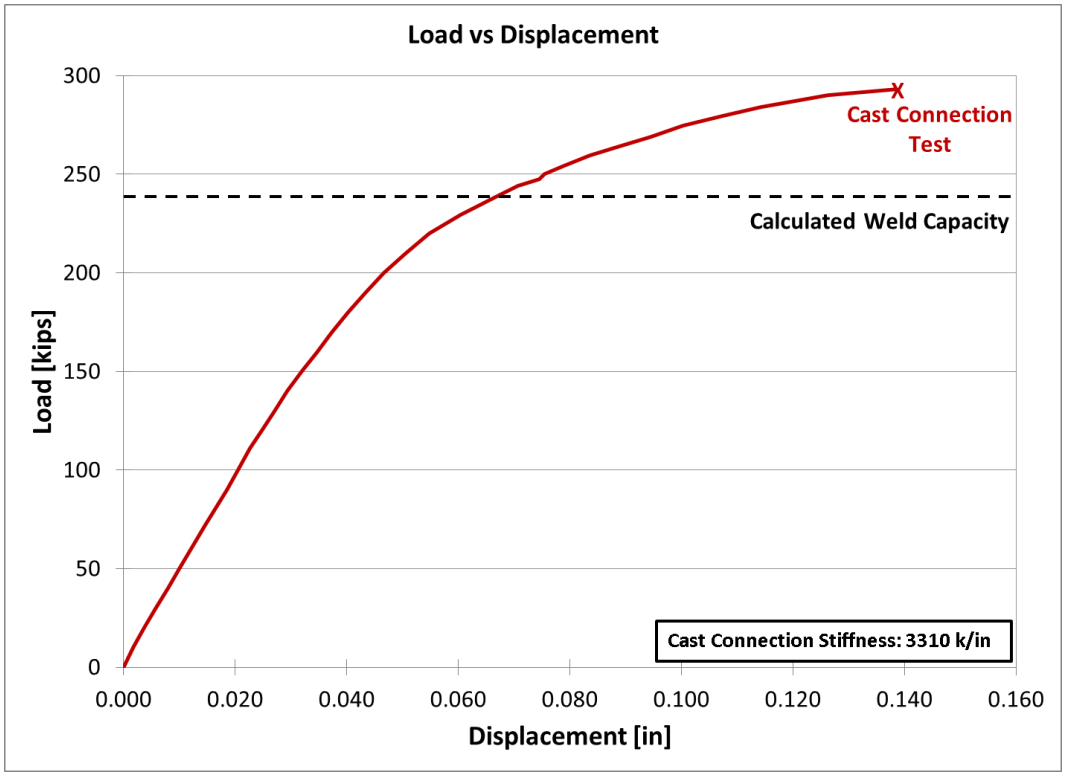

Figure 5.21: Cast Steel Connection Ultimate Strength Test Results

5.4.3 Fatigue Tests

Test specimens similar to those tested in the tension test were carried out under cyclic loading until fracture occurs. One of the key aspects of these tests was to make sure the fatigue crack initiates at the welded connection and does not originate in the casting. The tests were also used to classify the cast connection according to the fatigue categories given in the AASHTO Bridge Design Specifications.

Figure 5.22 shows the results of two fatigue tests on the cast connection and tube specimen. The stress range was computed by dividing the nominal applied load by the area of the tubular member. Since the cast connection is concentric, no shear lag factor was included. Unfortunately, the results indicated the fatigue behavior of the welded cast connection was poor.

The connection was designed to be a transversely loaded fillet weld which would transfer the force from the rim of the casting into the tube wall. It was designed as a fillet weld to facilitate the fabrication process and prevent the need for costly inspection procedures. However, while the connection is concentric on the whole, at the local level it is eccentric. Figure 5.23 depicts how the load is transferred locally through the weld.

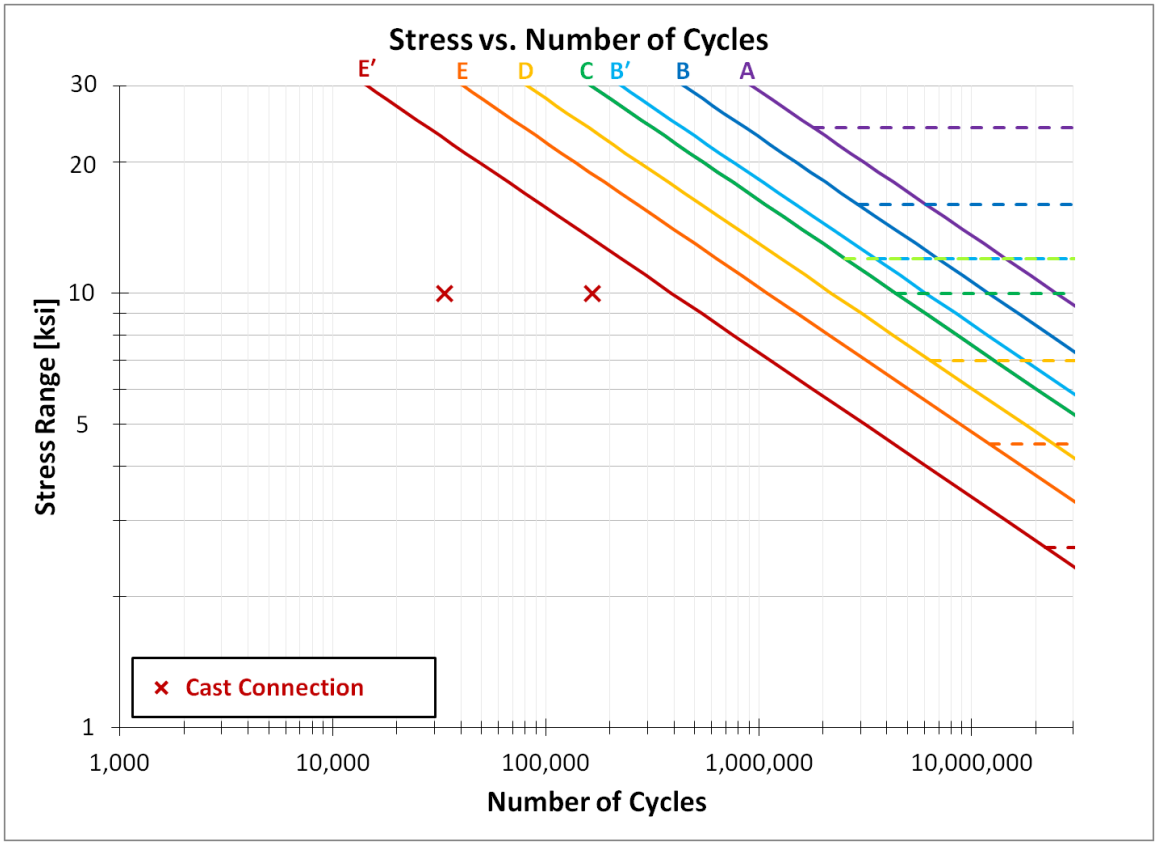

Figure 5.22: Cast Steel Connection Fatigue Results

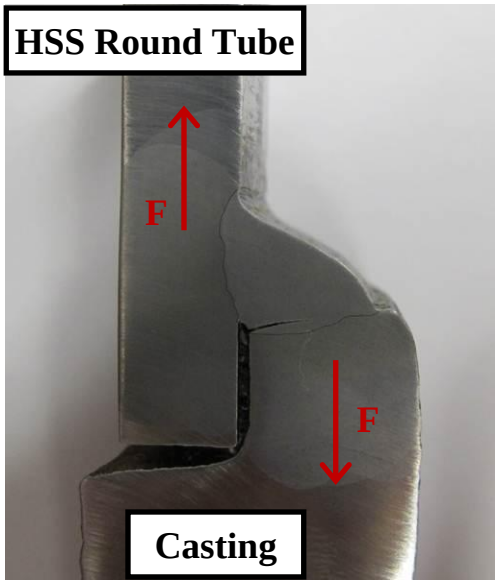

Figure 5.23: Eccentric Nature of Fillet Weld

The result of the eccentric loading pattern is a low fatigue life. The fatigue crack begins at the notch located at the root of the weld, and then propagates through the weld throat until it reaches the surface. Unfortunately, since the notch is built into the connection as a result of the geometry of the fillet weld, it cannot be improved. Therefore, a second specimen was prepared to improve the connection. The specimen was sand blasted to improve surface conditions and preheated to improve weld penetration, while the weld electrode diameter was reduced and a multi-pass weld was employed to further the level of penetration. The result was a significant improvement in fatigue life, as shown in Figure 5.22, however, the number of cycles achieved was only half of what is required to meet the minimum E′ category as specified by AASHTO for use in bridge components.

Additionally, when the crack becomes visible on the surface of the weld, the majority of the fatigue life of the detail has been used, meaning that there is little warning before imminent failure. An example of a fatigue crack in the cast steel connection weld is shown in Figure 5.24.

Figure 5.24: Cast Steel Connection Fatigue Crack

5.5 CAST CONNECTION TEST CONCLUSIONS

The results of the cast steel connection designed in this research indicated that it was not a suitable connection for typical cross frame braces. The strength tests showed the cast connection provided a safe detail when using standard connection checks to predict strength. The connection uniformly engaged the tube and provided one of the stiffer connections of all those discussed within this chapter (see Section 5.22). However, the poor fatigue life of the designed fillet weld detail leads to its exclusion from potential cross frame connections for this project. Further refinements in the design of the cast connection may be possible to improve the fatigue performance of the connection to tube weld. However, such further refinements were not undertaken in this project.

Part II: T-Stem Connection

5.6 T-STEM CONNECTION DESIGN

As an alternative to casting a steel connection piece to connect the tubular members of the cross frames, fabricated connections were also considered as part of the

research. The second detail investigated as part of this research program was the T-stem detail.

5.6.1 Features

The T-stem detail involves the use of a WT section to connect to the ends of the tube to a flat plate. The tubular member meets the flange of the WT shape at 90° and is fillet welded to create the connection. The stem of the WT can then be easily attached to the flat cross frame connection plate or to a cross frame gusset plate. Figure 5.25 shows the basic geometry of a T-stem connection.

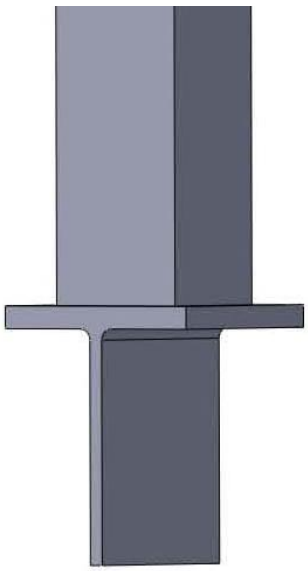

Figure 5.25: T-Stem Connection Detail Concept

One of the major advantages of the T-stem connection is it consists of standard steel rolled shapes. In comparison to the cast connection which requires special manufacture, the T-stem is readily available for fabrication. In addition, the material properties of the steel are better understood by most designers. The T-stem connection can also offer a variety of tube sizes to be used, allowing the bridge designer to customize the size of tube and connection for each particular scenario. In addition, like the cast connection, the T-stem connection seals the end of the tube protecting the inside of the

tubular member from atmospheric elements. Lastly, because of the increased availability, the T-stem connection may offer improved economy over the cast connection.

5.6.2 Dimensions

Determining the optimum size of WT section to use for a connection required several considerations. The two main criteria to evaluate were the yielding/fracture strength of the WT stem and the bending capacity of the WT flange. At the same time, the width of the flange should be selected so it does not grossly exceed the width of the HSS tube, resulting in poor efficiency of material.

For the experimental test program, it was the goal of the research team to select the WT sizes such that the full yielding capacity of the tubular members could be attained. While this is possible for thinner walled tubes, it was apparent that it was unlikely to be the case for thicker walled tubes. Furthermore, the capacity of the proposed fillet welded connection tended to control the design for some cases. Therefore, the research team decided to select two different WT sections for the experimental program, and to use them in different combinations to study the variety of failure modes possible for this design.

Using Table 5.1, the WT 9 x 35.5 and the WT 12 x 31 shapes were selected. With flange widths of 7.64 in and 7.04 in respectively, the use of 5 in square HSS members seemed reasonable, allowing about an inch along the sides in which to make the fillet weld. While the WT connection can be cut to any length and attached to the tubular member, it was proposed the WT be cut to a square flange area so the tube and flange are concentric, primarily for aesthetic purposes. The following table shows the experimental test program; more tests were originally planned, but not completed due to poor performance of this detail in fatigue loading.

Table 5.2: Experimental Test Program for the T-Stem Connection

Laboratory Test Program			
	Connection Description	**HSS Member**	**WT Connection**
Tension Tests	Square	HSS 5 X 5 X 3/8	WT 9 X 35.5
	Square	HSS 5 X 5 X 3/16	WT 12 X 31
Fatigue Tests	Square	HSS 5 X 5 X 3/8	WT 9 X 35.5
	Square	HSS 5 X 5 X 3/8	WT 9 X 35.5
	Square	HSS 5 X 5 X 3/8	WT 9 X 35.5
	Square (CJP)	HSS 5 X 5 X 3/8	WT 9 X 35.5
	Round	HSS 5.563 X 0.375	WT 9 X 35.5
	Round	HSS 5.563 X 0.375	WT 9 X 35.5
	Diamond	HSS 5 X 5 X 3/8	WT 9 X 35.5

5.6.3 Analysis

As shown in Table 5.2, round HSS members were also considered for use with the T-stem connection. The decision to consider round HSS members arose when preliminary analyses were performed on the connection geometries, indicating the square HSS members had a very large stress concentration. The following subsections discuss more detail on the finite element analyses.

5.6.3.1 Square HSS Connection

In an effort to understand the flow of forces through the T-stem connection, a finite element model was constructed in ANSYS. The model used 8-noded shell elements (SHELL93) to construct the plate regions of the WT section and the square HSS tube. The model did not account for the fillet region between the stem and flange of the WT, nor did it consider the curved corners of the square HSS members.

A major goal of the connection tests was to better understand the axial behavior of the tubular members in conjunction with the connections. The preliminary boundary conditions were simplistic: the applied load was discretized into several point loads

applied along the WT stem edge. To connect the tubular member to the WT flange, multipoint constraint elements (MPC184) were used to join the nodes.

Figure 5.26 shows a typical plan for a square HSS specimen with WT connections. Figure 5.27 shows typical boundary conditions for these analyses using a square HSS member.

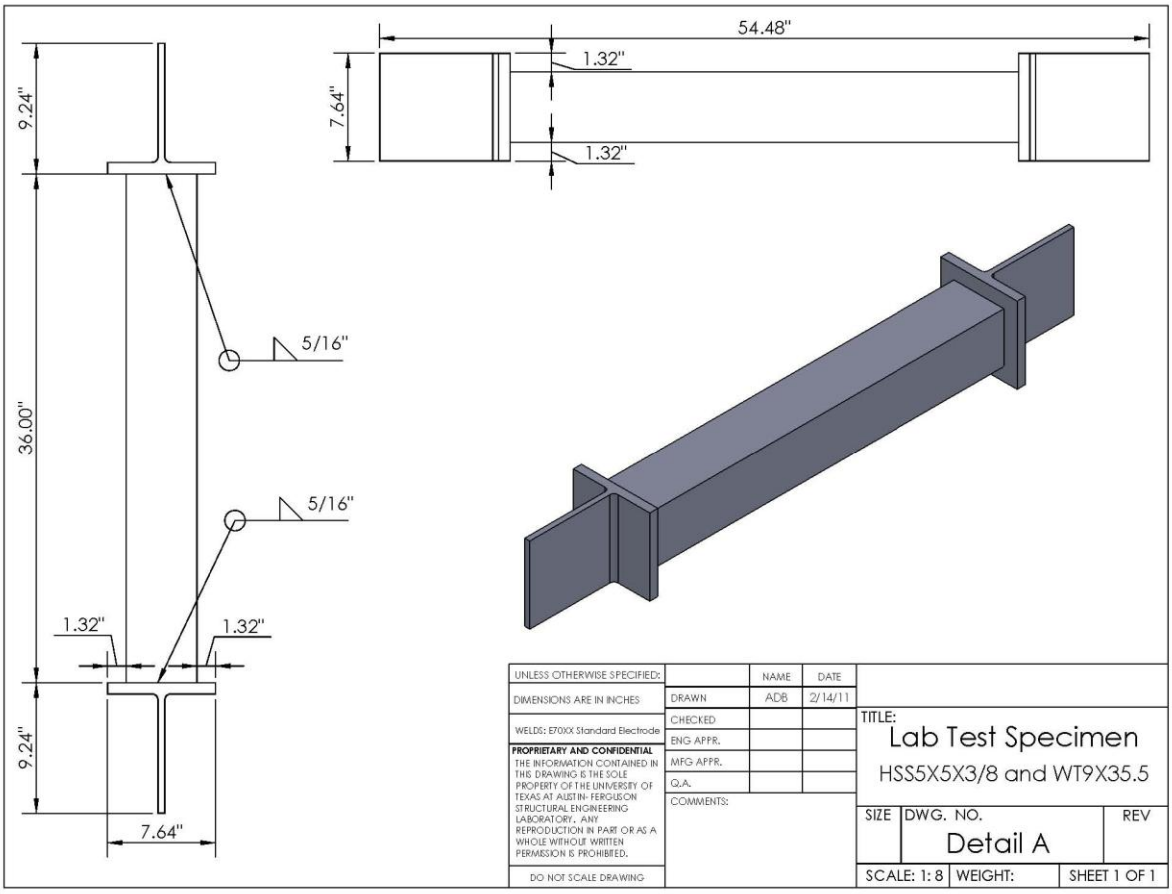

Figure 5.26: Square HSS Specimen with T-Stem Connection Detail

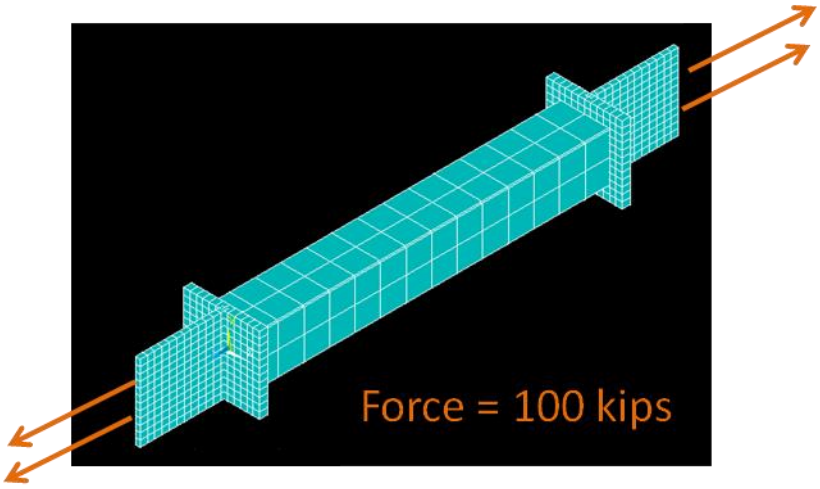

Figure 5.27: Typical Boundary Conditions Used for T-Stem Analysis

Results from these analyses showed that an intense stress concentration developed in the wall of the HSS tube perpendicular to the WT stem (see Figure 5.28(a)). Conversely, the stress in the wall parallel to the stem is less than the average stress expected in the tube section (Figure 5.28(b)). The presence of a stress concentration in the detail is problematic because it has the potential to lead to early, unexpected failures, especially in fatigue loading.

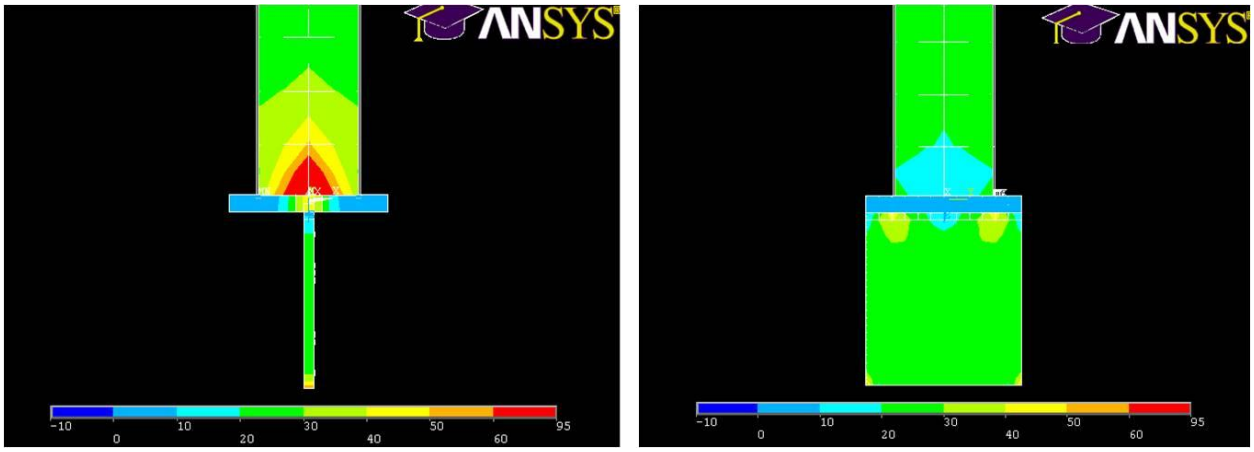

Figure 5.28: Longitudinal Stress [ksi] in HSS Tube Wall (a) Perpendicular to Stem and (b) Parallel to Stem

5.6.3.2 Round HSS Connection

Due to the stress concentration issue arising in the square HSS detail, the research team explored alternative arrangements of tubular members to determine if there was a reduction in the longitudinal stress. The first alternative used round HSS members instead of square members. The proposed detail geometry remained the same as the circular tube was centered in the square WT flange and connected with fillet welds. Figure 5.29 shows typical plans for a round HSS specimen with WT connections.

Figure 5.30 shows the preliminary analysis conducted for the round HSS members. In comparison to the square HSS detail, the round HSS seemed to reduce the magnitude of the stress concentration by about 40%.

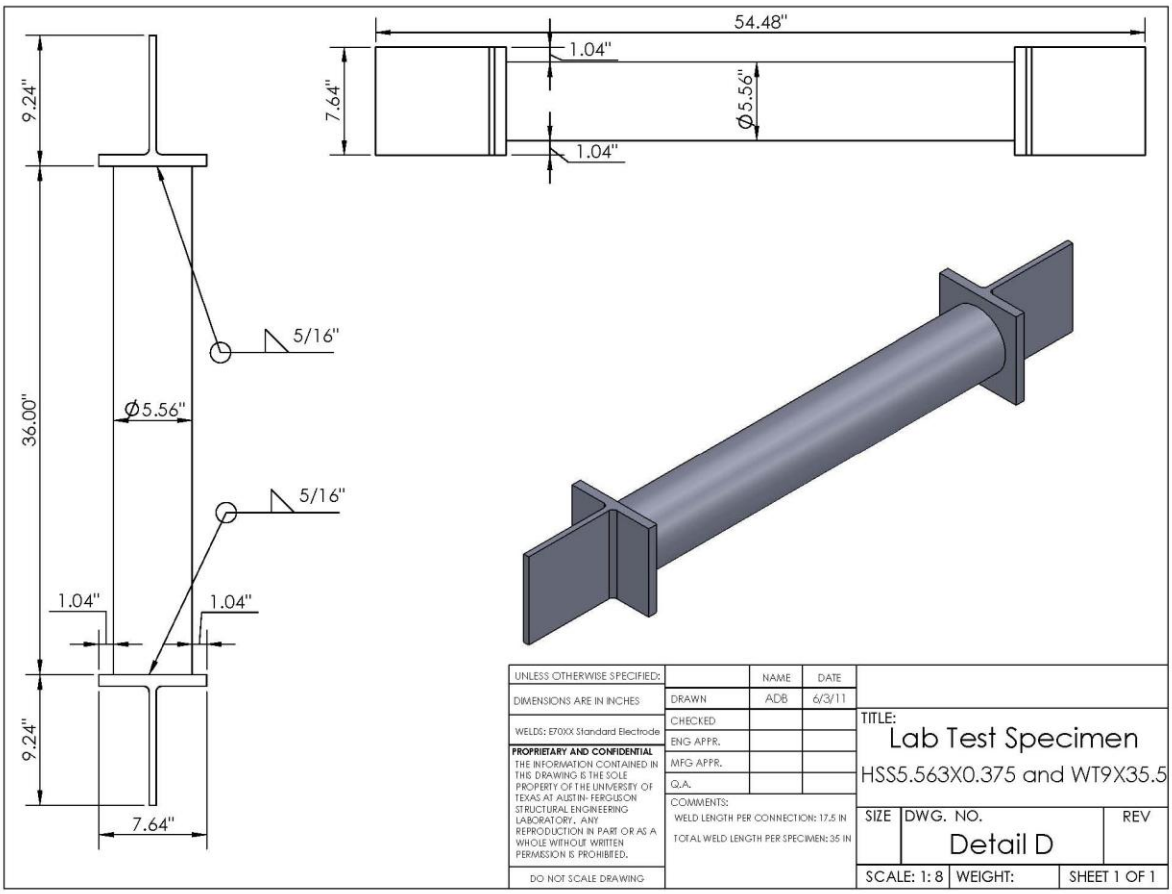

Figure 5.29: Round HSS Specimen with T-Stem Connection Detail

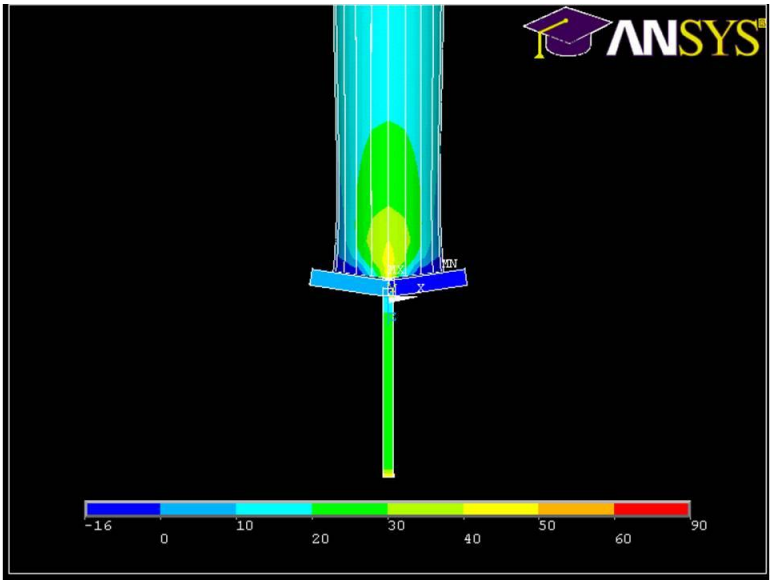

Figure 5.30: Longitudinal Stress [ksi] in Round HSS Tube Wall

5.6.3.3 Diamond HSS Connection

The second alternative to the square HSS detail was the "diamond" HSS connection. Utilizing the same square HSS sections, the tube is rotated 45 degrees about its longitudinal axis and attached to the flange of the WT section, as shown in Figure 5.31.

Performing an analysis on the rotated square specimen showed a further reduction in stress concentration as compared to the round HSS member, suggesting this detail may have the best fatigue performance of the three proposed options. Results of the analysis are given in Figure 5.32. The results showed a stress reduction of about 40% compared to the square T-stem connection, but unlike the round specimen, the peak stress zone was smaller in area, and the stresses along the length of the member more evenly distributed.

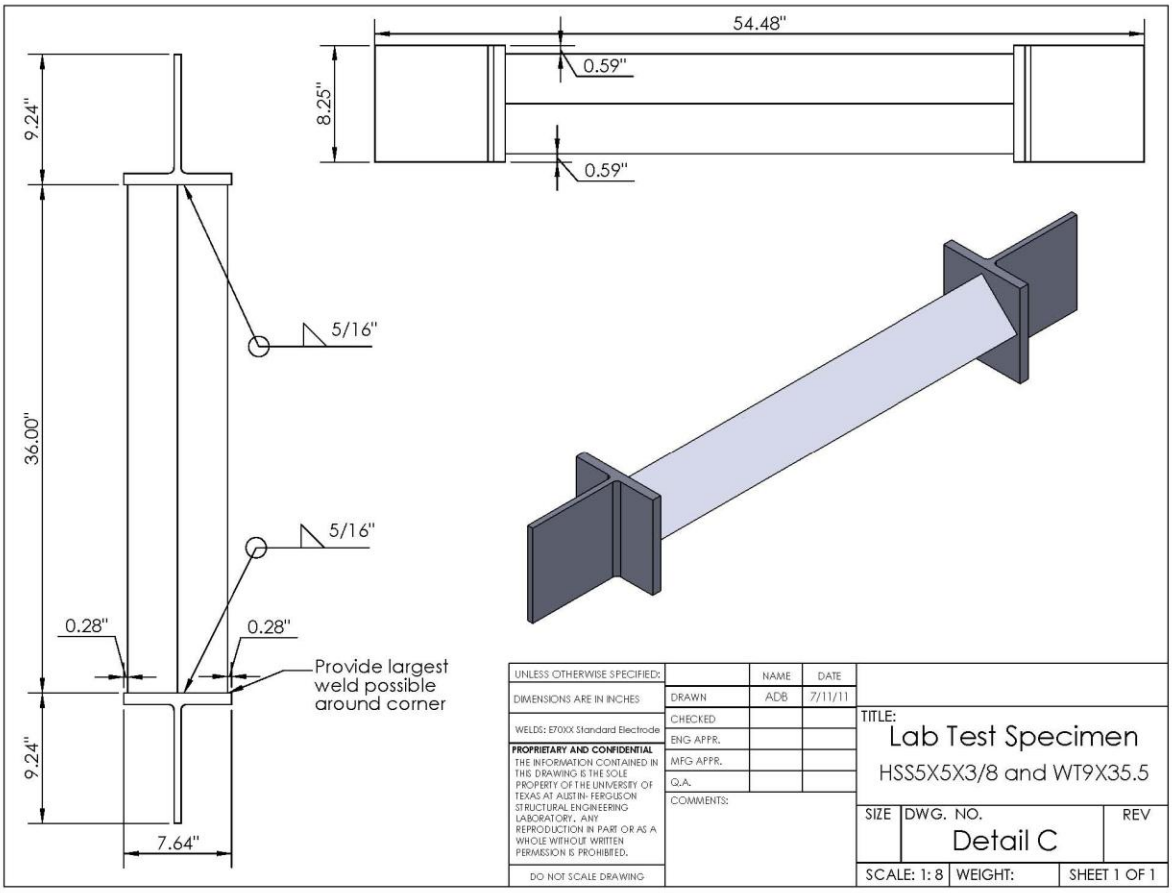

Figure 5.31: Diamond HSS Specimen with T-Stem Connection Detail

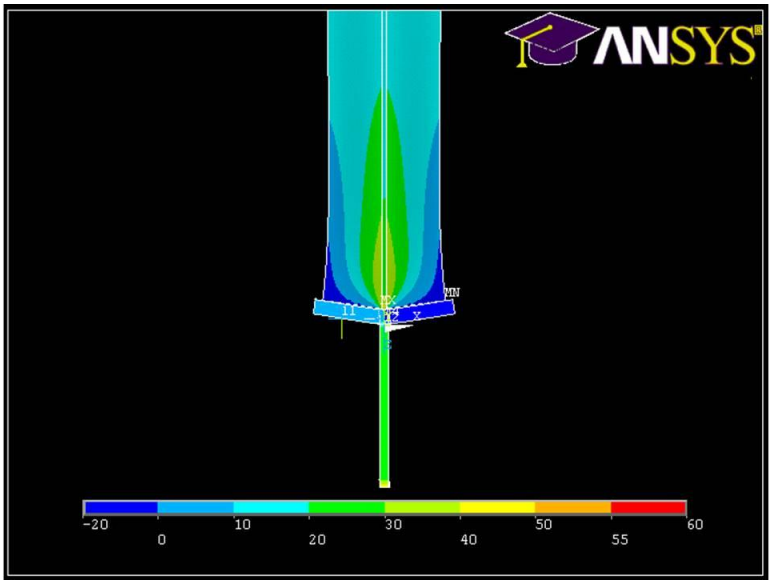

Figure 5.32: Longitudinal Stress [ksi] in Diamond HSS Tube Wall

In order to improve the finite element model associated with the experimental tests, numerous strain gages were attached to the HSS tube walls to measure the strain at various load levels. The general purpose strain gages were manufactured by Vishay Micro-Measurements with a 350 Ω resistance. In order to further examine the stress concentration effect, many gages were used in that particular region, as shown in Figure 5.33. Gages were also applied in the same pattern on the opposite wall to eliminate any effects from bending occurring due to an out-of-straightness of the specimen in the testing machine.

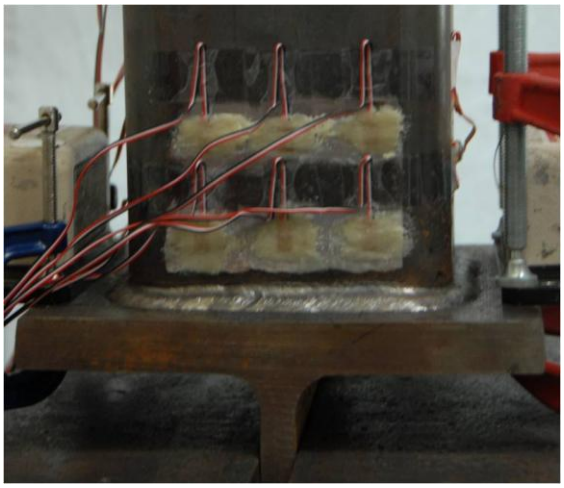

Figure 5.33: Strain Gages Applied to Tube Wall

5.7 T-STEM CONNECTION LABORATORY EXPERIMENTS

5.7.1 Stiffness Tests

A series of stiffness tests were performed on the T-stem connection using an HSS 5 x 5 x 3/8 member fillet welded to the flange of WT 9 x 35.5 connections. The tests included the square, round, and diamond HSS detail as outlined in the previous section. An additional test utilizing a complete joint penetration groove weld with the square HSS connection was also performed and showed similar results to the fillet weld specimen. Figure 5.34 shows the stiffness data obtained from the tests.

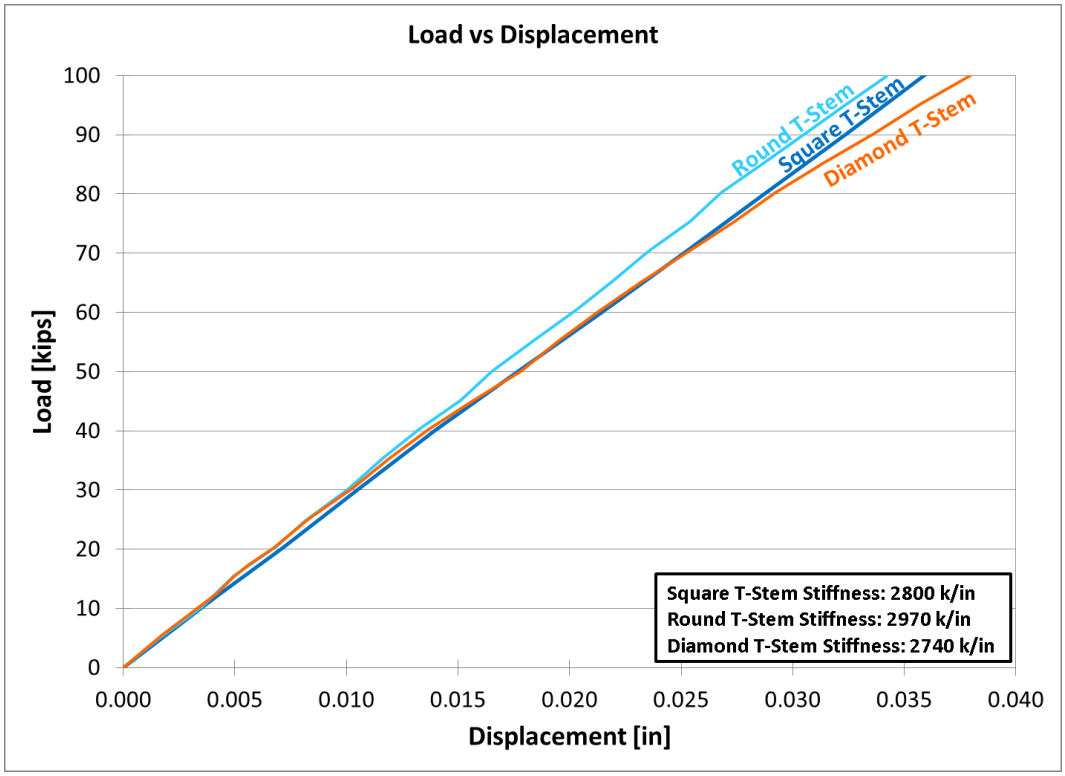

Figure 5.34: T-Stem Connection Stiffness Data

In order to compare the various connections' performance, it is necessary to account for the area of the tubular member used. This will be discussed later in this chapter. However, since the square and diamond HSS connections use the same connections and tubes, their performance can be directly compared. Looking at the graph, we see the Square HSS connection is slightly stiffer than the Diamond HSS connection; however, they are practically the same, which is expected since the two specimens utilize the same connections and member.

5.7.2 Ultimate Strength Tests

After obtaining the stiffness of the T-stem connections, the tests were continued into the inelastic range to determine the ultimate strength and failure mechanism of the detail.

5.7.2.1 Square HSS 5 x 5 x 3/8 and WT 9 x 35.5 Connections

Using standard connection strength calculations, it was determined the limiting strength without resistance factors was approximately 204 kips corresponding to yielding of the WT stem. However, the weld fractured much before this at an applied load of 152 kips. The premature failure of the connection indicates the danger the aforementioned stress concentration poses on the behavior of the tubular member. The failure also highlights the necessity for a more accurate prediction method of the ultimate strength of the connection. Figure 5.35 shows the force versus displacement behavior of this connection type and Figure 5.36 shows the fractured condition of the specimen.

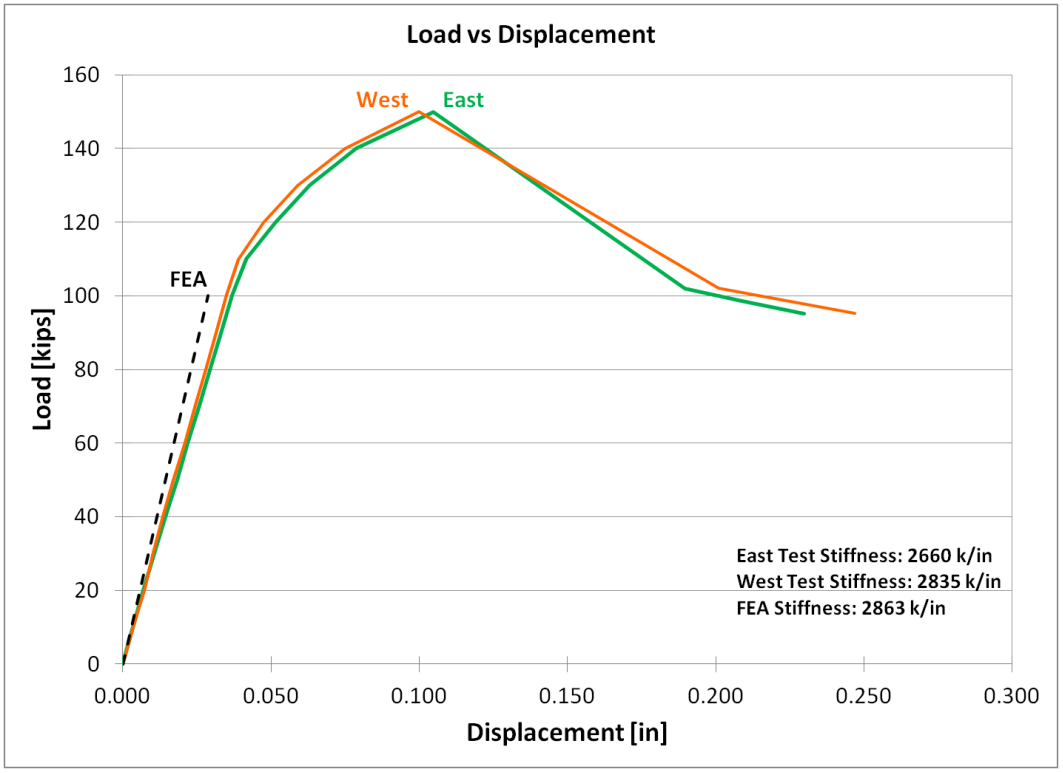

Figure 5.35: Ultimate Strength Test of Square HSS 5 x 5 x 3/8 and WT 9 x 35.5

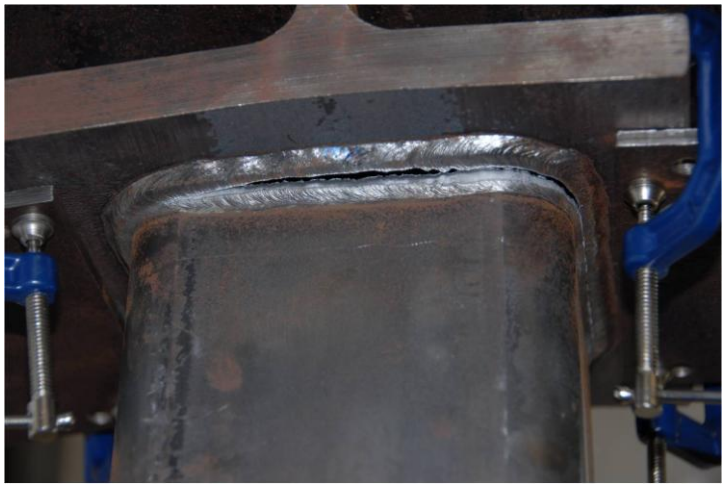

Figure 5.36: Fracture in Fillet Weld Connection

5.7.2.2 Square HSS 5 x 5 x 3/16 and WT 12 x 31 Connections

A second square HSS specimen tested in tension consisted of an HSS 5 x 5 x 3/16 fillet welded to WT 12 x 31 connections. Similar to the previous test, the failure occurred in the weld prior to reaching its calculated strength. According to the strength calculations, yielding in the tube should have been the limiting state at a load of 187 kips. However, the welded connection fractured at a load of 114 kips. Load-displacement data for the test is given in Figure 5.37 and a photo of the fractured member is shown in Figure 5.38. As opposed to the thicker walled specimen, this specimen exhibited a substantial amount of ductility as the fracture in the weld spread along the tube face perpendicular to the T-stem. Figure 5.38 also exemplifies the bending in the WT flange that occurs as the weld begins to fracture.

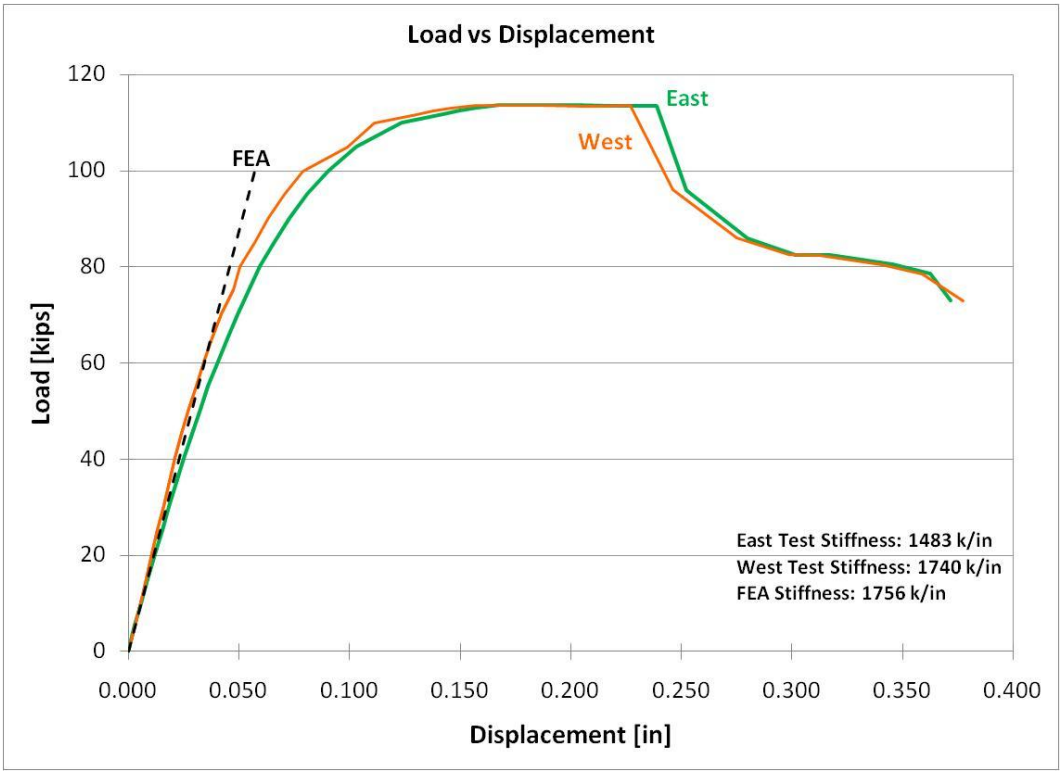

Figure 5.37: HSS 5 x 5 x 3/16 and WT 12 x 31 Stiffness Data

Figure 5.38: Fractured Connection

5.7.3 Fatigue Tests

In addition to the stiffness and strength behavior of the connections, it was necessary to determine the appropriate fatigue category for the connections according to the AASHTO Bridge design Specification. In order to assess the fatigue life, the test specimens were subjected to cyclic axial load to determine the fatigue design category.

Similar to the cast steel connection, the T-stem connection (square, round, or diamond) was designed to be concentric, however, at the local level, an eccentricity exists where the force is transferred from the flange of the T-stem into the wall of the tube. A cross section of the weld profile is shown in Figure 5.39.

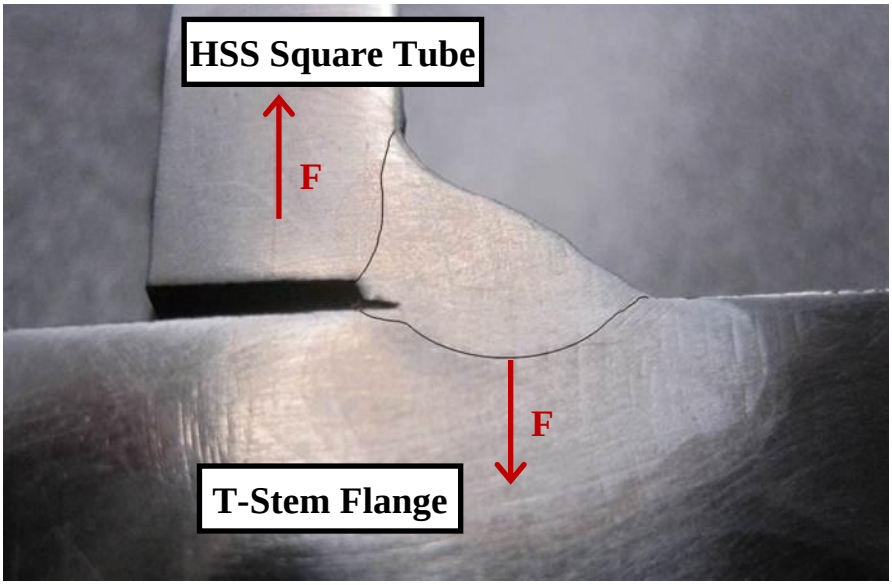

Figure 5.39: T-stem Connection Weld Eccentricity (with Weld Penetration Enhanced)

To highlight this effect, see the stress data obtained in Figure 5.47 though Figure 5.52. As will be seen, strain gages very close to the weld (less than 1 in away from the weld toe) indicate significant tension stresses where the FEA model would indicate compression, or low tensile stresses. But since the connection has the eccentricity shown in Figure 5.39, shear lag effects and localized bending would explain why these gages are actually experiencing larger tensile forces.

Unfortunately, this eccentricity drastically reduced the fatigue life of the connection. Due to the early failures of these HSS fillet welded specimens, a specimen utilizing a complete joint penetration groove weld was fabricated. The detail included a backup bar on the inside of the tube and was extremely difficult to fabricate. Plans of the detail are given in Figure 5.40.

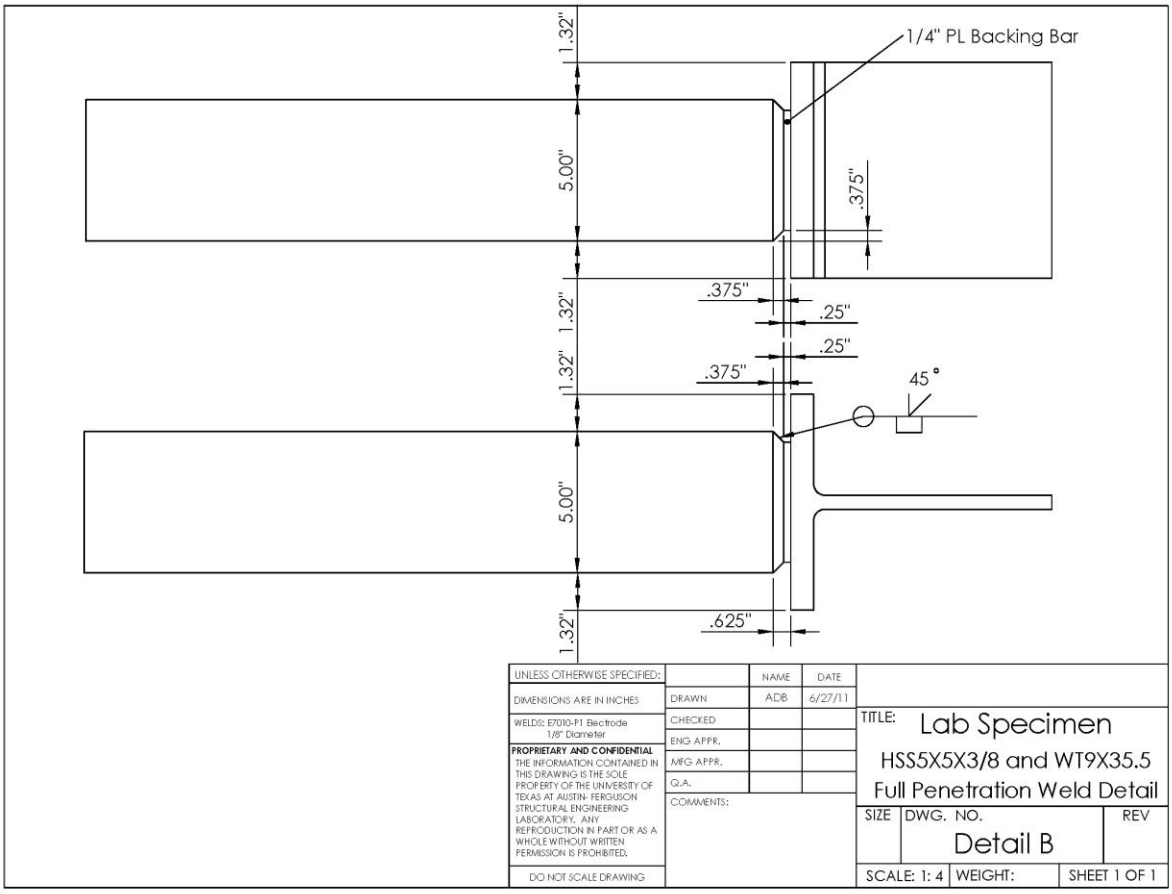

Figure 5.40: Complete Joint Penetration Groove Weld Detail

While this may not be a practical design option due to the high cost of complete joint penetration groove weld, it represented the maximum strength that could be expected from this detail.

The tests presented in this section were conducted at stress cycles of 5 and 10 ksi applied at a 1.4 Hz frequency. The HSS tubes were connected to the WT 9 x 35.5

connections with 5/16″ fillet welds. The following S-N plot was created with the results. The stress range plotted is the applied load divided by the area of the tube. Similar to the cast connections, no shear lag factor was included since the T-stem connection was concentric. Examples of fatigue cracks in the different details are presented in Figure 5.42 to Figure 5.45.

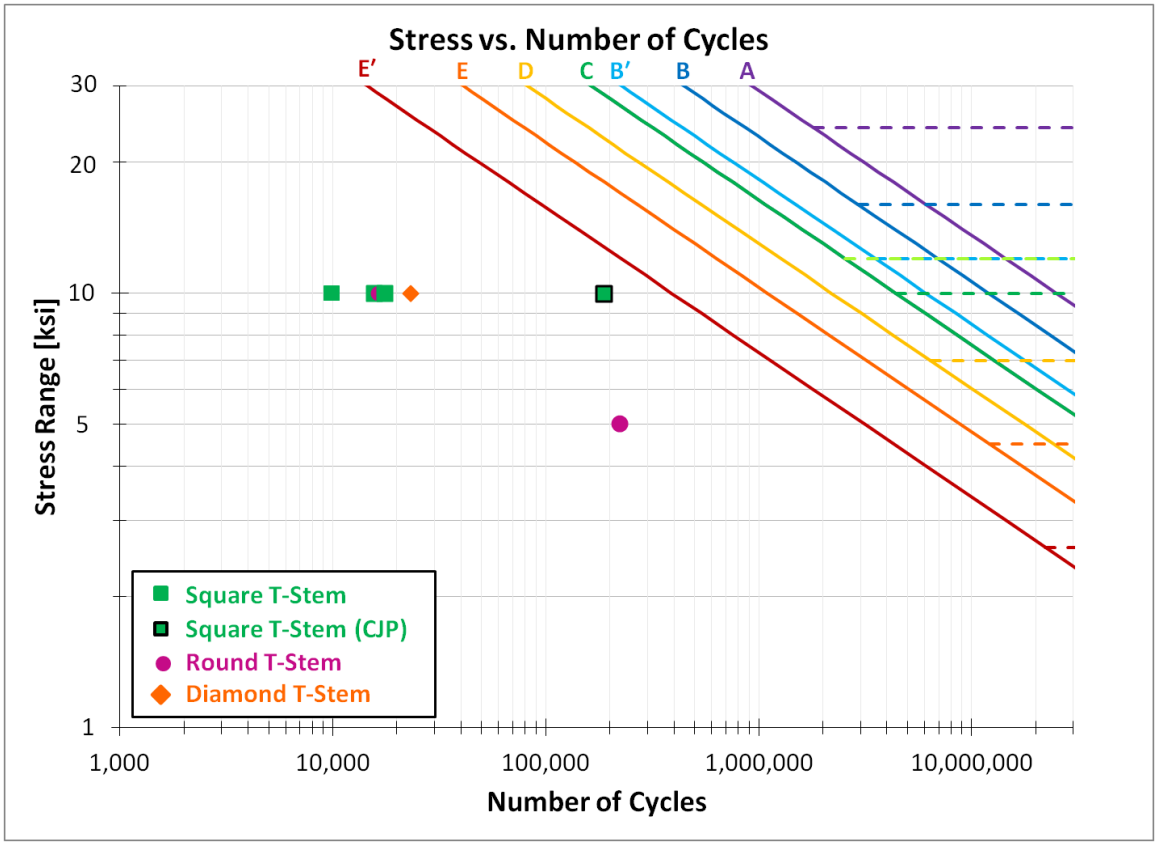

Figure 5.41: Fatigue Test Results

Figure 5.42: Example of Fatigue Crack Forming at Fillet Weld Root in Square HSS Connection

Figure 5.43: Example of Fatigue Crack Forming at CJP Weld Toe in Square HSS Connection

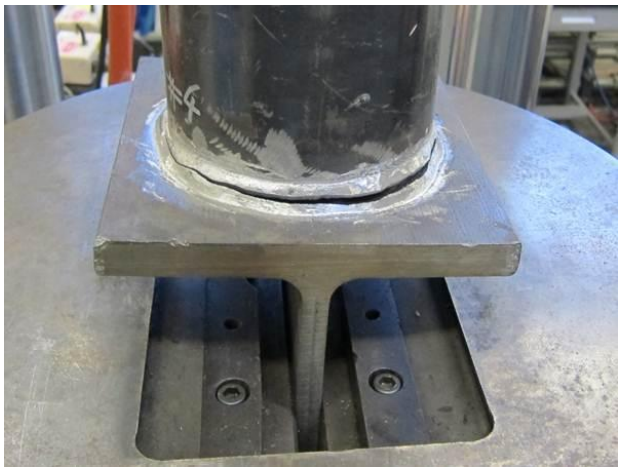

Figure 5.44: Example of Fatigue Crack Forming at Fillet Weld Root in Round HSS Connection

Figure 5.45: Example of Fatigue Crack Forming at Fillet Weld Root in Diamond HSS Connection

Unfortunately, none of the specimens reached the required number of cycles for fatigue categories allowed by AASHTO for use in steel bridge construction. Even the CJP specimen only reached half the life required by the E′ detail, the lowest of the AASTHO allowed categories. The reason the CJP specimen failed was the aforementioned stress concentration in the wall of the tubular member perpendicular to

the stem. The high concentration of stress severely reduces the fatigue life of the specimens.

5.8 T-STEM CONNECTION MEASUREMENTS

Limited finite element analyses were carried out on the T-stem connection. The model was validated using strain and displacement measurements from the connection test. To directly compare the results of the model to the experiment, each specimen was accurately measured to match all dimensions, including the thickness of the tube walls, width of the tube walls, and the thicknesses of the WT stems and flanges. The following subsections describe the model validation process. Although this detail was not studied extensively using FEA software, the procedure and measurements outlined was conducted for all finite element models of the remaining small scale connection tests.

5.8.1 Strain Comparisons

Using the strain data provided by the gages placed on the specimens, the associated stress was calculated by multiplying by the modulus of elasticity. The test stress data was then compared to the stress in the FEA model at various locations.

5.8.1.1 Square HSS 5 x 5 x 3/8 and WT 9 x 35.5 Connection

The first specimen had numerous gages attached along the length of the member for validation of the FEA model. The following plots summarize the information. In general, the data for gages located away from the welded connection matched better than those very near the connection and therefore most affected by the stress concentration.

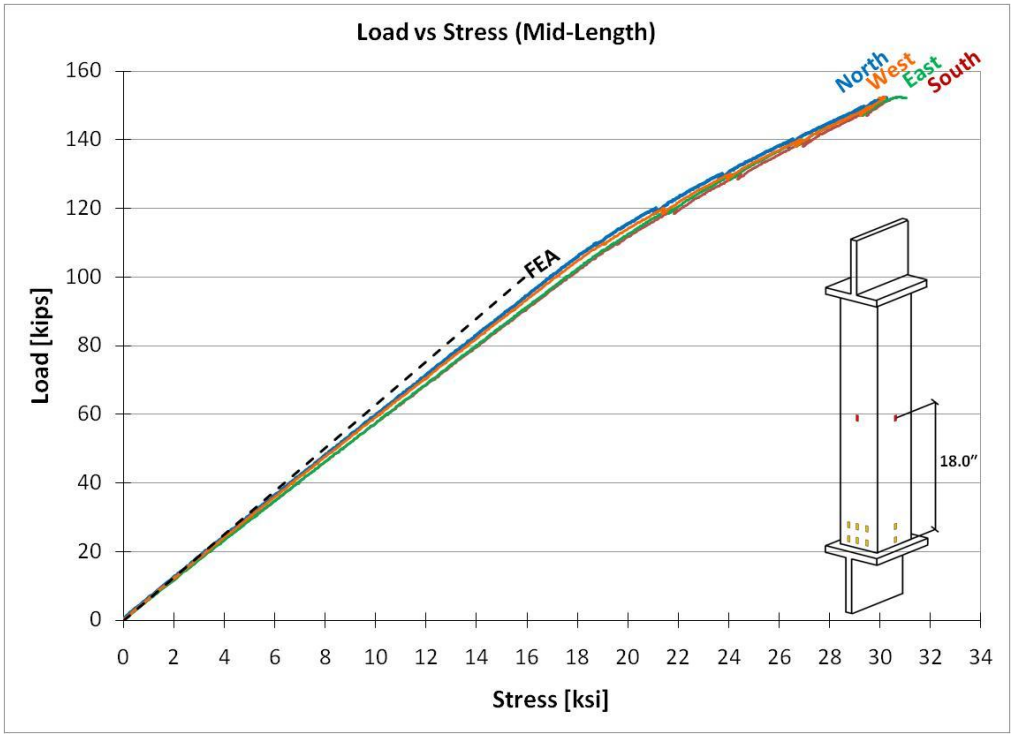

Figure 5.46: Load vs Stress at Mid-Length

Figure 5.46 shows the results for gages located at mid-length. It is important to note that at this location, the gages indicate the member is experiencing uniform stress, which is the general assumption used when calculating the strength and stiffness of the member. The length of the members was selected to obtain this condition so that edge effects resulting from the connections would not play a factor in the data obtained for any of the specimens.

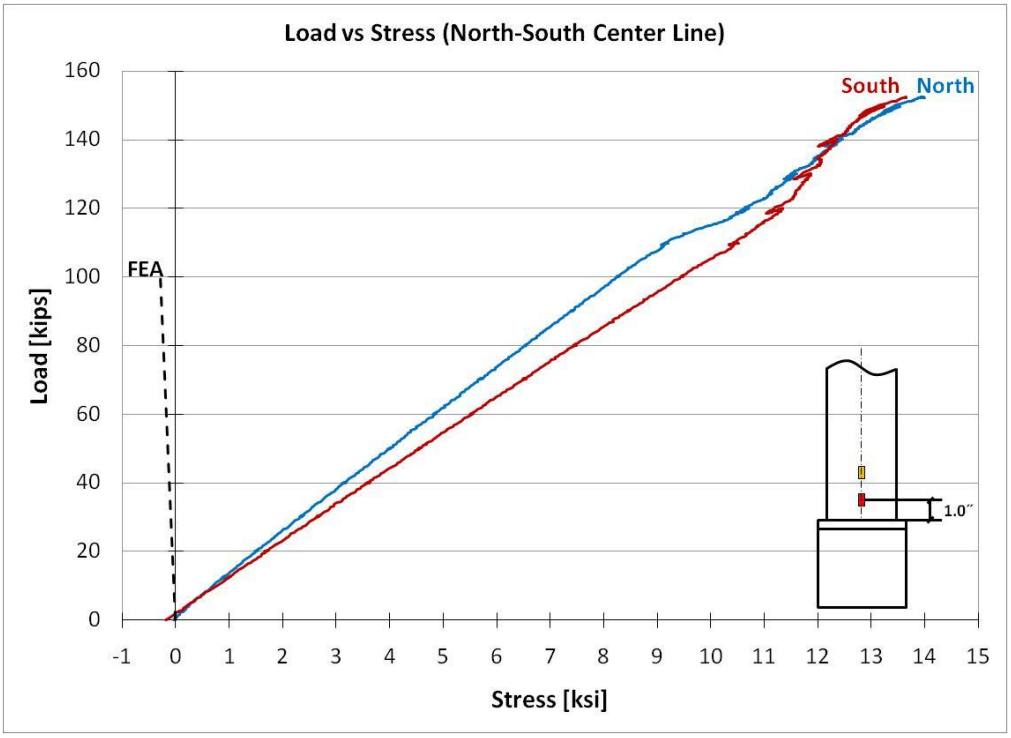

Figure 5.47: Load vs Stress at 1.0" from Connection (N-S Faces)

Figure 5.47 shows the load versus stress response for gages located on the tube walls parallel to the T-stem. From the analysis, these locations should experience compression, however the data measured indicated tension, showing that the connection may not be behaving as predicted. The stress readings on both faces do have similar values, which confirm the specimen was well aligned in the testing machine and that any bending of the member due to out-of-straightness was negligible. It is believed the complicated stress pattern near the welded connection is the reason for this large error, which was confirmed by comparing the results further from the connection in Figure 5.48.

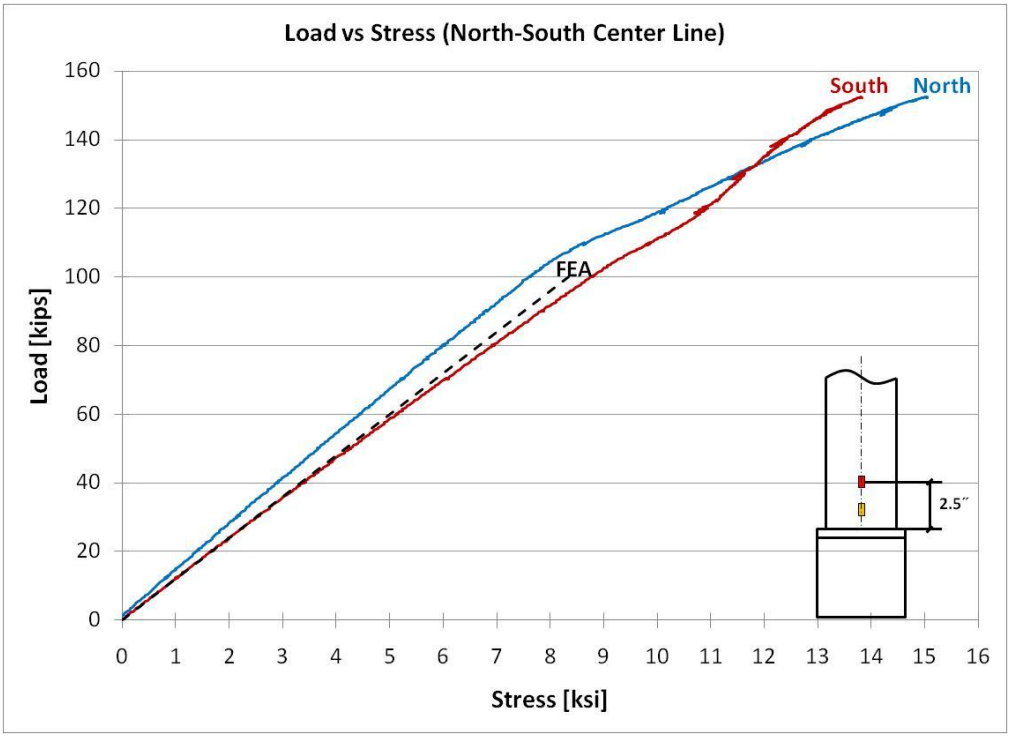

Figure 5.48: Load vs Stress at 2.5″ from Connection (N-S Faces)

Figure 5.48 also shows the stress response for the tube on the wall parallel to the T-stem. The gage readings shown further confirm the member did not experience bending (as described in the previous paragraph); in addition, these readings show that our FEA model was able to accurately capture the response of the member at the welded connection.

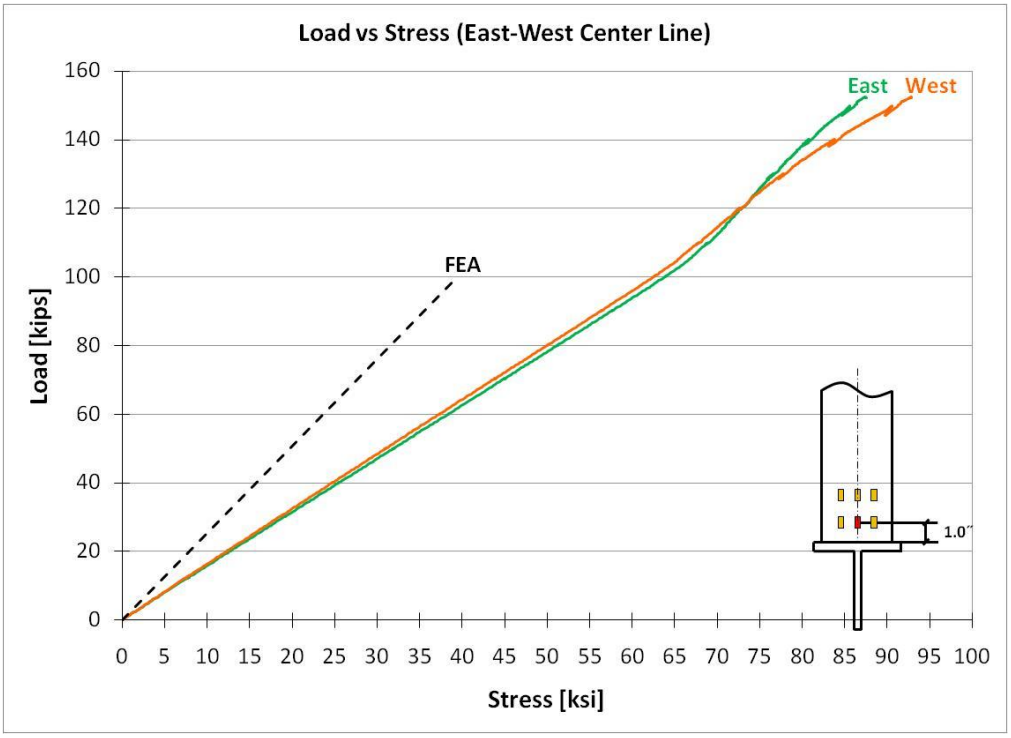

Figure 5.49: Load vs Stress at 1.0" from Connection (E-W Faces)

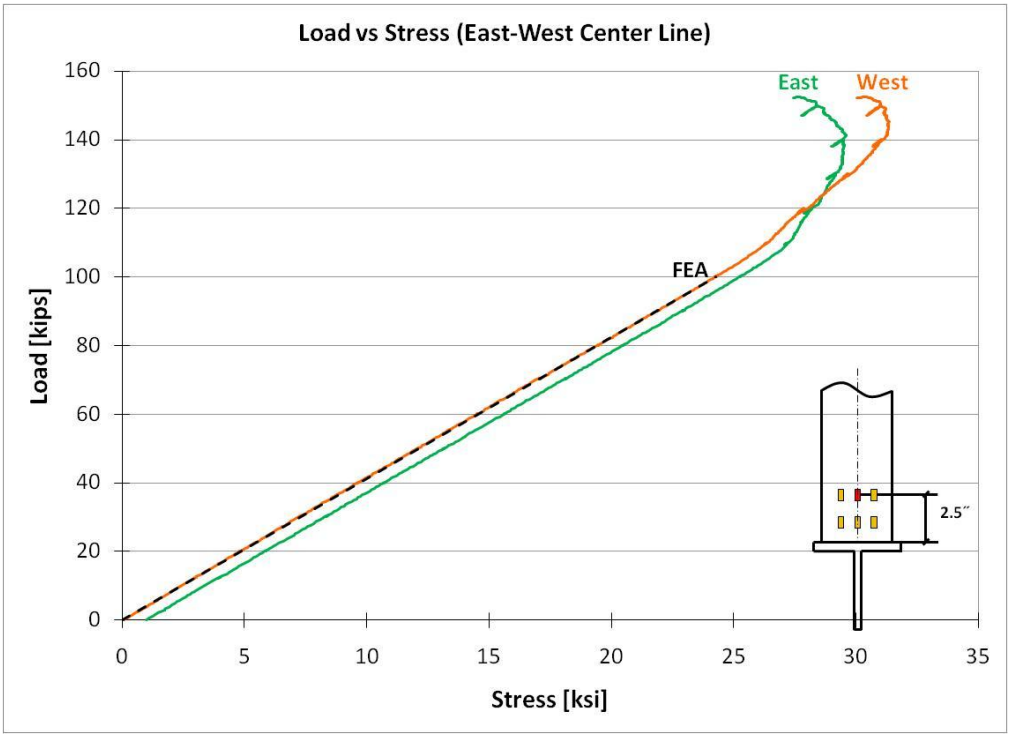

Figure 5.50: Load vs Stress at 2.5" from Connection (E-W Faces)

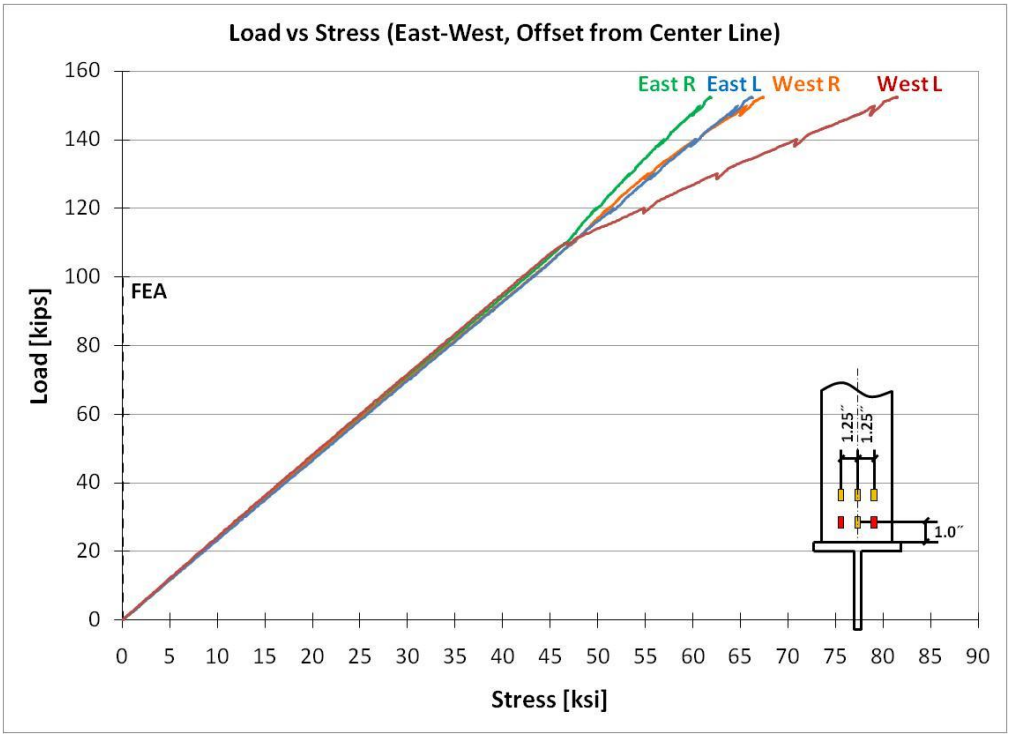

Figure 5.51: Load vs Stress at 1.0" from Connection (E-W Faces, Off Center)

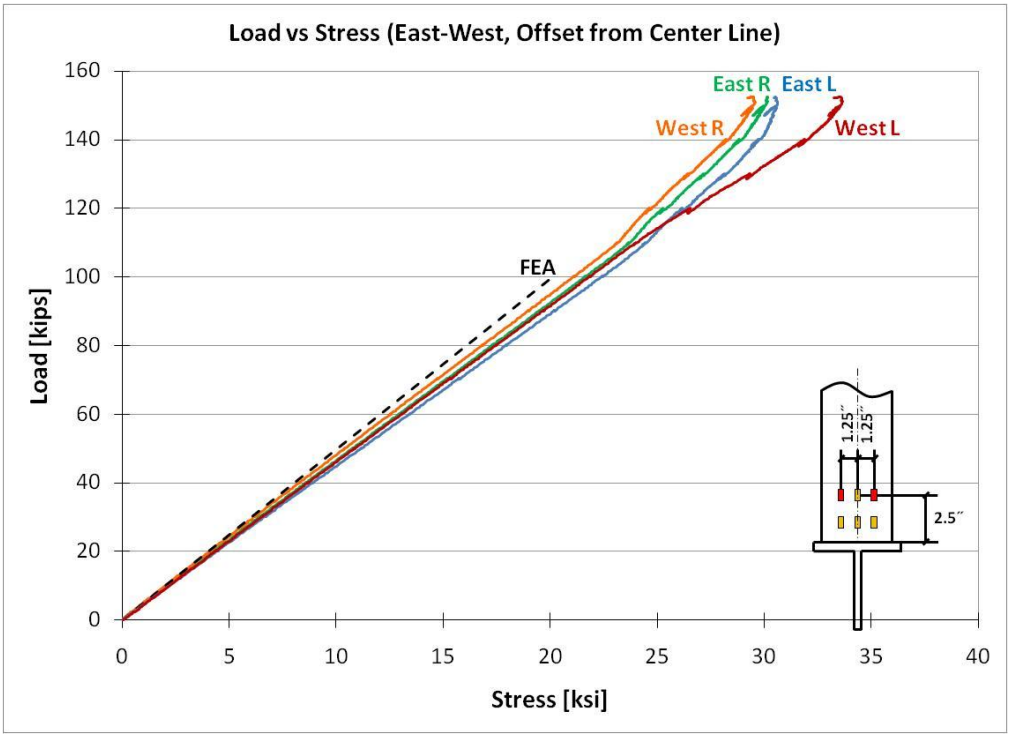

Figure 5.52: Load vs Stress at 2.5" from Connection (E-W Faces, Off Center)

Similarly, Figure 5.49 through Figure 5.52 corroborate the observations from Figure 5.47 and Figure 5.48. Near the connection (1 in away), the data measured had large discrepancies with the FEA results, but further from the connection (2.5 in away), the model was accurately capturing the behavior.

5.9 T-STEM CONNECTION TEST CONCLUSIONS

Multiple tests were performed on HSS members with T-stem connections. Due to the large stress concentration in the wall of the tube perpendicular to the stem, failure occurred in the welded connection prior to calculated failure loads using standard connection limit states. In terms of fatigue, the T-stem detail with square, round, and diamond HSS combinations performed very poorly and is not recommended for use in bridge applications where fatigue problems are critical.

Part III: Knife-Plate Connection

5.10 KNIFE-PLATE CONNECTION DESIGN

A third option for a connection to a tubular member investigated in this research was the knife-plate connection (or slotted tube connection). The connection involves creating a slot in the tube in which the gusset plate can be inserted, then fillet welding the tube to the plate. Figure 5.53 shows a picture of the completed knife-plate connection.

Figure 5.53: Knife-Plate Connection

Due to shear lag in this type of connection, a stress concentration will develop at the forward edge of the fillet weld in the tubular member. Further details on the failure mechanisms and fatigue test results from previous research were discussed in Chapter 3.

5.10.1 Stress Relief Hole

One way to improve the stress concentration at the forward edge of the fillet weld is to drill a stress relief hole. The hole creates a small region of compression in the vicinity of the start of the fillet weld, improving the fatigue life of the detail. The hole forces the tension stress to be "diverted" away from the forward edge, engaging the weld more uniformly along the length and minimizing the stress concentration. Figure 5.54 shows the knife-plate connection with the stress relief hole drilled.

Figure 5.54: Knife-Plate Connection with Drilled Stress Relief Hole

5.10.2 Slot Fabrication

To make the slot in the tube to receive the gusset plate, two methods were employed to determine if the fabrication had any effect on the fatigue performance of the detail. The first method involved drilling the stress relief hole and then saw-cutting the slot from the tube edge into the hole. The second method used a plasma torch to create the rectangular slot without the stress relief hole. The finishes obtained with both methods are shown in Figure 5.55.

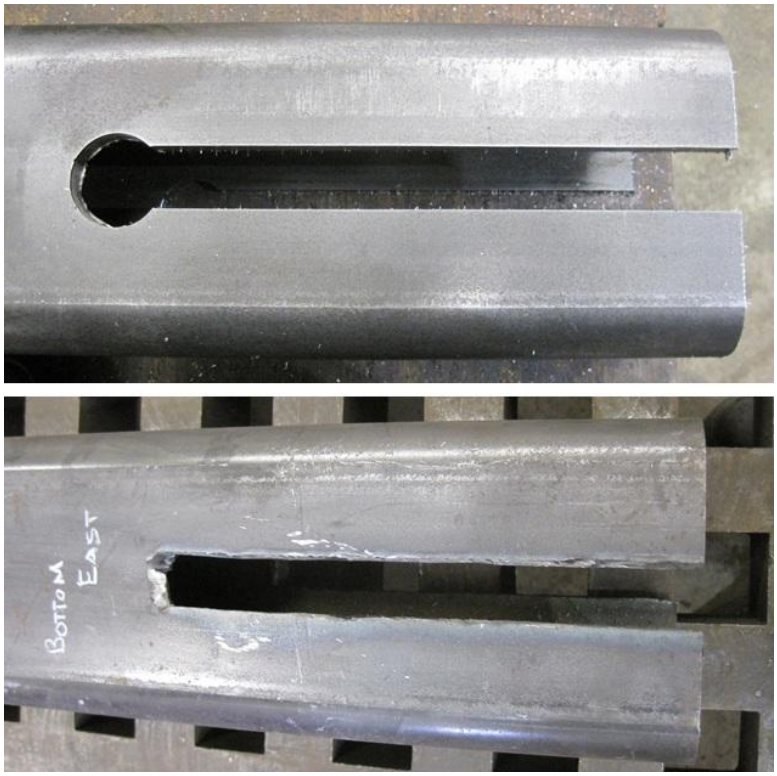

Figure 5.55: Fabrication of Knife-Plate Connection Using (a) Band Saw and (b) Plasma Torch

In all cases, the slot was centered on the wall of the square HSS 5 x 5 x 3/8 tube and the fillet weld connection length was 8 inches. The specimens with stress relief holes had diameters of 1-5/16 inches, 1-5/16 inches, and 1-1/2 inches respectively. The gusset plates were cut from PL7 x 0.75 flat bar and were 20 inches long to allow for the connection length and suitable grip length for the MTS Universal Testing Machine. The weld was specified to be 5/16 inches. Table 5.3 summarizes the six test specimens tested in the experimental test program.

Table 5.3: Experimental Test Program for the Knife-Plate Connection

Laboratory Test Program					
	Test Designation	**HSS Member**	**Connection**	**Slotted Connection Fabrication**	**Stress Relief Hole Diameter**
Fatigue Tests	KP1	HSS 5 X 5 X 3/8	PL 7 x 0.75	Band Saw	1-5/16″
	KP2	HSS 5 X 5 X 3/8	PL 7 x 0.75	Plasma Torch	None
	KP3	HSS 5 X 5 X 3/8	PL 7 x 0.75	Band Saw	1-5/16″
	KP4	HSS 5 X 5 X 3/8	PL 7 x 0.75	Plasma Torch	None
	KP5	HSS 5 X 5 X 3/8	PL 7 x 0.75	Plasma Torch	None
	KP6	HSS 5 X 5 X 3/8	PL 7 x 0.75	Band Saw	1-1/2″

5.11 KNIFE-PLATE CONNECTION LAB EXPERIMENTS

Laboratory experiments were performed on the knife-plate connection to determine the stiffness of the tube and connection system as well as to determine the appropriate AASHTO fatigue category.

5.11.1 Stiffness Tests

The stiffness tests for the knife-plate specimen followed the parameters outlined at the beginning of the chapter. Figure 5.56 shows the stiffness test results.

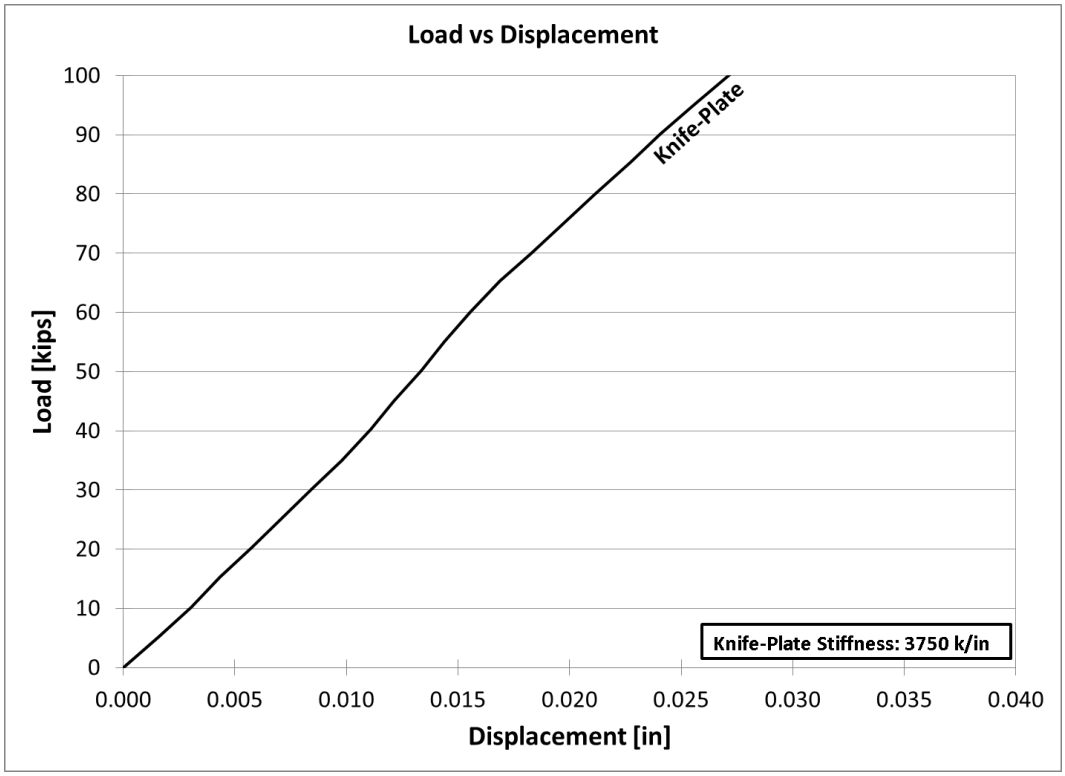

Figure 5.56: Knife-Plate Connection Stiffness Test Results

5.11.2 Ultimate Strength Tests

No ultimate strength tests were undertaken for the knife-plate connections. Numerous tests are described in the literature, and were mentioned in Chapter 3. In addition, for the HSS 5 x 5 x 3/8 tube, the MTS testing apparatus used in all the stiffness and fatigue tests did not have the necessary capacity.

5.11.3 Fatigue Tests

In total, six knife-plate specimens were tested in fatigue, three with the stress relief hole and three with only plasma torch-cut slots. The specimens with the stress relief hole achieved the AASHTO Category E detail, with one specimen achieving Category D. The specimens without the stress relief hole ranged from Category E′ to Category E. The one specimen failing prematurely had very large gaps in the fabrication of the torch cut slot. The results are plotted in Figure 5.57, with the plotted stress range

including the effect of shear lag, using the AISC shear lag factor for rectangular HSS [AISC Table D3.1 2010].

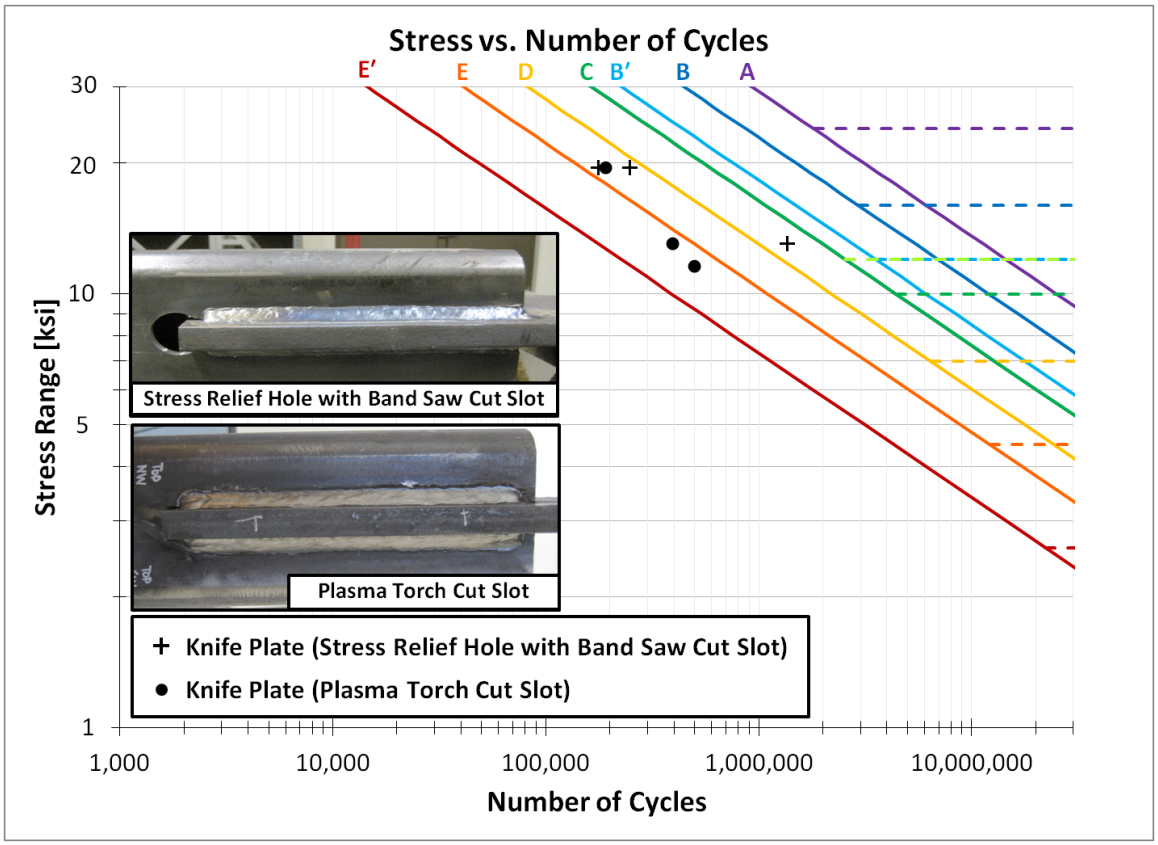

Figure 5.57: Fatigue Tests of Knife-Plate Connections

The fatigue tests indicated the knife-plate connection as a possible solution for cross frame connections. Examples of fatigue cracks in the stress relief hole specimens and the torch-cut slot specimens are shown in Figure 5.58 and Figure 5.59 respectively.

Figure 5.58: Knife-Plate Connection Fatigue Crack (Stress Relief Hole)

Figure 5.59: Knife-Plate Connection Fatigue Crack (Torch-Cut Slots)

5.12 KNIFE-PLATE CONNECTION FINITE ELEMENT ANALYSIS

Results from the stiffness tests were used to validate both a shell element and solid element FEA model of the knife-plate connection. The solid element model is shown in Figure 5.60.

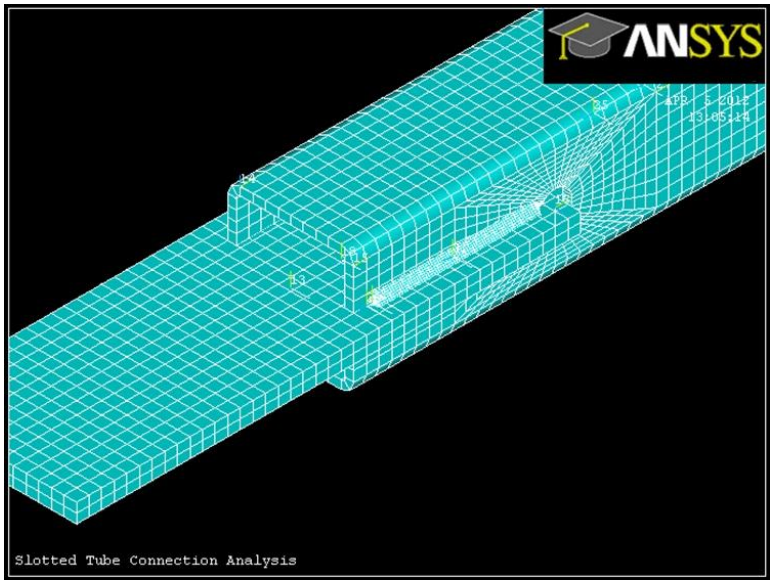

Figure 5.60: Knife-Plate Connection FEA Model

5.13 KNIFE-PLATE CONNECTION CONCLUSIONS

The test data suggests that the knife-plate connection is feasible for use with tubular members in cross-frames. In terms of fabrication, careful plasma-torching of the slot seems to not affect the fatigue performance as significantly as the presence of the stress relief hole. It is possible to combine the two fabrication techniques, using a plasma-torch cut slot and a drilled hole, which was performed on some of the cross frames tested in the large scale program described in Chapter 7. From the small scale component tests, the knife-plate connection achieves at minimum Category E′, and when including the stress relief hole can meet Category E behavior.

Part IV: Double Angle Connection

5.14 DOUBLE ANGLE CONNECTION DESIGN

A fourth option for single diagonal cross frame layouts is to use a double angle member. The connection detail would be similar to the current TxDOT X-type braces except that only a single diagonal member would be used, where the diagonal is a double angle member. One major advantage of using a double angle along the diagonal is the

elimination of connection eccentricity. The connections should have similar fatigue ratings as the current details, and may improve as the concentric connection may reduce out-of-plane bending. The angle diagonals may still be connected at the midpoint by welding the angles to a spacer plate as this helps the double angle to work as a single member. But the resulting fabrication requirements and material usage would be nearly identical to the current system, and may reduce as smaller angles may be possible for use on the diagonal. A picture of the double angle detail is shown in Figure 5.61.

Figure 5.61: Double Angle Detail

5.15 DOUBLE ANGLE CONNECTION LABORATORY EXPERIMENTS

Laboratory experiments for the double angle connection included stiffness, strength, and fatigue tests. The tests involved using a double angle member sized at L4 x 4 x 3/8, a typical size utilized in current TxDOT designed braces. The connection length to both gusset plates was 8 inches.

Three different gusset plate sizes were used, each with a length of 20 inches to allow for connection and grip length. The PL7 x 0.75 connections were sized to develop the strength of the double angle member in tension in the stiffness and strength tests, and were used in the first three fatigue tests. Since the majority of gusset plates used in real cross frames are only 0.5 in, three additional tests were conducted using PL7 x 0.5

connections. Lastly, a PL10.5 x 0.5 connection was tested, which offers the half inch thick plate while having the same area as the PL7 x 0.75 connections.

5.15.1 Stiffness Tests

The double angle detail was tested in tension according to the plan outlined at the beginning of the chapter. The results from the test are shown in Figure 5.62.

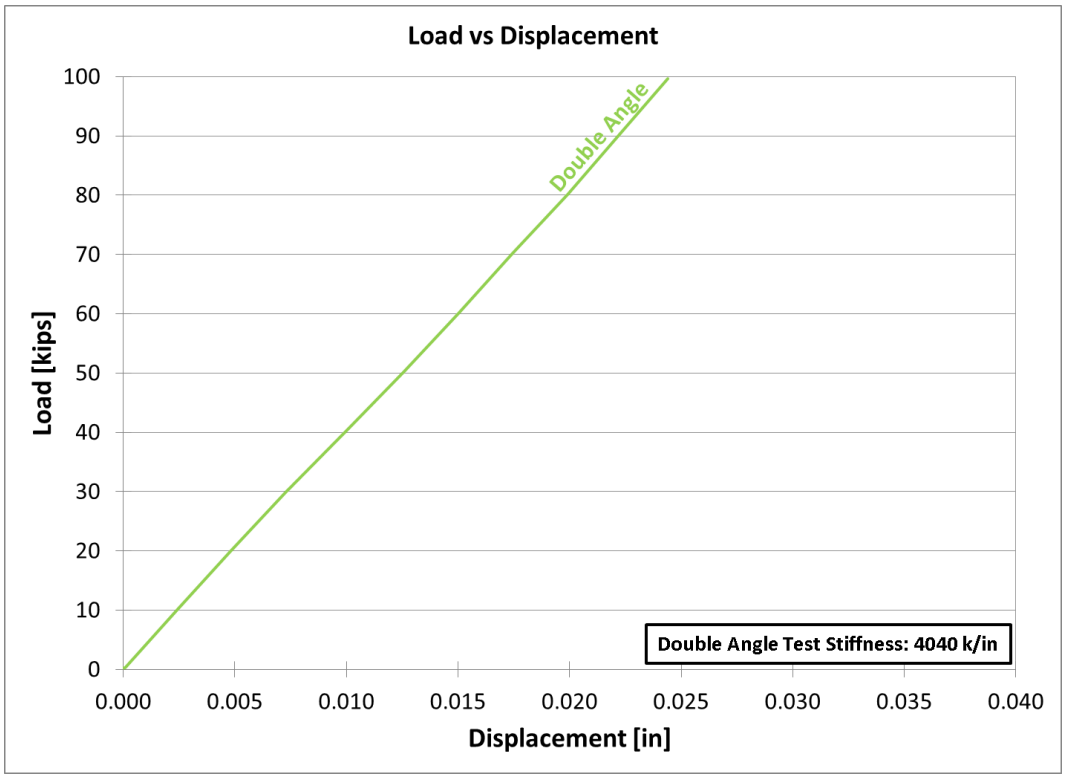

Figure 5.62: Double Angle Connection Stiffness Test Results

5.15.2 Ultimate Strength Test

To determine the strength and ductility offered by the double angle connection, tension was applied to the specimen to reach failure. However, the 220 kip MTS Universal Testing Machine did not have enough capacity to load the specimen to failure. The double angle reached the yield criteria and began to enter the strain hardening region. Before its ultimate strength was achieved, the machine reached its capacity. The

indication was significant ductility near yielding, and results from the single angle connection ultimate strength test support this observation. Figure 5.63 shows the data obtained from the test.

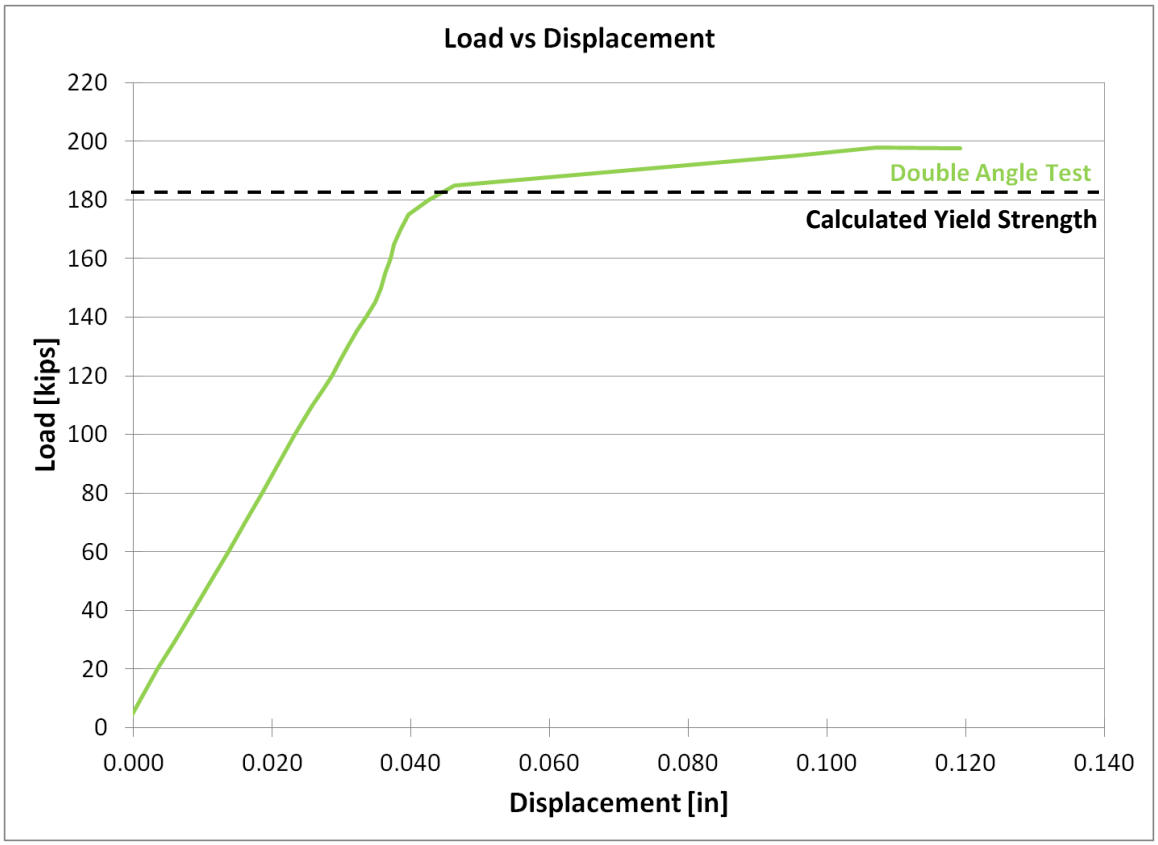

Figure 5.63: Double Angle Connection Strength Test Results

5.15.3 Fatigue Tests

As discussed in the introduction to Section 5.15, three different gusset plate sizes were tested in fatigue. The results from the experiments are given in Figure 5.64. The stress range was computed by dividing the nominal force by the double angle area, including the effect of shear lag as prescribed by AASHTO Table 6.6.1.2.3-1 [AASHTO 2012] and discussed in Chapter 3. The shear lag factor was calculated using the AISC equation for double angle members [AISC Chapter D 2010]. The inset figures in Figure 5.64 show a typical test from the side of the connection (top figure) and facing the connection (bottom figure).

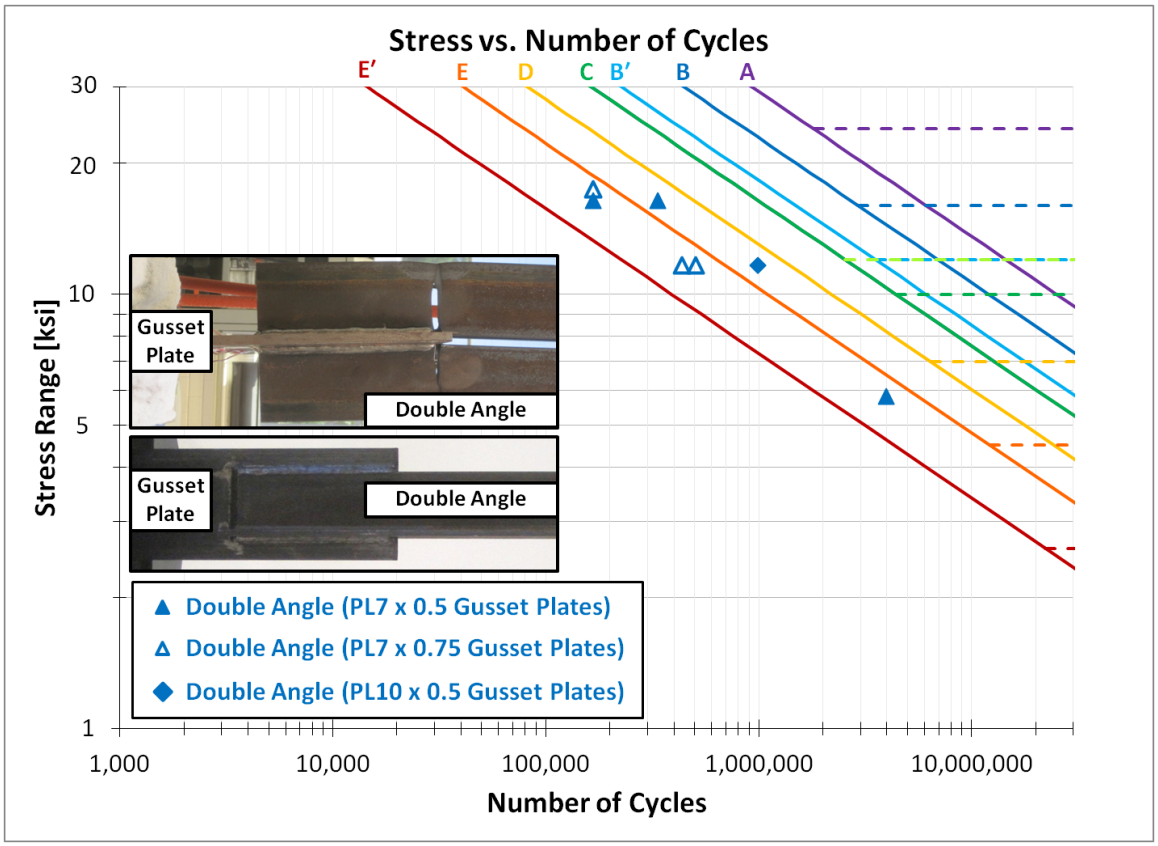

Figure 5.64: Double Angle Fatigue Test Results

From the fatigue tests, it is evident the double angle connection ranged from AASHTO Category E′ to E. Examples of fatigue cracks observed in the tests are shown in Figure 5.65 and Figure 5.66. When reducing from the 0.75 in gusset plate to the 0.5 in gusset plate, two specimens experienced fatigue cracks in the gusset plate. A review of the FEA model indicates there is a second area of stress concentration at the back edge of the angles, with the effect magnified as the stress in the gusset plate increases. Since the stress in the PL7 x 0.5 plates was substantially larger than in the 2L4 x 4 x 3/8 members, the fatigue crack initiated in the plate. The PL10.5 x 0.5 specimen shows that it is only a function of the stress range in the plate and not the thickness of material as the cracks in this test occurred in the angles.

Figure 5.65: Double Angle Connection Fatigue Crack (Angle Member)

Figure 5.66: Double Angle Connection Fatigue Crack (Gusset Plate)

5.16 DOUBLE ANGLE CONNECTION FINITE ELEMENT ANALYSIS

As with all the connections, an FEA model was validated using the strain/stress and displacement results measured from the experiments. Figure 5.67 shows the model with stress in the longitudinal direction plotted. The stress concentrations at the forward edges of the fillet weld in the angle are evident, as well as the second concentration at the bottom of the angle. Owing to further complexities of this type of member in the full-

scale cross frame fatigue tests (discussed in Chapter 7), limited analyses were performed on this connection type.

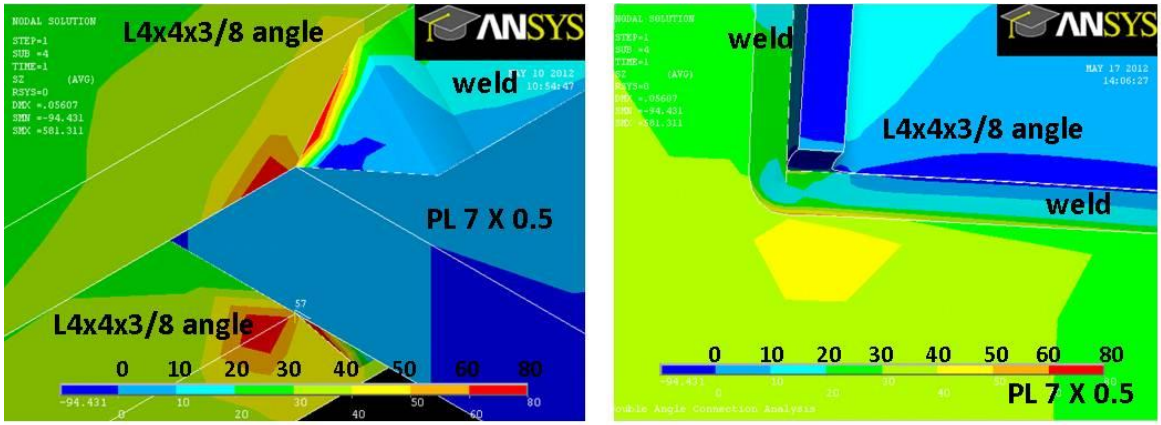

Figure 5.67: Double Angle Connection FEA Model with Stress Concentrations in the (a) Angle and (b) Gusset Plate

5.17 DOUBLE ANGLE CONNECTION CONCLUSIONS

Based on the individual member tests, the double angle seems to offer a suitable alternative to the existing single angle connection as it has the same AASHTO fatigue category (E′). However, the tests performed in fatigue seem to have the same boundary conditions as previous work for the single angles [McDonald and Frank 2009], potentially indicating that single angles may likely have worse fatigue behavior. Using the double angle along the diagonal only results in the same material usage as the X-type cross frame and offers the possibility of reducing the angle size to meet the same compression demands.

Part V: Single Angle Connection

5.18 SINGLE ANGLE CONNECTION DESIGN

The single angle connection tested was the L4 x 4 x 3/8 member fillet welded to a PL7 x 0.75 gusset plate, with an overlap of 8 inches. This detail is currently used in

practice and its performance was of interest to the researchers. Figure 5.68 shows the basic connection.

Figure 5.68: Single Angle Connection

5.19 SINGLE ANGLE CONNECTION LAB EXPERIMENTS

Laboratory experiments for stiffness, strength, and fatigue were desired for study in TxDOT Project 0-6564. However, due to the eccentric loading of the angle, fatigue tests were not possible. Therefore, another test setup involving fatigue testing of full scale cross frames was completed, and will be discussed in Chapter 7. In addition, extensive stiffness tests of various single angle cross frame types were conducted [Wang 2013].

5.19.1 Stiffness Tests

The single angle member was subjected to tension and the associated stiffness measured. Results from the stiffness test are plotted in Figure 5.69.

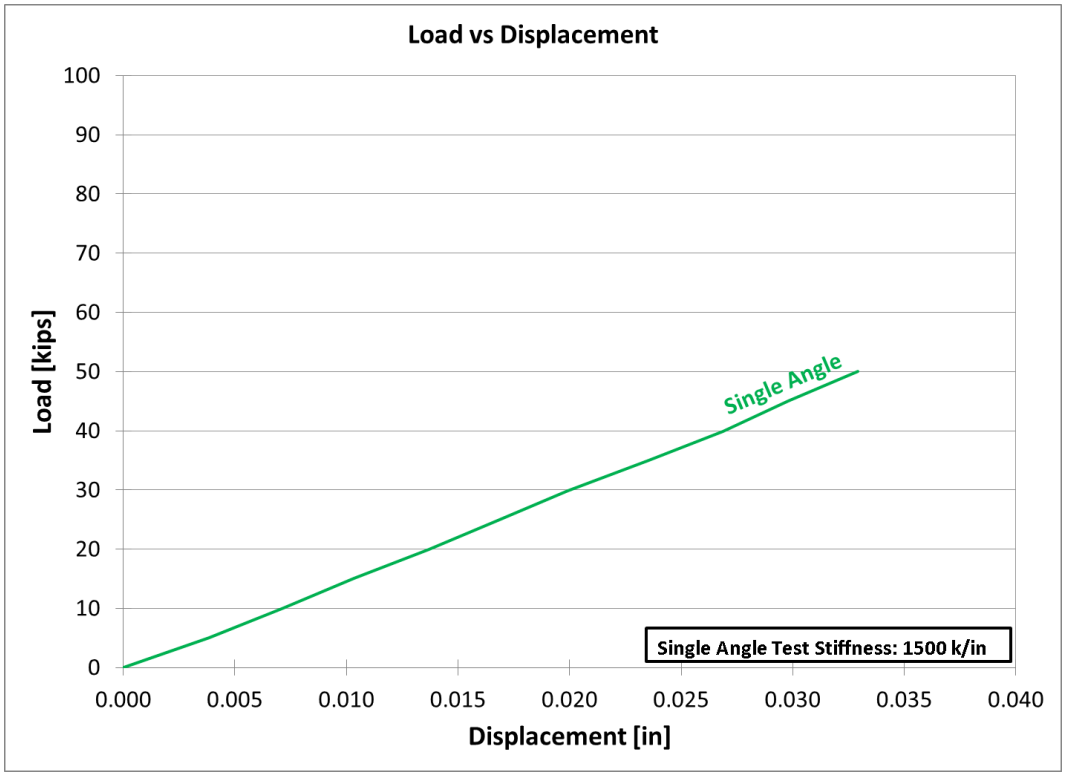

Figure 5.69: Single Angle Connection Stiffness Test Results

The eccentric loading of the angle significantly impacted the measured stiffness. Figure 5.70 shows the eccentricity of the member relative to the load through the gusset plate. The result is a substantial amount of bending, which reduces the stiffness.

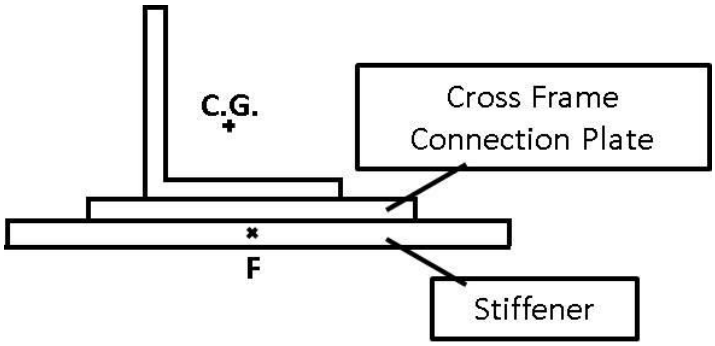

Figure 5.70: Single Angle Connection Eccentricity

5.19.2 Ultimate Strength Test

The single angle was tested to failure in the 220 kip MTS Universal Tension Machine. A significant amount of bending at the connection was observed. As the angle was loaded into the inelastic region, the angle yielded along the entire length, leading to a substantial amount of displacement. Unfortunately, the testing machine ran out of stroke length prior to fracture of the member. The data obtained is shown in Figure 5.71 and a picture of the deformed member is shown in Figure 5.72.

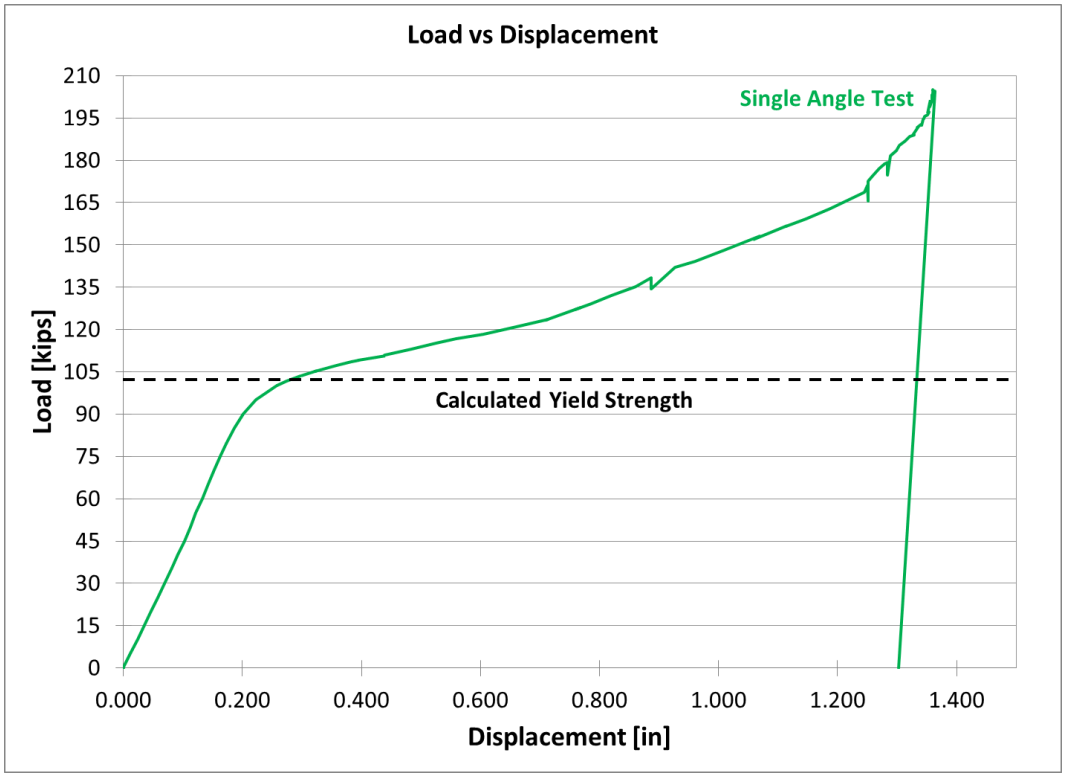

Figure 5.71: Single Angle Connection Ultimate Strength Test Results

Figure 5.72: Deformed Single Angle Connection in Tension

5.19.3 Fatigue Tests

As previously mentioned, concern for the testing machine due to the amount of bending of the single angle connection precluded the performance of any fatigue tests. Chapter 7 details an alternate test setup that was used to determine this detail's fatigue behavior.

5.20 SINGLE ANGLE CONNECTION FINITE ELEMENT ANALYSIS

Results from the stiffness test were used to validate a solid element FEA model of the single angle connection. Figure 5.73 shows the model in its deformed state, showing the out-of-plane deformation exhibited by the single angle connection.

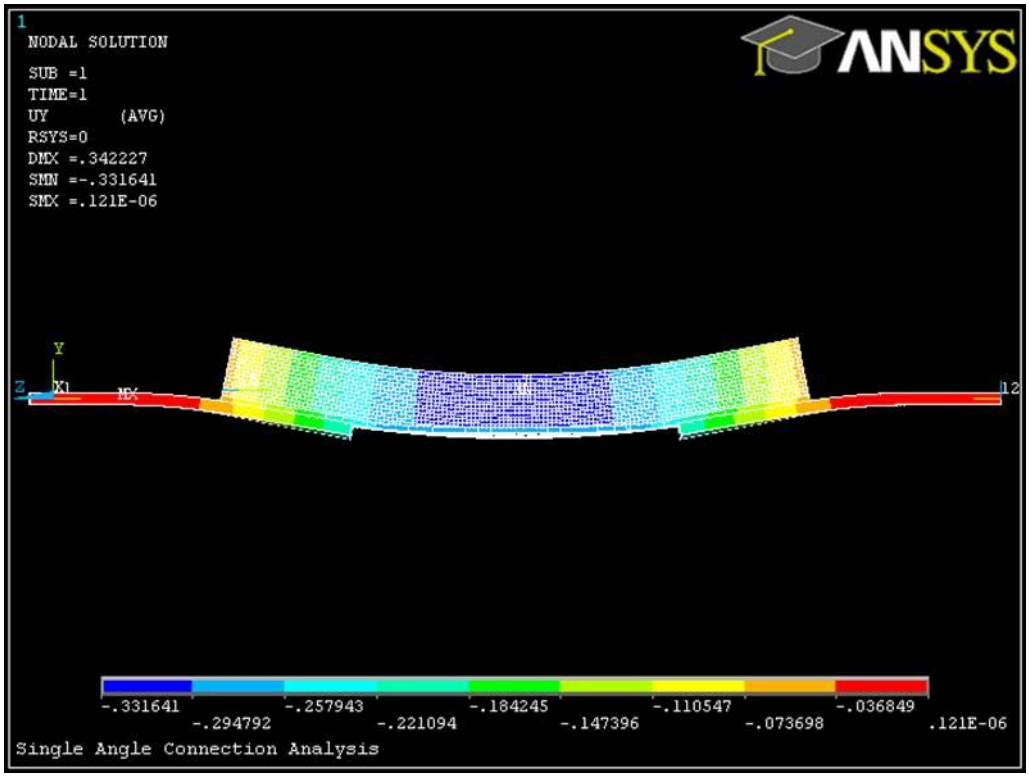

Figure 5.73: Single Angle Connection FEA Model

5.21 SINGLE ANGLE CONNECTION CONCLUSIONS

The single angle does not provide a very stiff connection due to the effect of the member bending under the eccentric loading. From a strength perspective, the detail meets typical strength checks and provides a significant amount of ductility. The fatigue behavior will be further examined in Chapter 7.

Part VI: Connection Comparison

5.22 CONNECTION STIFFNESS COMPARISON

In order to examine the overall performance of the five connection types tested, comparative analysis of the test results was conducted. The following sections describe methods of comparing the details to one another, and the results for both stiffness and fatigue behavior.

5.22.1 Modification of Torsional Brace Stiffness Formula

When calculating the in-plane stiffness of the cross frame, an elastic truss analysis is often employed [Yura 2001]. As previously stated in Chapter 2, for a tension-only system, the contribution of the compression diagonal is ignored, and the single diagonal model shown in Figure 5.74 (a) is analyzed.

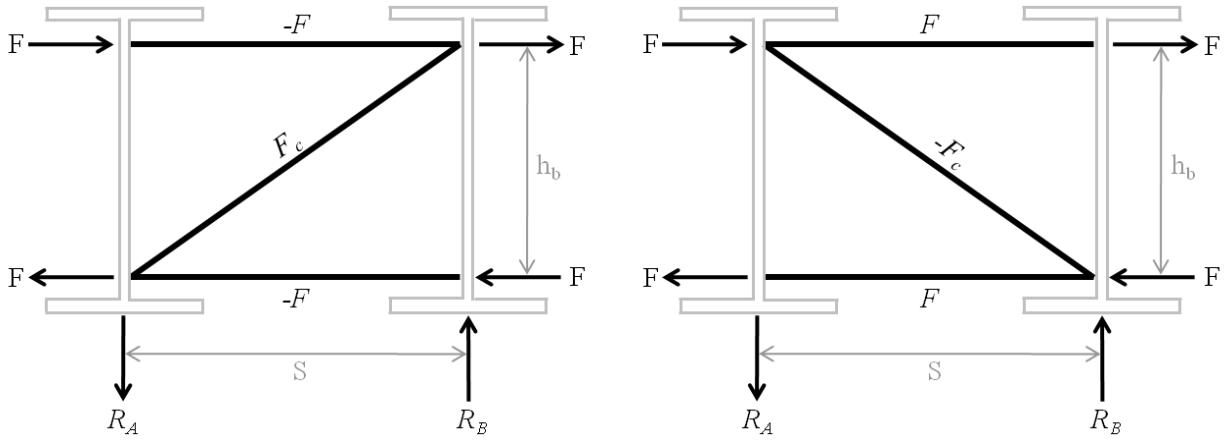

Figure 5.74: (a) Tension Diagonal System and (b) Compression Diagonal System

Following the derivation provided by Quadrato [2010], a deflection analysis on the tension-only diagonal system is performed to determine the rotation of the cross frame, and ultimately the torsional brace stiffness is (in accordance with the formula given by Yura [2001]):

$$\beta_{braxial} = \frac{E h_b^2 S^2}{\frac{2L_c^3}{A_c} + \frac{S^3}{A_h}} \tag{5.1}$$

where $\beta_{braxial}$ is the torsional brace stiffness of the cross frame considering only the axial stiffness of the cross frame members, E is the modulus of elasticity (29000 ksi), h_b is the height of the brace (centroid of top strut to centroid of bottom strut), S is the girder spacing, L_c is the length of the diagonal member, A_c is the area of the diagonal member, and A_h is the area of each strut. Eq. 5.1 assumes that the ends of the cross frame members are pinned.

Conversely, if the diagonal has significant buckling strength, the truss analysis could be performed on the geometry of Figure 5.74 (b), resulting in the same torsional brace stiffness as Eq. 5.1, with the diagonal member in compression instead of tension.

Eq. 5.1 offers a useful design calculation to determine the torsional brace stiffness of the cross frame, but it simplifies the typical cross frame geometry and it neglects the possible impact of the member connections. To better isolate the effects of the connection, it is useful to put Eq. 5.1 in terms of the stiffness of the strut and diagonal. Eq. 5.1 assumes the strut member stiffness to be defined as:

$$k_h = \frac{A_h E}{S} \tag{5.2}$$

and the diagonal member stiffness as:

$$k_c = \frac{A_c E}{L_c} \tag{5.3}$$

Revisiting the derivation of Eq. 5.2, but substituting Eqs. 5.2 and 5.3 where appropriate, the following formula for $\beta_{braxial}$ is obtained:

$$\beta_{braxial} = \frac{h_b^2}{\frac{2L_c^2}{k_c S^2} + \frac{1}{k_h}} \tag{5.4}$$

5.22.2 Calculation of the Connection Stiffness, $k_{connection}$

In order to determine the stiffness of the members, the equation for springs in series will be used:

$$\frac{1}{k_T} = \frac{1}{k_{member}} + \frac{1}{k_{connection}} + \frac{1}{k_{connection}} \tag{5.5}$$

where k_T is the total stiffness, k_{member} is the analytic stiffness of the member (Eqs. 5.2 and 5.3), and $k_{connection}$ is the stiffness of each connection including the effect of the eccentricity.

Using the MTS universal tension machine, test data for the total stiffness, k_T of the members and connections was obtained. Specifically, the stiffness was determined by dividing the forces obtained from the load cell on the MTS machine by the measured axial deflections read from the dial gages.

To calculate k_{member}, Hooke's Law was utilized. The length of the axial portion of the member was considered to be the length between the connections, not including any portion of the connection. For the T-stem and casting specimens, the length used was 36 in, where as the length of the knife-plate and angle specimens was 20 in (36 in, less two 8 in welded connections). Figure 5.75 graphically depicts the location of the stiffnesses used to calculate the connection stiffness.

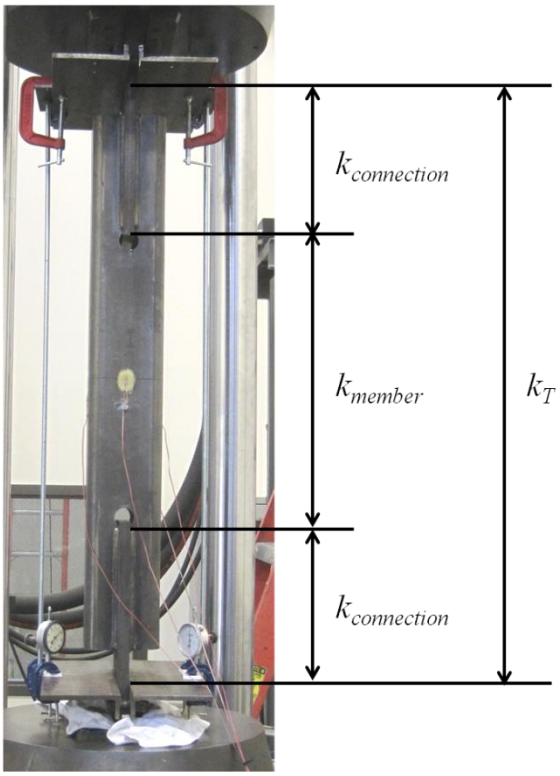

Figure 5.75: Location of Member Stiffness Measurements

Using the preceding values, $k_{connection}$ can be determined using Eq. 5.5. It is noted that the connection stiffness includes 2 in of the connected element due to the positioning of the dial gages.

5.22.3 Calculation of the Torsional Brace Stiffness with Member Connection Stiffness

Once $k_{connection}$ is calculated, , Eq. 5.5 can be applied to the cross frame geometry to determine k_c and k_h (now including the contribution of the member and connection). Substituting k_c and k_h in Eq. 5.4 will give the torsional brace stiffness of the cross frame including member connection flexibility.

While Eqs. 5.4 and 5.5 may better represent the actual condition, it is recognized the process may not be suited for design calculations. The goal is to use the equations to

estimate the magnitude of the effect of the connections and determine if it is necessary to include in design.

5.22.4 Review of Test Specimen Geometrys

The T-stem connection specimens consisted of two sections of a WT 9 x 35.5 connected to square HSS 5 x 5 x 3/8 tubes and round HSS 5.563 x 0.375 tubes. The WT was sized to meet expected strength requirements based on the HSS tube strength, while also meeting the geometric constraint that the WT flange width had to exceed the tube width allowing enough space for the weld. The tube was centered on the flange of the WTs and welded to create the connection. Three types of T-stem connection specimens were created: (1) square HSS welded with the tube walls parallel to the edges of the WT flange, (2) square HSS welded with the tube walls at a 45 degree angle to the edges of the WT flange (diamond), and (3) round HSS. Examples of the HSS specimens and WT connections are shown in Figure 5.76 (a-c).

The cast steel connection specimen comprised a round HSS 5.563 x 0.375 member connected to two steel castings. The castings were designed to seal the tube, to minimize stress concentrations at the connection, and to allow for easy assembly. To achieve these effects, the casting fits to the outside diameter of the tube and tapers to a flat plate which can then connect to cross frame gusset plates or directly to girder stiffeners (Figure 5.76 (d)). More detailed description of the steel casting design was presented earlier in this chapter.

The knife-plate connection was fabricated by first drilling a 1-5/16 in stress relief hole (1.75 times the 0.75 in thickness of the knife-plate), centered approximately 8.8 in from the either end of the HSS 5 x 5 x 3/8 member. A 3/4 in slot was then saw cut to allow insertion of the gusset plate. The tube was then welded longitudinally to the knife-plates to create the connection, which was specified to be 8 in long (Figure 5.76 (e)).

The double angle connection was fabricated using 2 L 4 x 4 x 3/8 members. The members overlapped the gusset plate by 8 in, and were welded around all sides of the angles. Although designers will sometimes detail the welds for a balanced condition, i.e.

the center of gravity of the weldment will align with the center of gravity of the angle, it was found the fully welded condition usually results in decreased fatigue behavior [McDonald and Frank 2009]. The fully welded condition was selected for testing in this research as it would represent the worst-case scenario. Additionally, discussion with fabricators at Hirschfeld Industries seemed to indicate the fully welded condition to be the most common specified. TxDOT typical details also do not explicitly require balanced fillet welds.

Similar to the double angle specimen, the single angle specimen was constructed from an L 4 x 4 x 3/8 member, overlapping the gusset plate by 8 in, and utilizing the fully welded condition. Additionally, a second transverse weld was situated on the back side of the angle, consistent with standard practice. The double and single angles specimens can be seen in Figure 5.76 (f) and (g) respectively. Table 5.4 also summarizes the total weld lengths for each of these variations to be used in standard steel connection calculations.

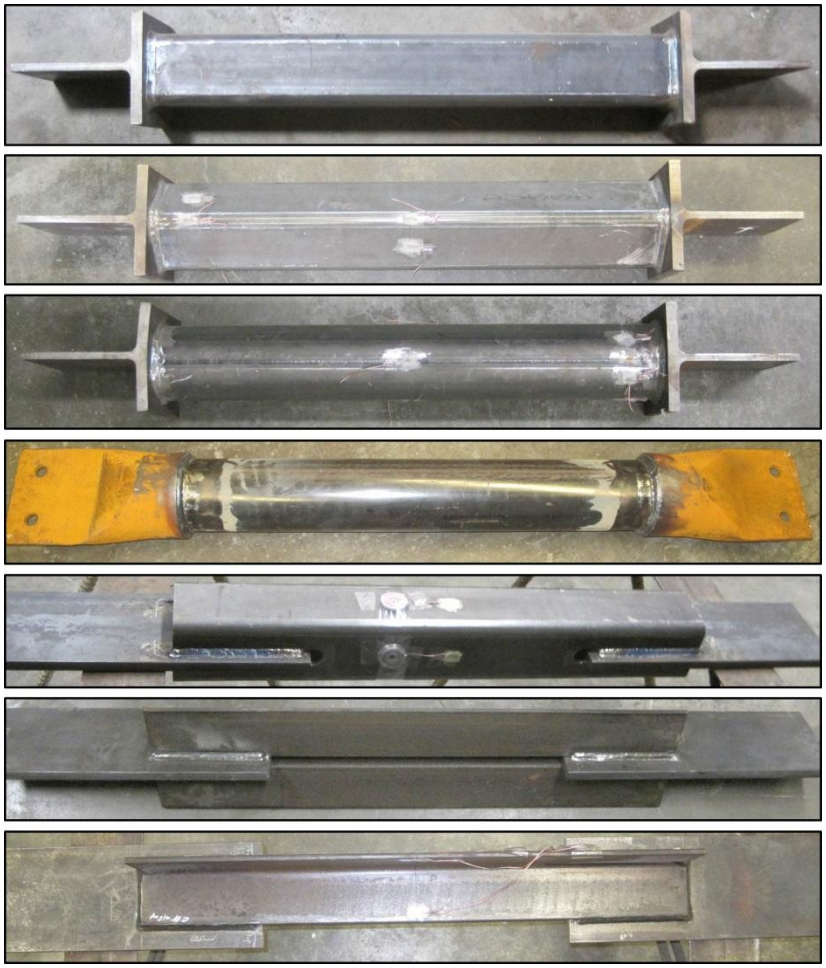

Figure 5.76: Test Specimens- (a) T-Stem and Square HSS, (b) T-Stem and Diamond HSS,(c) T-Stem and Round HSS, (d) Cast Connection, (e) Knife-Plate Connection, (f) Double Angle Connection, and (g) Single Angle Connection

Table 5.4: Test Specimen Geometry

Specimen	Member	Connection	Member Area [in^2]	Member Length[1] [in]	Connection Length[2] [in]
T-Stem Square	HSS 5 x 5 x 3/8	WT 9 x 35.5	6.18	36	4
T-Stem Diamond	HSS 5 x 5 x 3/8	WT 9 x 35.5	6.18	36	4
T-Stem Round	HSS 5.563 x 0.375	WT 9 x 35.5	5.72	36	4
Cast Connection	HSS 5.563 x 0.375	Steel Casting	5.72	36	4
Knife-Plate	HSS 5 x 5 x 3/8	PL 7 x 0.75	6.18	20	20
Double Angle	2L 4 x 4 x 3/8	PL 7 x 0.75	5.72	20	20
Single Angle	L 4 x 4 x 3/8	PL 7 x 0.75	2.86	20	20

1. The member length is the distance between connections shown in Figure 5.75.
2. The connection length is the longitudinal distance of the welded connections plus the additional length to the dial gages as shown in Figure 5.75.

5.22.5 Test Results

Each of the specimens was placed in a uniaxial tension test machine and loaded to determine the stiffness of the assembly, as described earlier in this chapter. The stiffness of each specimen was determined by plotting the load versus deflection curve based on the measured force from the load cell in the MTS machine and the deflection readings from the dial gages. Using a best-fit line through the data, the slope represents the stiffness of the specimen. Since the displacement readings include some region of the connection, which varied in width and thickness amongst the tests, the stiffness results from all the connection types are not directly comparable.

The knife-plate connection, double angle connection, and single angle connection utilized the same plate material to make the connections (PL 7 x 0.75), thereby allowing comparisons to be made between the tests. The total stiffness of the knife-plate specimen

was measured to be 3750 kip/in, about 7% less than the stiffness of the double angle specimen despite having a 5% larger area. The lower stiffness may indicate the connection has a greater shear lag than the double angle specimen. Results for the knife-plate specimen, as well as the angle specimens are plotted in Figure 5.77.

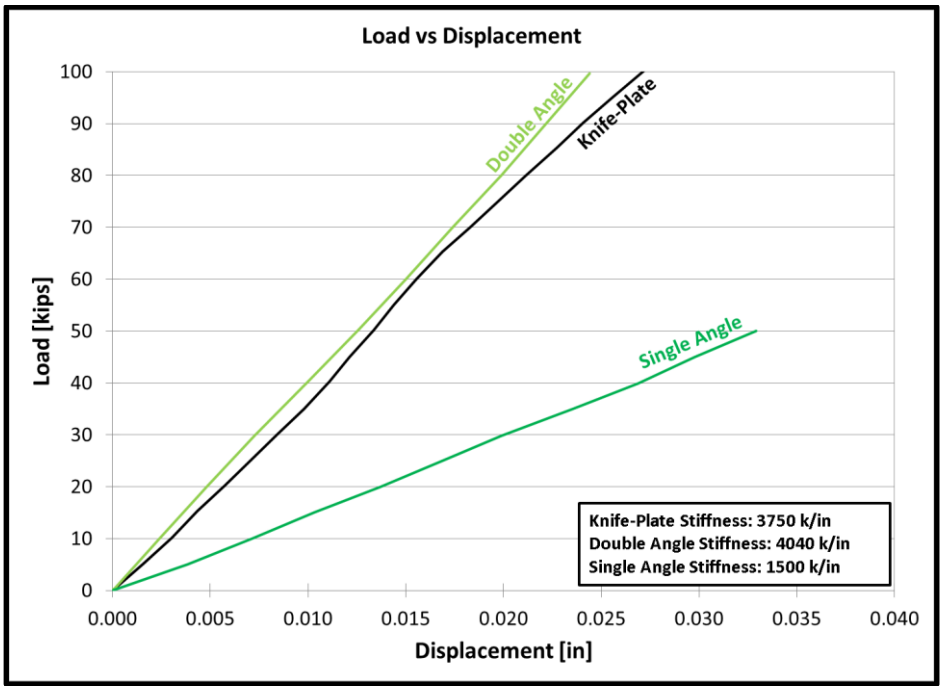

Figure 5.77: Summary of Stiffness Test Results- Knife-Plate, Double Angle, and Single Angle

The double angle specimen performed the best of these three connections, with a total stiffness of 4040 kip/in. On the contrary, the single angle specimen, representing the vast majority of cross frame members currently used, had a low stiffness of 1500 kip/in. While it would be expected the stiffness would reduce by half due to the cross-sectional area, the single angle stiffness is only 37% of the stiffness of the double angle. The most likely explanation is the eccentricity of load relative to the member. All of the other connections are concentric, reducing the amount of bending that occurs under direct tensile load. However, the single angle member is loaded through one leg only, causing substantial bending of the member and therefore decreasing the stiffness available.

5.22.6 Relative Behavior of the Connections

In order to better understand the behavior of the connections relative to one another, an average stress versus average strain plot was created as shown in Figure 5.78. The stress was calculated using the measured force from the MTS machine and the measured area of the member. The area of the member was calculated based upon the length of the member and the member weight, assuming a unit weight of steel of 490 lb/ft^3. The strain was calculated by dividing the measured displacement by the sum of the length of the member and the length of the connections to the gage location/attachment point as depicted in Figure 5.75. The displacement was calculated by taking the average of the two dial gages. By normalizing the force by the area of each member, and the strain by the length, Figure 5.78 shows the approximate performance offered by each connection.

It is observed the cast connection and the double angle connection perform the best, while the T-stem connections connected to the HSS 5 x 5 x 3/8 tubes are the most flexible. The current standard using single angle connections is not as effective as the casting, double angle, or knife-plate connections.

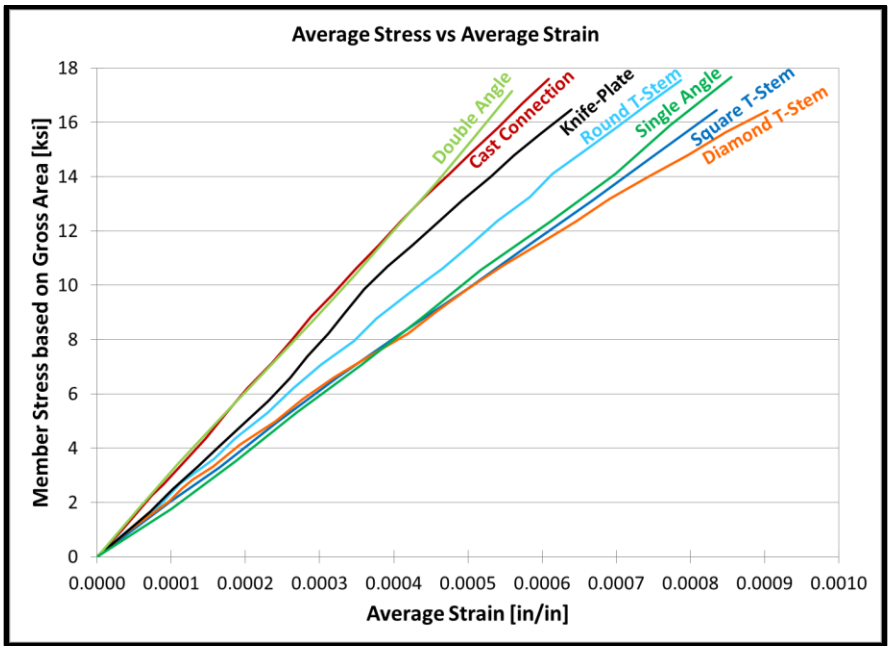

Figure 5.78: Relative Performance of Different Connections

5.22.7 Connection Stiffness

As outlined in Section 5.22.1, the connection stiffness can be calculated from the test data using Eq. 5.5. The results of these calculations are displayed in Table 5.5 and are grouped into the connections that could be compared to one another.

Table 5.5: Calculation of Connection Stiffness based upon Laboratory Tests

Specimen	Member Area [in^2]	Member Length [in]	Total Stiffness k_T [kip/in]	Member Stiffness k_{member} [kip/in]	Approximate Connection Stiffness $k_{connection}$ [kip/in]
T-Stem Square	6.09	36	2800	4910	13000
T-Stem Diamond	6.09	36	2740	4910	12400
T-Stem Round	5.69	36	2970	4580	16900
Cast Connection	5.69	36	3310	4580	23900
Knife-Plate	6.10	36	3750	4910	31700
Double Angle	5.81	36	4040	4680	59100
Single Angle	2.83	36	1500	2280	8800

Note: The connection stiffness includes the stiffness of the connecting plate, which varied between tests. It also contains the bending of the single angle member due to the member eccentricity. Therefore, the connection stiffnesses shown are not comparable to one another.

The T-stem connection combined with square tubular members produced similar values of stiffness for the connection, about 13,000 kip/in. However, use of the round tube with the T-stem offered better performance at 16,900 kip/in.

The cast connection stiffness was determined to be 23,900 kip/in. The stiffness value of the cast connection is very useful in understanding the behavior since the casting was designed to fit a specific diameter of tubes, but multiple tube thicknesses. Therefore, the stiffness will not fluctuate due to connection plate thickness changes, weld length variations, or tube thickness changes.

The knife-plate connection had a test stiffness of 31,700 kip/in. The double angle connection was more rigid with a stiffness of 59,100 kip/in and performed better than the knife-plate while having a smaller overall area. Finally, the single angle connection was

the most flexible, supplying only 8800 kip/in. It is interesting to see the detrimental effect of the eccentric loading on the single angle connection, by comparing it to the double angle comprised of the same cross-section.

Finally it is noted that the connection stiffness values obtained could be used in the prediction of the torsional brace stiffness provided by the in-plane axial deflection of the brace, or $\beta_{braxial}$. behavior of the completed cross frame. As Battistini [2009] indicated (discussed in Chapter 2), when calculating the total torsional brace stiffness, $\beta_{braxial}$ should be incorporated as follows:

$$\frac{1}{\beta_T} = \frac{1}{\beta_{braxial}} + \frac{1}{\beta_{\sec}} + \frac{1}{\beta_g} + \frac{1}{\beta_{conn}} \tag{5.6}$$

where:

$\beta_{braxial}$ = *torsional brace stiffness provided by the axial deflection behavior of the brace*
β_{sec} = *torsional brace stiffness provided by the web including any stiffeners*
β_g = *torsional brace stiffness provided by the girder*
β_{conn} = *torsional brace stiffness provided by the cross frame to connection plate connections*

It is important to note the values provided in Table 5.5 do not substitute for β_{conn} in the preceding formula, but are incorporated into the determination of $\beta_{braxial}$.

5.22.8 Effect on Cross Frame Stiffness

Once the stiffness of each connection has been determined, the values can be combined with the cross frame member lengths to determine the effect of including connection behavior in the calculation of the torsional brace stiffness. Two extreme cases for plate girder depth, 54 in and 96 in, will be considered to identify the effect of connection stiffness on different cross frame sizes.

Using Eq. 5.5, total member stiffnesses for the struts and diagonal were found including the effect of the connection. These calculations utilized the dimensions shown in Figure 5.74, along with the standard areas given in the AISC Steel Construction Manual [2010]. Once solved for, the stiffnesses from Table 5.5 were substituted into Eq.

5.4 to determine the total torsional brace stiffness. The value was compared to Eq. 5.1 which does not include connection behavior. The results are summarized in Table 5.6.

From Table 5.6 it is observed the inclusion of connection behavior can reduce the cross frame stiffness by up to 19%. The square and diamond T-stem connections cause the largest reduction in cross frame stiffness, ranging from 16-17% at the larger 96 in girder depth, and from 18-19% at the shallower 54 in depth. The castings performed fairly well only reducing the stiffness by 9-10% at both girder depths considered. In reference to the double angle cross frame, it is anticipated that single angles would be used for the top and bottom struts, with a double angle along the diagonal. The inclusion of the single angles reduced brace stiffness around 7-9%. Meanwhile, using all single angle sections in the tension-only calculation caused errors of 12-13%. The knife-plate cross frame was comparable to the double angle with errors of 7-9%.

Referencing Table 5.6, it is also concluded the reduction in axial brace stiffness due to connection effects is not highly sensitive to the girder depth. Comparing each connection at the two extreme depths considered, the percent decrease does not vary significantly between the two cases.

Table 5.6: Calculation of Cross Frame Stiffness Including the Effect of Member Connections

Girder Web Depth = 96 in, Girder Spacing = 10 ft							
Cross Frame Member Type	**Member**	**Connection**	**k_h [kip/in]**	**k_c [kip/in]**	**$\beta_{braxial}$ (Eq. 5.1) [10^6 kip-in/rad]**	**$\beta_{braxial}$ (Eq. 5.4) [10^6 kip-in/rad]**	**Percent Decrease**
T-Stem Square	HSS 5 x 5 x 3/8	WT 9 x 35.5	1210	1040	2.172	1.810	16.7%
T-Stem Diamond	HSS 5 x 5 x 3/8	WT 9 x 35.5	1200	1030	2.172	1.793	17.4%
T-Stem Round	HSS 5.563 x 0.375	WT 9 x 35.5	1190	1010	1.992	1.744	12.4%
Cast Connection	HSS 5.563 x 0.375	Steel Casting	1240	1050	1.992	1.814	8.9%
Knife-Plate	HSS 5 x 5 x 3/8	PL 7 x 0.75	1360	1150	2.172	2.008	7.6%
Double Angle	2L 4 x 4 x 3/8	PL 7 x 0.75	600	1090	1.721	1.596	7.3%
Single Angle	L 4 x 4 x 3/8	PL 7 x 0.75	600	500	1.048	0.921	12.1%

Girder Web Depth = 54 in, Girder Spacing = 10 ft							
Cross Frame Member Type	**Member**	**Connection**	**k_h [kip/in]**	**k_c [kip/in]**	**$\beta_{braxial}$ (Eq. 5.1) [10^6 kip-in/rad]**	**$\beta_{braxial}$ (Eq. 5.4) [10^6 kip-in/rad]**	**Percent Decrease**
T-Stem Square	HSS 5 x 5 x 3/8	WT 9 x 35.5	1210	1170	0.683	0.560	18.0%
T-Stem Diamond	HSS 5 x 5 x 3/8	WT 9 x 35.5	1200	1160	0.683	0.555	18.7%
T-Stem Round	HSS 5.563 x 0.375	WT 9 x 35.5	1190	1140	0.616	0.532	13.6%
Cast Connection	HSS 5.563 x 0.375	Steel Casting	1240	1190	0.616	0.556	9.7%
Knife-Plate	HSS 5 x 5 x 3/8	PL 7 x 0.75	1360	1300	0.683	0.624	8.6%
Double Angle	2L 4 x 4 x 3/8	PL 7 x 0.75	600	1250	0.550	0.503	8.5%
Single Angle	L 4 x 4 x 3/8	PL 7 x 0.75	600	570	0.357	0.311	12.9%

Note: The calculations for the double angle cross frame assume single angle struts and a double angle diagonal

5.22.9 Connection Stiffness Conclusions

Often in design, simplified formulas are used to determine the axial brace stiffness of the cross frame. These formulas typically do not consider the effect the connection may have on the stiffness of the brace. As part of using a single diagonal cross frame, experimental tests were conducted to characterize the stiffness of five different connections: (1) the T-stem connection, (2) the cast steel connection, (3) the knife-plate connection, (4) the double angle connection, and (5) the single diagonal connection. The tests showed that the round HSS tube with T-stem connections offers higher stiffness than using square HSS members, despite having a lower cross-sectional area. Subsequent analysis showed the WT 9 x 35.5 T-stems to have a major impact on the torsional stiffness of the cross frame, reducing the value calculated by the current analytical formula by 12-20%. The cast connection performed fairly well, only resulting in a 9-10% decrease of stiffness relative to the current analytical formula.

The knife-plate connection reduced the brace stiffness by 7-9%, assuming the connection plates are similarly sized to the specimen. The eccentric loading of the single angle connection caused the reduction in brace stiffness to be larger (12-13%), but when combined with a double angle along the diagonal, the loss was limited to 7-9%. Again, these expected reductions are based on similarly sized connection plates and weld lengths.

Lastly, comparing brace stiffness reductions at a larger and smaller girder depth, the effect of including the connections led to roughly the same percent decrease between the two cases.

These stiffness calculations were determined based on specific connection sizes and details. Future parametric studies should be used to isolate the effect of the connection to apply to a broader range of connection geometries. While including the connection behavior in determining the torsional stiffness of the brace may be more accurate, it is not practical for design. For now, it seems the expected loss in stiffness is

less than 10% for the connections commonly used, which can be accounted for by using appropriate safety factors, or by incorporating the reduction factor discussed in Chapter 6.

5.23 CONNECTION FATIGUE COMPARISON

The fatigue behavior of the various connections is more easily compared than the stiffness properties. Using the S-N plot, the fatigue performance of all the different connections are shown in Figure 5.79 with the stress ranges, number of cycles to failure, and fatigue crack location shown in Table 5.7.

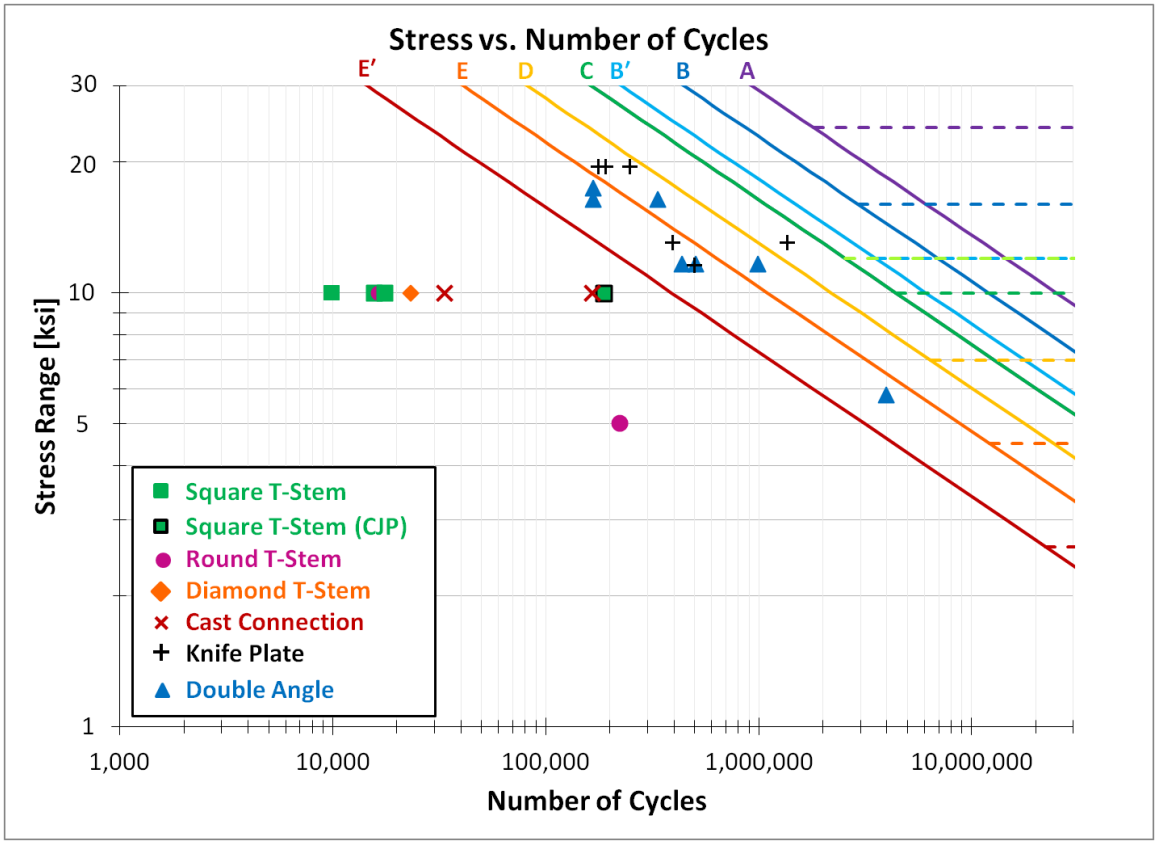

Figure 5.79: Fatigue Performance of Various Details

The following is a summary of the results of the fatigue tests:

- The Square, Round, and Diamond T-stem connections performed poorly in fatigue due to the transversely loaded fillet weld that has a slight load

eccentricity when examined on the local level. The large stress concentration noted in the FEA further exacerbates the fatigue problem.

- The cast steel connection performed poorly in fatigue, similar to the T-stem connections.
- The knife-plate connections offered adequate performance, with 5 of 6 specimens achieving AASHTO Category E. The stress relief hole further increases the fatigue life, while using the saw or torch to cut the slots seems to have no effect.
- The double angle members meet the requirements of AASHTO Category E′. The cracks should form in the angles as long as the stress range in the gusset plate is not larger than in the member.
- The single angle member could not be tested due to the amount of bending that occurs due to the eccentric load pattern. An alternative test setup described in Chapter 7 will determine the fatigue behavior of these members.

Table 5.7: Fatigue Test Summary of Various Details

Fatigue Test	Member				Connection		Weld		Controlling S_R (ksi)	N	Crack Location
	Size	Nominal S_R (ksi)	Shear Lag Factor U	S_R (ksi)	Size	S_R (ksi)	Type	Size			
F-ST1	HSS 5 x 5 x 3/8	10	-	10	WT 9 x 35.5	16.61	Fillet	5/16	10	9884	Weld
F-ST2	HSS 5 x 5 x 3/8	10	-	10	WT 9 x 35.5	16.61	Fillet	5/16	10	17603	Weld
F-ST3	HSS 5 x 5 x 3/8	10	-	10	WT 9 x 35.5	16.61	Fillet	5/15	10	15669	Weld
F-ST4	HSS 5 x 5 x 3/8	10	-	10	WT 9 x 35.5	16.61	CJP	5/16	10	186692	Weld
F-RT1	HSS 5.563 x 0.375	10	-	10	WT 9 x 35.5	15.04	Fillet	5/16	10	16394	Weld
F-RT2	HSS 5.563 x 0.375	5	-	5	WT 9 x 35.5	7.53	Fillet	5/16	5	222184	Weld
F-DT1	HSS 5 x 5 x 3/8	10	-	10	WT 9 x 35.5	16.61	Fillet	5/16	10	23228	Weld
F-CC1	HSS 5.563 x 0.375	10	-	10	Casting	14.20	Fillet	5/16	10	33557	Weld
F-CC2	HSS 5.563 x 0.375	10	-	10	Casting	14.20	Fillet	5/16	10	165756	Weld
F-KP1	HSS 5 x 5 x 3/8	10	0.766	13.05	PL 7 x 0.75	11.62	Fillet	5/16	13.05	1360317	Tube
F-KP2	HSS 5 x 5 x 3/8	10	0.766	13.05	PL 7 x 0.75	11.62	Fillet	5/16	13.05	392727	Tube
F-KP3	HSS 5 x 5 x 3/8	15	0.766	19.58	PL 7 x 0.75	17.77	Fillet	5/16	19.58	190226	Tube
F-KP4	HSS 5 x 5 x 3/8	10	0.766	13.05	PL 7 x 0.75	11.62	Fillet	5/16	11.62	497842	Gusset
F-KP5	HSS 5 x 5 x 3/8	15	0.766	19.58	PL 7 x 0.75	17.77	Fillet	5/16	19.58	176546	Tube
F-KP6	HSS 5 x 5 x 3/8	15	0.766	19.58	PL 7 x 0.75	17.77	Fillet	5/16	19.58	246176	Weld
F-DA1	2L4 x 4 x 3/8	10	0.859	11.64	PL 7 x 0.75	11.12	Fillet	5/16	11.64	436278	Angle
F-DA2	2L4 x 4 x 3/8	15	0.859	17.46	PL 7 x 0.75	16.13	Fillet	5/16	17.46	166983	Angle
F-DA3	2L4 x 4 x 3/8	10	0.859	11.64	PL 7 x 0.75	10.73	Fillet	5/16	11.64	507435	Angle
F-DA4	2L4 x 4 x 3/8	10	0.859	11.64	PL 7 x 0.5	16.39	Fillet	5/16	16.39	166809	Gusset
F-DA5	2L4 x 4 x 3/8	10	0.859	11.64	PL 7 x 0.5	16.39	Fillet	5/16	16.39	335986	Gusset
F-DA6	2L4 x 4 x 3/8	5	0.859	5.82	PL 7 x 0.5	8.2	Fillet	5/16	5.82	3971604	Angle
F-DA7	2L4 x 4 x 3/8	10	0.859	11.64	PL 10.5 x 0.5	10.65	Fillet	5/16	11.64	986449	Angle

5.24 CROSS FRAME CONNECTION CONCLUSIONS

There are a variety of connections that can be used to connect the cross frame members to the gusset plates. The T-stem connections, while convenient from a fabrication perspective, do not provide a very stiff connection, typically fail below calculated loads, and have poor fatigue performance. Therefore, the research team did not consider this detail further.

The cast steel connection provides a stiff connection and meets standard strength checks. However, its poor performance in fatigue prevents it from being a suitable option for steel bridge cross frames.

The knife-plate connection offers the best fatigue performance of those details investigated, but fabrication and material costs will be higher. From a fatigue standpoint, plasma torching could be used to streamline the fabrication of the slot with minimal effect on fatigue life. The knife-plate connection provides one of the stiffest connections. One of the disadvantages of the knife-plate connection is that it does not seal the end of the tube.

The double angle connection provides a reasonably stiff connection and meets typical strength calculations. The fatigue performance meets the minimum AASHTO Category E′ requirements.

The single angle connection is relatively flexible due to the eccentric loading on the angle, which leads to substantial bending of the angle at the connection. This bending prevents fatigue tests from being performed in the MTS Universal Testing Machines due to damage concerns. Chapter 7 highlights an alternative test setup to categorize the fatigue performance of the single angle cross frame. In addition, Z-type cross frames with the knife-plate and double angle details will be investigated.

CHAPTER 6
Large Scale Cross Frame Stiffness Test Summary

6.1 INTRODUCTION

In addition to the small scale cross frame connection tests described in Chapter 5, large scale cross frame stiffness and fatigue tests were conducted as part of the research project. The large scale fatigue tests will be covered in detail in Chapter 7 of this dissertation, while the large scale stiffness tests is the main topic of Wang's dissertation "Stiffness of Steel Bridge Cross Frames of Various Designs and Connections" [2013]. This summary of work reported by Wang [2013] is provided here, as results of these tests will be used in computational study described in Chapter 8.

The following chapter provides a brief summary of the important results of the large scale stiffness tests. As discussed in Chapter 5, the eccentric nature of the single angle connection reduces the stiffness of the member, which in turn reduces the overall stiffness of the cross frame. The large scale cross frame test results provide experimental data on the stiffness of currently used and proposed cross frame layouts. A comparison of the stiffness obtained with commonly used equations and analysis techniques based on truss idealizations is also provided. Lastly, FEA analysis was conducted on numerous layout geometries, and an equation for a cross frame stiffness reduction factor was developed. The reduction factor allows a simplified technique to better model cross frame stiffness and was used in the computational studies described in Chapter 8.

6.2 LARGE SCALE STIFFNESS TEST SETUP

In order to replicate the forces induced in the cross frame at the onset of girder buckling as described in Chapter 2, an experimental test setup was fabricated at Ferguson Structural Engineering Laboratory at The University of Texas at Austin. The setup, shown in Figure 6.1, used three hydraulic tension-compression actuators and three reaction struts to apply equal and opposite moments to the cross frame. Load cells were

connected to each actuator and strain gages were applied to the reaction struts and the cross frame members to monitor the forces during the test. The forces in the angles were calculated using a numerical regression technique that had been successful in previous research [Helwig and Fan 2000] and was verified in this project during the small scale connection tests. The rotation of the cross frame was measured with linear potentiometers located at the corners and mid-height of the cross frame. In order to supply equal loads to each hydraulic actuator, a load maintainer was used. For more details on the test setup, measurement techniques, and specimen geometry see Wang [2013].

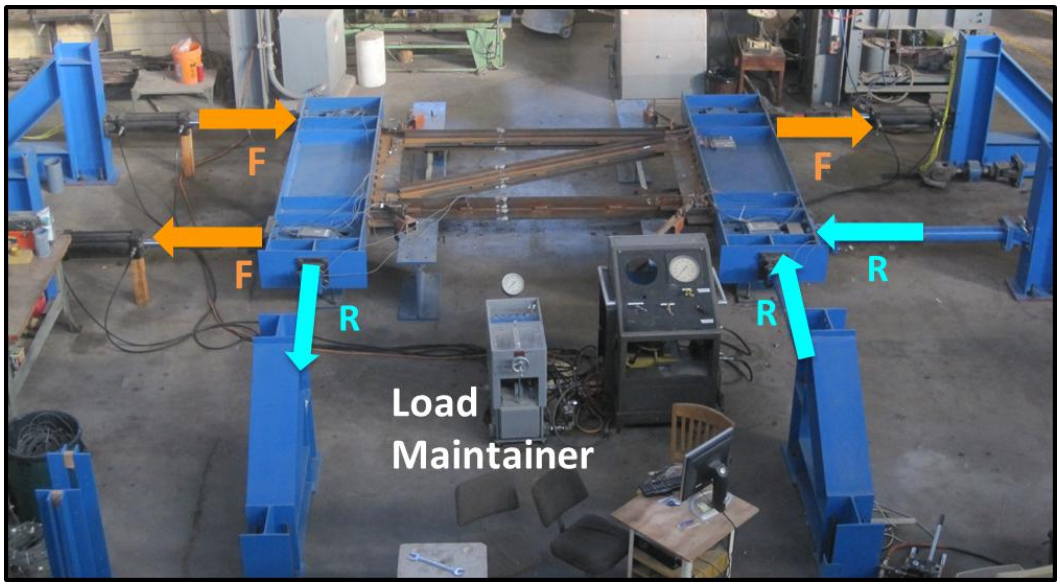

Figure 6.1: Cross Frame Stiffness Test Setup with Z Frame

Each cross frame type was loaded in both directions, meaning the forces were applied in the direction shown in Figure 6.1 and then reversed to verify the stiffness of the cross frame was not dependent upon loading direction in the elastic range. The applied moment and measured rotation were plotted at various load levels and the test was repeated multiple times within the linear elastic range. A line was fit to the data using linear regression; the slope of the line represents the experimentally determined planar stiffness of the brace, in units of kip-in/rad. A sample plot of the results for the unequal leg angle X frame is shown in Figure 6.2, with the torsional brace stiffness of the

cross frame highlighted in the box. For this cross frame, the torsional brace stiffness was approximately 1,054,000 kip-in/rad.

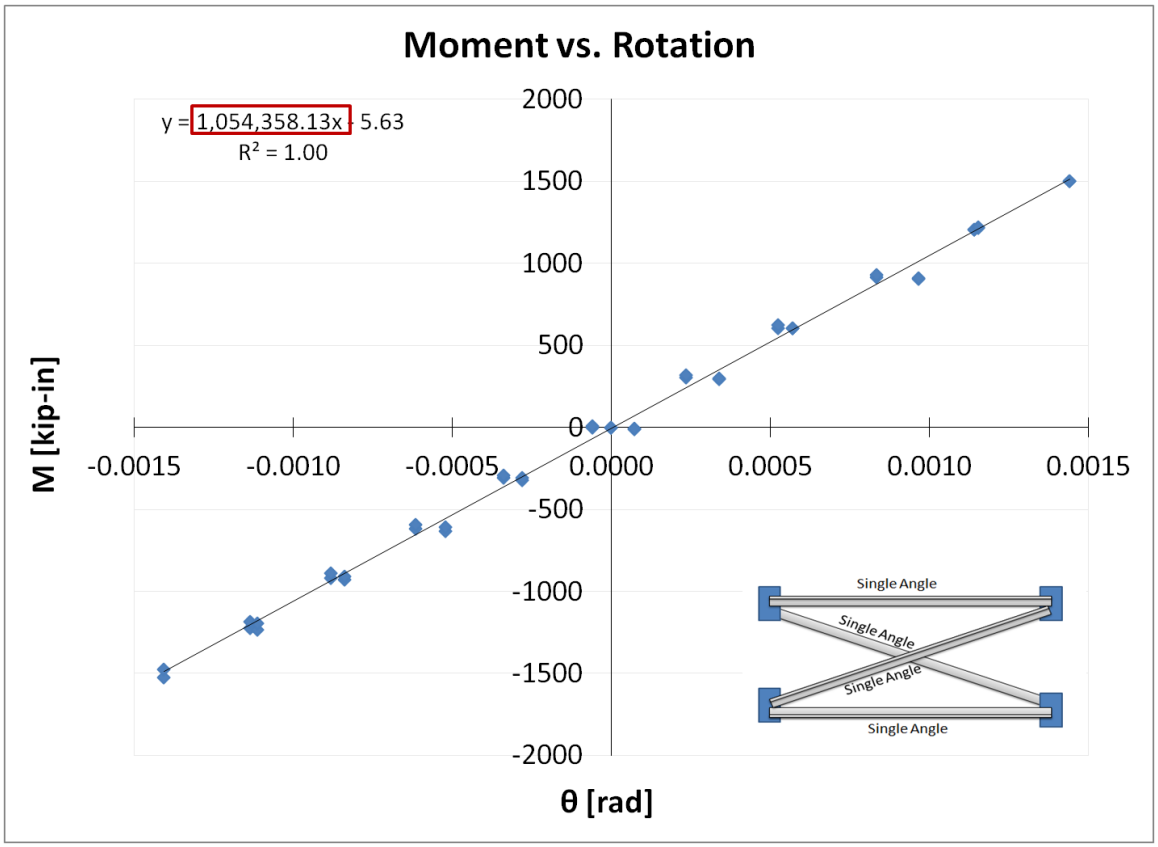

Figure 6.2: Determination of Torsional Brace Stiffness for X Frame

6.3 LARGE SCALE STIFFNESS TEST RESULTS

Following the outlined procedure, the torsional brace stiffness was obtained for various X frame, K frame, and Z frame specimens. The measured stiffness was compared to the analytical formulations discussed in Chapter 2, as well as a line element solution obtained using Risa 2D and an 8-noded shell element model using ANSYS finite element analysis software. Note that the Risa 2D model represented the cross frame members using truss elements. In addition to the cross frame, the loading beams and reaction struts were included in both the line and shell element models, with the analysis restraining the

out-of-plane displacements of the load beams. The results are summarized in Table 6.1. The "Line Element" values listed in this table are the Risa 2D results.

Table 6.1: Cross Frame Stiffness Comparison

Type of Cross Frame	Test Results [k-in/rad]	Solution [k-in/rad]		Error [%]
Single Angle X Frame 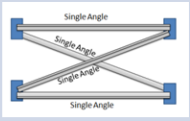	872,000	Analytical	1,579,000	82%
		Line Element	1,572,000	81%
		Shell Element	867,000	-1%
Single Angle K Frame 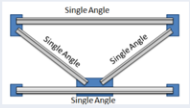	760,000	Analytical	1,189,000	56%
		Line Element	1,180,000	55%
		Shell Element	781,000	3%
Unequal Leg Angle X Frame 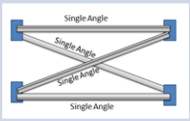	1,054,000	Analytical	1,609,000	53%
		Line Element	1,602,000	52%
		Shell Element	1,065,000	1%
Double Angle Z Frame (Single Struts) 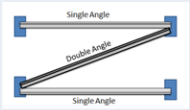	597,000	Analytical	907,000	52%
		Line Element	905,000	52%
		Shell Element	616,000	3%
Double Angle Z Frame (Double Struts) 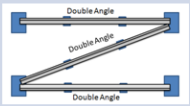	1,182,000	Analytical	1,152,000	-2.5%
		Line Element	1,150,000	-3%
		Shell Element	1,164,000	-1.5%
Square Tube Z Frame 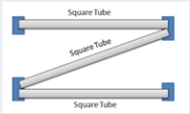	658,000	Analytical	649,000	-1%
		Line Element	647,000	-2%
		Shell Element	657,000	0%

From the results, it is evident there is a large error when using the analytical formula or line element solution for any of the cross frames containing single angle members. As was previously discussed, the error is mainly due to the eccentric single

angle connection between the cross frame member and connection plate. The analytical calculations and the line element solutions show good agreement because both use a truss element model approach in which only axial shortening/elongation are considered. In contrast, the shell element FEA model can accurately predict the measured stiffness of the cross frames because it allows the single angle members to bend out-of-plane due to the applied forces. When examining the Z frame with square HSS tubes or all double angle members, the solution types seem to agree quite closely with the results from the laboratory tests. Since the tubes are connected using a knife-plate connection, the forces from the gusset plates are transmitted through the centroid of the tube, minimizing the out-of-plane bending of the cross frame members. Similarly, the double angle members are also concentrically connected. Therefore, a truss-type model is representative of the actual behavior of the brace and will provide an accurate solution.

The effect of member eccentricity is further demonstrated by the unequal leg angle X frame specimen. The single angle X frame used equal leg L4x4x3/8 angles, while the unequal leg specimen used L6x3-1/2x5/16 angles, long legs back-to-back. The cross sectional areas of these two angle shapes are 2.86 in^2 and 2.89 in^2 respectively. Referencing Table 6.1, the analytical solutions and line element solutions for each of these specimens were very similar, since both of these solution types rely only upon the member area provided. However, it was observed the actual measured stiffness for these two specimens were quite different, with the unequal leg specimen providing 21% more stiffness than the equal leg counterpart. The increase in stiffness is primarily a result of the reduced member eccentricity which leads to less out-of-plane bending of the member. Figure 6.3 qualitatively shows the reduction in member eccentricity gained by using unequal leg angle cross frames.

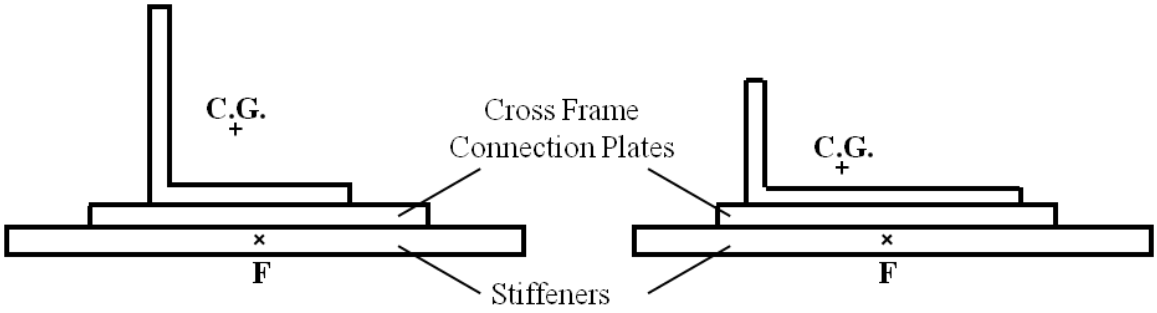

Figure 6.3: Reduction of Connection Eccentricity by Using Unequal Leg Angles

6.4 DEVELOPMENT OF REDUCTION FACTORS FOR CROSS FRAME STIFFNESS

Throughout the testing phase of the large scale cross frame stiffness specimens, force and displacement measurements were compared with the results from computational models. In particular, the researchers used the test data to validate a shell element model of the cross frame that would be able to accurately determine the real cross frame stiffness provided by the brace by capturing the out-of-plane bending of the member. The accuracy of the model has already been shown in Table 6.1, where it is observed the shell element model was within 3% of the measured stiffness for all cross frame layouts considered. For more details on the validation of the FEA model, see Wang [2013].

The validated model was then used to conduct a parametric FEA study to examine the effects various parameters have on cross frame stiffness. In particular, angle sizes, cross frame depths, and girder spacings were changed to consider realistic permutations for design. The studies were performed to determine a reduction factor for single angle X- and K-type cross frames. The reduction factor is defined as follows:

$$R = \beta_{FEA} / \beta_{analytical} \tag{6.1}$$

where:

β_{FEA} = *torsional brace stiffness calculated by the finite element analysis which represents the expected actual stiffness of the brace*

$\beta_{analytical}$ = *torsional brace stiffness calculated using analytical equations or line element solutions*

Therefore, the reduction factor *R* (also referred to as the R factor) represents the percentage of the analytical stiffness that is actually provided by the real cross frame. Since the eccentricity of the single angle members reduces the cross frame stiffness, *R* will always be less than 1.0.

In the course of the parametric study, it was found the reduction factor was dependent upon the ratio of the girder spacing to the height of brace (S/h_b), the member eccentricity ($\bar{y}$), and the thickness of the angle (t) [Wang 2013].

Performing a regression analysis on the FEA stiffness results, the following equation was obtained for the reduction factor for the X-type cross frame:

$$R_{est-SX} = 1.063 - 0.087\frac{S}{h_b} - 0.159\,\bar{y} - 0.403t \tag{6.2}$$

Likewise, the following equation was obtained for the reduction factor for the K-type cross frame:

$$R_{est-SK} = 0.943 - 0.042\frac{S}{h_b} - 0.048\,\bar{y} - 0.420t \tag{6.3}$$

6.5 VERIFICATION OF REDUCTION FACTORS FOR CROSS FRAME STIFFNESS

To verify the accuracy of the reduction factor, two methods were employed. First, comparison with the test results for the X- and K-type frames was conducted. The use of the R factor was also extended for application to unequal leg cross frames. Secondly, comparison of the R factor with the FEA results for all the permutations considered was performed.

6.5.1 Comparison to Test Results

To determine the adequacy of the reduction factor *R* for a given scenario, the results from the regression analysis were applied to the brace geometries tested as part of the large-scale stiffness test program. The R factor was calculated for each test specimen, and subsequently multiplied by the analytical brace stiffness ($\beta_{analytical}$). The ensuing

value is the expected brace stiffness measured from the test. The following table summarizes the results.

Table 6.2: Cross Frame Stiffness Test Results Comparison using R Factor

Type of Cross Frame	Test Results [k-in/rad]	Solution [k-in/rad]		Error [%]
Single Angle X Frame 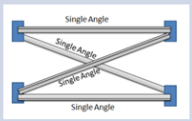	872,000	Analytical	1,579,000	82%
		R*Analytical	860,000	-1.4%
Single Angle K Frame 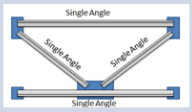	760,000	Analytical	1,189,000	56%
		R*Analytical	762,00	0.3%
Unequal Leg Angle X Frame 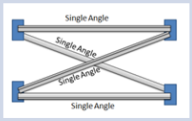	1,054,000	Analytical	1,609,000	53%
		R*Analytical	1,018,000	-3.4%

As observed in Table 6.2, the reduction factor does a very good job of predicting the actual cross frame stiffness provided by the brace. The reduction factors given by Equations 7.2 and 7.3 result in an accuracy of 1.4% and 0.3% respectively for the X-type and K-type frames. When the reduction factor is extended for use with the unequal leg angle, it is noted the error is about 3.4% conservative, which is within reasonable accuracy for the determination of brace stiffness, especially since a designer would typically want to supply 2-3 times the absolute minimum, or ideal stiffness, for stability.

6.5.2 Comparison to FEA Results

The reduction factors were also applied to all the FEA cases used to generate the data for the regression analyses. To assess the accuracy globally, plots were created for the X frames and K frames with $R^*\beta_{analytical}$ on the vertical axis, and β_{FEA} on the horizontal axis. Effectively, these plots are graphing the predicted stiffness (using the R

factor) versus the actual stiffness (determined from the validated FEA model). Figure 6.4 and Figure 6.5 show the results.

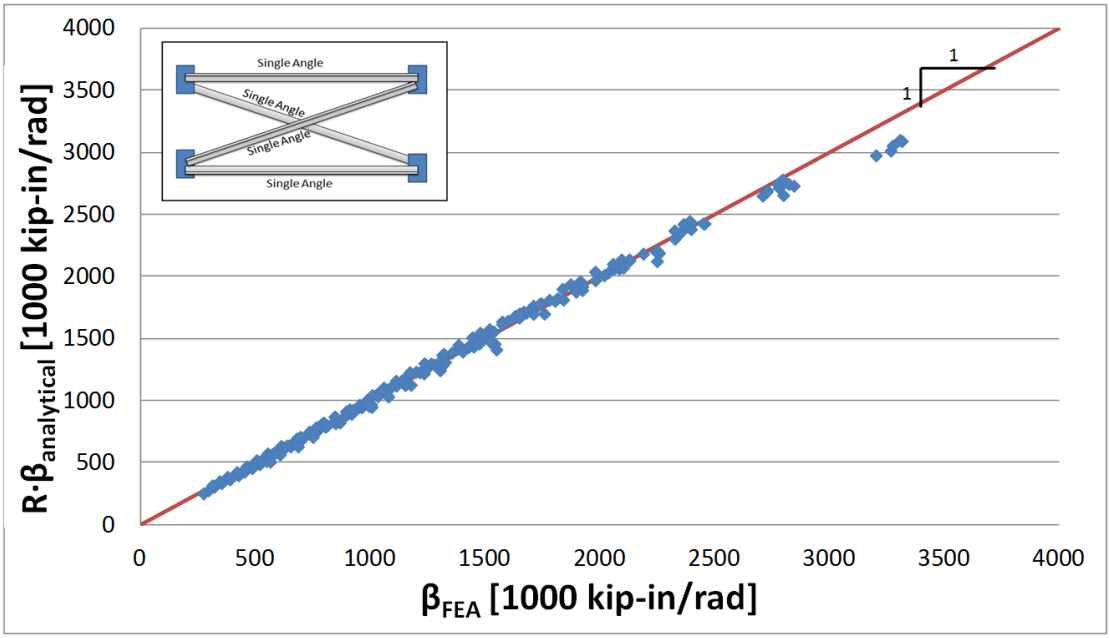

Figure 6.4: Accuracy of Reduction Factor for X-type Cross Frames [Wang 2013]

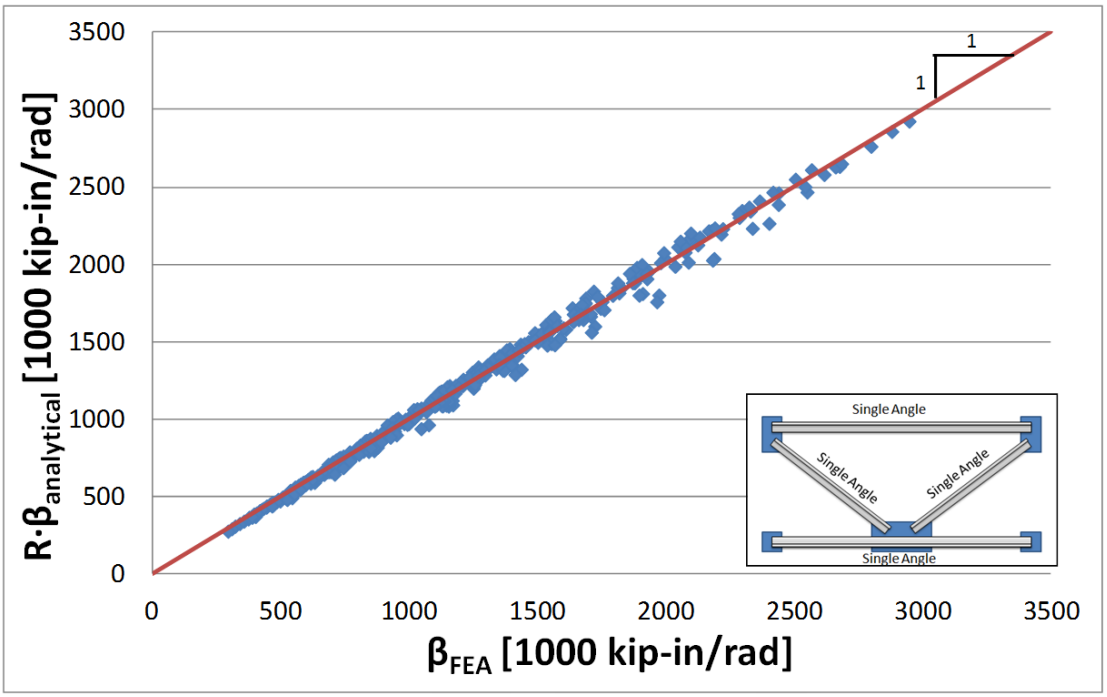

Figure 6.5: Accuracy of Reduction Factor for K-type Cross Frames [Wang 2013]

To help evaluate the accuracy of the R factor for both the X- and K-type cross frames, a line with a slope of 1 has been plotted in both Figure 6.4 and Figure 6.5. If the R factor exactly predicts the actual stiffness of the cross frame, than the point representing that particular geometry will fall directly on this line. As demonstrated from both figures, the data points tend to fall on or very near the line, meaning the R factor does a very good job in predicting the actual stiffness of the brace.

6.6 CONCLUSION

The preceding sections have provided an overview of the stiffness behavior of cross frames in steel bridges as observed in large scale laboratory tests and further analyzed using computational models. It should be apparent that the eccentric connection of the single angle member reduces the stiffness of the individual member (as described in Chapter 5), which in turn, contributes to a reduction in the stiffness of the completed cross frame. Other factors such as the angle thickness, girder spacing, and brace height were also found to affect the total brace stiffness.

The reduction in stiffness due to the eccentric connection can be fairly substantial, leading to very large errors when trying to use analytical equations or line element models which do not account for the out-of-plane bending of the brace; unconservative errors up to 80% were seen in the test results for cross frame stiffness. By using the reduction factor developed in the research, designers can easily and accurately predict the actual stiffness supplied by the cross frame.

6.7 IMPLICATION OF THE R FACTOR FOR CROSS FRAME DESIGN

In addition to being able to better predict the stiffness of the cross frame systems, the R factor has another important implication in terms of cross frame design. In general, structural elements with higher stiffness will tend to attract higher forces due to their rigidity. If designers are modeling these braces using line elements (or using programs that use line element analyses internally), than the predicted forces in the cross frames may actually be higher than the forces experienced in the real structure. While this may

be a conservative approach from a strength and fatigue perspective, it can lead to design difficulties and uneconomical designs. For example, if an analysis using an incorrectly high estimate of brace stiffness shows that the predicted stress range is too high for fatigue, the designer may increase member sizes to reduce the stress range. This, in turn, will increase the brace stiffness, attract more force to the brace, further increase the stress range, and require even large members. Thus, errors in computing brace stiffness can result in significantly uneconomical designs that can be avoided by correctly modeling brace stiffness.

By applying the R factor to the brace stiffness, the designer can more accurately predict the forces in the completed structure. Chapter 8 describes a case study involving a curved steel bridge that experienced fatigue issues during design. Using typical commercial software which would overestimate the stiffness of the brace, engineers were required to increase the cross frame member sizes, add more cross frame lines, and add an additional girder line to satisfy the AASHTO bridge specification requirements for fatigue. By applying the R factor within the analysis, the force ranges in the cross frame members would have been reduced, possibly indicating the extreme measures taken to satisfy the design requirements were not completely necessary.

CHAPTER 7
Large Scale Cross Frame Fatigue Tests

7.1 INTRODUCTION

One of the priorities of the research study documented in this dissertation was to evaluate the performance of existing cross frame layouts and offer improved details for a more efficient brace. In Chapter 5, proposed connections were tested on the individual members of the cross frame to determine stiffness, strength, and fatigue behavior. The MTS Universal Testing Machine utilized in the experiments was able to measure the stiffness and strength of the single angle detail, but was not used for fatigue tests on the detail due to concerns about damaging the machine. The single angle detail attached to a gusset plate through one leg has an eccentric connection, as depicted in Figure 7.1.

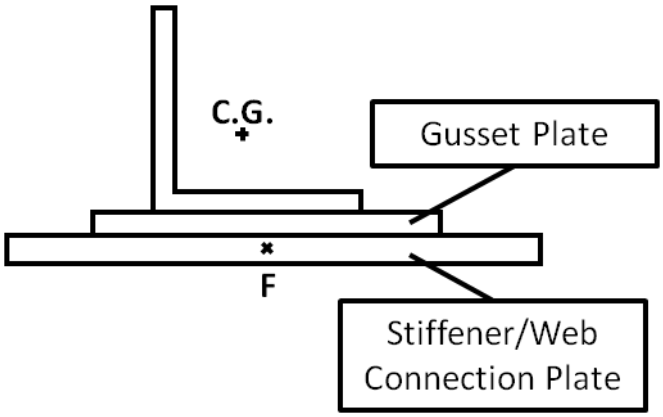

Figure 7.1: Eccentric Single Angle Connection

Due to the eccentricity, a substantial amount of bending is induced in the member, and in turn, a bending moment is applied to the testing machine. Figure 7.2 depicts the magnitude of the bending as seen in the tension test performed to the ultimate strength of the angle.

Figure 7.2: Single Angle Strength Test Bending

With the large amount of observed bending, there was a concern that the testing machine could be damaged if cyclic fatigue tests were performed. A previous study conducted for the American Institute for Iron and Steel [McDonald and Frank 2009] had similar issues with the angle bending. As an alternative, the researchers opted to eliminate bending to the cross head by incorporating symmetry and testing two angle specimens back-to-back, to achieve concentric behavior from the combined members and eliminate the potential damage to the cross head. Although the two angles had separate gusset plates, the symmetry of the resulting orientation was very similar to the double angle member tested as part of the current project. The AASHTO fatigue category determined by McDonald and Frank [2009] for the single angles was E′, the same as was determined for the double angle connection as outlined in Chapter 5.

While the previous fatigue tests on the back-to-back single angle tests provide a baseline understanding of the connection, the boundary conditions of the angles are not representative of the real structure since the effects of bending are not captured. In the cross frame, the gusset plates are fastened to connection plates that allow bending of the single angle members, which may have a diminishing impact on the fatigue life of the detail. Therefore, full scale cross frame fatigue tests were necessary to determine the

appropriate category for these members in the existing brace details. The test setup also provided a realistic measure of the fatigue performance of the other proposed details in a full cross frame system.

In addition, the stiffness of the cross frames utilizing the single angle details obtained in the large scale laboratory tests and accompanying finite element analyses showed a large discrepancy as compared to the appropriate truss analogy for brace stiffness. Treating the members as axial elements with concentric connections is not likely a good representation of the actual behavior, thus necessitating a different test evaluation for the fatigue performance.

In order to verify the fatigue performance of the various cross frame connection details, a test setup was fabricated to allow cyclic loading of the entire cross frame so as to be similar to cross frames in actual bridge applications. This chapter outlines the features of the test setup, discusses the results for five different cross frame types, and makes recommendations for improved cross frame behavior based on the test data and accompanying finite element analyses.

7.2 CROSS FRAME FATIGUE TEST SETUP

A CAD view of the large scale cross frame fatigue test setup using SolidWorks 2011 software is shown in Figure 7.3 and the completed laboratory setup is shown in Figure 7.4.

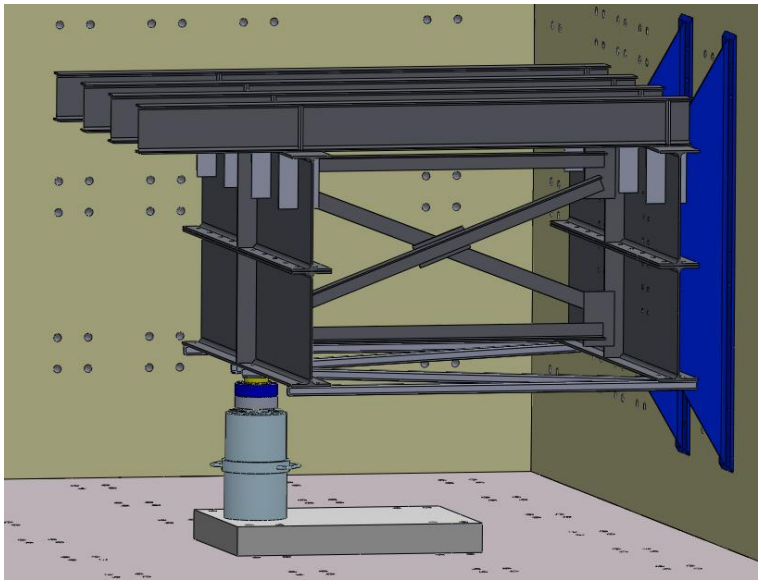

Figure 7.3: CAD Drawing of Cross Frame Fatigue Setup

Figure 7.4: Completed Cross Frame Fatigue Test Setup

Figure 7.5 through Figure 7.8 shows front views and side views of the test setup as well as identifies some key features of the experiment. The following subsections will discuss the various pieces of the test frame and the purpose of each.

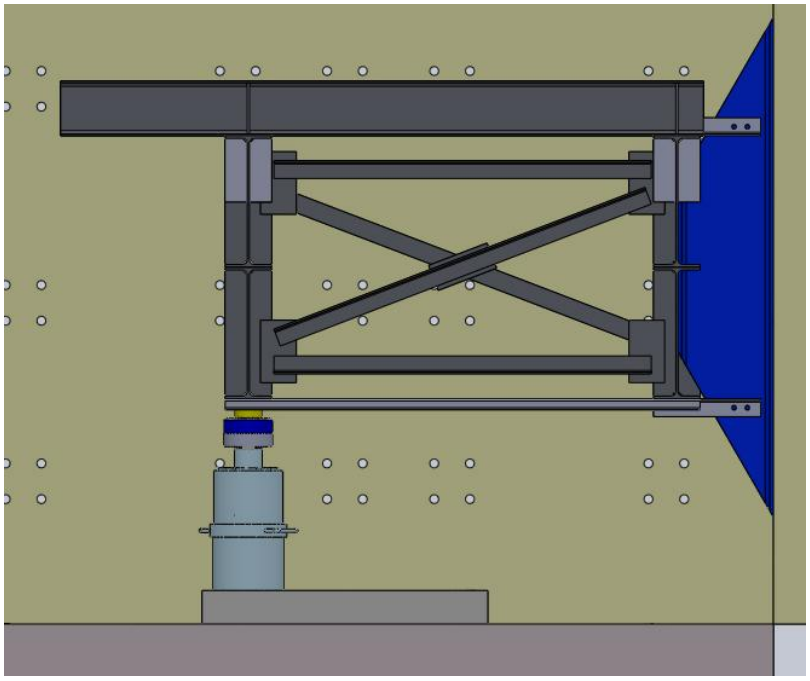

Figure 7.5: Front View of Cross Frame Fatigue Setup

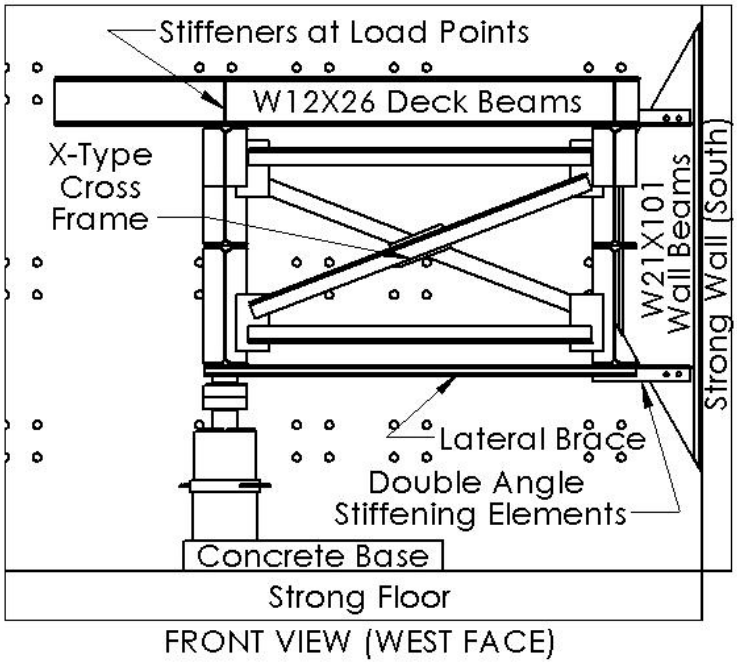

Figure 7.6: Front View of Cross Frame Fatigue Setup (Details)

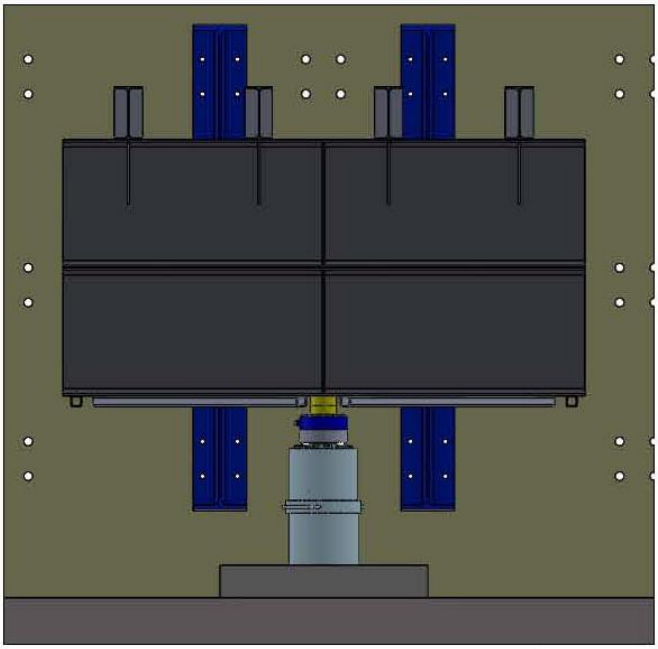

Figure 7.7: Side View of Cross Frame Fatigue Setup

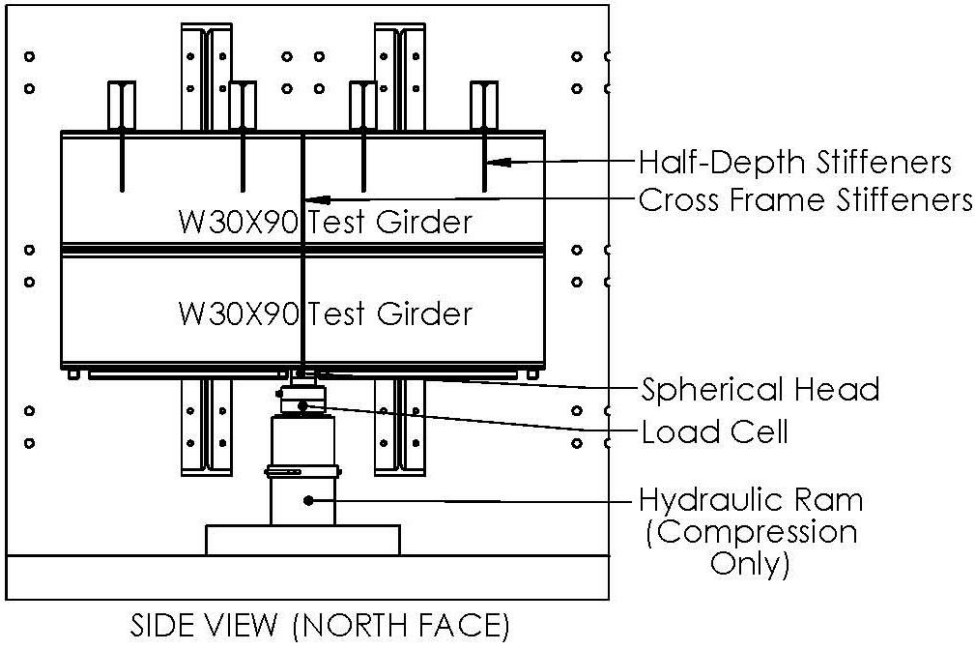

Figure 7.8: Side View of Cross Frame Fatigue Setup (Details)

7.2.1 Built-Up Test Girders

In order to avoid the fabrication of built-up sections but to still simulate the plate girders typically used in the construction of steel bridges, the researchers used two 10 ft long W30x90 rolled sections, stacked on top of one another, and bolted together along the length of the flange at a 12 in spacing. The bolt spacing was selected using FEA to ensure that the fully tightened bolts controlled slip between the two wide flange sections and simulated a built-up girder. The bolts used were ASTM A490 bolts and were tightened with the assistance of a pneumatic torque wrench. The resulting cross section is approximately 5 ft deep, with a web thickness of 0.47 in. The associated web slenderness ratio (web depth to thickness) is 123, well within the typical range for plate girders frequently used in steel bridges.

7.2.2 Deck Beams

Although a composite concrete deck between the two girders was considered during the design phase of the setup, such a deck would make the removal and installation of cross frames very difficult. Therefore a simulated concrete deck was used by including W12x26 sections spanning between the two test girder sections. Once the concrete deck is cured in a real bridge system, it can provide substantial bracing to the girder sections by providing both lateral and torsional restraint at top flanges of the girders. For simplicity in fabrication and repeatability between tests, the W12x26 beams were selected to provide similar rotational restraint to the flanges. Using typical values of the concrete deck thickness, reinforcement ratios, and material properties, the EI/L of the concrete deck section was calculated and equated to that of an equivalent steel section, resulting in the placement of four W12x26 beams for the 10 ft girder sections being tested. The W12x26 beams correspond to an approximate deck thickness of 8-10 inches, with a girder spacing of 8 ft, and an assumed modulus of elasticity based on approximate elastic behavior of normal weight concrete. The deck beams are indicated in Figure 7.6.

7.2.3 Wall Beam Supports

The desired loading condition was to represent the deflection in the cross frame when a truck passes over the brace location. Since the truck will typically cause differential deflections between adjacent girders, the cross frame will experience a live load induced stress. To practically achieve this condition, a vertical load was applied to one test girder, while the deflections of the adjacent test girder were restricted. The differential deflection was achieved in the tests by using a hydraulic actuator to displace one girder while the other girder was anchored to a reaction wall. Two W21x101 girder sections were fabricated and anchored to the wall. One of the test girder webs was then bolted to the W21x101 sections. The wall support is shown in blue in Figure 7.5 and is called out in Figure 7.6.

7.2.4 Double Angle Stiffening Elements

When statically loading the cross frame setup before the first test, a large amount of flange bending occurred at the test girders as a result of the limited attachment length of the wall beam to the girder web. The excessive bending lead to large displacements required to achieve realistic forces in the cross frame members. As a result, double angle sections were bolted to the top and bottom flanges of the test girder adjacent to the wall and bolted to the web of the wall beam. Figure 7.5 and Figure 7.6 show the locations of the double angles.

7.2.5 Lateral Bracing

The 10 ft. simulated girder sections lacked the continuity that would be present in an actual bridge section and there were concerns about the deformational behavior of the bottom flange of the girders. Due to the eccentric loading of the single angle members, deflection out of the plane of the cross frame occurs. This deflection could cause the entire test setup to rotate about the load point. To prevent the rotation and simulate the stiffening effects that would come from girder continuity, bracing was supplied in the form of a lateral truss on the bottom flange. The lateral truss consisted of

HSS2.5x2.5x1/4. FEA results showed that these members did not significantly change the forces in the cross frame and the stresses using the selected member would be minimal so as not to create a fatigue issue. The bottom flange bracing can be seen Figure 7.3 and Figure 7.4 and is indicated in Figure 7.6.

7.2.6 Connection Plates

Connection plates were provided to help limit distortion at the cross frame locations as well as the helping to distribute the stiffness of the simulated deck beams. Half-depth stiffeners cut from 5in x 1/2 in plate material were selected to help transfer the forces from the test girders into the deck beams. The same plate material comprised the full depth stiffeners situated above the loading ram, which also acted as the cross frame connection plates.

7.2.7 Loading System

To load the cross frame vertically, a 200 kip hydraulic actuator was used to apply compression-only loads, transferred to the girders through a 200 kip load cell and spherical head which allowed rotation of the test girder relative to the loading system. The hydraulic actuator was placed on a concrete pad. Holes were drilled into the concrete pad so that threaded rods screwed into the base of the actuator would extend into the concrete pad to act as a shear key to prevent the actuator from shifting out of position during cycling. The actuator, load cell, and spherical head are shown in Figure 7.9. A preload was applied to the system to achieve a baseline stress of 5 ksi in the critical bracing member and was the minimum stress level in the cyclic test. The maximum stress was set to provide the desired stress range.

Figure 7.9: (a) Hydraulic Actuator, (b) Load Cell, and (c) Spherical Head

7.2.8 Fabrication Methods

To accommodate the wall beam, the flanges on one side of the test beam were coped to provide continuous support along the depth of the web. The wall support beams had to be long enough to provide sufficient anchor points to the reaction wall, but also needed fit within the flanges of the test beams. The wall support beams were therefore tapered to form a trapezoid that was long enough to provide sufficient anchoring points to the wall and to fit within the flanges. Since the components of the setup were to be used on a fatigue setup, care was taken in cutting the test setup pieces to the proper length and shape since rough, jagged cuts would present possible fatigue crack initiation points on the test setup. After flame cutting the sections, grinding was performed to improve the surface condition. Figure 7.10 to Figure 7.13 depict the wall support fabrication process.

All the holes were constructed using a magnetic drill, lubricated by hydraulic oil, to produce holes with minimal defects to minimize potential points of fatigue crack initiation. The smaller lateral truss tubes, double angle stiffening elements, connection plates, and cross frame members and gusset plates were cut using a metal band saw.

Figure 7.10: Drilling Holes for Wall Beams

Figure 7.11: Flame Cutting Web

Figure 7.12: Completed Wall Support

Figure 7.13: Surface Condition (a) After Flame Cut and (b) After Subsequent Grinding

7.3 CROSS FRAME SPECIMEN DETAILS

The majority of the cross frames were fabricated by the researchers and welded by a certified welding technician at the Ferguson Structural Engineering Laboratory. The following subsections outline the general procedures performed to create the braces and the measures taken for quality assurance.

7.3.1 Cross Frame Fabrication and Specimen Designation

The cross frame members were cut to appropriate length using a horizontal band saw, which is consistent with the cutting methods used in standard bridge fabrication

shops. Different cross sections were used for the members based on the cross frame type and detail summarized in Table 7.1. Also, the specimen designation adopted for reference in the project is introduced.

Table 7.1: Cross Frame Types and Specimen Designation

Cross Frame Type	**Specimen Designation[1]**	**Cross Frame Member**
X Frame, Equal Leg Angles	XF_#	L4x4x3/8
X Frame, Unequal Leg Angles	XF_UL_#	L6x3.5x5/16
K Frame, Equal Leg Angles	KF_#	L4x4x3/8
Z Frame, HSS Tubes	ZF_HSS_#	HSS5x5x3/8 HSS6x3x5/16
Z Frame, Double Equal Leg Angles	ZF_DA_#	2L4x4x3/8

1. The # symbol denotes the specimen number for that type of cross frame.

Once cut, the pieces were laid out on a welding table according to the individual specimen details. In order to assure the proper height of brace, 4 in x 4 in wood posts were cut and placed between the top and bottom struts of the cross frame. Using the posts guaranteed the struts were parallel to one another and the proper distance apart. The plates were held in place to the struts using C-clamps, and squared up using the edges of the welding table. The diagonals were then set in place and clamped. Once the cross frame was complete, tack welds were used to maintain the geometry until the prescribed welded details were completed. In general, the tack welds were placed at locations away from potential stress concentrations and were ground smooth before completing the fillet welds. An example of the cross frame layout during fabrication is shown in Figure 7.14.

Figure 7.14: Cross Frame Layout during Fabrication

Based upon test results, changes were incorporated into some of the details to improve the fatigue behavior and constructability and/or to investigate the effects of different variables. A summary of each specimen is given in Appendix A.

7.3.2 Cross Frame Welding Process

The welding processes performed for each cross frame were conducted in accordance with TxDOT standards regarding weld size and material. The welding machine used was a Miller XMT 450 CC/CV multiprocess inverter with a Miller 70 series wire feeder. The welding process employed was flux-cored arc welding (FCAW).

At an early stage in the full scale fatigue tests, the researchers had some of the cross frames fabricated in the Bridge shop of Hirschfeld Industries in San Angelo, Texas. The cross frames were cut and tack welded at FSEL with the final welding completed at Hirschfeld to ensure that the fatigue performance of specimens welded at FSEL were consistent with the quality that would be expected from a bridge fabricator. Members of the research team including the FSEL welding technician were present at Hirschfeld to observe the welding process and note the welding electrode and settings.

During the visit, a Hirschfeld worker provided the researchers with an index card specifying the TxDOT prescribed welding parameters for cross frame fabrication. The values suggest a voltage range of 25.8-30 V, an amperage range of 275-342.9 Ω, and a

wire-feed speed of 14.5-16.5 in/min. These values were utilized in the test specimens constructed at Hirschfeld, as well as the remaining specimens welded at FSEL (all specimens *except* XF_1,2,3,4; KF_1,2; ZF_HSS_1; ZF_DA_1).

The TxDOT specified welding procedure obtained from Hirschfeld also requires the minimum preheat in accordance with AWS D1.5, which includes a minimum temperature of 50˚F for steel 1/8 - 3/4 in thick and 70˚F for 3/4 - 1-1/2 in thick members. These minimum temperatures were satisfied for all specimens.

7.3.3 Cross Frame Welding Electrode

Three types of wire were used throughout the cross frame fatigue tests. The first was a Lincoln Electric Ultracore® 71A85 flux-cored gas-shielded wire with a 1/16 in diameter. The 71A85 wire is designed for all position welds, meets seismic structural fabrication standards, and should be used with a mixed Argon-CO_2 shielding gas [Lincoln Electric 2013]. The wire was used primarily to weld the cross frame specimens to the connection plates in the test setup due to its ability to better perform vertical and overhead welds. The cross frame specimens fabricated prior to the researchers' visit to Hirschfeld Industries (a steel bridge fabricator) had welds connecting the cross frame members to the gusset plates using this type of welding wire (Specimens XF_1,2,3,4; KF_1,2; ZF_HSS_1; ZF_DA_1).

The second type of wire is the Lincoln Electric Ultracore® 70C wire, with a 5/64 in diameter electrode wire. The larger diameter of this wire (5/64 in vs. 1/16 in) greatly increased the heat input and available weld metal. This wire type was used by Hirschfeld to weld four cross frame specimens so that the test results would include cross frames actually produced by a typical bridge fabricator. The specimen designations for these cross frames were XF_5, KF_3, ZF_HSS_2, and ZF_DA_2.

The third type of wire is the Lincoln Electric Outershield® 70 series for mild steel in the flat and horizontal position and is suited for structural fabrication [Lincoln Electric 2013]. This wire has consistent properties to the consumable used at Hirschfeld which

was a Lincoln Electric Ultracore® 70C wire. The wire also had a 5/64 in diameter. This wire was used for all remaining specimens tested.

Since the third type of wire is only suited for flat and horizontal positions, it was used only in the fabrication of the remaining cross frames. The previous Lincoln Electric Ultracore® 71A85 wire was used to attach the specimens to the connection plates in the test setup, since that connection requires a vertical weld.

7.3.4 Testing Procedures and Stress Range Determination

Once the specimens were welded into the setup, researchers would load the cross frames statically to measure the vertical stiffness of the system and to verify the deflections were similar to the FEA model predictions. A view of the test setup and loading application is given in Figure 7.15.

Figure 7.15: Test Setup and Load Application

Since the hydraulic actuators used in the research could only apply compression loads, the stresses in the cross frame members never experienced a reversal. The load was statically applied until the critical member in the brace reached an average tensile stress of 5 ksi based on the readings collected from the member strain gages and

accounting for shear lag in the member. As discussed in Chapter 5, the AISC guidelines for the calculation of shear lag was used for the single angle, double angle, and knife-plate connections [AISC Chapter D 2010]. The use of the effective stress range is suggested by the AASHTO Specification to determine the appropriate fatigue category [AASHTO 2012]. For the Z Frame HSS specimens, strain gages were attached to each tube wall at the mid-length of the critical member and averaged to obtain the measured stress in the tube. For the angle members, four gages were applied to each angle at mid-length for the K Frame Single Angle and Z Frame Double Angle specimens and at a quarter point for the X Frame Single Angle and X Frame Single Unequal Leg Angle specimens. A linear regression technique described by Helwig and Fan [2000] was used to determine the measured stress in the angles. Once the gross stress away from the connection was measured, it was multiplied by the appropriate shear lag factor to determine the effective stress. All strain gages used were Vishay Micro-Measurements CEA-06-250UN-350/P2 gages, which are thermally compensated for mild carbon steel.

The 5 ksi stress was the minimum stress value in the loading cycle. The desired stress range of the test was then added to this minimum to give the maximum stress value in the loading cycle (i.e. a test with a S_R = 15 ksi, would have S_{min} = 5 ksi and S_{max} = 20 ksi including shear lag effects). Once the applied load to achieve the minimum stress value was established, the load was increased to determine the value at the maximum stress and force and displacement measurements were taken.

Due to the complexity of the setup, the force at the minimum stress range was not always uniform for all cross frame specimens of the same type. In addition, once the load range was established, the setup was cycled 2-5 times until the force and displacement measurements had stabilized, making minor adjustments during the process.

Using the load range determined by the described process, the cross frame member stress cycled between the maximum and minimum following a sine curve. The frequency of the test was gradually increased until the setup was no longer stable, meaning the max/min stresses were not being reached, the force feedback error became larger than 10 kips, or the setup or hydraulic ram made uncharacteristic noises. The

frequency was then reduced to maintain proper control of the setup and the test was begun.

Each test was run until failure. Researchers monitored the stress ranges in the appropriate elements and recalibrated the applied force range if discrepancies arose. Due to the time-consuming fabrication of the braces, specimens were sometimes temporarily repaired to evaluate fatigue crack growth at secondary locations. These tests are indicated with the letters 'A' and 'B' following the test specimen designation to indicate reuse of the specimen. The test results at the first failure have the 'A' while the results of at the second failure after repairing the cross frame have the 'B'.

7.3.5 Testing Equipment

The test was conducted utilizing a closed-loop force-controlled system. A 30 gallon per minute (gpm) hydraulic pump was used to provide hydraulic oil to the system. The oil flowed into an MTS high-pressure accumulator, which was connected to an MTS Flextest® SE Controller and a 15 gpm servo-valve. The system was monitored by a portable data acquisition system.

The computer software monitors the force response from the load cell attached to the hydraulic ram and controls the flow of the oil into the system via the servo-valve to make sure the desired force range was attained. The following figure graphically depicts the force-controlled system.

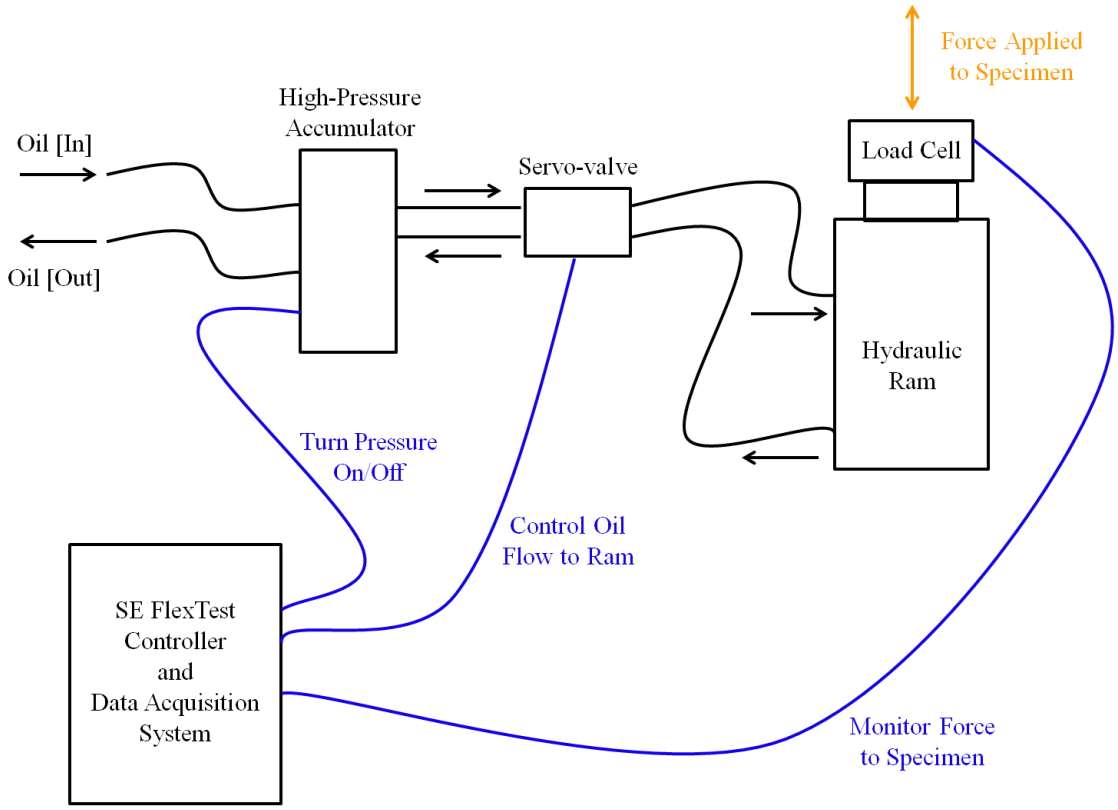

Figure 7.16: Schematic of Force Controlled System

Part I: X Frames- Equal Leg Angles

7.4 X FRAME- EQUAL LEG ANGLE DESIGN

The initial design of the X frame using equal leg angles followed the TxDOT standard detail for Type E cross frames shown in Figure 7.17. The angle size selected was L4x4x3/8, which, based on a review of several completed bridge designs, would be appropriate for the test frame spacing and girder depth. In addition, the L4x4x3/8 angles were used in the large scale cross frame stiffness tests, providing continuity in the research.

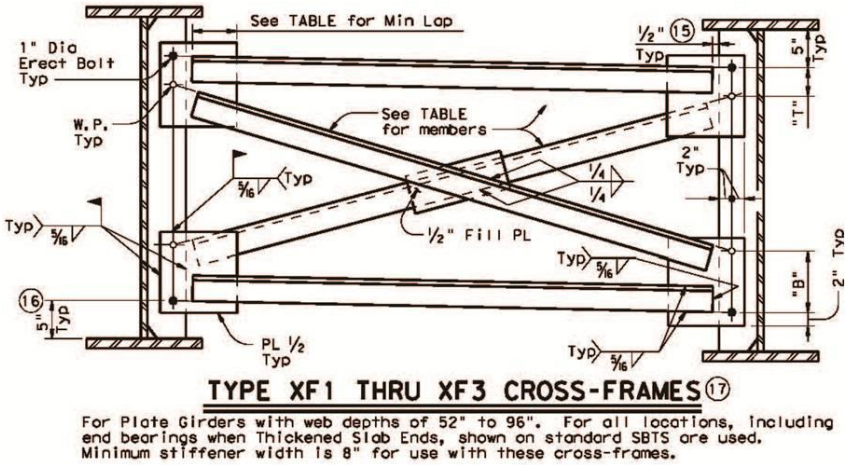

Figure 7.17: Typical TxDOT X Frame Detail [TxDOT 2010]

A typical view of the X frame specimens in the testing frame is shown in Figure 7.18.

Figure 7.18: Typical X Frame Specimen in Test Setup

When the outside girder is loaded through the hydraulic actuator, the outside edge of the cross frame specimen displaces vertically, inducing tension in one diagonal and compression in the other as depicted in Figure 7.19. The load range in the tests were established to achieve the desired stress range based upon the corresponding output from

axial forces calculated based upon the strain gage readings from the cross frame diagonals. Since angle members are not symmetric, the strain gage readings cannot be directly used to determine the axial force in the member. Helwig and Fan [2000] present a linear regression technique in which the measurements from four strain gages at one cross section location can be used to calculate the axial force in the angle member. This technique has been used successfully in previous research [Helwig and Fan 2000; Wang 2013].

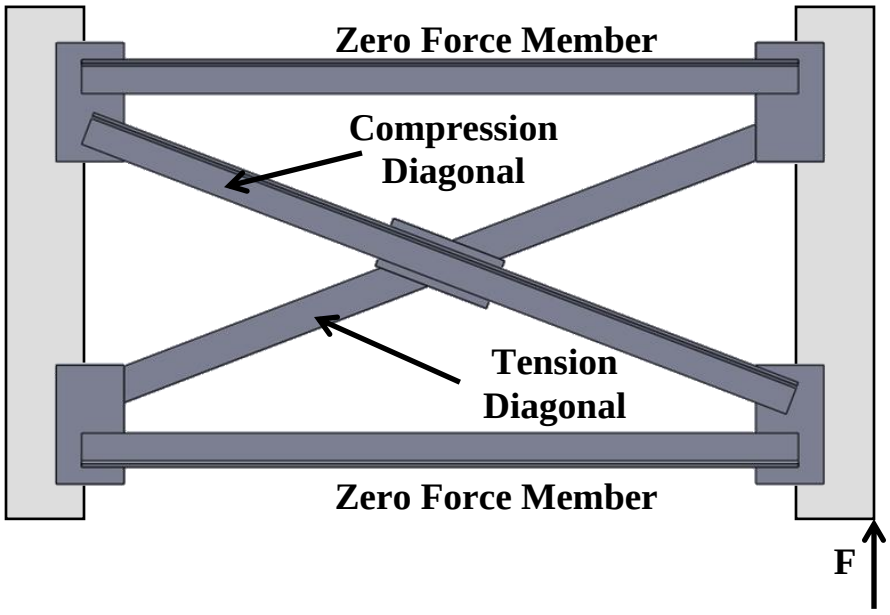

Figure 7.19: Typical X Frame Internal Forces from Load Applied

7.4.1 X Frame Test Variables

A total of 8 X frames with L4x4x3/8 equal leg angles were tested in fatigue with varying geometries. The complete details of each test are summarized in Appendix A.

For discussion purposes, the tests are divided into three primary groups of interest. First, there are the tests that most closely follow the geometry called for in the typical TxDOT detail shown in Figure 7.17. These correspond to test specimens XF_1,3,4. The weld positioning are indicated for these specimens in Figure 7.20.

The specifics of the other specimens are detailed in Figure 7.21. These tests had the same basic overall dimensional geometry, but required some changes in the layout of the gusset plates and welding. The tension diagonal for specimens XF_2, 5, and 8 was oriented on the side of the gusset away from the gusset-connection plate connection. The ramification is the critical tension member welds in these specimens do not directly interact with the gusset-connection plate welds. Additionally these tests examined the effect of placing a weld along the back edge of the angle-gusset weld, currently not specified in the typical TxDOT detail.

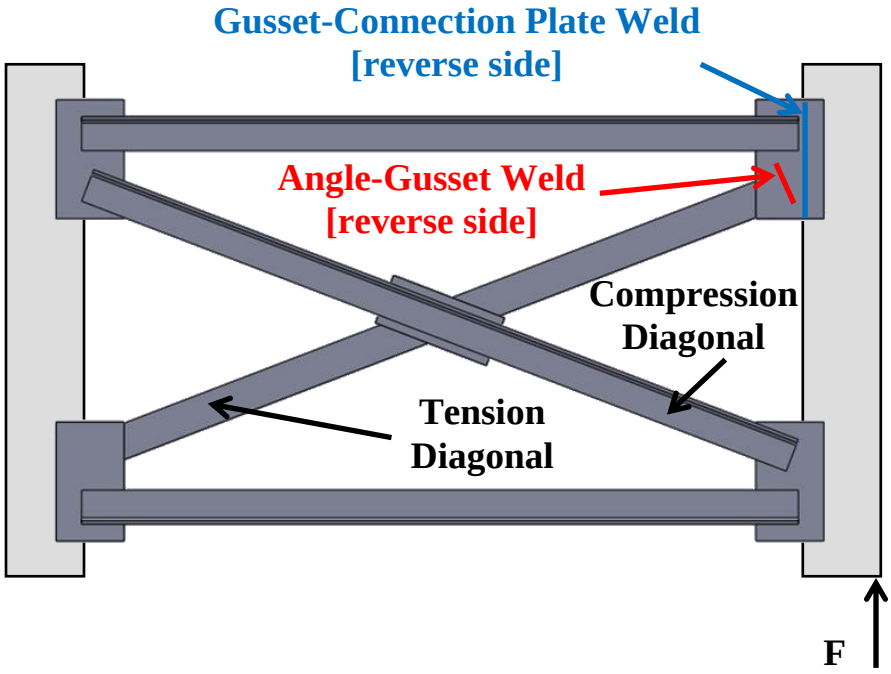

Figure 7.20: X Frame with Tension Diagonal on Connection Plate Side of Cross Frame (i.e. XF_1,3,4)

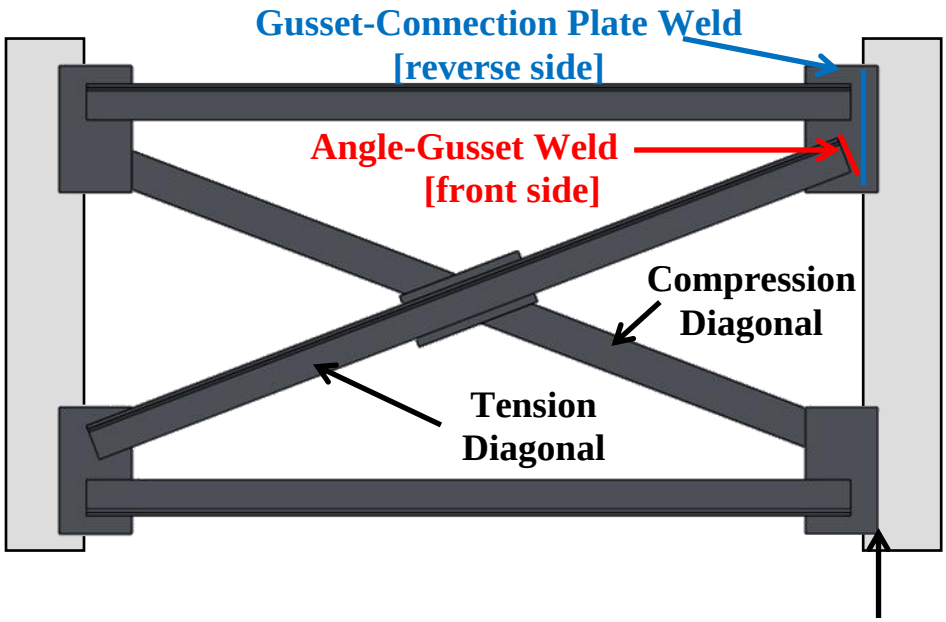

Figure 7.21: X Frame with Tension Diagonal away from Connection Plate Side of Cross Frame (i.e. XF_2,5,8)

Lastly, the research team investigated an increased spacing between the end of the angle weld and the gusset-connection plate weld. The tests used a wider gusset plate so that the overlap of the angle diagonals remained constant. These tests correspond to XF_6,7.

7.4.2 X Frame Tests of Current TxDOT Detail (XF_1,3,4)

Specimens XF_1,3,4 were fabricated following details most similar to the current TxDOT detail. The cross frame was welded together and then welded into the test frame. Upon running the first test, a fatigue crack began propagating from the toe of the angle-gusset weld into the gusset plate at a relatively low fatigue life, much lower than the AASHTO minimum Category E′. Upon subsequent inspection, it was seen the gusset-connection plate weld, typically performed in the field, intersected the angle-gusset weld, as seen in Figure 7.22 and Figure 7.23.

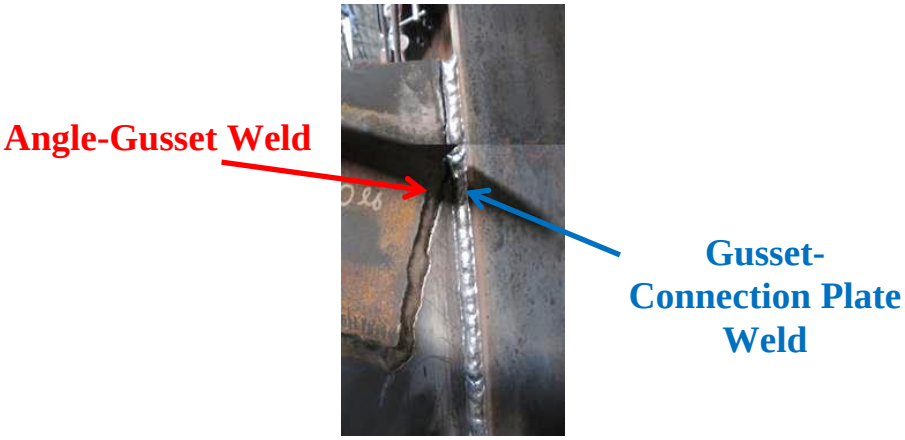

Figure 7.22: Overlap of Angle-Gusset Weld and Gusset-Connection Plate Weld (XF_1)

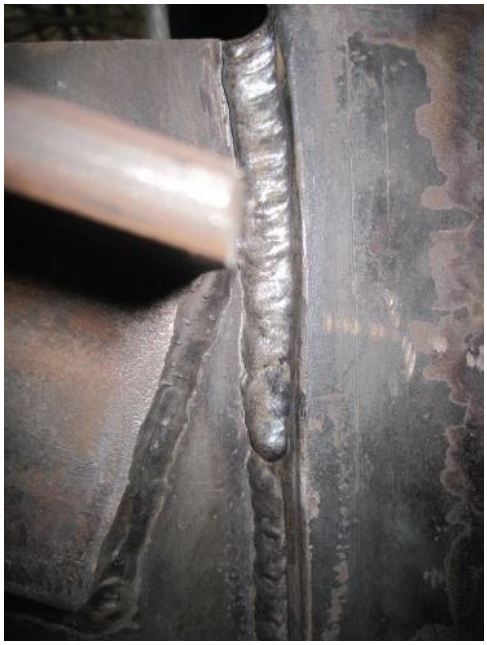

Figure 7.23: Overlap of Angle-Gusset Weld and Gusset-Connection Plate Weld (XF_4)

The overlap of any welds in a structure can lead to significant stress concentrations. The stiffness provided by welded details tend to attract larger forces, elevating the stresses in the connections. In this case, the overlap significantly reduced the fatigue life of the welds.

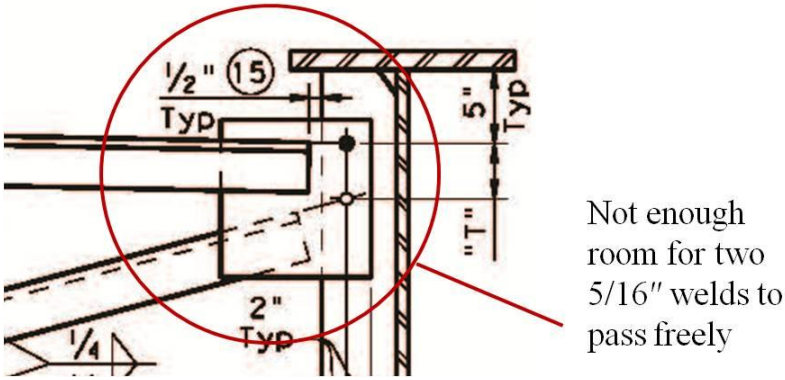

Figure 7.24: Typical TxDOT Spacing between End of Angle and Edge of Connection Plate [TxDOT 2006]

The intersecting welds are a direct result of the specified 1/2″ spacing between the end of the diagonal and the connection plate edge as shown in Figure 7.24. The fillet dimension of a 5/16″ fillet weld used for the angle to gusset plate weld combined with the 5/16″ fillet dimension for the gusset to connection plate weld adds up to 5/8″ which exceeds the 1/2″ spacing and therefore the welds must overlap. It is the recommendation of the researchers to modify this detail immediately to include a larger spacing, as the fatigue behavior is relatively poor, as indicated in Figure 7.25. The details with the overlapping welds had a rating below E′.

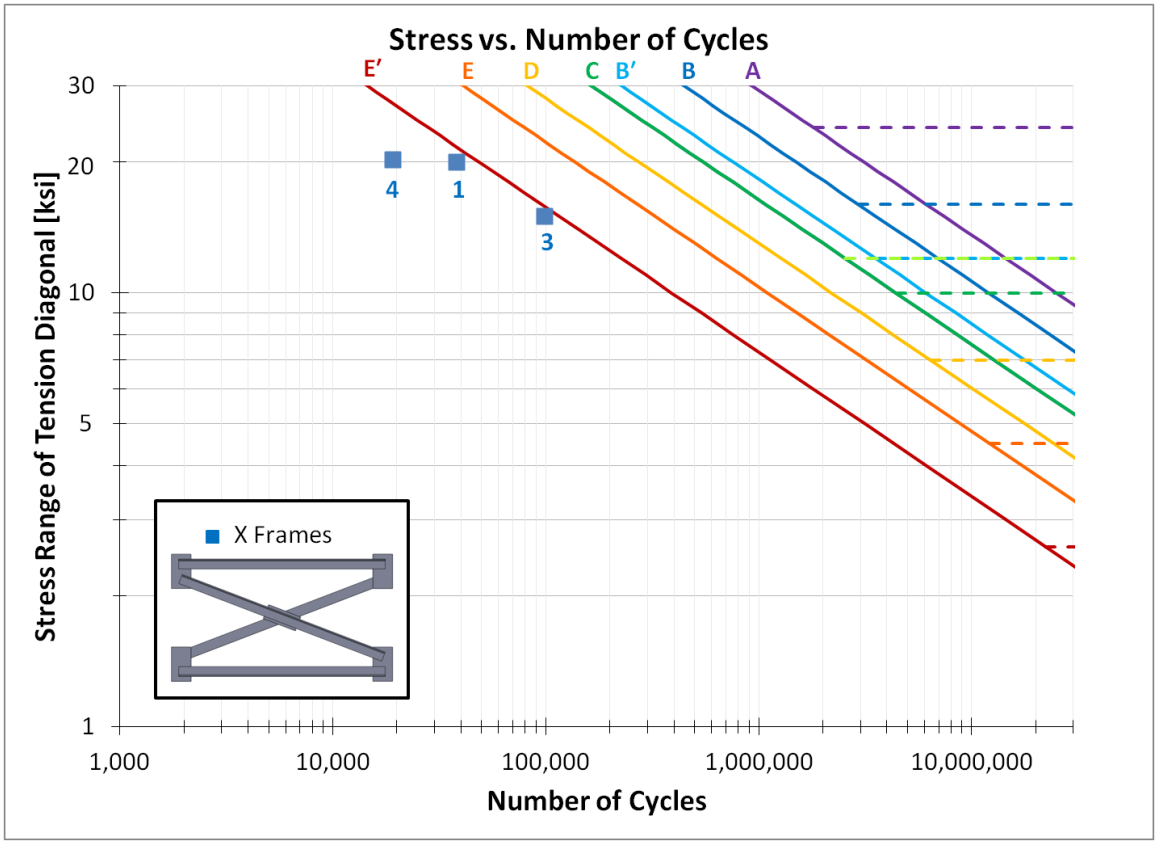

Figure 7.25: Cross Frame Fatigue Results of Specimens XF_1,3,4 with Weld Intersection

7.4.3 X Frame Tests of TxDOT Detail with Tension Diagonal away from Gusset-Connection Plate Weld (XF_2,5,8)

Specimens XF_2,5,8 were fabricated with the tension diagonal away from the gusset-connection plate weld to prevent the intersection of the welds. As the tension/compression diagonal behavior varies depending on location and force placement on the bridge, it was necessary to consider this alternate scenario.

With the lack of stress concentration at the end weld of the angle-gusset connection as in the other XF tests, these specimens experienced failure at the forward edge of the fillet weld connection propagating into the angle member. This type of failure was consistent with the observations of McDonald and Frank [2009]. An example of the type of fatigue crack that occurred is shown in Figure 7.26.

Figure 7.26: Fatigue Crack at Forward Edge of Fillet Weld into Angle Member (XF_2)

In discussing the X frame detail with fabricators and TxDOT engineers, it was determined an additional transverse fillet weld is sometimes not included along the reverse side of the angle-gusset connection that is shown in Figure 7.27. The primary reason for including the weld is to seal the connection from moisture and minimize the propensity for corrosion in the connection; however it is not required by the detail specification.

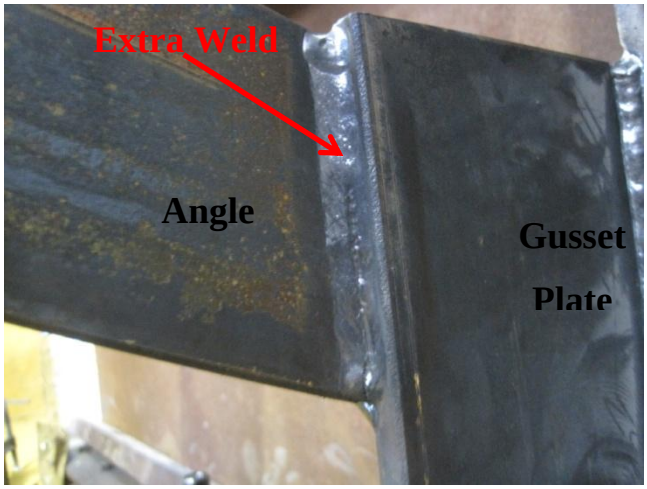

Figure 7.27: Additional Transverse Fillet Weld on Reverse Side of Angle-Gusset Connection (XF_2)

The research team decided to investigate the performance of this connection with and without this detail. Two similar specimens to XF_2 had the same basic geometry, but did not include these welds. Data from the tests indicate the fatigue performance without the weld is worse than when it is included. Both XF_5 and XF_8 failed to achieve category E′ at failure due to lack of the weld. As mention before, XF_5 was repaired with plates welded to reinforce the cracked portion, so that additional test data could be obtained. The test marked XF_5B corresponds to a second failure in the tension diagonal at the other end of the diagonal from failure XF_5A.

A summary of the test data for this set of specimens is given in Figure 7.28.

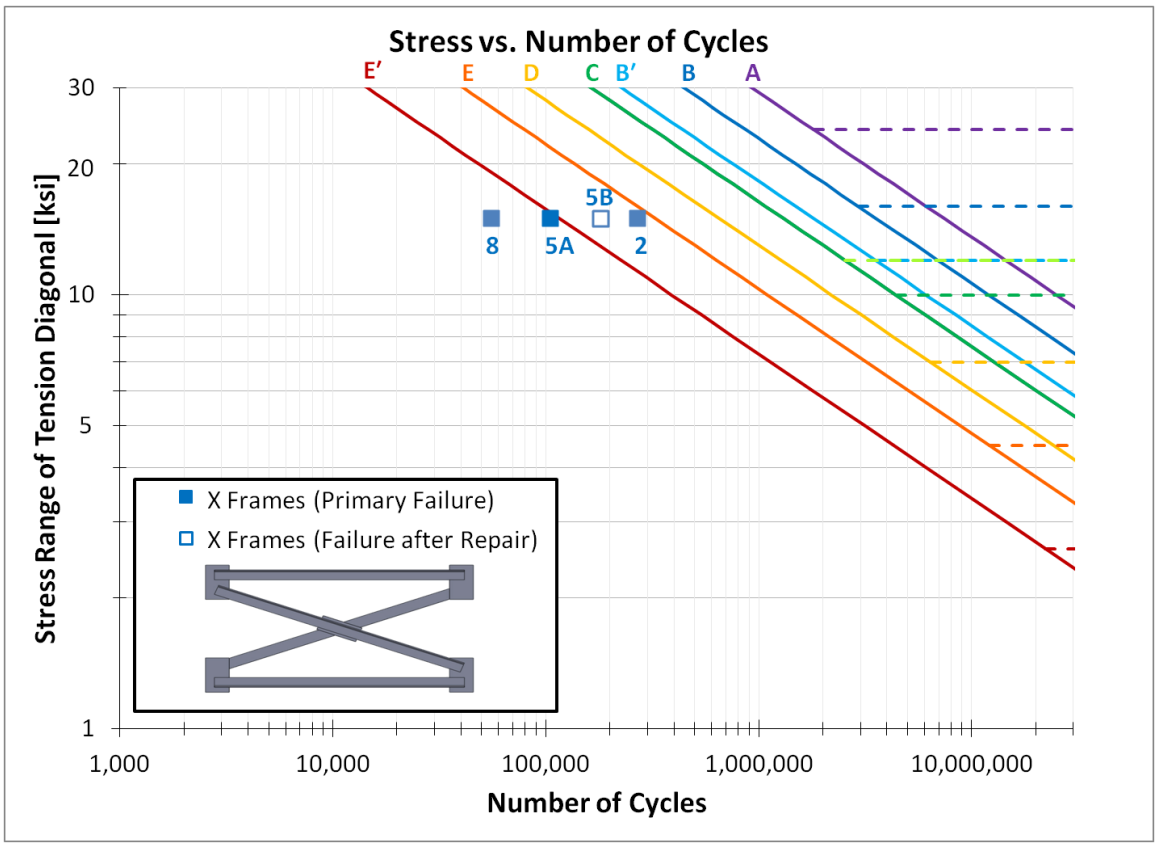

Figure 7.28: Cross Frame Fatigue Results of Specimens XF_2,5,8 with Tension Diagonal away from Gusset-Connection Plate Weld; XF_5,8 has No Additional Transverse Weld

7.4.4 X Frame Tests of TxDOT Detail with Increased Spacing between Angle-gusset Weld and Gusset-Connection Plate Weld (XF_6,7)

The final series of tests on the X frames with equal leg angles examined the effect of an increased gusset width, which in turn allowed a larger space between the end weld of the angle-gusset connection and the gusset-connection plate weld. Recall the overlap of these welds in XF_1,3,4 led to a significant reductions in the fatigue life.

To determine the spacing, finite element modeling was used to vary the gap until an optimal distance was found. When the angle is placed in tension, a hot spot stress develops in the gusset plate approximately 0.75″-1″ away from the gusset toe of the angle-gusset weld as shown in Figure 7.29.

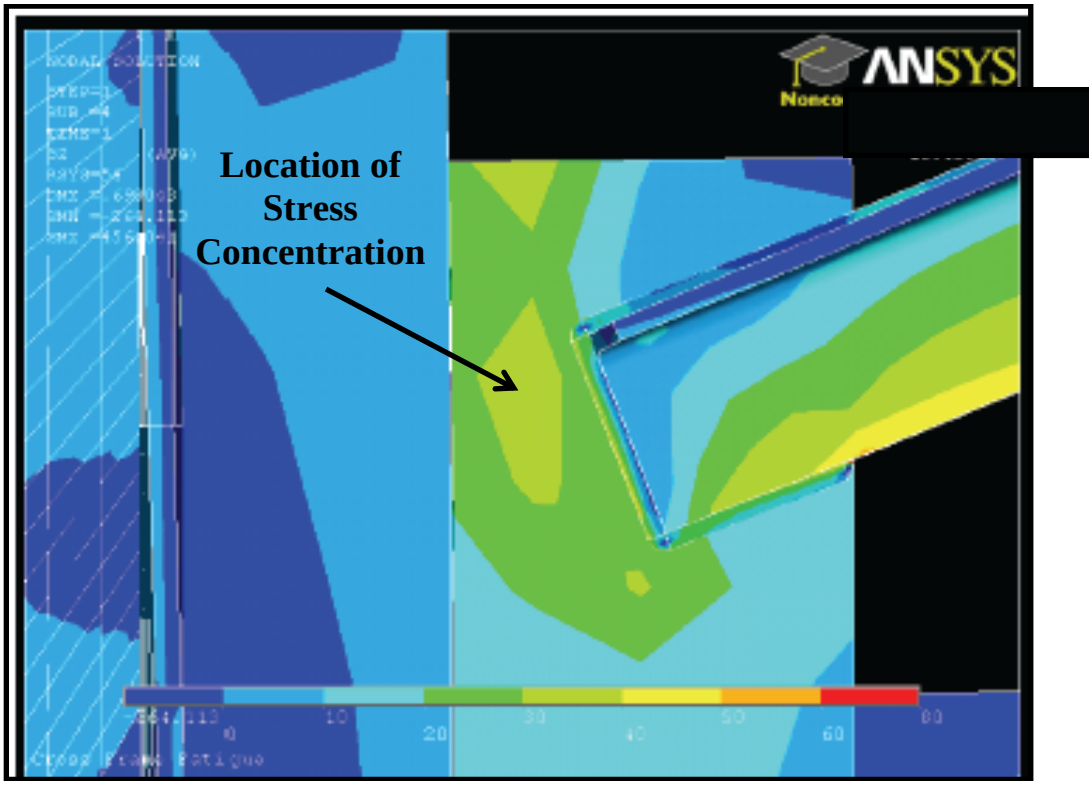

Figure 7.29: Hot Spot Stress in Gusset Plate due to Angle-Gusset Connection

Due to the location of the stress concentration, the distance between the connection plate edge and tension angle was increased from 0.5″ to 2.5″. The extra

spacing allows the highest portion of the stress concentration to be in the gusset plate, instead of at the toe of the gusset-connection plate weld. To keep the details comparable, the gusset plate width was also increased by 2″ so the angle overlap remained similar.

The extra spacing substantially increased the fatigue performance, as shown in Figure 7.30 with tests XF_6,7 reaching Category E.

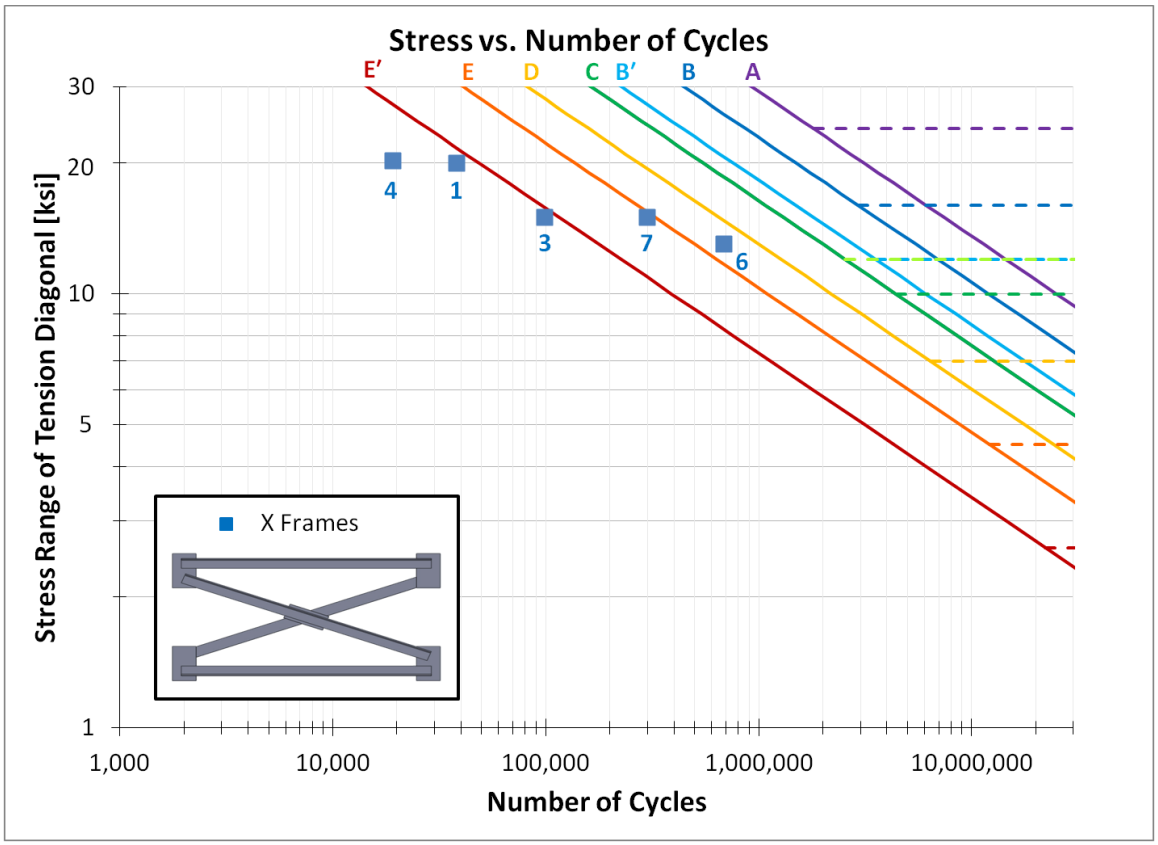

Figure 7.30: Cross Frame Fatigue Results of Specimens XF_6,7 with Increased Weld Spacing (Relative to Typical TxDOT Details in XF_1,3,4)

Although the stress concentration was reduced, failure emanated from the toe of the angle-gusset weld and propagated into the gusset plate. However, the overall performance of these cross frames was superior to the other specimens. A typical failure crack from these tests is shown in Figure 7.31.

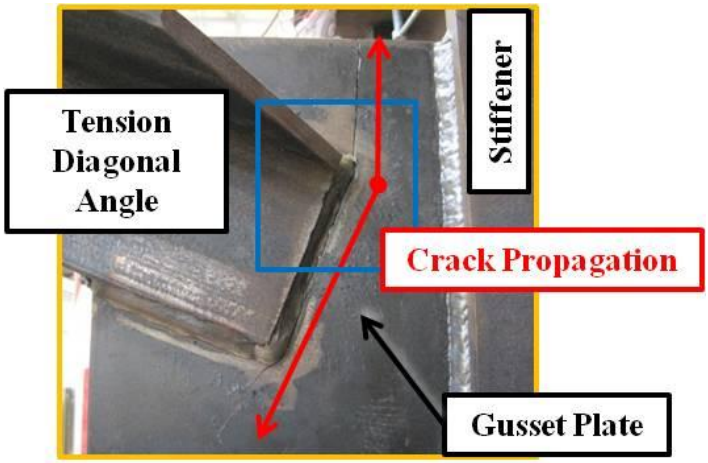

Figure 7.31: Typical Failure Crack in X Frame with Increased Weld Spacing (XF_6)

7.4.5 X Frame Conclusions

The following figure summarizes the cross frame fatigue test data on the series of X frames with equal leg angles.

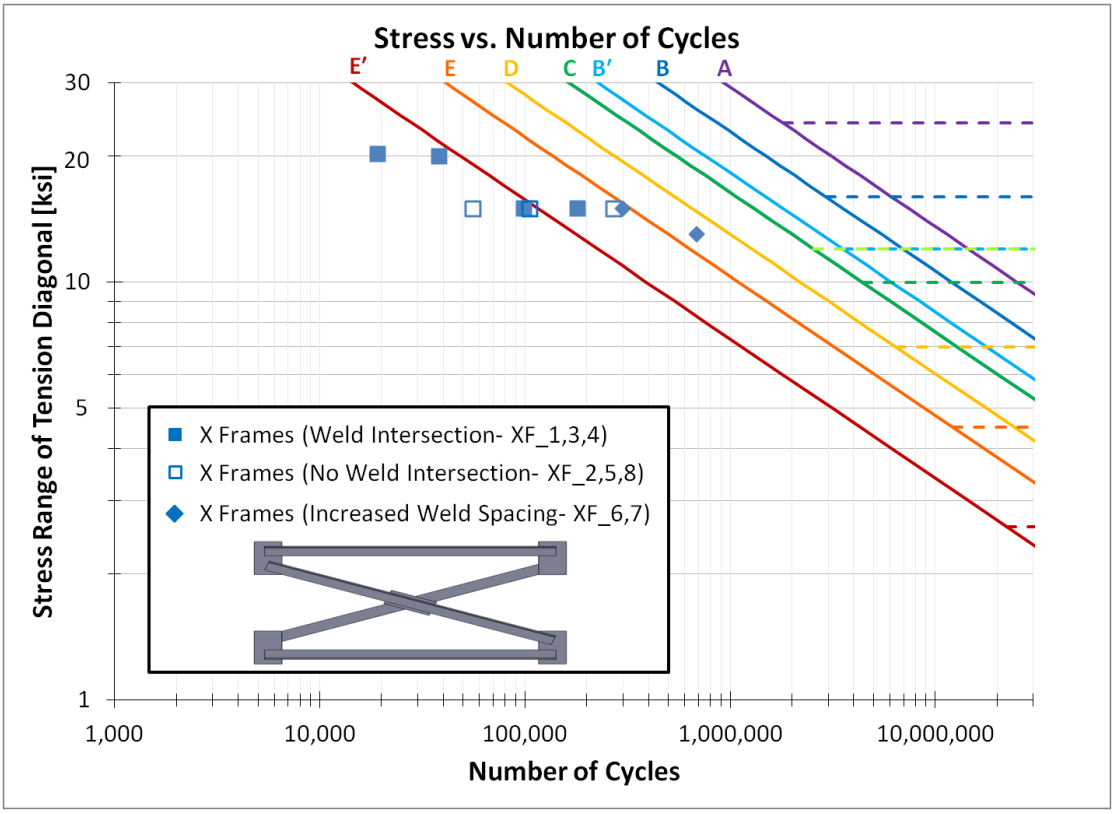

Figure 7.32: Cross Frame Fatigue Results of X Frames with Equal Leg Angles

The testing showed a variety of failure mechanisms. First and foremost, the TxDOT recommendation of 0.5 in between the end of the diagonal member and the connection plate shown in Figure 7.17 leads to poor fatigue behavior. Increasing this spacing to 2.5 in. resulted in significant improvement of life. In addition, in cases where the likely direction of tension in the diagonals is known, such as curved or severely skewed bridges, the angle in tension should be detailed so it attaches to the gusset plates on the same side as the top and bottom struts. Finally, increased fatigue life was observed in specimens that included the additional transverse weld on the reverse side of the angle along the gusset plate edge. Due to the fabrication techniques for X frames, this additional weld will not substantially increase the cost.

Part II: X Frames- Unequal Leg Angles

7.5 X FRAME- UNEQUAL LEG ANGLE DESIGN

In addition to the equal leg specimens, three specimens with unequal legs were examined using L6x3.5x3/16 members. The primary purpose of investigation was to examine the performance of the unequal leg angle cross frame relative to the equal leg X frames. As discussed in Chapter 6, the unequal leg X frame provides moderately more stiffness than the equal leg counterpart for the same area of steel. The result is mainly due to the reduced eccentricity of the angle member. With a reduced eccentricity of the unequal leg angle, it is perceived the fatigue performance should be the same as the equal leg angle X frame, if not better.

The typical TxDOT details for X frames were followed for the unequal leg specimens, however, the gusset plate depths were increased to accommodate the wider angle sections. Details on the test specimens are given in Appendix A. The unequal leg angle specimen is depicted in Figure 7.33 and a typical test is shown in Figure 7.34.

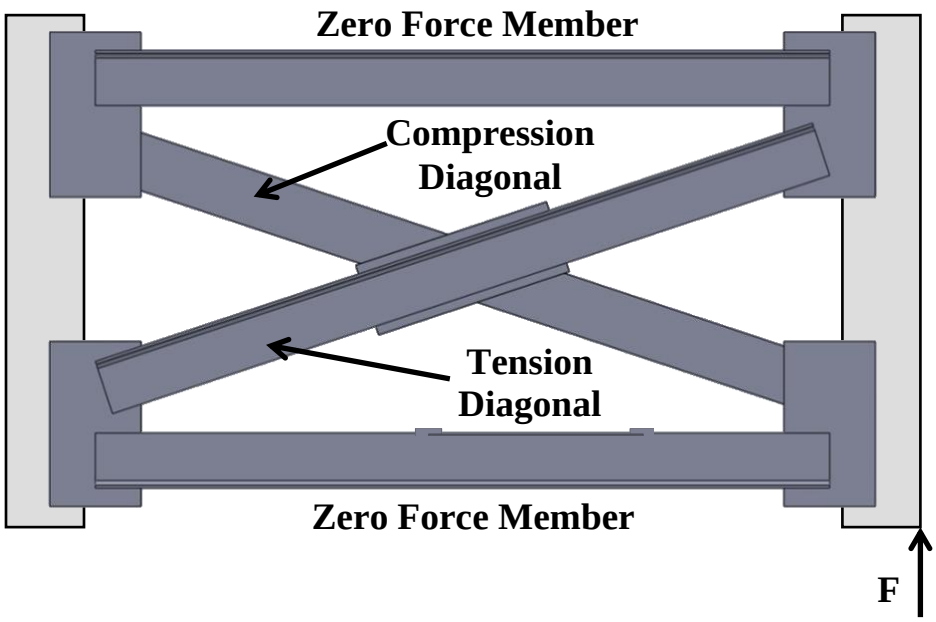

Figure 7.33: Typical Unequal Leg X Frame Specimen with Internal Forces due to Load

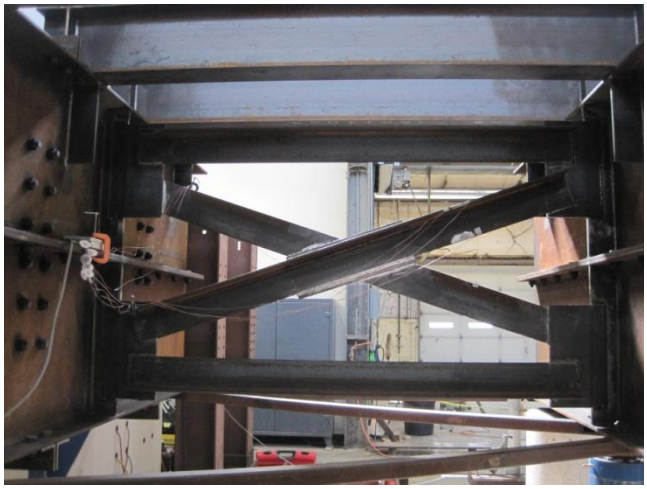

Figure 7.34: Typical Unequal Leg X Frame in Test Setup

Similar to the X Frame Equal Leg series, specimens with the tension diagonal on both sides of the gusset plate were considered. The specimens with designation XF_UL_1,2 had the tension diagonal on the side away from the gusset-connection plate weld, while XF_UL_3 had the tension diagonal on the same side as the gusset-connection

plate weld. XF_UL_3 also included the increased spacing between the end of the diagonal and the gusset plate spacing which helped to reduce the stress concentration discussed in XF_6,7.

Typical unequal leg X frame fatigue cracks are shown in the following figures.

Figure 7.35: Typical Unequal Leg X Frame Fatigue Crack (XF_UL_1,2)

Figure 7.36: Typical Unequal Leg X Frame Fatigue Crack (XF_UL_3)

Results from the fatigue tests seem to indicate the reduced eccentricity may lead to the formation of a fatigue crack at the forward edge of the fillet weld propagating into the angle member. All three specimens failed in this manner.

Additionally, specimen XF_UL_3 did not have additional transverse welds along the reverse side of the angle at the gusset edge. Based upon this fatigue test result, it seems that the weld on the reverse side of the connection does not significantly change the behavior of the unequal leg angle cross frames. The following is a summary of the X frame unequal leg angle fatigue test results plotted with the equal leg cross frames.

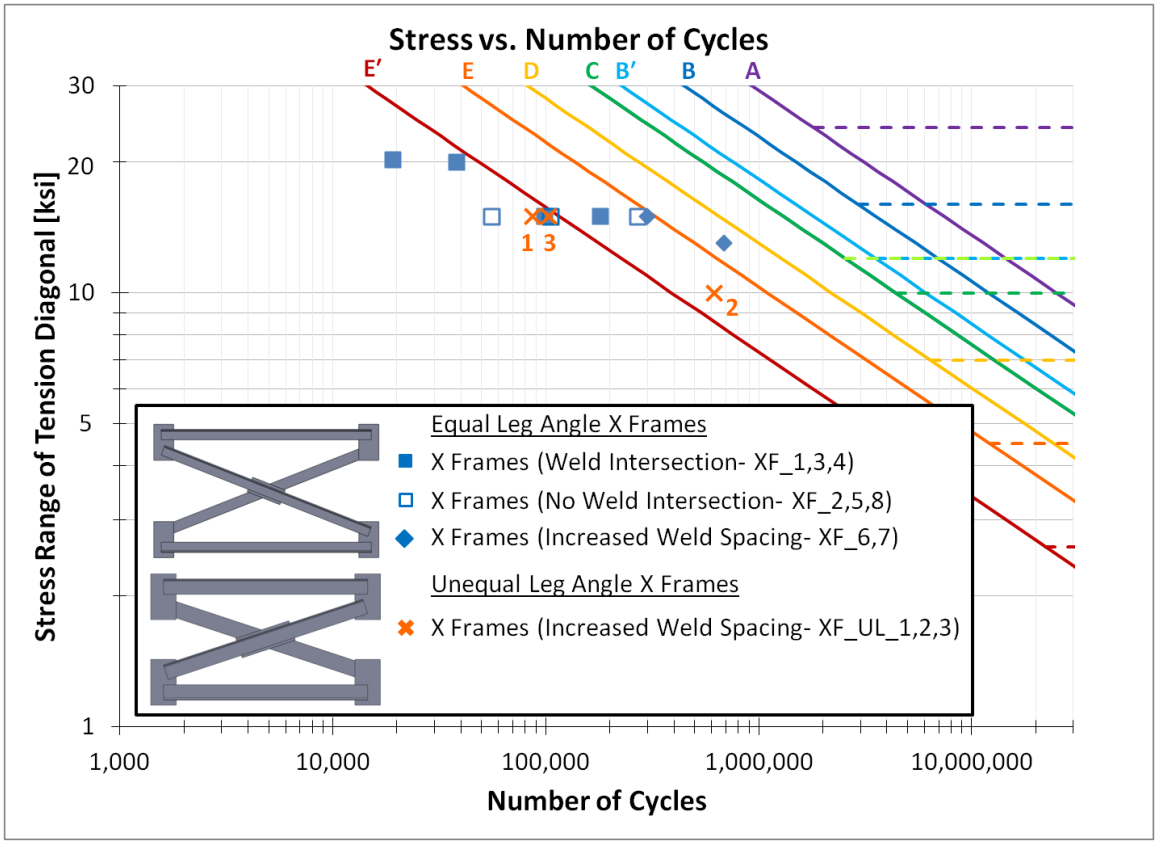

Figure 7.37: Cross Frame Fatigue Results of Unequal Leg Angles

Results from the tests indicate the unequal leg angles provide about the same performance as their equal leg counterparts when similar testing conditions are examined. It is concluded the unequal leg angles may offer a viable alternative to equal leg angles, as their fatigue performance is similar but they have slightly higher cross frame stiffness results.

Part III: K Frames- Equal Leg Angles

7.6 K FRAME- EQUAL LEG ANGLE DESIGN

K frames were also tested as part of the research program. The K-frames utilized L4x4x3/8 angles and were constructed in accordance with the typical TxDOT standard details [2010]. The following figure indicates the requirements for the K frame geometry.

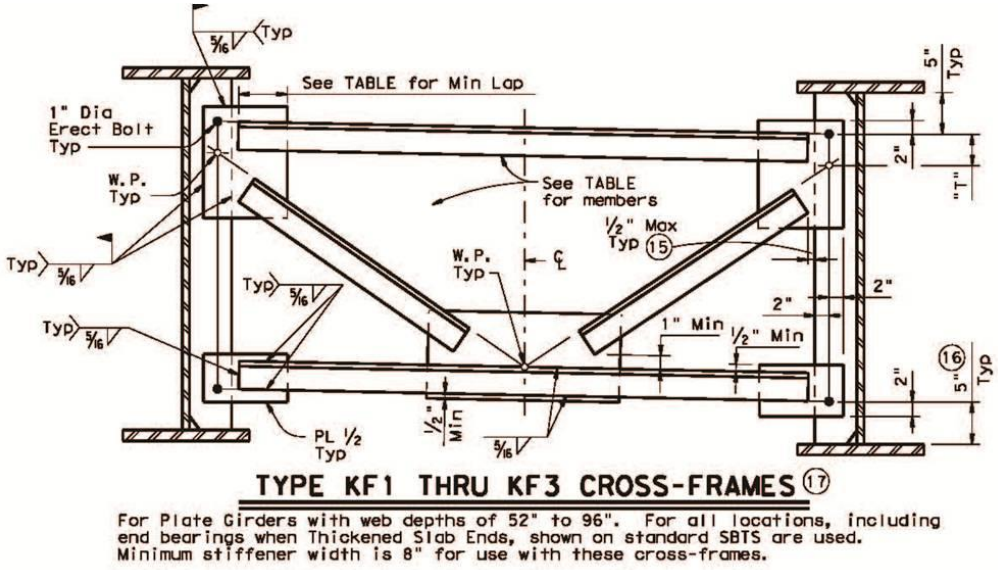

Figure 7.38: TxDOT Standard K Frame Detail [2010]

The K frame specimen in the testing frame is shown in Figure 7.39.

Figure 7.39: Typical K Frame Specimen in Test Setup

As with the other tests, the hydraulic actuator lifted the outside girder causing a differential vertical displacement between the ends of the cross frame. The cyclic load induced tension in one diagonal and compression in the other (see Figure 7.40). Similar to the previously described tests, the axial forces in the diagonals and struts were monitored using strain gages and the load range was set to achieve the desired stress range.

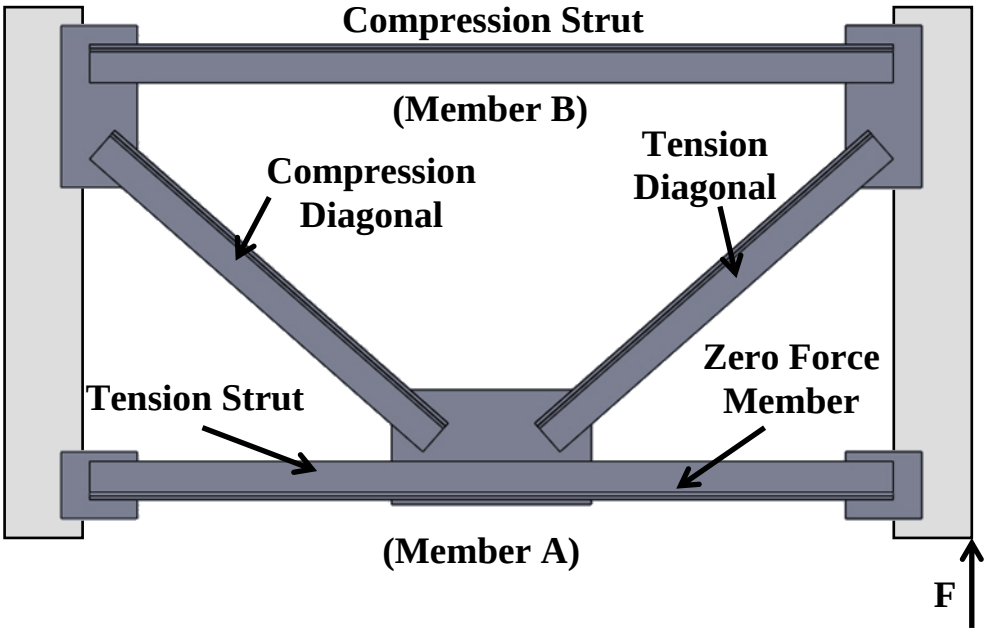

Figure 7.40: Typical K Frame Internal Forces from Load Applied

7.6.1 K Frame Test Variables

A total of seven K frames with equal leg angles were tested in fatigue with varying geometries. Five of the tests utilized L4x4x3/8 angles for all of the K-frame members. The other two tests utilized L4x4x3/8 angles for all members except for "Member A" (identified in Figure 7.40) which was an L4x4x3/4 angle and attached to a center gusset plate connection with an increased thickness of plate. More details on the tests are provided in Appendix A.

The seven tests performed on K frames are divided into three groups of test parameters. First, the tests most similar to the TxDOT detail are assessed. These correspond to specimens KF_2,3,4 and used equal leg L4x4x3/8 sections for all members.

Secondly, tests were run on K frames whose orientation was rotated 180 degrees (flipped vertically to change the orientation of the diagonals) from the TxDOT standard, corresponding to specimens KF_1,5. These tests incorporated the same basic geometry as KF_2,3,4 with the L4x4x3/8 sections for all members.

Lastly, tests were performed on K frames whose "Member A" (see Figure 7.40) was increased to L4x4x5/8 members and the center gusset plate thickness was increased from 0.5″ to 0.75″. The reasoning behind these changes is presented, as well as the difference in fatigue performance.

Similar to the X frames, tests were performed with and without a transverse weld on the reverse side of the angle connecting the angle to the gusset plate edge. The necessity of the backside weld is very important from a fabrication standpoint. If the weld can be omitted, the ease of fabrication is dramatically improved since the K-frame can be fabricated without the necessity of flipping the cross frame.

7.6.2 K Frame Tests of Current TxDOT Detail (KF_2,3,4)

Specimens KF_2,3,4 were fabricated following details most similar to the current TxDOT detail. The cross frame members were welded to the gusset plates, and the cross frame system was then welded into the test frame.

The primary cause of fatigue in cross frames is from the differential deflection of adjacent girders due to truck traffic passing over the girders. The loading that was used was the same as in the previously discussed tests with the outside girder deflected upwards. In order for the tests to be comparable to the TxDOT detail shown in Figure 7.38, the orientation of the cross frames had to be rotated to match the loading, as shown in Figure 7.41.

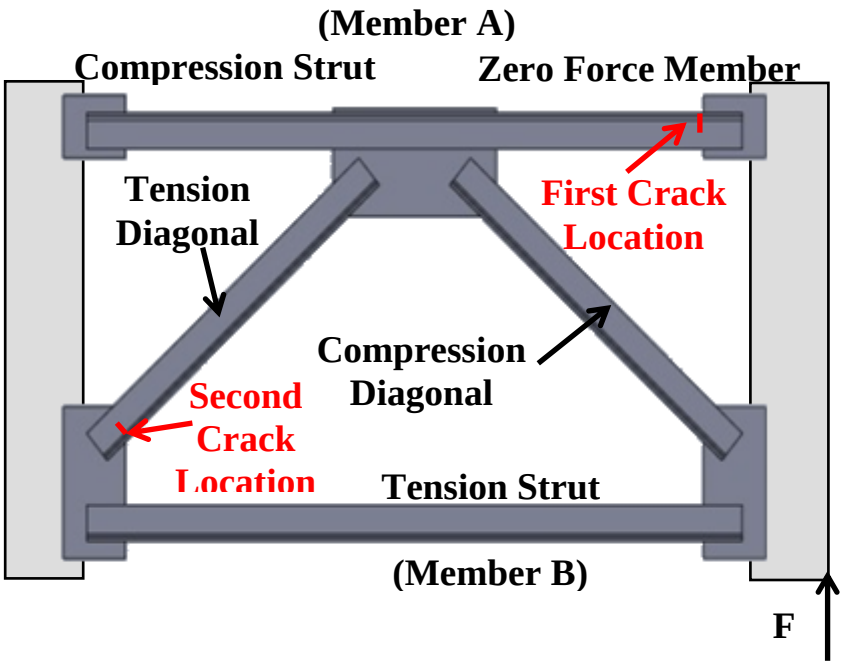

Figure 7.41: K Frame Orientation in Test Setup as given by TxDOT Detail with Member A Rotated Longitudinally (KF_2,3,4)

One potential concern in flipping the cross frame was the positioning of the steel deck girders (which simulate the concrete deck), relative to the struts. Using the finite element model of the test specimen, axial forces were measured for the struts with the load applied upward (as in the lab tests) and downward (as in typical bridge loading). The change in axial force was deemed minimal, and there was virtually no difference in the subsequent magnitude of deflection.

Finally, it is important to note the axial forces labeled in Figure 7.41 are those based on a simplistic truss analysis of the cross frame. Measured forces, along with finite element models, indicated the "zero force member" in fact had substantial stress at the connections and in specimens KF_2,3,4 was the first location to fail. An example of a fatigue crack at this location is shown in Figure 7.42.

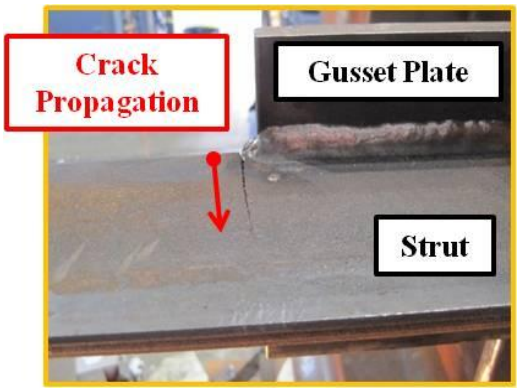

Figure 7.42: K Frame with Fatigue Crack in Strut (KF_2)

In order to consider why the K frames failed at this location, it is necessary to examine the main mode in which forces are induced in the cross frame. As previously stated, differential deflection of the cross frame leads to fatigue of the brace. If the cross frame shown in Figure 7.41 undergoes a displacement, rather than an applied force, the struts must rotate to accommodate the movement. In a true truss analysis, the "zero force member" labeled in the figure would simply undergo rigid body rotation and would not pick up force. However, since the angle-gusset welds are not perfect hinges and develop moment in the connection, the strut undergoes double curvature bending, similar to a beam. This bending of the member caused stress/strain, which is what the strain gages measured. The stress due to the bending led to a stress concentration that eventually resulted in a fatigue crack.

In order to gain further information on the fatigue behavior of the axially loaded angle members (the diagonals), the fatigue crack was repaired to permit additional testing. An example of the repair is shown in Figure 7.43.

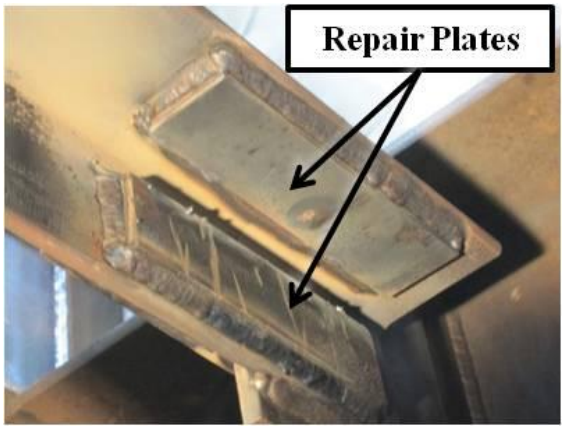

Figure 7.43: K Frame Fatigue Crack Repair in Strut (KF_2)

Once repaired, the cross frames continued to cycle until failure occurred in the tension diagonal, as seen in Figure 7.44.

Figure 7.44: K Frame Fatigue Crack in Tension Diagonal (KF_2)

The results from the fatigue tests indicate the current TxDOT K frame detail to be between the AASHTO Category E′ and E details (see Figure 7.45). Due to the relatively low stress range in the struts, the failure due to the bending stresses significantly decreased the life (Failure A). Once repaired, the failure in the angle members (Failure B) behaved similar to the predicted behavior of McDonald and Frank [2009] as well as the behavior seen in X frame specimens XF_2,5,8. In fact, the K frame angles provide better performance than the X frames if there was a mechanism to ensure failure in the diagonals.

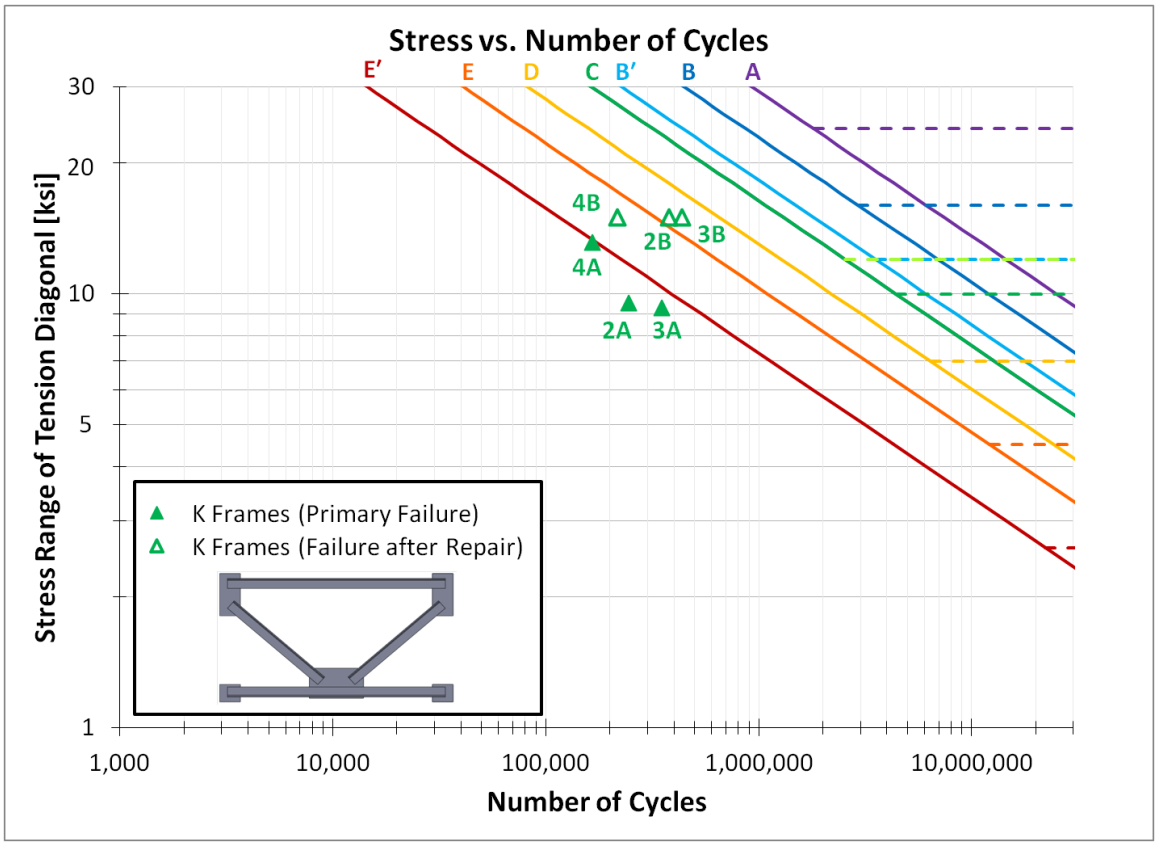

Figure 7.45: Cross Frame Fatigue Results of Specimens KF_2,3,4

Finally, one additional observation was taken from this series of tests. The current typical detail shown in Figure 7.38 has the outstanding leg of both struts on the same side (see figure below). The orientation for the bottom strut as shown was used in KF_4, while KF_2,3 had the outstanding legs symmetrical as shown in Figure 7.40.

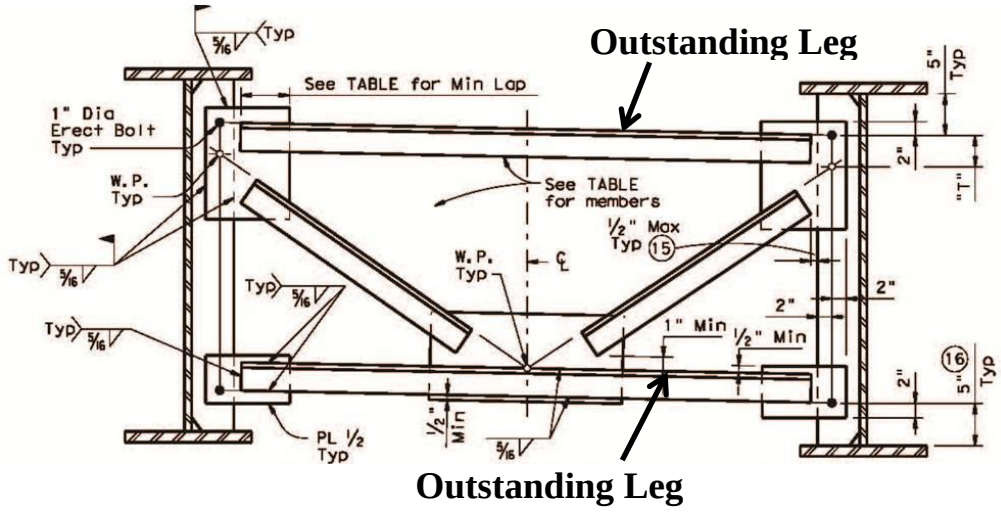

Figure 7.46: TxDOT Standard K Frame Detail with Strut Orientation Indicated [2010]

As seen in the test data of Figure 7.45, the TxDOT typical orientation increases the amount of bending stress at the connection of the strut, reducing the fatigue strength . Therefore, it is recommended to flip the bottom strut to have the outstanding leg on the bottom of the K-frame as depicted in Figure 7.40.

7.6.3 K Frame Tests of TxDOT Detail Rotated 180 Degrees (KF_1,5)

Specimens KF_1,5 were fabricated with the same geometry as KF_2,3,4 but were positioned in the test frame upside down relative to the location of the applied load as depicted in Figure 7.47. In construction, the K frames may be installed in either orientation. In terms of cross frame stiffness, both orientations provide the same torsional restraint. Therefore, the researchers wanted to determine the most advantageous arrangement of the brace.

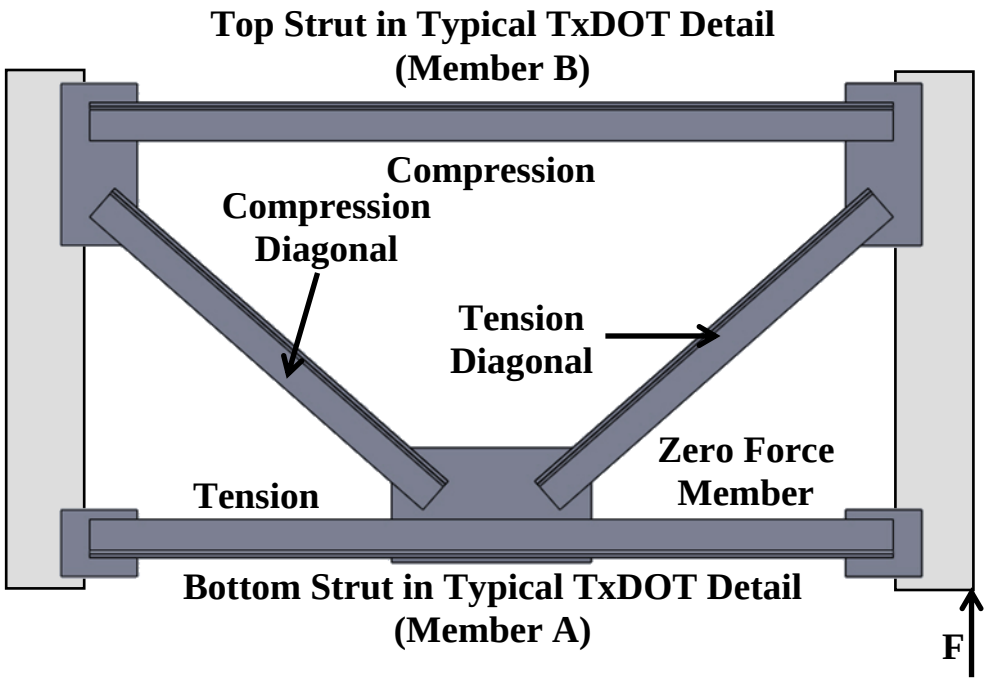

Figure 7.47: Cross Frame Orientation of KF_1,5

Following the aforementioned truss analogy, the expected failure location would be expected in either the tension diagonal or the tension portion of the bottom strut. Monitoring the stress in the cross frame members showed the tension strut to have nearly the same axial force as the diagonal, partially due to the vertical bending deformation at the connection. The results of two tests are shown in Figure 7.48 and an example of the crack forming in the tension strut is shown in Figure 7.49. As mentioned before, KF_5 developed a fatigue crack in the tension portion of Member A (see Figure 7.47) and the result is designated KF_5A, which never made it to a Category E′. A retrofit was applied to the member and the test was continued with the final failure occurring in the tension diagonal, the result of which is graphed as KF_5B and made it to a Category E′ rating.

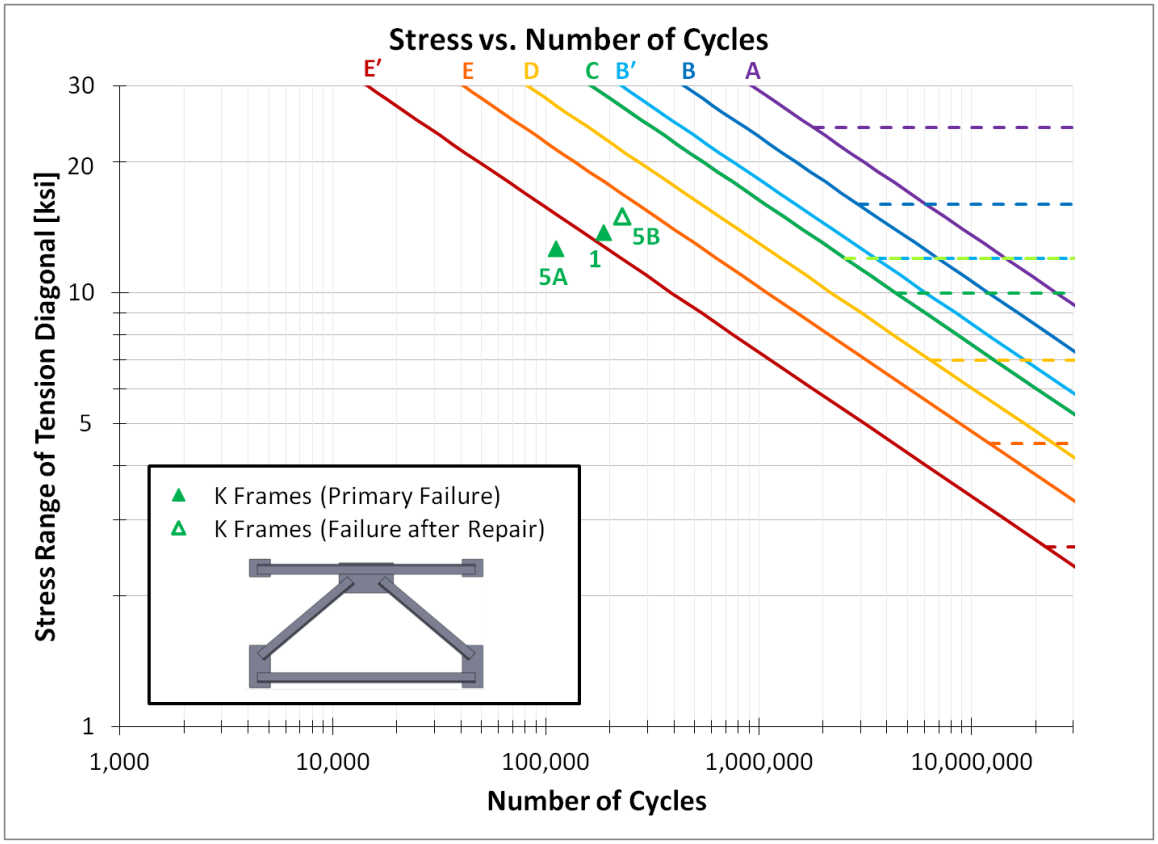

Figure 7.48: Cross Frame Fatigue Results of Specimens KF_1,5

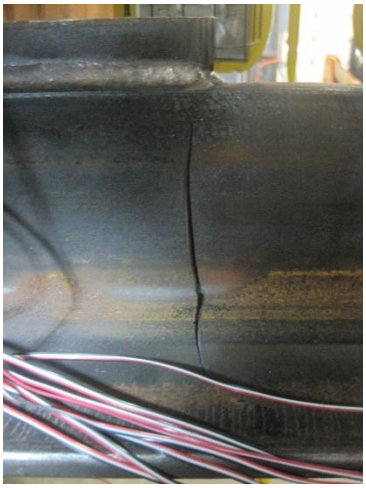

Figure 7.49: Crack in Tension Strut (KF_1)

When compared to the normal orientation of the K Frame in the previous section, the fatigue performance of the rotated specimens are inferior to the former. Therefore, the orientation shown in the typical TxDOT Standard Details provides longer fatigue life for this type of brace.

7.6.4 K Frame Tests with L4x4x5/8 Strut (KF_6,7)

As noted earlier, the failure of many of the cross frames consisted of cracking in the top strut (in the flipped orientation) of the strut due to excessive bending of the angle members. In many instances the crack was repaired so that the test could be extended to look at the behavior of other components of the cross frame. These tests are labeled with the "A" and the "B" to denote a cross frame in which the initial crack was repaired. The research team wanted to try to avoid the cracking problem in the struts and therefore the final series of tests on the K frames involved using a larger, stiffer "Member A" (see Figure 7.45) to decrease the bending stress in the member and a thicker center gusset plate. The purpose of these modifications was to extend the life of the cross frame by eliminating failure in the gusset plates and struts, so the K frame would fail by fatigue in the diagonal members. The preferred mode of failure is a fatigue crack at the forward edge of the fillet weld, propagating into the angle as discussed in the X frame test series. This failure mode correlates with the results published by McDonald and Frank [2009] and subsequently referenced in the AASHTO Specification [2012].

The primary geometry remained the same as KF_2,3,4, but with the modifications indicated by the following figure.

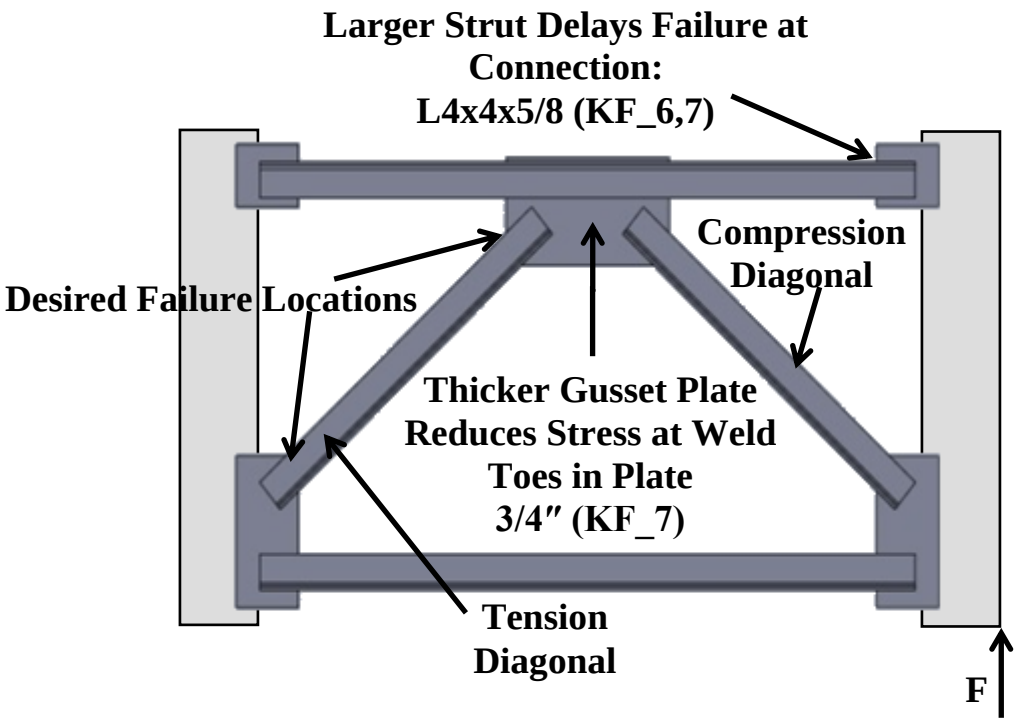

Figure 7.50: K Frame Specimen Details (KF_6,7)

The tests showed these modifications to improve the fatigue behavior of the K frame, with the result of cracking in the tension diagonal member. Results for KF_6,7 are plotted with the other data for comparison in Figure 7.51 and an example of the fatigue crack at failure is shown in Figure 7.52.

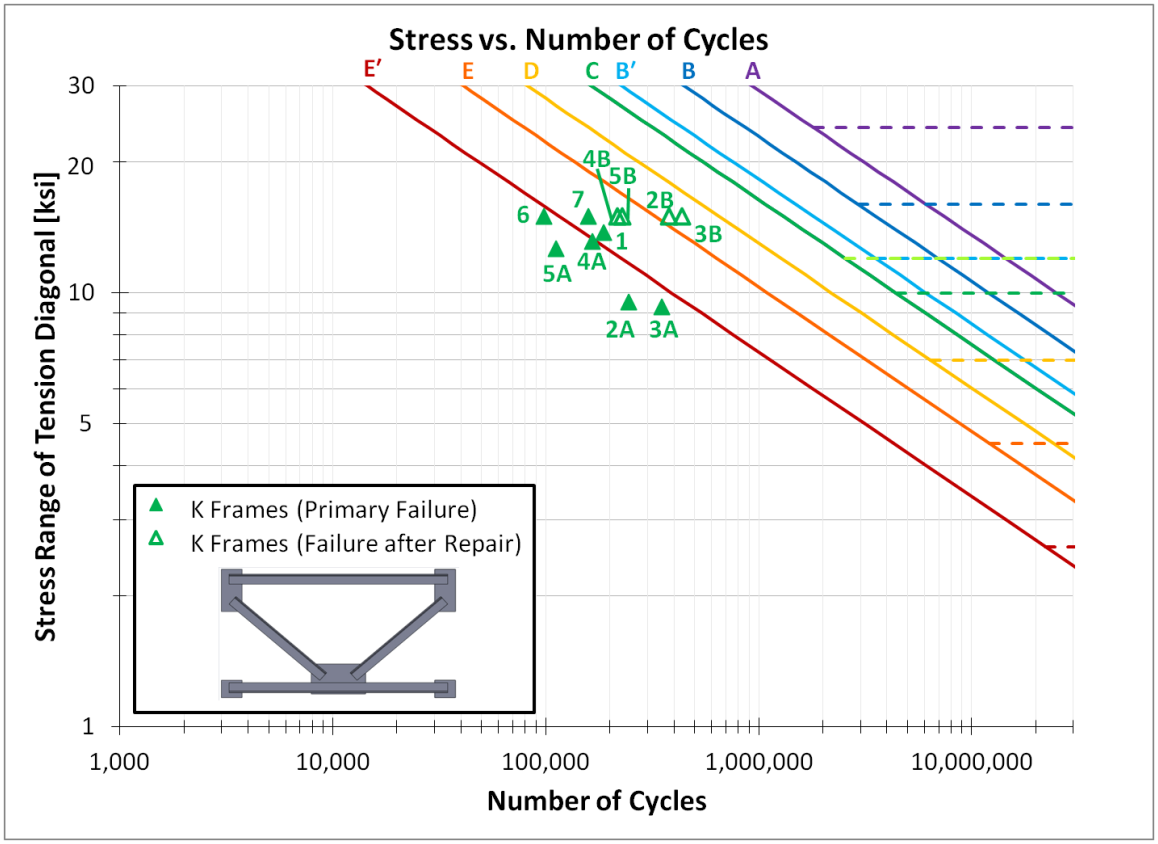

Figure 7.51: Cross Frame Fatigue Results of K Frame Specimens

Figure 7.52: Fatigue Crack in Tension Diagonal (KF_7)

7.6.5 K Frame Conclusions

Figure 7.51 summarizes the results for the K frame tests. The testing showed two primary failure mechanisms: bending of the struts leading to relatively low fatigue life and failure in the tension diagonal, either at the forward edge of the fillet weld connection propagating into the angle member, or at the back weld of the connection propagating into the plate as seen in the X Frame series of tests.

It is concluded the current orientation of the TxDOT Standard Detail offers the highest fatigue performance, and the following modifications can be made to increase fatigue life:

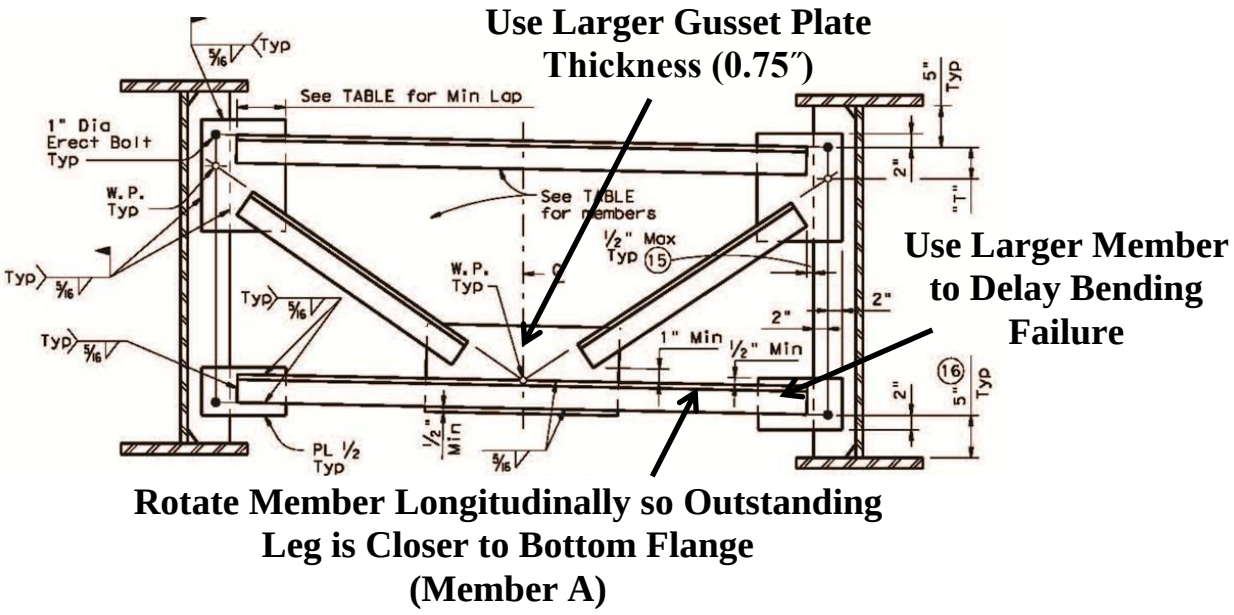

Figure 7.53: Suggested Improvements to TxDOT Standard K Frame Detail

For the tests conducted using L4x4x3/8 members, an L4x4x5/8 was an adequately larger "Member A" to cause cracking to occur first in the tension diagonal. Additionally, it is noted the extra transverse weld on the reverse side of the angles does not have a correlation to fatigue life based on the tests conducted herein; therefore, for ease of fabrication, these welds should not be required.

In terms of stiffness, K frames generally offer lower stiffness than X frames for typical girder spacings and girder depths (except for shallow, wide cross frames). However, if the stiffness calculated is still adequate for a given bridge design, then K frames would be preferred due to the more simple fabrication that does not require flipping of the cross frame. The following graph compares the stiffness ratio of K frames to X frames for various inclinations (degrees) for the diagonal (based on the X frame i.e. a 45 degree angle corresponds to a height of brace equal to the girder spacing). Results are shown for several different angle sizes. The results given include the stiffness reduction factor outlined in Chapter 6.

One can observe the plot indicates that for diagonal inclinations between 20-30 degrees utilizing the larger angle sections, the K frames can offer better stiffness than the X frames. However, as the angle of inclination increases, X frames become much more efficient.

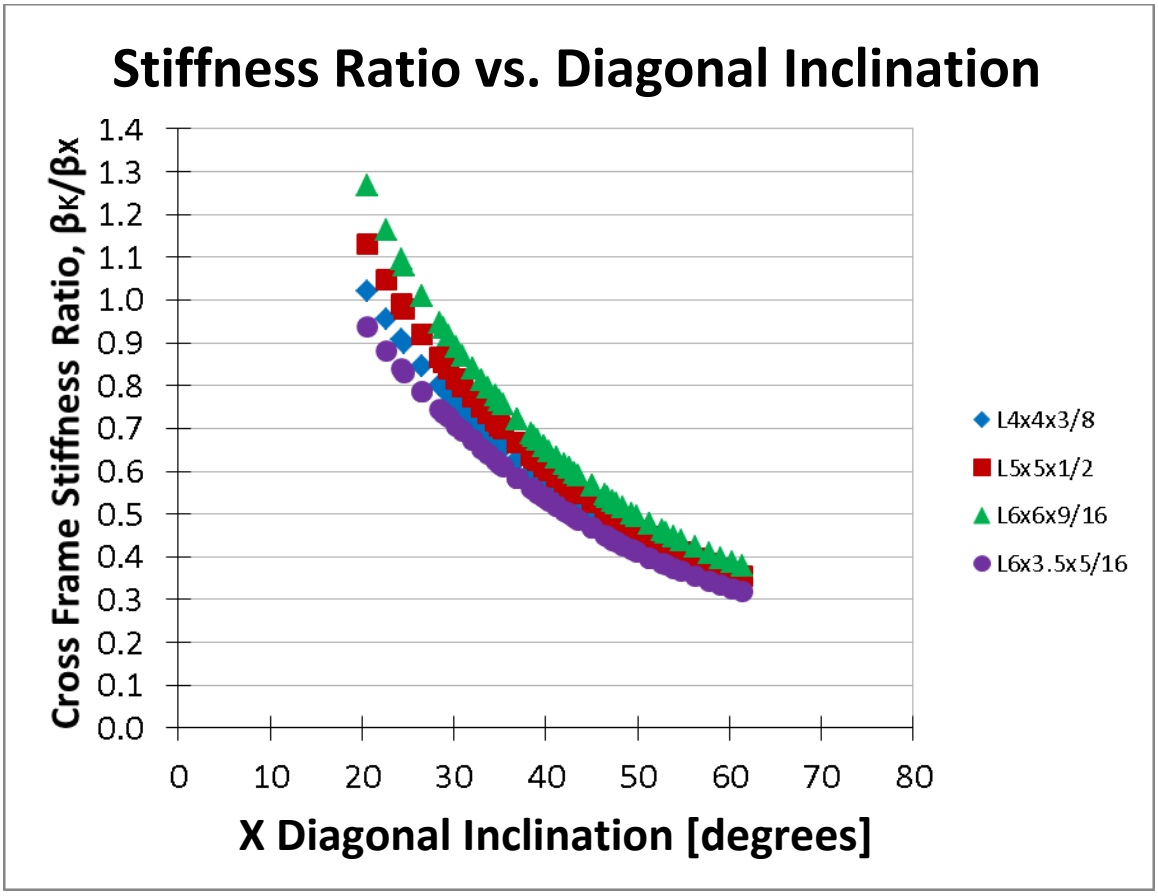

Figure 7.54: X Frame to K Frame Comparison for Different Geometries and Cross Sections

The following table compares the stiffness ratio (β_K/β_X) for various girder spacings and brace heights for cross frames utilizing L4x4x3/8 angles.

Table 7.2: Comparison of K Frame Stiffness to X Frame Stiffness Using L4x4x3/8 Members for Various Girder Spacings and Brace Heights

Ratio of K Frame Stiffness to X Frame Stiffness (β_K/β_X) Using L4x4x3/8 Members					
		Girder Spacing			
		6 ft	8 ft	10 ft	12 ft
Height of Brace	60 in	0.57	0.72	0.85	0.96
	72 in	0.50	0.62	0.74	0.85
	84 in	0.44	0.55	0.66	0.76
	96 in	0.40	0.50	0.59	0.68
	108 in	0.37	0.45	0.54	0.62
	120 in	0.35	0.42	0.50	0.57
	132 in	0.34	0.40	0.46	0.53

Table 7.2 further illustrates the effectiveness of X frames relative to K frames for many geometries. It is observed for typical sized cross frames using the L4x4x3/8 angle, the X frames provide a higher stiffness than the K frames. As the height of brace increases for a given spacing (or the angle of inclination increases), the effectiveness of the K frame decreases. However, as the girder spacings increase, the K frames become more effective. It is important to note in all of these cases that as long as the K frame provides the required stiffness, this type of brace is adequate for design.

7.7 Effect of Weld on Reverse Side of Angle-Gusset Connection

Another variable of interest in the currently used X and K cross frame details is the lack of a weld on the reverse side of the angle-gusset connection, as seen in the following figure.

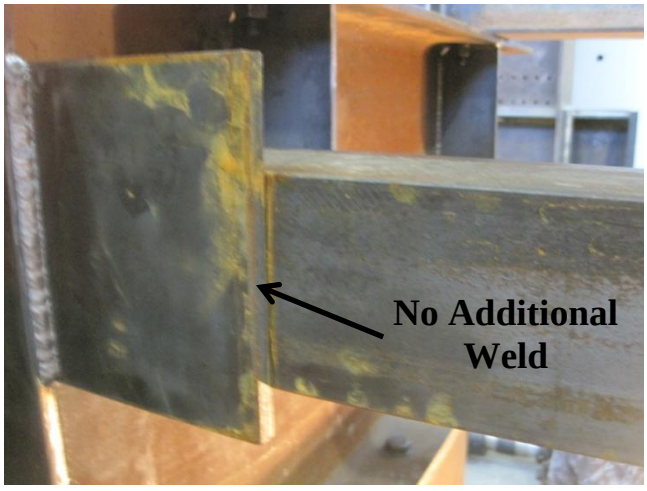

Figure 7.55: Absence of Additional Transverse Weld on Reverse Side of Angle

In discussion with the fabricators at Hirschfeld Industries, this reverse side weld is sometimes included and other times it is not**Error! Reference source not found.**. It is particularly advantageous to not include this weld on K frames because the cross frame can be laid out, welded, and then immediately stacked without requiring the frame to turned over and welded. This is possible since all the K frame members are situated on one side of the gusset plates. On the other hand, due to the crossing diagonals, X frames require at least one rotation during fabrication.

In analyzing the fatigue test data from the K frames, it is noted that specimens KF_3,4,5,6, and 7 did not have these extra welds. Referring to the S-N plot of all the K frame specimens (Figure 7.51), there is no obvious correlation between fatigue life and the presence of the backside weld. It is recommended for design these welds be optional, especially due to the advantage for reducing fabrication time and costs.

However, the X frames do show possible benefit from the reverse side welds. Referencing Figure 7.56, it seems the backside welds significantly improve the fatigue

behavior. It is noted that the two data points to the far right include an increased gusset plate width, which helps reduce the stress concentration at his location, as well as the reverse side welds. It is therefore recommended that the reverse side welds be included on X frames since there is no major fabrication savings from not including the welds.

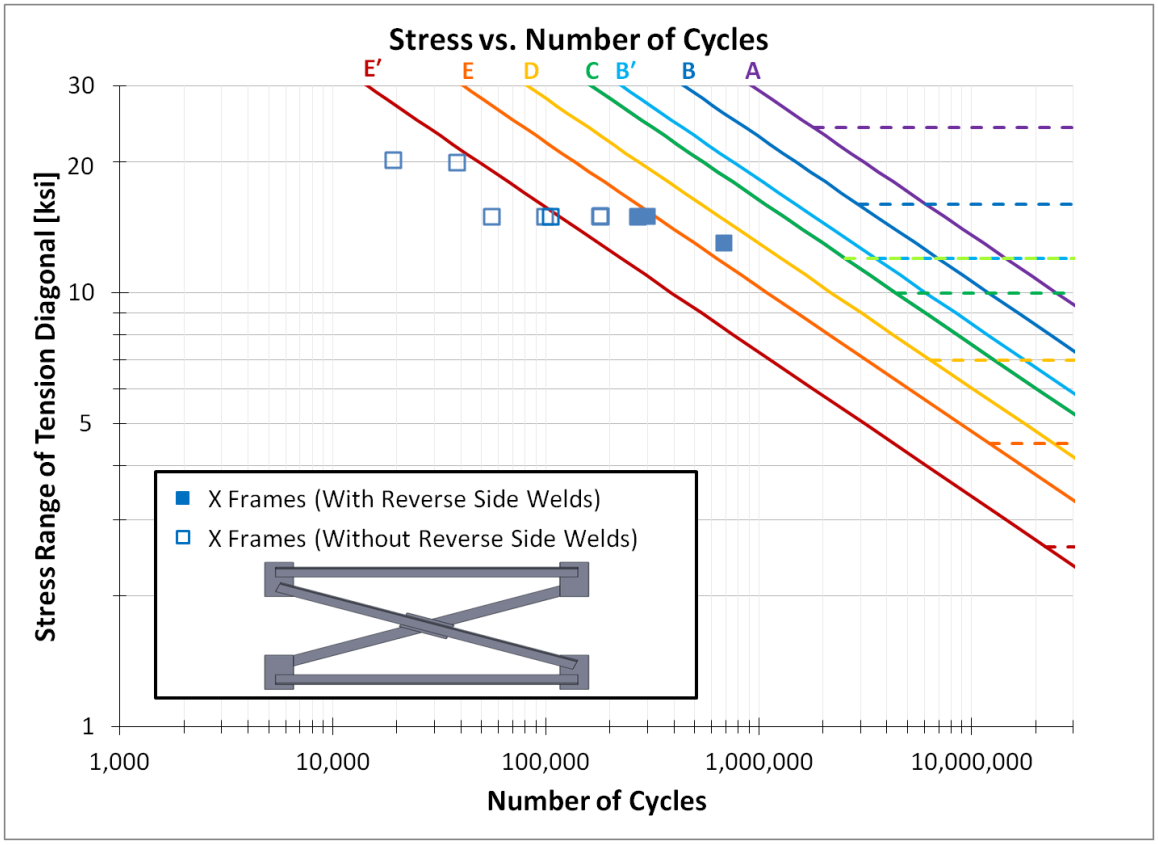

Figure 7.56: Cross Frame Fatigue Results of X Frame Specimens with and without Reverse Side Angle-Gusset Welds

Part IV: Z Frames- HSS Tubes

7.8 Z Frame- HSS Tube Design

Based on the results from the small scale experiments, Z frames were also further investigated to examine their fatigue behavior. The first series of Z-frames utilized HSS 5x5x3/8 square tubes with knife plate connections. A second size diagonal, rectangular

HSS 6x3x5/16, was used in the final test with the HSS section to investigate the impact of the member proportions on the fatigue behavior. The following figures show the specimen in the setup and internal forces generated by the applied loading.

Figure 7.57: Z Frame HSS Specimen in Fatigue Test Setup

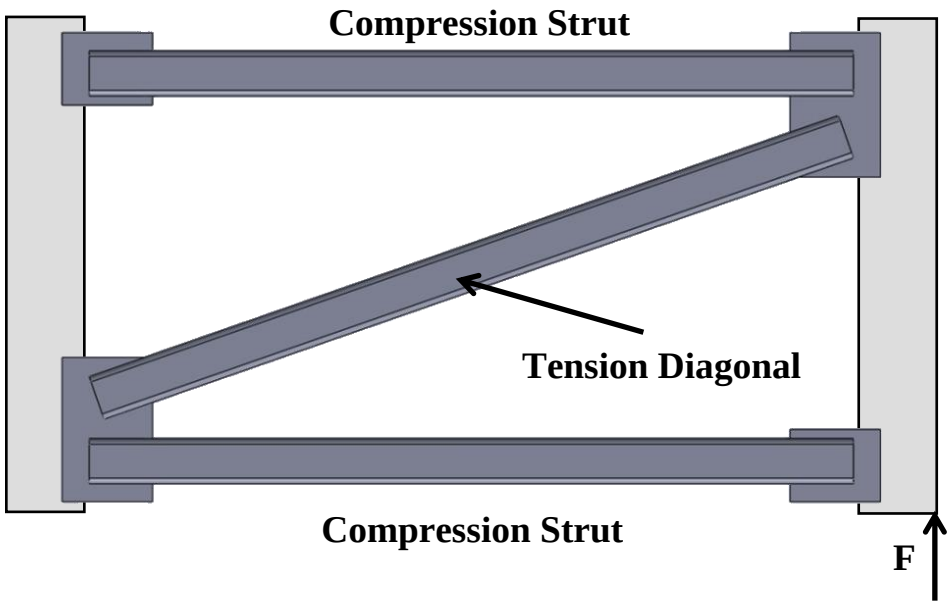

Figure 7.58: Z Frame HSS Internal Forces due to Fatigue Test Loading

7.8.1 Z Frame HSS Test Variables

A total of four Z frames with HSS members were tested in fatigue. The geometry of the specimens was adapted from the TxDOT Standard Details for X frames, using the width of the HSS tubes to size the gusset plate widths and depths.

The first three tests utilized HSS5x5x3/8 members connected to the gusset plates using the knife plate detail. The same size tube was studied in the small scale laboratory experiments and showed a promising Category E or better detail in axial fatigue. These specimens are noted as ZF_HSS_1,2,3.

A fourth test was conducted near the termination of the project using a rectangular HSS6x3x5/16 to better compare to the stiffness of the angle cross frames, and to examine the effect of the height of the tube.

7.8.2 Z Frame Tests using HSS5x5x3/8 Members (ZF_HSS_1,2,3)

As discussed in Chapters 2 and 4, the HSS5x5x3/8 member was chosen as an equivalent size tube to provide a similar capacity in compression as an L4x4x3/8 angle in tension.

To help alleviate stress concentrations at the forward toe of the fillet weld, a stress relief hole was included on specimens ZF_HSS_1,2. While this technique showed promise in improving the fatigue life of the axial specimens, it was readily apparent to the researchers that construction of this detail in cross frames would be difficult. During fabrication, it was difficult to precisely locate the drilled hole to provide the stress shadowing effect and to achieve fit it with the gusset plates accordingly since the hole location was often difficult to accurately locate prior to fit up.

The third specimen, ZF_HSS_3 did not contain the stress relief hole, and provided similar performance to the other specimens. In addition, this specimen was fabricated using a plasma torch rather than a band saw to cut the slots. From the test results, no difference in fatigue behavior was noted. The following figures show typical cracks in the square HSS members.

Figure 7.59: Typical Z Frame HSS Fatigue Crack (ZF_HSS_2)

Figure 7.60: Typical Z Frame HSS Fatigue Crack (ZF_HSS_3)

The typical mode of failure was the introduction to cracks at the tube toe of the forward edge of the fillet weld propagating into the tube. Additionally, cracks may have initiated at the critical stress point on the circular stress relief hole, or at material notches in the plasma cut slot. These failures were consistent with the small scale fatigue tests. Once fatigue cracking had initiated, some specimens developed cracks through the throat of the fillet weld, typically only after the primary cracks had become quite large.

The results from the fatigue tests are given in Figure 7.61.

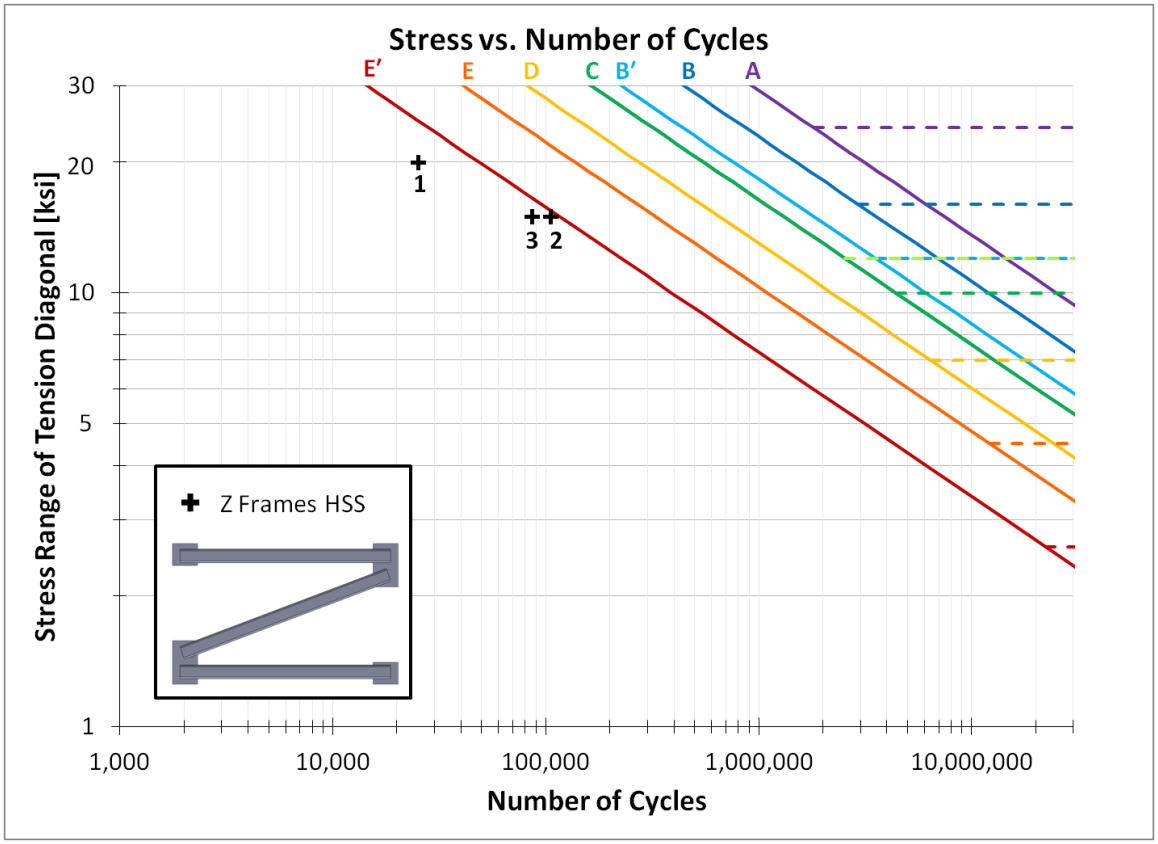

Figure 7.61: Cross Frame Fatigue Results of Specimens ZF_HSS_1,2,3

From the test data, it is seen the HSS tube specimens failed at a stress state corresponding to less than a Category E′ detail using the AASHTO Specification. This result was surprising considering the superior performance determined by the small scale laboratory tests and underscored the importance of full scale testing. Based upon the small scale component tests, the Z-frame with the HSS sections would have been the top recommendation based upon fatigue performance. However, the full scale tests demonstrated shortcomings in some HSS sections for application in cross frames bracing.

Upon further investigation, it was determined, that like the K frames, the singular diagonal in tension is subjected to a substantial amount of bending due to the fixity of the connections and the applied vertical load. To determine the magnitude, specimen ZF_HSS_2 was instrumented with strain gages at the quarter points of the tube (rather

than mid-length as done in ZF_HSS_1). The stress on the top face of the tube was nearly double the average stress of the member. This correlates to a significant increase in stress concentration at the connection (see Figure 7.62).

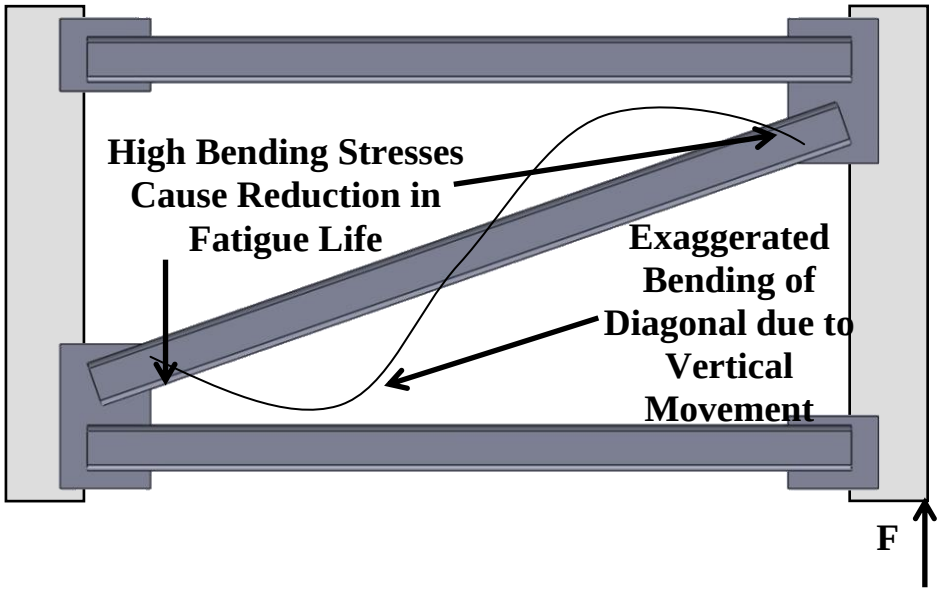

Figure 7.62: Large Bending Stress Causes Loss of Fatigue Life in Z Frames

7.8.3 Z Frame Tests using HSS6x3x5/16 Members (ZF_HSS_4,5)

Since the bending stress is proportional to the distance from the centroid, it was theorized that a rectangular tube, with the short width in the vertical direction, would help to lower the bending stress and improve fatigue performance. The following figures show the specimen in the test setup along with examples of fatigue cracks. It is noted the ZF_HSS_4 and ZF_HSS_5 also included the stress relief hole.

Figure 7.63: Rectangular HSS Z Frame in Test Setup

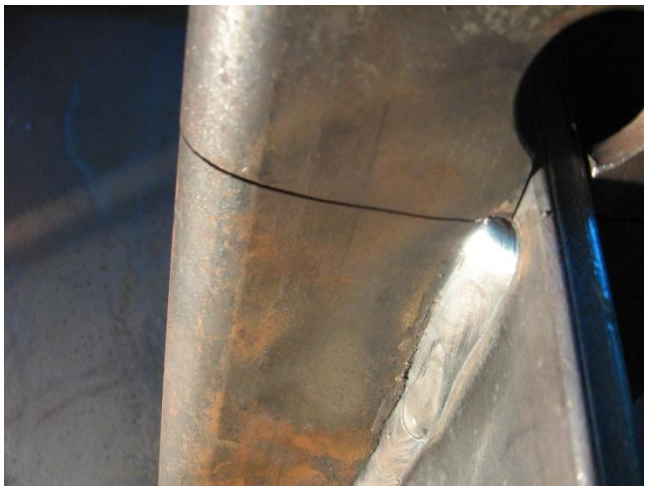

Figure 7.64: Example of Fatigue Crack (ZF_HSS_4)

The result from these tests showed the rectangular HSS tube significantly improved the fatigue life to Category E. The stress increase due to bending of the tube was reduced from 2.0 times to 1.6 times. Figure 7.65 shows the fatigue test results for all the Z frame HSS specimens.

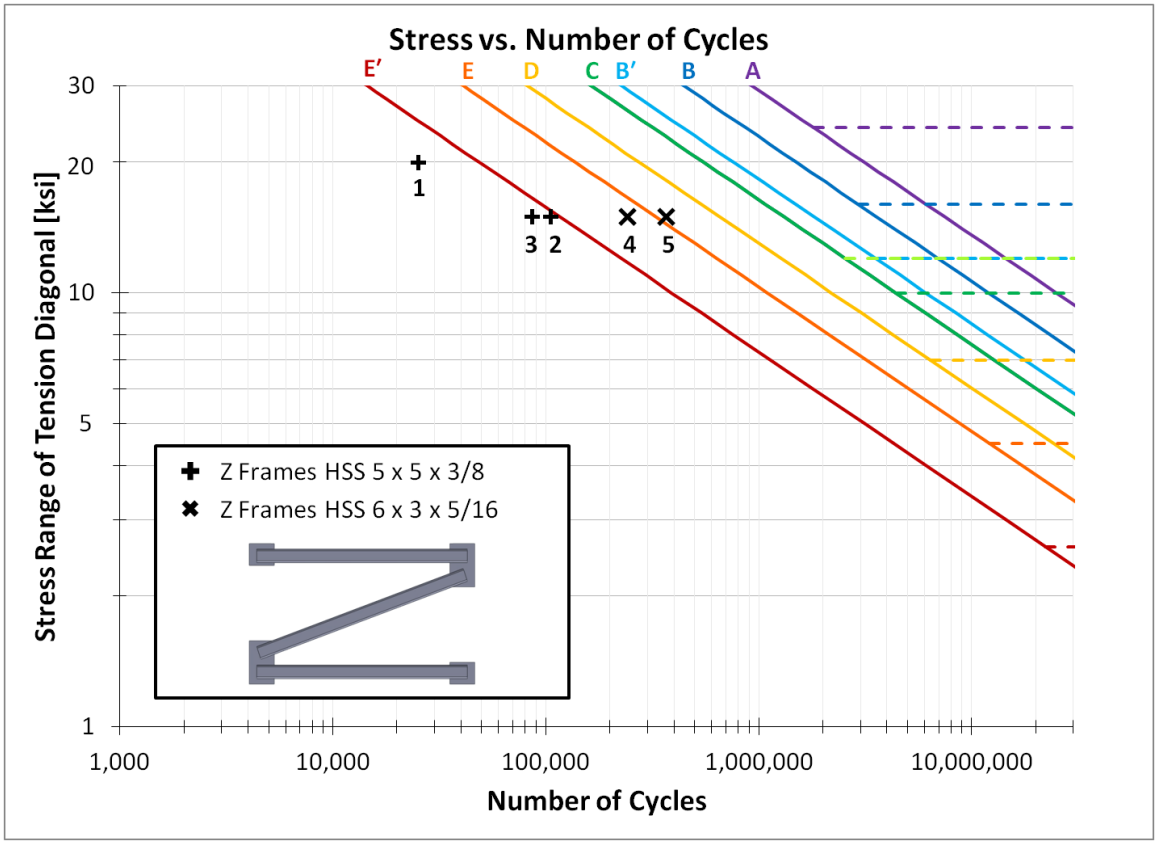

Figure 7.65: Cross Frame Fatigue Results of Z Frame HSS Specimens

7.8.4 Z Frame HSS Conclusions

Due to the relatively large cross frame stiffness of the Z Frame HSS, differential girder deflection tended to introduce a substantial amount of bending into the cross frame members and particularly the diagonal. When the tension bending stress is added to the axial tension induced from differential deflection, the fatigue performance was significantly reduced. However, despite cracking early, the tubes exhibit a large amount of resiliency since cracks propagated to nearly 3/4 the perimeter of the member before sudden fracture.

The final specimen tested utilized a rectangular HSS tube with the gusset plate inserted into slots made in the longer portion of the tube. The rectangular tube resulted in significant decreases in the bending induced stresses (since it is proportional to the

distance from the neutral axis) and resulted in a specimen that achieved adequate fatigue life for design and may offer improved life relative to the single angle X and K frames.

Part V: Z Frames- Equal Leg Double Angles

7.9 Z FRAME- EQUAL LEG DOUBLE ANGLE DESIGN

Z frames with L4x4x3/8 double angles were tested in the full scale cross frame fatigue setup as well. Although the fatigue performance of the single angles couldn't be tested with the small scale tests, these tests indicated that the built-up double angles offer improved structural performance versus the single angle detail due to the concentric nature of the geometry. The following figures highlight the test details.

Figure 7.66: Z Frame Double Angle Specimen in Fatigue Test Setup

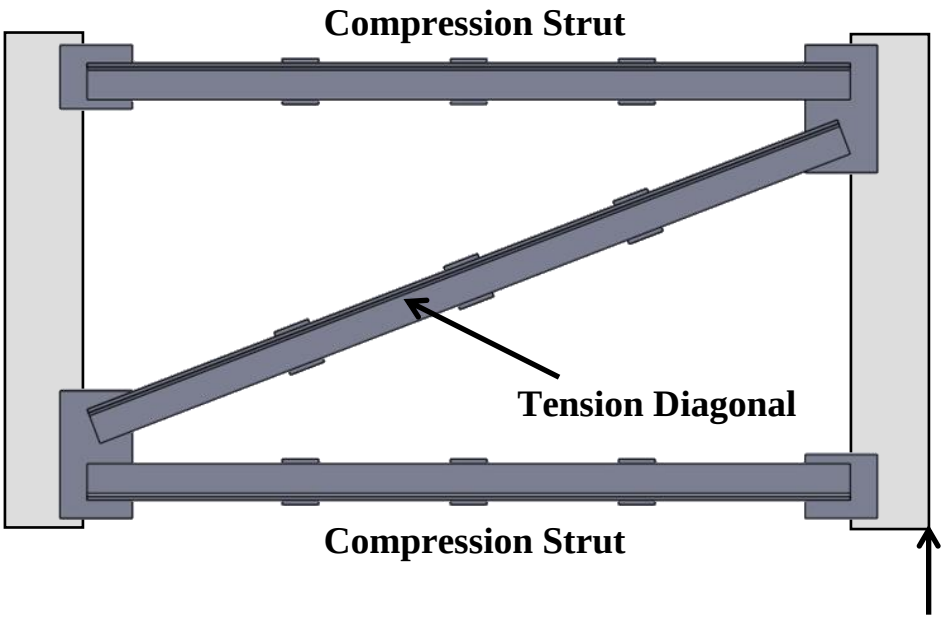

Figure 7.67: Z Frame Double Angle Internal Forces due to Fatigue Test Loading

7.9.1 Z Frame Double Angle Test Variables

A total of three Z frames with 2L4x4x3/8 members were tested in fatigue. The geometry of the specimens were adapted from the TxDOT Standard Details for X frames, but eliminating one diagonal and using double angle members. The gusset plates were modified where only a single member framed into the connection. The specimen designation for these tests are ZF_DA_1,2,3.

7.9.2 Z Frame Tests using 2L4x4x3/8 Members (ZF_DA_1,2,3)

As discussed in Chapters 2 and 5, from a stiffness and strength perspective, the double angle members offer the same if not better performance than the single angle counterparts due to the concentric nature of the connection. To verify their use in full scale cross frames, fatigue tests on the entire assembly were performed. Results from the tests are shown in Figure 7.68 and example of fatigue cracks are given in Figure 7.69 to Figure 7.71.

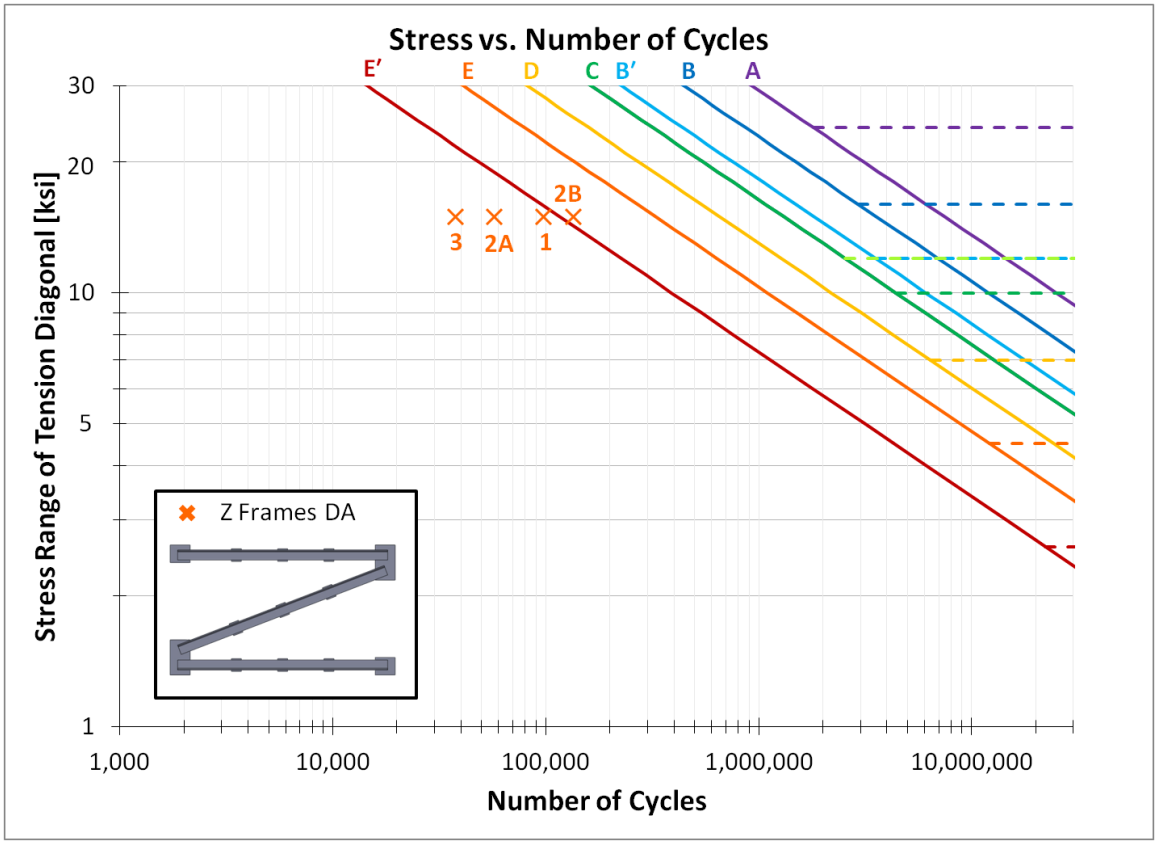

Figure 7.68: Cross Frame Fatigue Results of Z Frame DA Specimens

Figure 7.69: Typical Z Frame Double Angle Fatigue Crack (ZF_DA_1)

Figure 7.70: Typical Z Frame Double Angle Fatigue Crack (ZF_DA_2)

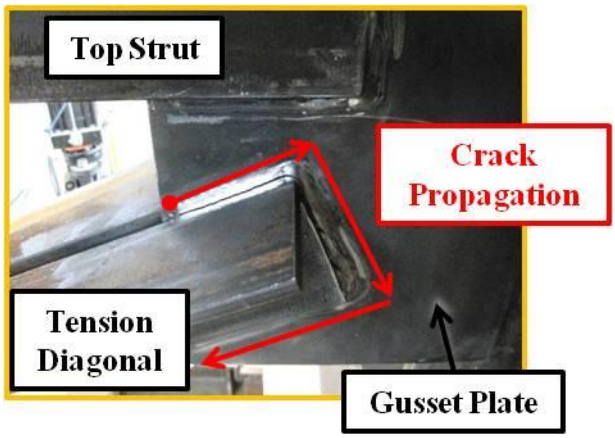

Figure 7.71: Typical Z Frame Double Angle Fatigue Failure Mode (ZF_DA_3)

Similar to the Z Frame HSS specimens, the diagonal of the ZF_DA specimens undergoes a substantial amount of bending due to the displacement of the system (see Figure 7.62). The bending significantly reduces the fatigue life, and in the case of the double angles, that rating was reduced to less than Category E′ in the AASHTO Specification.

Like the X frame series of tests, some cracks formed at the forward edge of the fillet weld, but into the heel of the double angle members. Other failure cracks were observed due to interaction between the angle-gusset welds and gusset-connection plate field weld. The most interesting failure mechanism, observed in two of the three

specimens at the end of the fatigue life, was the failure depicted in Figure 7.71. The failure began at the heel of the angle, but rather than propagating into the angle or into the plate, the crack ran along the weld throat of the connection. Once through the longitudinal weld, it continued through the transverse weld, and then worked its way forward on the other longitudinal weld. Once the member disconnected, the test was complete.

7.9.3 Z Frame Double Angle Conclusions

Due to the high cross frame stiffness of the Z Frame Double Angle, a substantial amount of bending was introduced to the diagonal, similar to the HSS specimens. The bending stresses cause the angles to crack early and have a low fatigue life. Although the concentric nature of the angles improves the stiffness, it seems to have a detriment on fatigue life and the researchers believe that this layout may not achieve adequate fatigue life for design. The Z frame double angle layout is currently not recommended for design, based upon the full scale cross frame fatigue tests.

7.10 SUMMARY OF CONCLUSIONS

Fatigue tests on 26 full scale cross frames were conducted as part of the dissertation research. The major conclusions from the test program are as follows:

- K frames may be a desirable choice for cross frame applications since the layout of the members can save fabrication time since the welding can be conducted from one side, thereby eliminating the need to flip the cross frame. However, the designer must check the K frame can provide adequate stiffness for bridge stability.
- K frames and X frames have very similar fatigue performance.
- Improvements to the TxDOT Standard Detail for K frames are:
    - Thicker center gusset plate extends fatigue life.
    - Use of larger angle on the bottom chord improves the fatigue performance.
    - Flipping the bottom chord vertically so that the outstanding leg is closer to the bottom flange improves the fatigue performance.

    - The transverse weld between the gusset plate and the angle of the K-frame on reverse side of the angle does not change performance and should therefore not be required in the detail.
- Improvement to the TxDOT Standard Detail for X frames are:
    - The minimum spacing between the end of angles and edge of connection plate should be increased from 0.5″ to 2.5″ to minimize interaction/stress concentration between the angle-gusset end weld and gusset-connection plate edge field weld. The current detail does not allow enough room for the two welds to pass freely, resulting in overlap of welds and a reduction in the fatigue life.
    - The inclusion of an additional transverse weld on the reverse side of the angle improves fatigue performance and should be included. Since the cross frame already needs to be flipped to facilitate other welds, this additional well has a relatively minimal cost.
- X frames with unequal leg angle members have similar performance as the X frames with equal leg angles. The reduced eccentricity of unequal leg angles moderately increases the stiffness but does not seem to change the fatigue performance.
- Z frames with square HSS tubes can have substantial bending in the diagonal. The performance is similar to the use of angles, so the additional cost is therefore not justified.
- Z frames with rectangular HSS tubes seem to offer a viable alternative to X frames and K frames, so long as the axis of bending vertical bending in the tubes is aligned with the weaker axis of the tube.
- Z frames with double angle members should not be used due to relatively poor fatigue performance relative to the other systems that were tested.

Part VI: Comparison of Full-Scale Cross Frame Fatigue Tests to Component Fatigue Tests

7.11 REVIEW OF FATIGUE PERFORMANCE

During this dissertation research, numerous small-scale component fatigue tests were carried out on members and their connections (See Chapter 5 for more details). This testing procedure is often used by researchers to understand the fatigue behavior of the connections as large-scale tests are difficult to perform, require specialized equipment, and can be costly. In fact, much of the AASHTO specification relies upon the results of component tests to develop the appropriate fatigue categories.

Due to the complexities in testing the eccentrically connected single angle member, the researchers felt that component tests would not provide a realistic representation of the fatigue behavior since the single angle specimen would need to somehow be restrained in the testing apparatus. The solution called for large-scale cross frame fatigue tests which would allow the angle members to deflect as they would in a real cross frame. The purpose of this section is to show the benefits of both test programs. Figure 7.72 shows the results of the component fatigue tests and Figure 7.73 shows the results of the full scale cross frame fatigue tests.

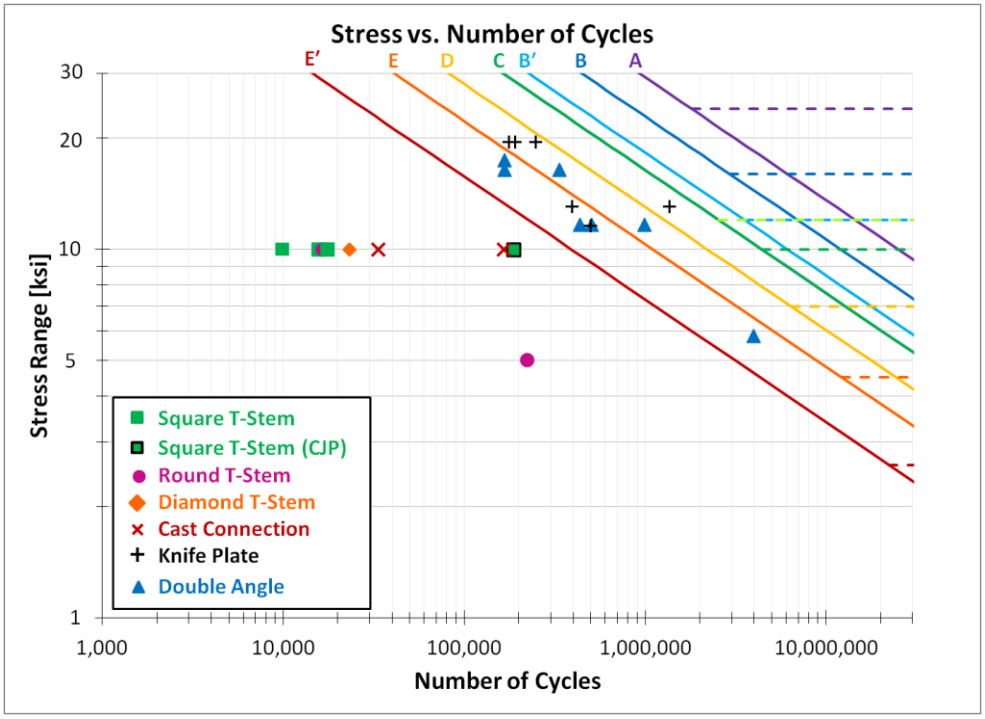

Figure 7.72: Small Scale Component Fatigue Test Results

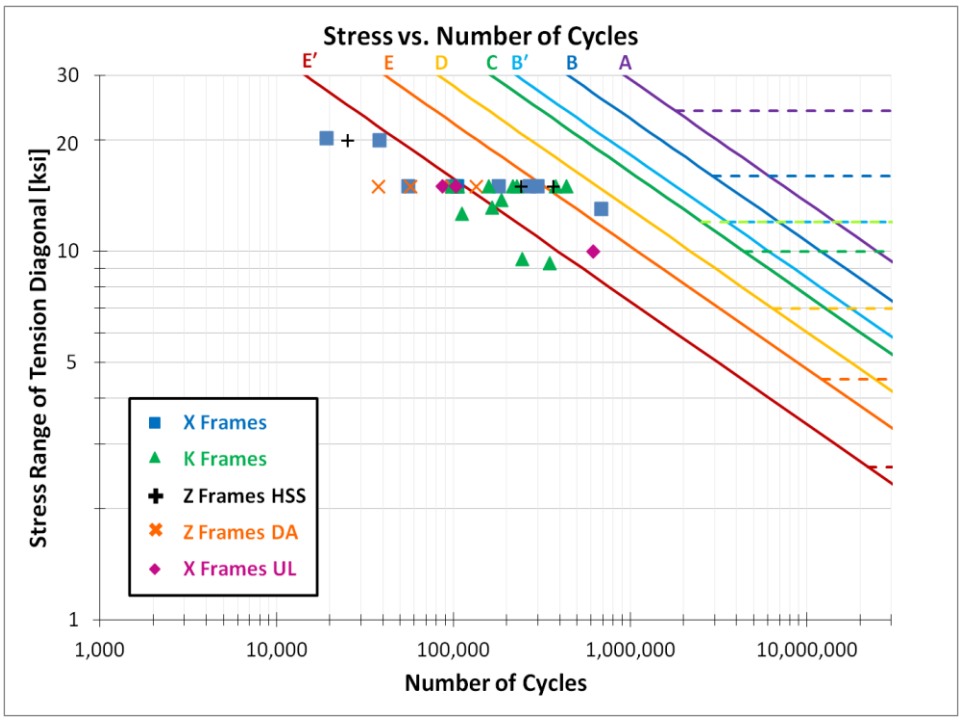

Figure 7.73: Full Scale Cross Frame Fatigue Test Results

The first observation is in reference to the T-stem and cast connections. From the component tests, it was clear that the transverse fillet welded detail required in both connection types resulted in a large stress concentration at the root of the weld leading to a short fatigue life. The component tests allowed the researchers to effectively identify this behavior, and preclude the testing of these details from the more costly large-scale tests.

Secondly, due to the flexibility of the eccentrically connected single angle member, component tests were not possible on this detail. The large scale testing allowed the researchers to observe the behavior of the members under cyclic loading and determine the fatigue rating of the connection. The large scale tests indicate the single angle detail should be classified as an AASHTO Category E′ detail, currently one level more severe than is currently in the specification. This finding will help ensure cross frames are being designed appropriately to prevent fatigue problems from being introduced, especially as engineers continue to use more advanced structural analysis tools and better material quality to push the boundaries of our profession.

Next, when considering the knife-plate detail, the small scale component tests would suggest the detail with the stress relief hole would be capable of providing Category E to maybe even Category D behavior. Had the large scale tests not been conducted, researchers may have missed the how the Z frames respond to applied loads, and may have strongly recommended this detail for use. In the course of the large-scale tests, researchers realized the Z frame diagonal is subject to a substantial amount of bending causing double curvature in the member. This curvature greatly increases the bending stresses at the connection, which substantially reduces the overall fatigue life of this detail. The full scale tests showed the Z frames with HSS 5 x 5 x 3/8 members to fall short of the minimum Category E′ rating; however, the researchers discovered that using rectangular HSS 6 x 3 x 5/16 tubes can reduce the bending stresses at the connection and can achieve Category E′ behavior.

Finally, the component tests would have indicated the double angle connection to be no worse than its single angle counterpart, namely Category E′. Large scale testing

again revealed the diagonal member to experience double curvature bending. Since angle members have relatively low bending stiffness, cracks readily formed at the connections and the Z frame with double angles could not achieve Category E′.

In conclusion, it is recognized that both testing methods had their advantages and the results highlight the need for engineers to investigate the true behavior of the completed structure when making design recommendations.

CHAPTER 8
Analysis of Live Load Cross Frame Forces: a Case Study

8.1 INTRODUCTION

To demonstrate the significance of modeling assumptions used in representing cross frames in steel girder bridges, a case study was conducted in which analysis of an actual steel bridge was undertaken. The case study bridge was analyzed to compute live load induced forces in cross frame members. In design, the live load induced forces are used to compute the stress range in the cross-frame members, which in turn are used to check the adequacy of the cross frame for satisfying fatigue design requirements in AASHTO. Since live load forces were of interest in this case study, the structural model must represent the completed composite bridge. Cross frame forces in the case study bridge were evaluated using a variety of modeling approaches and a variety of software, including commercial bridge design software. This chapter describes the details and results of this case study.

8.2 COMPARISON TO COMMERCIAL SOFTWARE

As discussed previously, the use of the typical eccentric single angle connection detail leads to a reduction in cross frame stiffness. The effect of the cross frame stiffness has a different impact on stability induced forces during the construction stage of the bridge versus forces induced due to passing truck traffic on the completed in-service bridge. From the perspective of stability bracing, a lower cross frame stiffness can lead to an unsafe system during construction since the cross frame must possess adequate stiffness to provide effective bracing. Even if the brace is adequate from a stiffness perspective, a reduction in the stiffness will result in a larger force induced due to stability effects on the system.

The effect of the cross frame stiffness on forces induced in the cross frame due to truck traffic on the in-service actually results in the opposite effect compared to stability induced forces. In analyzing bridge behavior, a reduction in stiffness of the cross frame usually results in a reduction in force in the cross frame members. In general, stiffer elements attract higher forces; therefore, modeling decisions related to the bracing that might be made by designers or within the computer software programs can have a significant impact on the resulting forces in the bracing. Overestimating the stiffness of the cross frame in the finished bridge may result in perceived fatigue problems that may not actually exist.

It is therefore of interest to further investigate the implications of the methods used by commercial bridge design software in modeling the cross frames. Discussions with TxDOT designers have revealed cases where the fatigue stresses in the cross frames have controlled the design of the braces on some projects. It is a difficult design predicament, as increasing the area of the cross frame members in hopes of reducing the fatigue stress range in turn, increases the axial stiffness of the member which increases the forces attracted by the brace. By using the reduction factor discussed in Chapter 6, the stiffness properties of the cross frame can be more accurately modeled, potentially reducing the forces in the members and lowering the fatigue stresses. The following sections highlight a case study in which the fatigue stresses of the cross frame members governed the design, ultimately requiring engineers to add an extra girder line to the project.

8.2.1 Case Study Bridge Details

The plans and details of the bridge modeled for comparison in this study were provided by TxDOT and consist of two phases that will be referred to as the "initial design" and the "final design". The initial design contains plans for a single span curved I-girder bridge using 8 girders and the TxDOT XF2 cross frame detail. During design, fatigue issues were indicated by the bridge software package, which consisted of a grillage model. After adjusting the girder cross sectional properties, cross frame spacing,

and cross frame member type, the fatigue stress range in the cross frames were still larger than acceptable. The solution resulted in the final design, which includes an additional girder line, adds two extra lines of cross frames, and increases the area of the cross frame members to the TxDOT XF3 detail. The following subsections describe the bridge in full detail.

8.2.1.1 Initial Design

The initial design of the bridge consisted of 8 single span curved girders spaced at 8.57 ft. The outermost girder on the curve had a length of 165.0 ft and a radius of curvature of 1944 ft. The girder cross section details are highlighted in Table 8.1 and the full bridge plans are given as Supplemental Files.

Table 8.1: Initial Design Bridge Details

Initial Design	
Girder Properties	
Number of Girders	8
Girder Spacing	8.57 ft
Deck Overhang	3 ft
Radius of Curvature	1884-1944 ft
Number of Spans	1
Span Length	159.7-165.0 ft
Web Depth	68 in
Web Thickness	0.625 in
Girder Spacing	8.57 ft
Flange Width	24 in
Top Flange Thickness	1-1.25 in
Bottom Flange Thickness	1-2.25 in
Dapped End Length	85 in (both ends)
Dapped End Depth	42 in (both ends)
Bracing Information	
Cross Frame Arrangement	Radial, Equal Spaces
Total Number of Cross Frames	12
Cross Frame Spacing	14.52-15.00 ft
Cross Frame Type	TxDOT XF2
Angle Type	L5x5x1/2
Angle Area	4.75 in^2
Brace Height	58 in
Intermediate Stiffeners	
Stiffener Width	8 in
Stiffener Thickness	0.50 in
Bearing Stiffeners	
Stiffener Width	11 in
Stiffener Thickness	1.25 in

The bridge geometry and cross sections were modeled using a commercial grillage type analysis program that helps designers check the various strength, service, and fatigue limit states required by the AASHTO LRFD Bridge Design Specification. Output from the software provided by TxDOT indicated the stresses in the cross frame

members in the initial design exceeded the Fatigue I limit state. Therefore, designers needed to modify the geometry to satisfy the requirements.

The easiest way to try to satisfy the requirements is to increase the area of the cross frame members, thereby lowering the stress in the members, assuming the force remains the same. However, when the area of the cross frame members is increased, the associated stiffness of the brace is also increased. The increase in system stiffness leads to the attraction of larger forces, potentially not reducing or even increasing the stress range in the members.

8.2.1.2 Final Design

TxDOT engineers attempted to satisfy the Fatigue I limit state by modifying the initial design cross frame member areas, girder spacing, and number of cross frame lines. Finally the designers were forced to add an additional girder line which reduced the girder spacing, and to add additional cross frame lines and larger cross frame member areas to satisfy the design requirements. The final design details are given in Table 8.2.

Table 8.2: Final Design Bridge Details

Final Design	
Girder Properties	
Number of Girders	9
Girder Spacing	7.5 ft
Deck Overhang	3 ft
Radius of Curvature	1884-1944 ft
Number of Spans	1
Span Length	159.7-165.0 ft
Web Depth	68 in
Web Thickness	0.625 in
Flange Width	24 in
Top Flange Thickness	1.25 in
Bottom Flange Thickness	1-2 in
Dapped End Length	85 in (both ends)
Dapped End Depth	42 in (both ends)
Bracing Information	
Cross Frame Arrangement	Radial, Equal Spaces
Total Number of Cross Frames	14
Cross Frame Spacing	12.28-12.69 ft
Cross Frame Type	TxDOT XF3
Angle Type	L6x6x9/16
Angle Area	6.45 in^2
Brace Height	58 in
Intermediate Stiffeners	
Stiffener Width	8 in
Stiffener Thickness	0.50 in
Bearing Stiffeners	
Stiffener Width	11 in
Stiffener Thickness	1 in

Output from the grillage software provided by TxDOT indicated the stresses in the cross frame members in the final design satisfied all fatigue limit states.

8.2.2 Software for Steel Bridge Analysis

The advantage of using a three dimensional finite element software package is the ability to extensively model the bridge girders, stiffeners, cross frames, deck, and other components in a more complete fashion. However, it is unrealistic that bridge designers would be able to model every project in such detail, and use of sophisticated modeling techniques requires specialized expertise and time. As an appropriate alternative, there are a variety of commercial software packages that allow the designers to input the bridge geometry, apply loads, and perform appropriate analyses to make sure the bridge meets the design specifications.

Many of these software packages perform a grillage or grid analysis on the completed bridge structure. In a grid analysis, the structure is simplified into a two-dimensional plane with all the applied loads acting perpendicular to the plane [Topkaya and Williamson 2003]. The members are usually modeled as line elements which are assumed to be axially rigid and have three degrees of freedom at each node, namely transverse displacement, rotation about the member's strong axis, and rotation about the member's longitudinal axis. Bending about the weak axis is typically ignored [Topkaya and Williamson 2003].

Grid analyses are computationally efficient, but can sometimes lead to over-simplification of the structure. Of particular concern is the modeling of the cross frames. In order to create the grid, the cross frames are simplified into an equivalent beam element. The equivalent beam is given a moment of inertia and torsional constant based on different structural analogies of the cross frame system. Some programs may use the equations outlined in Chapter 2 for torsional brace stiffness to size the equivalent beam. Other programs use a truss model analogy, performing a secondary analysis on the cross frame to determine the stiffness properties.

8.2.2.1 Determination of Equivalent Beam for Grid Analysis

Many bridge engineers make use of analysis software that carries out a grillage analysis on bridge projects involving complex geometry as well as curved girders. Cross

frames in the grillage models are modeled using a single line element (beam element) that must have a specific moment of inertia to capture the appropriate stiffness of the cross frame.

In order to determine the properties of the bracing beam elements, the cross frame is modeled as a truss, including both the cross frame members and the connection plates as part of the truss model. In many situations the software may internally use assumptions about the characteristics of the cross frame. A review of the documentation for the software will provide an indication of how the moment of inertia is determined. One modeling technique that is used consists of releasing one side of the brace and providing a roller type boundary condition while the other side of the brace is pinned [MDX 2013]. The top and bottom nodes of the brace are supported on both sides. A moment is applied to the released end by placing a unit force couple at the top and bottom nodes. Figure 8.1 denotes the boundary and loading conditions for this analysis. Figure 8.2 shows the associated deflected shape of the brace.

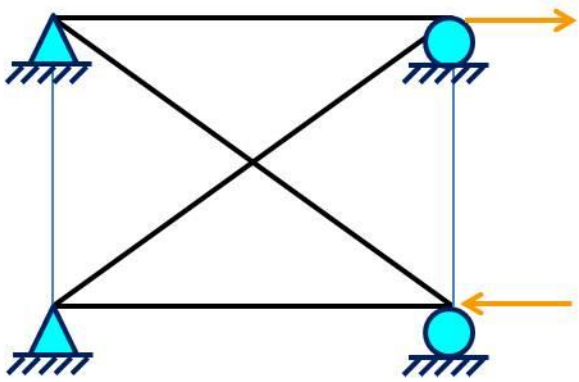

Figure 8.1: Boundary and Loading Conditions for Cross Frame Rotation Calculation in Typical Grillage Model

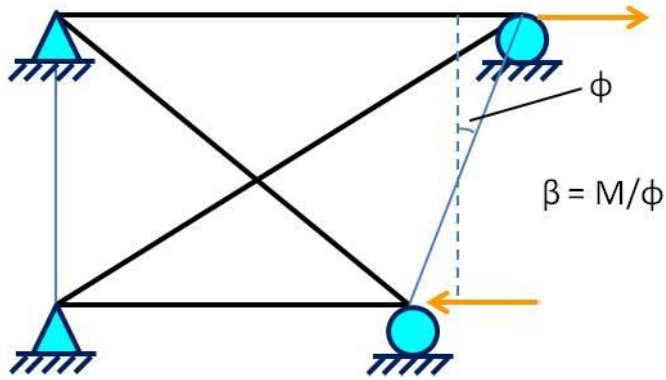

Figure 8.2: Displaced Shape for Cross Frame Stiffness Calculation in Typical Grillage Model

The horizontal displacements of the top and bottom nodes on the released side are calculated using a truss analysis. The resulting displacements are used to calculate the rotation of the brace (ϕ) as indicated in Figure 8.2. Ultimately, this provides the cross frame stiffness by dividing the applied moment by the rotation of the brace.

The rotational stiffness of a fixed-pinned beam subjected to a moment at the free end is given by the following equation:

$$M = 4\frac{EI}{L} \times \theta \tag{8.1}$$

where,

M = *Applied Moment*
E = *Young's Modulus*
I = *Moment of Inertia*
L = *Length of the Beam*
θ = *Rotation at the Free End*

Equating the rotation of the cross frame from the analysis (ϕ) to the rotation of the beam element at the free end (θ) for the same applied moment, an equivalent moment of inertia can be calculated for the beam element for use in the grid analysis. The torsional constant for the beam element is calculated by summing the torsional constants of the individual members of the cross frame.

A comparison of the truss model cross frame stiffness and the beam element equivalent moment of inertia was conducted for the two phases of this case study. The truss model analysis was conducted using MASTAN2 [2013]. A summary of the grillage model input and calculation results is presented in Table 8.3.

Table 8.3: Calculation of Beam Equivalent Moment of Inertia

	Original Design	**Final Design**
Girder Web Depth	68 in	68 in
Height of Brace	58 in	58 in
Girder Spacing	8.57 ft	7.5 ft
Distance from Cross Frame Connection to Center of Girder	6 in	0 in
Angle Member	L5x5x1/2	L6x6x9/16
Angle Area	4.75 in^2	6.45 in^2
Length of Strut	90.8 in	90 in
Length of Diagonal	107.8 in	107.1 in
MASTAN 2 Results		
UX of Top Node	0.0004125 in	0.0003019 in
UX of Bottom Node	-0.0004125 in	-0.0003019 in
Rotation (MASTAN2)	1.422×10^{-5} rad	1.041×10^{-5} rad
Equivalent Beam Calculations		
$I_{equivalent}$ (Calculated)	3194 in^4	4323 in^4
$I_{equivalent}$ (Actual Input)	3111 in^4	4133 in^4
Percent Difference	+2.7%	+4.6%

There were small discrepancies between the calculated moment of inertia for the beam element and the actual input for both the initial and final designs. Researchers contacted the software company to further discuss the calculation for equivalent moment of inertia to make sure the procedure was correct. It was determined that the general procedure was correct but perhaps the software was including additional options selected by the user. As researchers only had access to the output data files produced by the software and to the provided bridge plans, it was very difficult to determine which aspects of the input may have slightly changed the brace height, spacing, etc… With less

than a 5% difference in equivalent beam stiffness, the results from the case study should not be significantly affected.

8.2.2.2 Determination of Cross Frame Forces from Equivalent Beam

Once the grid analysis is complete, the grillage software often applies the resulting moments and shear forces on the equivalent beam to the truss model of the cross frame. Shear is distributed equally to both top and bottom nodes (provided the node location is able to resist vertical loads), and the moment is reapplied as a force couple. The forces in the cross frame members are determined using a structural analysis.

8.2.3 ANSYS Model

8.2.3.1 Geometry and Properties

In order to evaluate the cross frame forces predicted by the grillage model software, comparison to a three-dimensional finite element software was conducted. The model was constructed followed typical techniques used in previous research to obtain brace forces in plate girder systems [Quadrato 2010, Stith 2010]. The girders were constructed using 8-noded shell elements. The girders were modeled along a horizontal curve as given by the plan dimensions and contained the dapped end detail specified. Stiffeners were placed at each cross frame location, also made from the 8-noded shell elements. The stiffeners were placed at the exact location shown on the drawings and connected to the web elements using constraint equations.

The cross frames were modeled using line elements that framed into the web-flange interface, connecting at the nodes of the stiffeners. Shell element cross frames were considered for analysis, but greatly increased the computational time required. By using the reduction factor developed by Wang [2013] discussed in Chapter 6, line elements could be used to predict the forces in the real members. Additionally, line elements were necessary to compare with the results produced by the grillage model analysis.

A concrete deck was also provided using shell elements that framed in along the top flange of the girders. Elastic section properties of the concrete were employed, consistent with the deck thickness and compressive strength of concrete provided in the output from the TxDOT supplied grillage model analysis. Figure 8.3 and Figure 8.4 show portions of the ANSYS model.

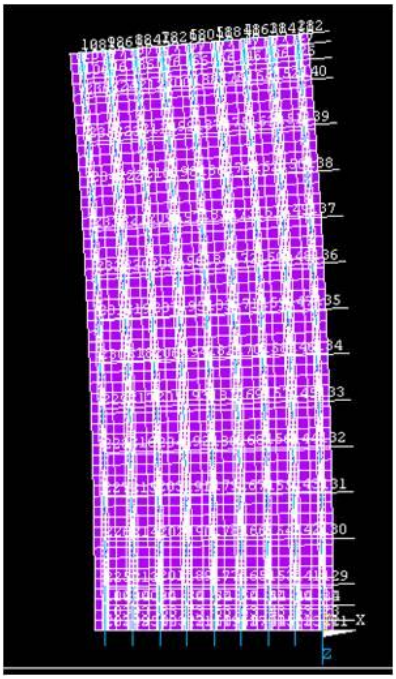

Figure 8.3: Top View of ANSYS Model

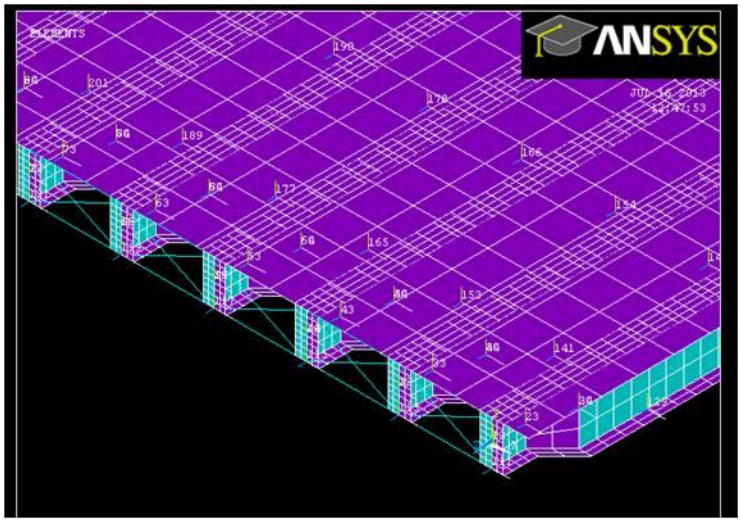

Figure 8.4: Isometric View of ANSYS Model

8.2.3.2 Application of Loads

Due to the proprietary nature of commercial bridge modeling software, determining the specific technique for placement of loads and their associated magnitudes was not possible. Therefore, loads were applied in ANSYS consistent with the current AASHTO LRFD Specification [2013] for Fatigue I and Fatigue II limit states as outlined in Chapter 3.

The specification calls for the design truck or tandem to be applied as moving point loads within the design lane. The design truck has a fixed 30 ft spacing between the rear axles as specified for fatigue analyses. The moving point loads are multiplied by the 1.15 impact factor.

A schematic is shown in Figure 8.5 on how the point loads were applied. Corner nodes of the deck shell elements were set on a 3 ft grid. The point loads were then applied at the nearest node for analysis. The truck (or tandem) was run along the outside girder first, and repeated across the width of the bridge.

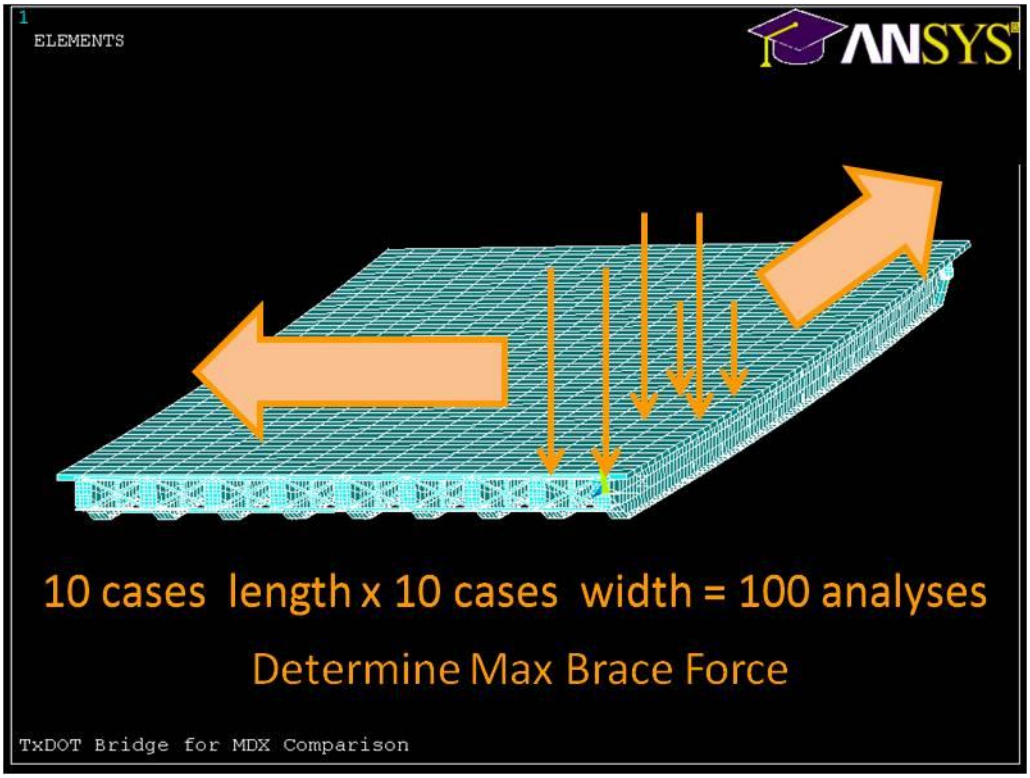

Figure 8.5: Application of Design Truck Loads in ANSYS

8.2.3.3 Determination of Cross Frame Line Element Area

In order to compare with the results given to the research team by TxDOT, the area of the line elements were selected to first model the equivalent stiffness calculated by the grillage model. Since the grillage model accounted for the actual height of brace, and the cross frames in the ANSYS model framed into the web-flange interface, slight modifications to the area of the line elements were made. For comparison of cross frame forces predicted by ANSYS versus the commercial grillage model, the cross frame stiffness reduction factor (R-factor) was initially not included in the ANSYS model. The R-factor was then later included in the ANSYS model to evaluate the impact on the stiffness adjustment on the predicted cross frame forces.

8.2.4 Initial Design Comparison

Analysis was performed on the initial design geometry to the best extent available from the provided plans. The fatigue truck and tandem were each run at the 100 different locations outlined in Figure 8.5, and the maximum force in each cross frame member was identified.

As previously discussed, the initial design was controlled by the Fatigue I limit state. Analysis in ANSYS showed the truck to induce much larger force in the cross frames than the tandem for the given geometry. The location of the maximum forces due to the suite of analysis cases was in the center bay, in the braces near the center. See Figure 8.6 for more detail.

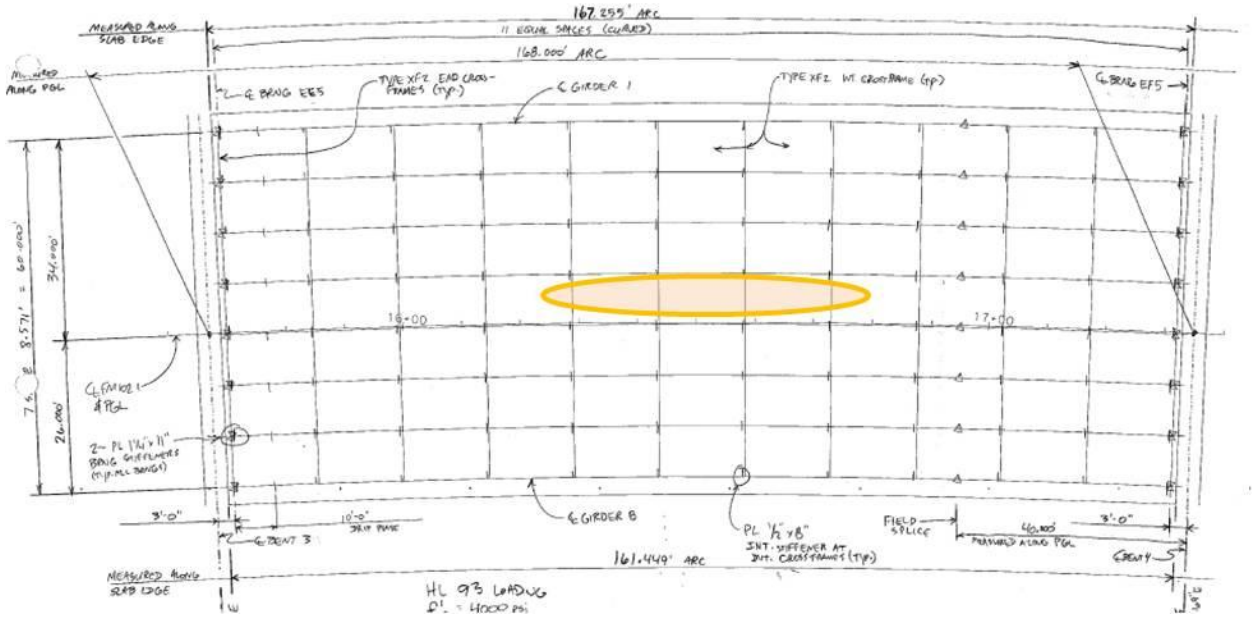

Figure 8.6: Location of Maximum/Minimum Forces in ANSYS and Grillage Model (Initial Design)

When considering fatigue, it is important to consider the range of force a given cross frame member may experience. The range of force is the value provided by the grillage model output and is what the ANSYS forces will be compared against. From the information obtained by the author, it seems the grillage model software takes the

maximum force in each cross frame member due to the series of loads and subtracts the minimum force in each member found for the same series of loads. This approach is very conservative as it assumes that every "cycle" must now consist of the placement of a truck in the precise locations to provide both the maximum and minimum possible forces.

Results from the initial design analysis showed fair agreement between the ANSYS and grillage model output. The results for the center bay are given in Table 8.4.

Table 8.4: Results for Cross Frame Member Forces in Center Bay of Initial Design (R-Factor not included in ANSYS model)

Initial Design Comparison- Bay 4

Loading Condition: Fatigue I, Design Truck

Maximum Brace Forces (ANSYS)				
Brace	Top Chord [k]	Bottom Chord [k]	Diagonal 1 [k]	Diagonal 2 [k]
1	1.90	0.00	3.10	3.30
2	1.27	9.67	8.63	6.33
3	1.75	16.49	12.01	9.44
4	2.06	20.05	13.33	10.45
5	2.37	21.29	14.12	10.60
6	2.49	21.91	14.58	10.43
7	2.50	22.22	14.84	10.63
8	2.41	22.27	14.79	11.22
9	2.11	21.97	14.40	11.56
10	1.77	18.55	13.12	10.67
11	1.30	10.84	9.21	7.00
12	1.92	0.96	2.67	3.54

Minimum Brace Forces (ANSYS)				
Brace	Top Chord [k]	Bottom Chord [k]	Diagonal 1 [k]	Diagonal 2 [k]
1	-0.13	0.00	-5.01	-4.44
2	0.00	-5.43	-3.44	-5.72
3	0.00	-8.40	-3.92	-6.17
4	0.00	-8.93	-3.45	-6.15
5	0.00	-9.72	-2.91	-6.63
6	0.00	-10.20	-2.78	-7.06
7	0.00	-10.60	-2.77	-7.24
8	0.00	-10.62	-2.91	-6.98
9	0.00	-10.48	-3.65	-6.83
10	0.00	-10.03	-4.06	-6.74
11	0.00	-6.91	-3.89	-5.96
12	0.00	-1.31	-4.41	-5.83

Force Range (ANSYS)				
Brace	Top Chord [k]	Bottom Chord [k]	Diagonal 1 [k]	Diagonal 2 [k]
1	2.04	0.00	8.11	7.75
2	1.27	15.10	12.07	12.05
3	1.75	24.88	15.93	15.61
4	2.06	28.98	16.78	16.60
5	2.37	31.01	17.03	17.23
6	2.49	32.11	17.36	17.49
7	2.50	32.81	17.61	17.86
8	2.41	32.89	17.70	18.20
9	2.11	32.44	18.05	18.38
10	1.77	28.59	17.18	17.40
11	1.30	17.75	13.10	12.96
12	1.92	2.27	7.07	9.37

Force Range (Grillage Model)				
Brace	Top Chord [k]	Bottom Chord [k]	Diagonal 1 [k]	Diagonal 2 [k]
1	0.25	0.25	3.00	3.00
2	13.47	13.47	4.45	4.45
3	24.27	24.27	6.09	6.09
4	31.50	31.50	5.85	5.85
5	35.92	35.92	6.17	6.17
6	38.69	38.69	6.53	6.53
7	38.69	38.69	6.53	6.53
8	35.92	35.92	6.17	6.17
9	31.50	31.50	5.85	5.85
10	24.27	24.27	6.09	6.09
11	13.47	13.47	4.45	4.45
12	0.25	0.25	3.02	3.02

One important observation from the obtained data is the discrepancy between the force range in the top chords of these braces. Since the ANSYS software includes modeling of the concrete deck as well as the three dimensional location of the cross frames relative to the deck, the force range in the top strut is very low. The grillage model cannot identify this extra restraint, making the force range in the top chord quite

high. Additionally, due to the way the cross frames are modeled as equivalent beams in the grillage model, the top and bottom chords undergo the same force range as well as the diagonals. This differs from the ANSYS model predictions.

In addition, there is a sizable discrepancy between the force ranges in the diagonals. Due to the roller and pin restraints inherent to the cross frame in the grillage model (see Figure 8.2), the diagonals are not experiencing larger forces since the roller/pin supports will take some of the applied load. This is contradictory to the findings given in Chapter 7 and Wang [2013] where the diagonals of the X frame are the primary load carrying members of the system.

Despite these differences, the maximum force range still occurs in the bottom strut in both models, the magnitude of which was similar for most locations, within approximately 20% for the most heavily stressed braces.

8.2.5 Final Design Comparison

The next stage in the case study was to compare the force ranges from the ANSYS model to the grillage model for the final geometry. The comparison was done for the Fatigue II limit state, which was indicated by the output of the grillage model software to be the controlling scenario. The location of the maximum force range was again identified at the braces towards the very center of the bridge, as indicated in Figure 8.7.

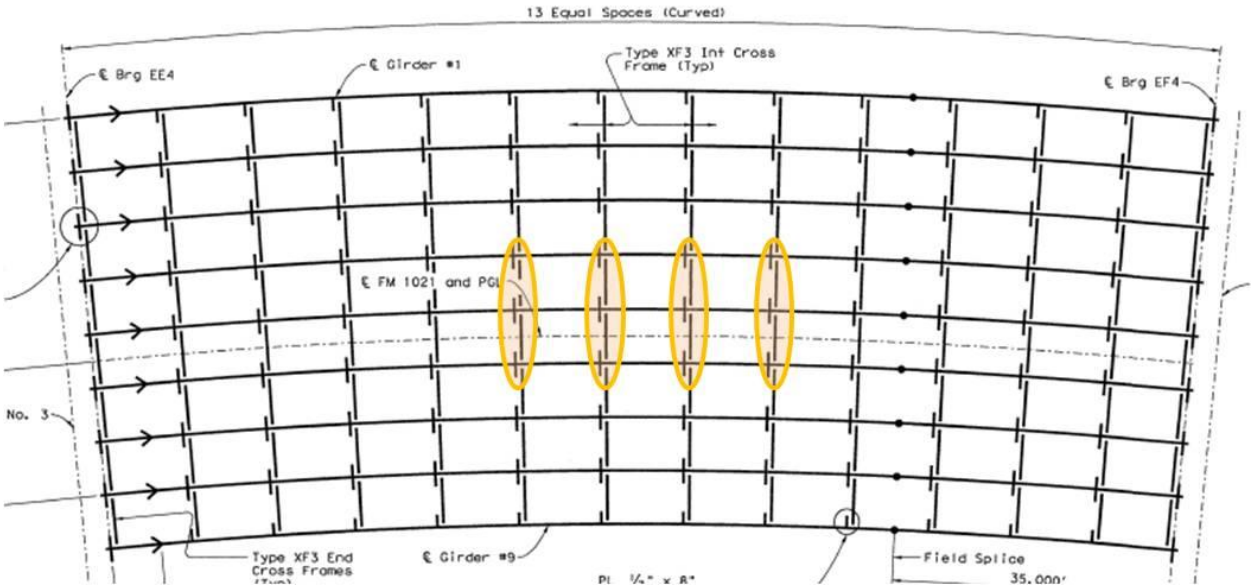

Figure 8.7: Location of Maximum/Minimum Forces in ANSYS and Grillage Model (Final Design)

As discussed for the initial design, the force ranges in the braces were compared and found to be in relative agreement for the maximum values. For this loading condition ANSYS indicated the force range to be slightly higher. A sample of the data is shown in Table 8.5.

Table 8.5: Results for Cross Frame Member Forces in Center Bays of Final Design (R-Factor not included in ANSYS model)

Final Design Comparison- Bay 5

Loading Condition: Fatigue II, Design Truck

Maximum Brace Forces (ANSYS)				
Brace	Top Chord [k]	Bottom Chord [k]	Diagonal 1 [k]	Diagonal 2 [k]
1	0.86	0.00	1.33	1.29
2	0.72	4.86	3.88	3.22
3	1.00	7.22	4.91	4.12
4	1.27	8.27	5.25	4.44
5	1.50	9.32	5.47	4.80
6	1.68	9.82	5.59	4.84
7	1.78	10.00	5.62	4.78
8	1.79	10.02	5.73	4.86
9	1.71	9.92	5.79	4.95
10	1.56	9.60	5.77	5.00
11	1.34	9.13	5.73	5.02
12	1.06	8.19	5.41	4.72
13	0.70	5.34	4.15	3.57
14	0.93	0.71	0.49	1.94

Minimum Brace Forces (ANSYS)				
Brace	Top Chord [k]	Bottom Chord [k]	Diagonal 1 [k]	Diagonal 2 [k]
1	-0.19	0.00	-3.02	-2.99
2	0.00	-2.71	-2.06	-2.48
3	0.00	-4.57	-1.89	-2.94
4	0.00	-5.30	-1.45	-3.25
5	0.00	-5.41	-1.42	-3.28
6	0.00	-5.42	-1.34	-3.36
7	0.00	-5.39	-1.24	-3.39
8	0.00	-5.58	-1.23	-3.46
9	0.00	-5.74	-1.32	-3.49
10	0.00	-5.92	-1.43	-3.51
11	0.00	-5.81	-1.58	-3.53
12	0.00	-5.34	-2.03	-3.35
13	0.00	-3.19	-2.14	-2.55
14	-0.02	-0.74	-3.04	-2.96

Force Range (ANSYS)				
Brace	Top Chord [k]	Bottom Chord [k]	Diagonal 1 [k]	Diagonal 2 [k]
1	1.05	0.00	4.35	4.28
2	0.72	7.57	5.94	5.70
3	1.00	11.79	6.80	7.06
4	1.27	13.57	6.70	7.69
5	1.50	14.73	6.89	8.07
6	1.68	15.24	6.92	8.20
7	1.78	15.39	6.86	8.17
8	1.79	15.60	6.96	8.32
9	1.71	15.66	7.11	8.44
10	1.56	15.52	7.20	8.51
11	1.34	14.94	7.31	8.55
12	1.06	13.52	7.44	8.07
13	0.70	8.53	6.29	6.13
14	0.95	1.44	3.54	4.90

Force Range (Grillage Model)				
Brace	Top Chord [k]	Bottom Chord [k]	Diagonal 1 [k]	Diagonal 2 [k]
1	0.01	0.01	0.08	0.08
2	6.39	6.39	0.59	0.59
3	9.28	9.28	1.15	1.15
4	11.56	11.56	1.00	1.00
5	13.25	13.25	1.44	1.44
6	13.73	13.73	0.67	0.67
7	13.99	13.99	0.63	0.63
8	13.99	13.99	0.63	0.63
9	13.73	13.73	0.67	0.67
10	13.22	13.22	1.44	1.44
11	11.48	11.48	0.99	0.99
12	5.95	5.95	2.98	2.98
13	3.98	3.98	2.26	2.26
14	0.00	0.00	0.06	0.06

The previously mentioned discrepancies in the force ranges in the top chords and diagonals are again observed in the data. The maximum force range was identified in the bottom strut of the braces and showed fair agreement between the two models, especially considering the number of unknown characteristics about the internal calculations of the grillage software.

8.2.6 Use of R Factor for Calculation of Force Range

The final stage of the case study was to examine the effect of properly modeling the cross frame stiffness of the system. As discussed in Chapter 6, the use of single angle members leads to significant reductions in cross frame stiffness due to the eccentricity of the member. The research has proposed the use of a reduction factor, R, in which the eccentricity can be accounted for and an accurate prediction of cross frame stiffness can be made utilizing the truss model equations.

Since stiffer members will tend to attract more force, it is expected that the predicted force ranges in the cross frame members using line element models are in fact, higher than the actual forces experienced. To quantify this effect, more analysis was performed on the initial TxDOT design to see if including the R factor reduced the cross frame forces. The results of the series of analyses are given in Table 8.6.

Table 8.6: Results for Cross Frame Member Forces in Center Bay of Initial Design Including the R Factor

Initial Design Comparison- Bay 4

Loading Condition: Fatigue I, Design Truck

Force Range without R Factor (ANSYS)				
Brace	Top Chord [k]	Bottom Chord [k]	Diagonal 1 [k]	Diagonal 2 [k]
1	2.04	0.00	8.11	7.75
2	1.27	15.10	12.07	12.05
3	1.75	24.88	15.93	15.61
4	2.06	28.98	16.78	16.60
5	2.37	31.01	17.03	17.23
6	2.49	32.11	17.36	17.49
7	2.50	32.81	17.61	17.86
8	2.41	32.89	17.70	18.20
9	2.11	32.44	18.05	18.38
10	1.77	28.59	17.18	17.40
11	1.30	17.75	13.10	12.96
12	1.92	2.27	7.07	9.37

Force Range with R Factor (ANSYS)				
Brace	Top Chord [k]	Bottom Chord [k]	Diagonal 1 [k]	Diagonal 2 [k]
1	1.32	0.00	7.01	6.85
2	0.41	8.70	7.54	7.47
3	0.65	15.80	10.94	10.78
4	0.82	20.12	12.55	12.37
5	0.93	22.39	13.27	13.23
6	0.97	23.89	13.76	13.77
7	0.97	24.56	13.97	14.07
8	0.93	24.13	13.93	14.16
9	0.81	22.49	13.68	13.80
10	0.66	18.29	12.21	12.11
11	0.43	10.80	8.29	8.11
12	0.96	0.82	6.43	7.24

Referencing the above results, one can see the force range is reduced significantly when the R factor is accounted for in the analysis. For reference purposes, the R factor for the given cross frame geometry was nearly 0.50.

For the cross frame members with the largest force ranges, including the reduction factor results in a 25% decrease in the cross frame force range. In terms of

design, this reduced force can help alleviate fatigue design problems. The following table examines the ratio between the force range with and without the R factor included in the ANSYS model.

Table 8.7: Ratio of Cross Frame Member Forces in Center Bay of Initial Design with and without the R Factor

Ratio of Force Range With/Without R Factor (ANSYS)				
Brace	Top Chord [k]	Bottom Chord [k]	Diagonal 1 [k]	Diagonal 2 [k]
1	0.65	-	0.86	0.88
2	0.32	0.58	0.62	0.62
3	0.37	0.63	0.69	0.69
4	0.40	0.69	0.75	0.74
5	0.39	0.72	0.78	0.77
6	0.39	0.74	0.79	0.79
7	0.39	0.75	0.79	0.79
8	0.39	0.73	0.79	0.78
9	0.38	0.69	0.76	0.75
10	0.37	0.64	0.71	0.70
11	0.33	0.61	0.63	0.63
12	0.50	0.36	0.91	0.77

Referencing Table 8.7 it is clear the proper modeling of the stiffness of the cross frame not only effects stability calculations, but also serves an important role in the determination of cross frame fatigue force ranges. Reductions of 20-30% were typical in the most heavily loaded braces, while other braces can see approximately 60-70% reductions.

8.2.7 Application of R to General Computer Software

In the analysis considered, the R factor was applied to the member cross sectional area and the resulting forces were obtained from the ANSYS finite element software. Although this is one possible approach, an alternative would be to apply the reduction factor to the modulus of elasticity. In this way, stress calculations performed by the program would remain accurate. In addition, the change in the modulus of elasticity may be an easier way to apply the reduction factor to all the cross frames. Since the stiffness of the members is proportional to AE/L, both methods are acceptable.

8.2.8 Case Study Conclusions

The following conclusions summarize the information obtained in performing this case study:

- The method in which grillage analysis software determine cross frame "beams" with an equivalent moment of inertia may not result in accurate predictions of stiffness and fatigue behavior of the cross frame.
- Increasing the stiffness of a cross frame in a bridge model will increase the amount of force the members of the brace experience.
- To more accurately predict the forces in the cross frames, the stiffness reduction factor R can be applied to the cross sectional area or modulus of elasticity of the line element cross frame members.
- Including the reduction factor can lead to 20-30% decreases in the fatigue force range for the most heavily loaded members.

The importance of using the R factor to better estimate the cross frame force ranges is highlighted by the initial and final design considered in this case study. Due to fatigue forces calculated by the analysis program, designers were forced to use 35% larger cross frame members, two additional intermediate cross frame lines, and one extra girder line. These additions significantly increased the cost of the project and may not have been necessary due to the overestimation of cross frame force ranges.

CHAPTER 9
Conclusions and Recommendations

9.1 INTRODUCTION

The research outlined in this dissertation was conducted as part of TxDOT Project 0-6564 and was directed at improving the basic understanding of the behavior of cross frames in steel bridges as well as developing improved details. The project sought to examine the current details used in practice and, if necessary, to propose alternative designs which could offer increased performance in strength, stiffness, and fatigue.

To accomplish these broad goals, the research team performed numerous experimental tests and computational analyses on the cross frame members, the member connections, the cross frame system, and the cross frame as part of the overall bridge geometry. The results of these tests and analyses are summarized in this chapter and multiple recommendations based upon the research are given.

9.2 APPLICABILITY OF CAST STEEL CONNECTIONS

In developing an efficient cross frame, the research team investigated the use of tubular members for inclusion in the cross frame design. Tubular members were considered in an attempt to determine if improved efficiency over traditional braces were possible using cross frames with only one diagonal as shown in the Z frame layout in Figure 9.1.

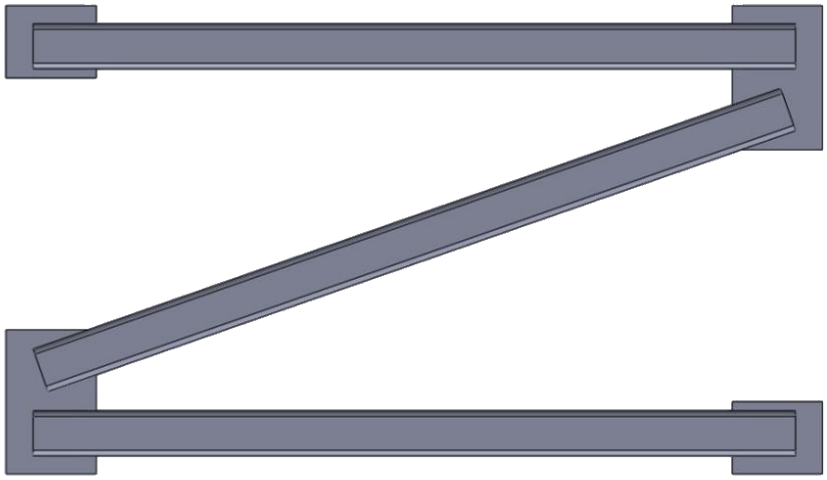

Figure 9.1: Z Frame Cross Frame Layout

However a problem associated with using tubular members is the development of an efficient connection to the gusset plates since the fabrication requirements for connecting a tubular member is more involved compared to traditional cross frame system that often utilize angles. One proposed solution was to develop a steel casting that was engineered to seal the end of the tube, connect easily to the tube via a fillet welded connection, and taper to a flat plate which could be welded to the gusset plate or cross frame connection plate. The casting developed as part of this research is shown in Figure 9.2.

Figure 9.2: Cast Steel Connection

Ultimately, the fillet weld between the cast steel connection and tube exhibited relatively poor fatigue performance compared to other members that have traditionally been used in cross frame applications. However, although the castings were not successful in the cross frame application, a great deal of valuable information was learned that may be useful in other applications. Based upon the experiences with the castings as part of this research the following conclusions can be drawn:

- Cast steel components can be engineered for use in steel bridge design.
- During the design and fabrication process, it is important to have a good working relationship with the foundry, which will assist the engineer in developing efficient molds used for creating the connection.
- Since the components are created from molten steel, the engineer is able to have control over the material properties of the final product.
- Steel castings can be made in a weathering steel grade satisfying the requirements of ASTM A709, Grade 50W.
- The steel castings produced for the research had very good strength properties, including a yield strength of 68.2 ksi, a tensile strength of 85.1 ksi, and 29% elongation at fracture.
- The steel castings developed had very good toughness, recording Charpy V-notch test values of 110.7 ft-lb at 40°F and 84.0 ft-lb at -40°F.
- A variety of quality control techniques are available to ensure the castings are free from internal and surface defects.

9.3 CROSS FRAME MEMBER STRENGTH, STIFFNESS, AND FATIGUE TESTS

The next stage of the research considered the individual cross frame member behavior with a variety of connections identified for potential use with the tubular members, as well as conventional connections with single and double angle members. Figure 9.3 shows each of the members tested for ultimate strength, stiffness, and fatigue performance.

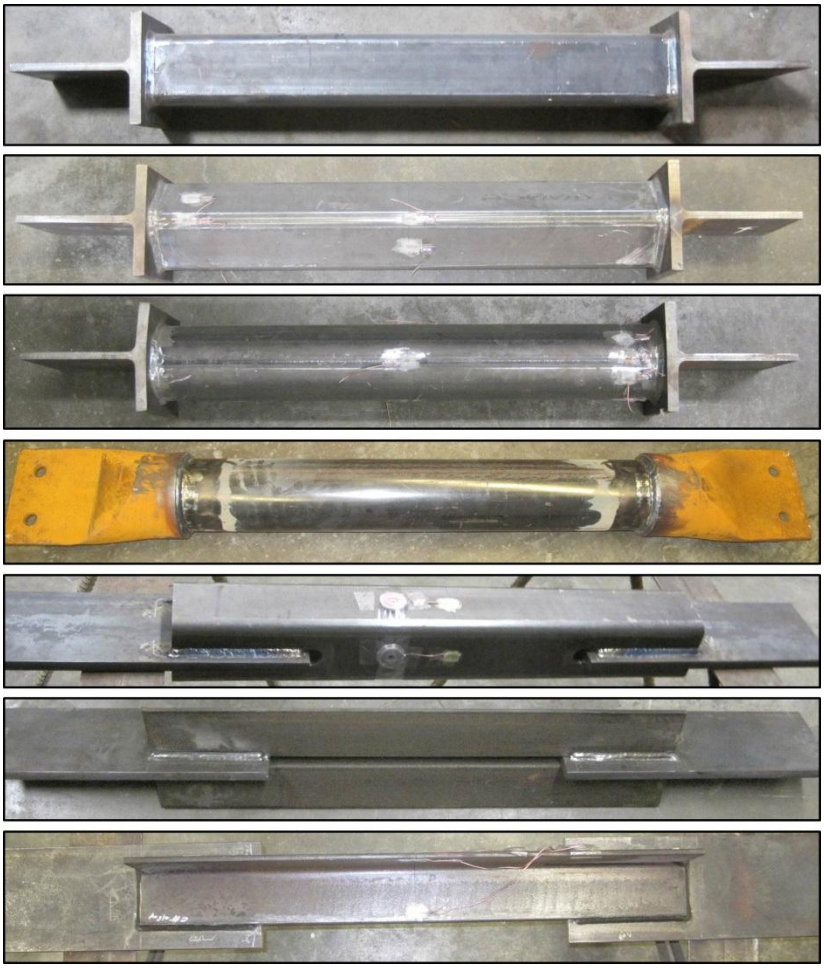

Figure 9.3: Test Specimens (from top to bottom): (a) T-Stem and Square HSS, (b) T-Stem and Diamond HSS,(c) T-Stem and Round HSS, (d) Cast Connection, (e) Knife-Plate Connection, (f) Double Angle Connection, and (g) Single Angle Connection

Based upon the individual member tests, the following conclusions were drawn:

9.3.1 Strength and Stiffness Tests

- Simplified formulas for design typically neglect the effect of the connections on the stiffness of the member (and subsequently of the overall cross frame system).
- The Square, Round, and Diamond T-stem connections performed poorly in strength due to a large stress concentration that forms in the tubular

member in line with the stem of the T. The T-stem members failed in strength at a lower value than predicted by conventional tension member and connection formulas.

- The cast connection provides a concentric connection with an even stress distribution to the tube. The strength properties exceeded the predicted strength of applicable tension member and connection formulas.
- The knife-plate connection was more difficult to fabricate than the other connections considered, but offered good strength and stiffness properties.
- The double angle connection offered good strength and stiffness properties. It is important to properly size the connection plate for this arrangement.
- The single angle connection has adequate strength properties, but relatively poor stiffness behavior. The eccentricity of the angle member relative to the applied load results in a moment on the member that leads to significant bending that reduces the axial stiffness of the member. A basic schematic is shown in Figure 9.4.

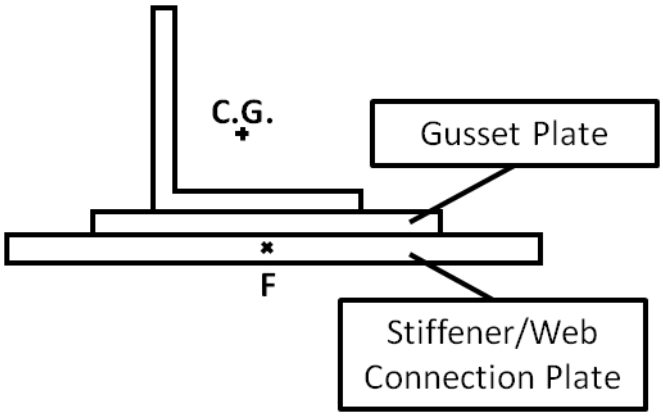

Figure 9.4: Eccentricity of Load Relative to Angle Center of Gravity

9.3.2 Fatigue Tests

- The Square, Round, and Diamond T-stem connections performed poorly in fatigue, most likely due to the transversely loaded fillet weld that has a slight load eccentricity when examined on the local level.
- The cast steel connection performed poorly in fatigue. Although the casting was streamlined to allow stress to flow into the tube and have a uniform distribution of stress in the tube itself, similar to the T-stem connections, the fillet weld connection had an eccentricity that greatly reduced the fatigue performance in the casting.
- The knife-plate connections offered adequate performance, with 5 of 6 specimens achieving AASHTO Category E. The stress relief hole included in some specimens further increases the fatigue life when properly sized and fabricated. Using the saw or torch to cut the slots for the knife-plate does not seem to have an effect on fatigue performance.
- The double angle members met the requirements of AASHTO Category E′. The cracks generally formed in the angles and not the gusset plates provided the stress range in the gusset plate is less than the stress range in the member.
- The single angle member was not tested in the small scale component test setup due to the amount of bending that occurs from the eccentric load pattern and concerns with damaging the testing machine. An alternative test setup described in Chapter 7 was used to obtain a measure of the fatigue behavior of these members.

9.4 FULL SCALE CROSS FRAME STIFFNESS TESTS AND ANALYSIS

Based on the success of the knife-plate and double angle member tests, full scale cross frame stiffness and ultimate strength tests were carried out for these members in the Z frame layout. In addition, the current TxDOT single angle X frame and K frame details

were considered to evaluate the performance. These standard details are given in Figure 9.5 and Figure 9.6.

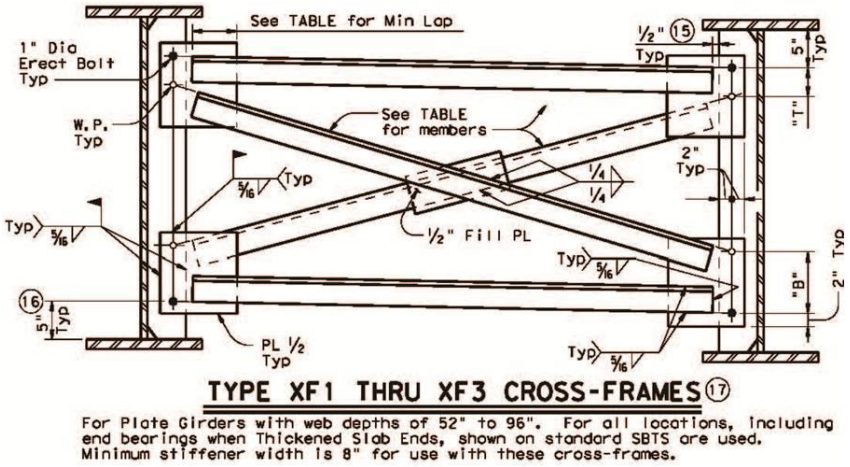

Figure 9.5: TxDOT Standard X Frame Detail [2010]

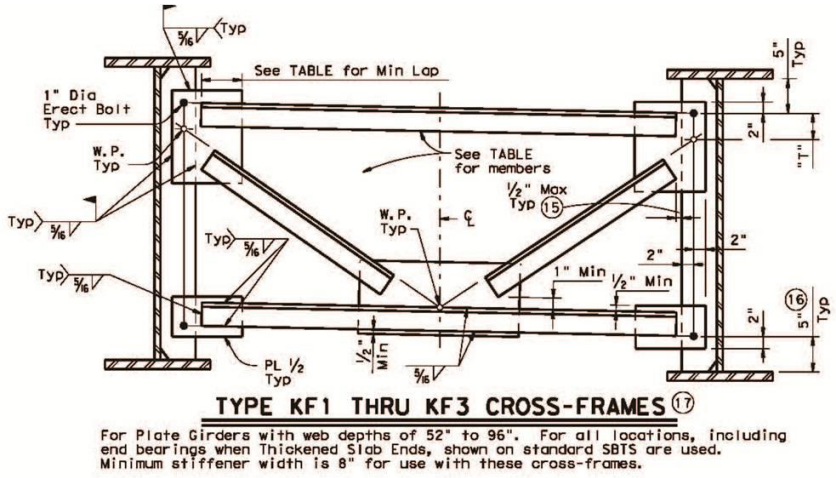

Figure 9.6: TxDOT Standard K Frame Detail [2010]

In total, 7 cross frame arrangements were tested to measure the stiffness and strength properties. Full results, analysis, discussion, and recommendations can be found in Wang [2013]. For the purposes of this dissertation, the following major conclusions were utilized.

- In all cross frames using single angle members, the reduction in member stiffness due to the eccentricity of the load severely lowers the overall cross frame stiffness by as much as 50% or more.
- The reduction in stiffness of the unequal leg X-frame was less than the equal leg X-frame with the same member area. Therefore, the reduced member eccentricities of unequal leg X-frames may provide improved performance.
- Line element truss models used to represent the cross frames consider the full stiffness of the member and will therefore not account for stiffness reductions due to eccentric loading.
- To better predict the stiffness and member forces of single angle cross frames using analytical procedures, a reduction factor R was developed using validate finite element models.

9.5 FULL SCALE CROSS FRAME FATIGUE TESTS

Fatigue tests on 25 separate specimens were conducted as part of the research. The major conclusions from the test program are as follows:

- To date, full scale cross frame fatigue tests had never been performed. The full scale experimental test setup allowed observation of behavior not present in the component testing, which provisions currently rely upon.
- The current AASHTO classification of the single angle detail as Category E was unconservative compared to the measured response in the laboratory tests. The eccentricity of the member when tested in the actual arrangement seems to indicate a lower bound to the data of Category E´.
- K frames are desirable for design as the layout and fabrication reduces labor time and costs, provided no additional transverse welds are used on the reverse side of the angles. However, the designer must check the K frame can provide adequate stiffness for bridge stability.

- K frames and X frames have similar fatigue performance.
- Z frames with square HSS tubes can have substantial bending in the diagonal member. The performance is similar to the use of angles, so the additional cost may not be justified.
- Z frames with rectangular HSS tubes may offer a viable alternative to X frames and K frames. To be effective, the major axis of the rectangular HSS should be oriented for bending in the out-of-plane direction. Using rectangular HSS can lead to Category E performance, an improvement upon the Category E′ performance measured in cross frames with angle members.
- Z frames with double angle members should be avoided.

In addition to these conclusions, the following recommendations are made to improve the performance of the currently used X-type and K-type cross frames:

- Possible improvements to the TxDOT Standard Detail for X frames are:
  - The minimum spacing between the end of angles and edge of stiffener should be increased from 0.5″ to 2.5″ to minimize interaction/stress concentration between the angle-gusset end weld and gusset-stiffener edge field weld. The current detail does not allow enough room for the two welds to pass freely, resulting in overlap of welds and a severe reduction in fatigue life (see Figure 9.7 and Figure 9.8).
  - The inclusion of an additional transverse weld on the reverse side of the angle improves the fatigue performance of the angles in X frames and should be included.
  - X frames with unequal leg angle members have similar fatigue performance as the X frames with equal leg angles. The reduced

eccentricity of unequal leg angles moderately increases the stiffness but did not significantly improve the fatigue performance.

- Possible improvements to the TxDOT Standard Detail for K frames are (see Figure 9.9 for clarification):
  - Thicker center gusset plate extends fatigue life.
  - Use of a larger angle on the bottom strut (as depicted in Figure 9.9) improves fatigue performance of the entire brace.
  - Rotating the bottom chord longitudinally so the outstanding leg is closer to the bottom flange improves fatigue performance.
  - Use of additional transverse weld on reverse side of angle does not seem to change performance and should therefore not be included in order to simplify fabrication.

9.6 COMPARISON OF CROSS FRAME FATIGUE FORCES TO COMMERCIAL SOFTWARE

A comparison using FEA software to commercial software was performed, which showed the reduction in stiffness inherent to the single angle members leads to a reduction in fatigue-induced forces. By including the reduction factor R, the forces experienced in fatigue were reduced by 20-30% in the case study, which could lead to significant savings in the number of cross frames necessary, the angle cross-section selected, and potentially less girder lines.

9.7 RECOMMENDATIONS TO IMPROVE CURRENT TXDOT CROSS FRAME DETAILS

Based upon the observations in the full scale cross frame fatigue tests, the following modifications to the existing TxDOT details are recommended [TxDOT 2006].

Figure 12.8

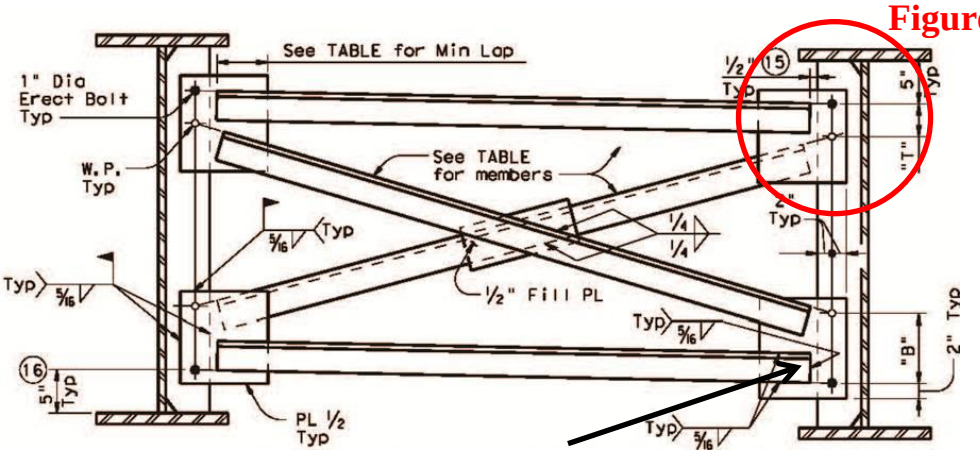

Include Weld on Reverse Side of Angle

Figure 9.7: Suggested Improvements to TxDOT Standard X Frame Detail

Increase Spacing from 0.5″ to 2.5″ (current spacing does not allow two standard 5/16″ welds to pass without overlap)

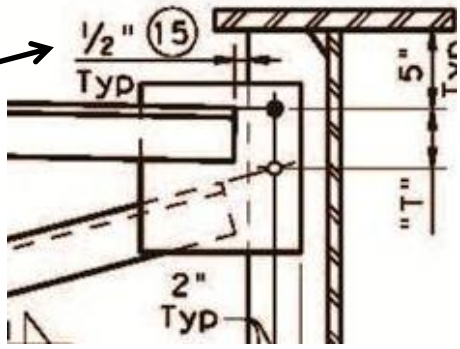

Figure 9.8: Increased Spacing between End of Angle and Edge of Stiffener

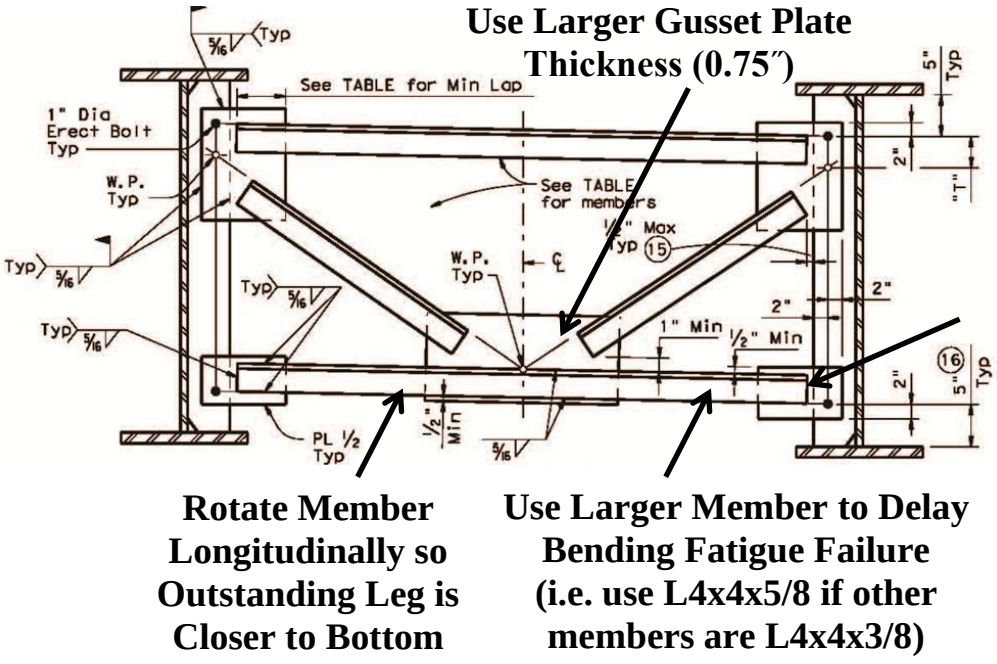

Figure 9.9: Suggested Improvements to TxDOT Standard K Frame Detail

APPENDIX A

Cross Frame Fatigue Test Results

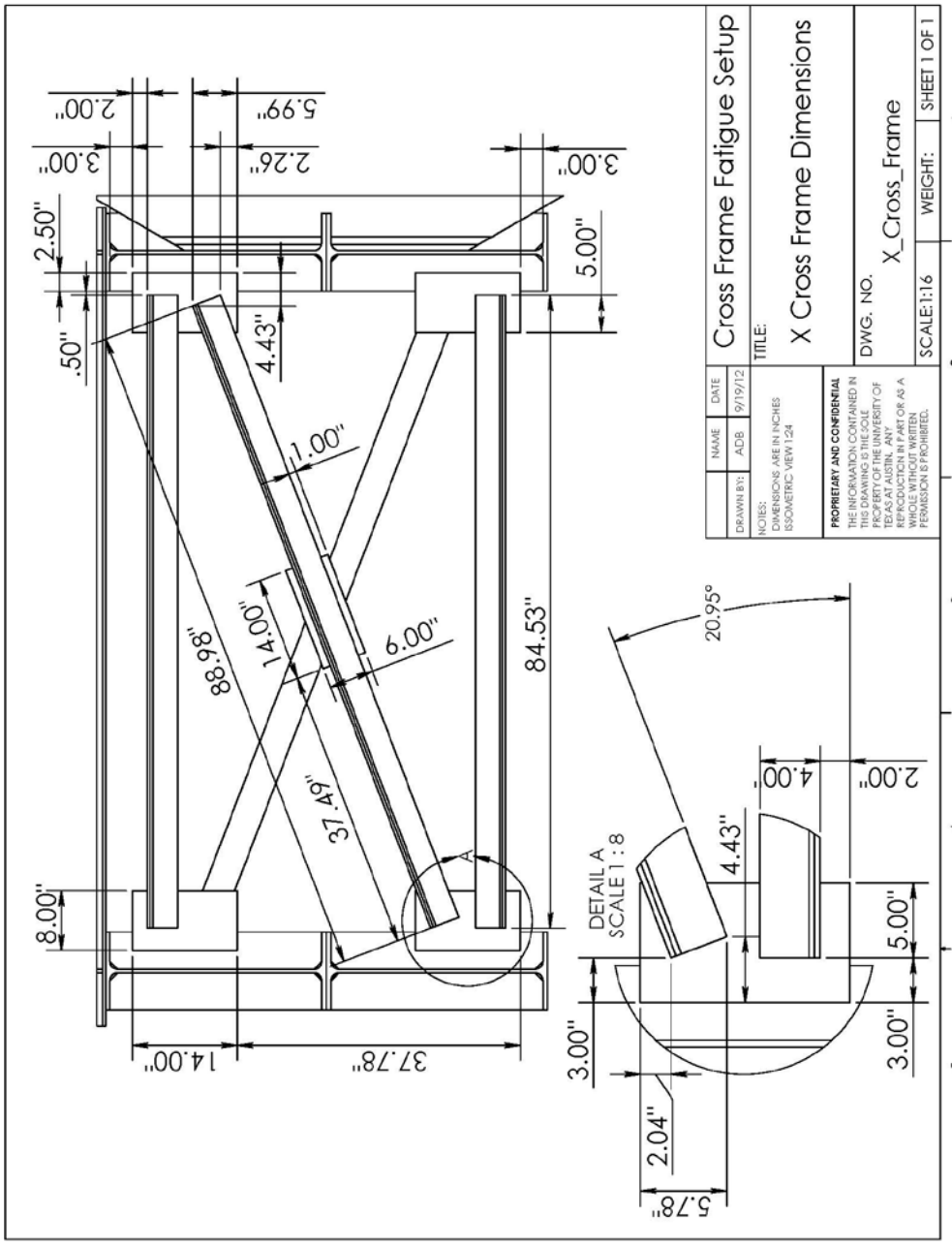
Cross Frame Fatigue Setup
X Cross Frame Dimensions
X_Cross_Frame
SCALE:1:16
WEIGHT:
SHEET 1 OF 1
DRAWN BY:
ADB
9/19/12
DIMENSIONS ARE IN INCHES
ISSOMETRIC VIEW 1:24
PROPRIETARY AND CONFIDENTIAL
2.50"
.50"
3.00"
2.00"
2.26"
5.99"
3.00"
5.00"
4.43"
1.00"
88.98"
14.00"
6.00"
37.49"
84.53"
8.00"
14.00"
37.78"
20.95°
DETAIL A
SCALE 1 : 8
4.00"
2.00"
4.43"
5.00"
3.00"
3.00"
2.04"
5.78"

Test Specimen: XF1

Test Dates: 11/2/2012 – 11/4/2012

Primary Failure Location: Gusset Plate

S_R = 20.03 ksi (tension diagonal)

N = 38,201 cycles

AASHTO Fatigue Category: < E′

Average Weld Size: Leg: 0.33″ **Throat:** 0.32″

Stiffness: **Initial:** 84.61 k/in **Final:** 79.34 k/in
6.23% loss of stiffness

Details:

- TxDOT Standard X-Type Cross Frame Detail
- First test completed in testing program
- MTS 407 controller used
- Tension diagonal of cross frame positioned on the back side of the cross frame
- Tension diagonal angle-gusset plate weld intersected gusset-stiffener field weld

Crack Locations:

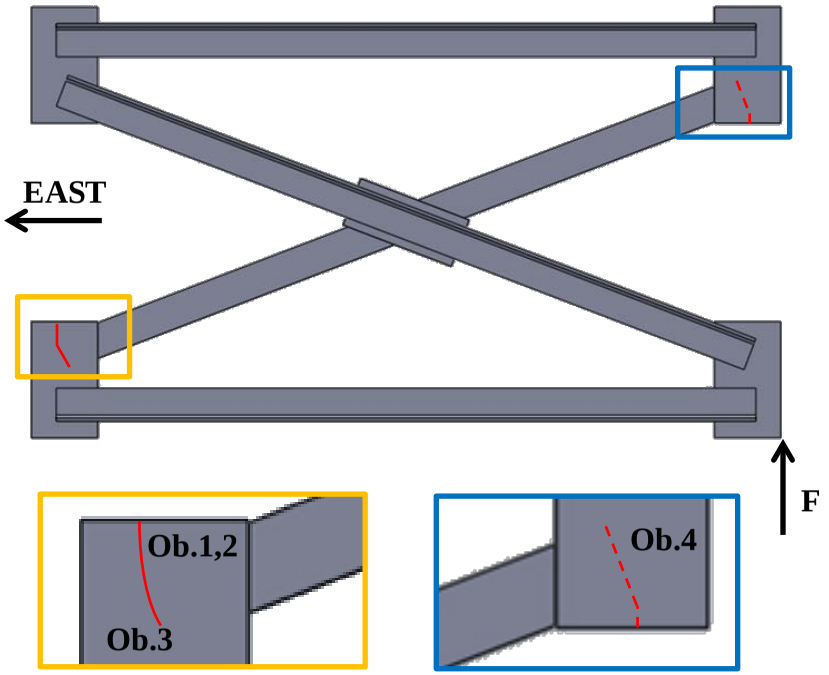

Observations:

1. Cracking occurred along the gusset toe of the gusset-stiffener weld above the weld intersection, and along the gusset toe of the angle-gusset weld below the intersection
2. The intersection of welds leads to a large tensile stress transfer, making it the likely point of crack initiation. The crack was already large when first observed, but Test Specimen XF4 confirmed this theory.
3. The curved nature of crack on back of gusset suggests downward propagation of crack by bending effects.
4. A smaller, hairline crack, similar in pattern, was seen at the opposite side of the tension diagonal.

Test Specimen: XF1

First Observed Crack
C1: N = 38,201 cycles
C2: N = 38,201 cycles

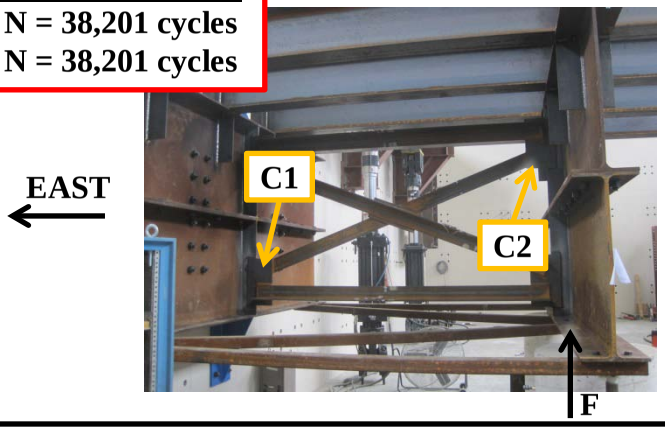

Crack 1: (Back)

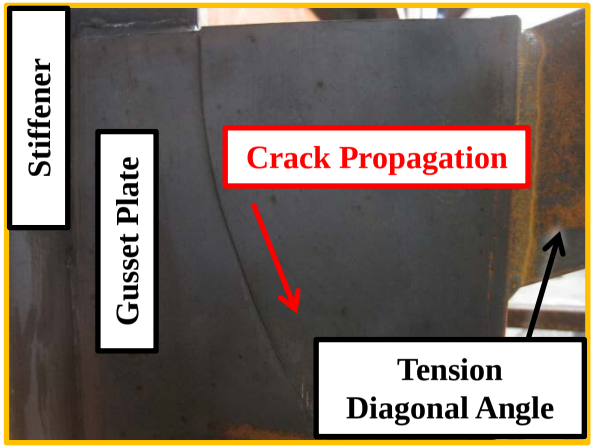

The curved nature of the crack suggests downward propagation due to bending.

Crack 1: (Front)

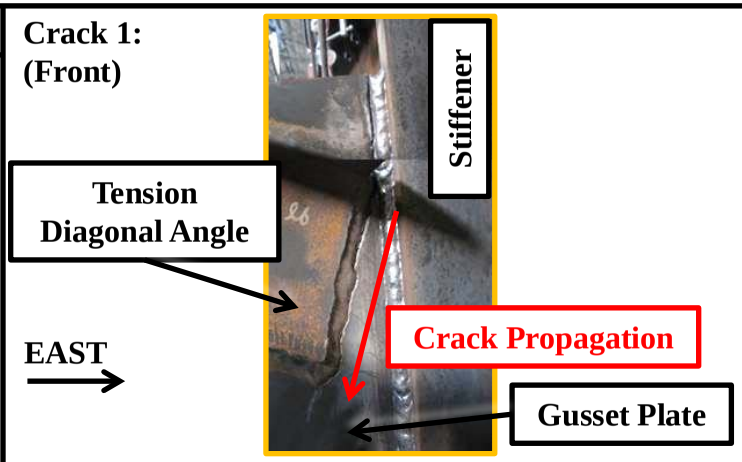

The crack was large when first observed. The crack is along the gusset toe of the gusset-stiffener weld and the gusset toe of the angle-gusset weld. It is believed to have initiated at the weld intersection, which would occur by strictly following the TxDOT Standard Detail.

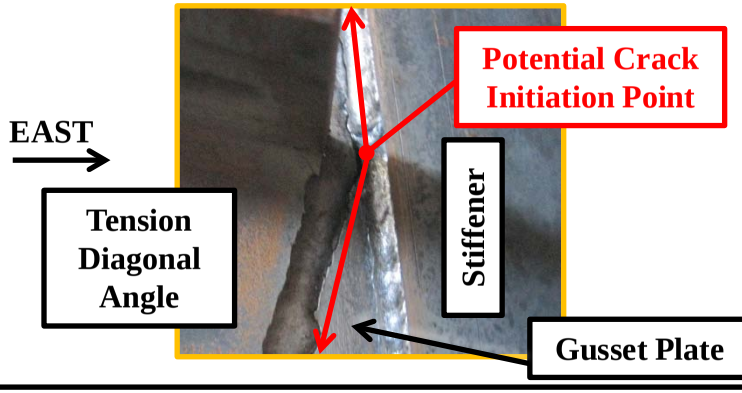

Test Specimen: XF1

Crack 2:

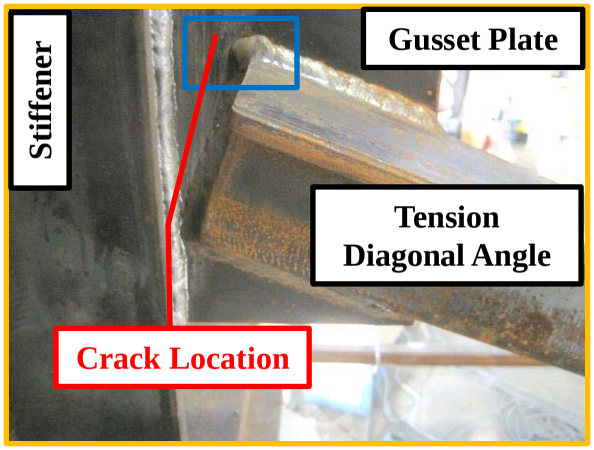

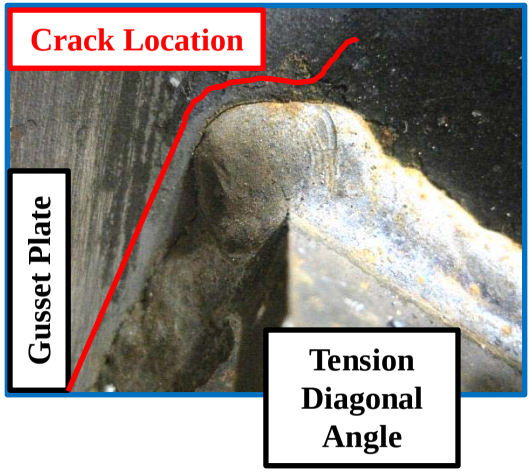

A similar crack to the primary failure occurred at the other end of the tension diagonal. The crack followed the gusset toe of the angle-gusset connection above the point of weld intersection and the gusset toe of the gusset-stiffener connection below the intersection.

Test Specimen: XF2

Test Dates: 11/12/2012 – 11/19/2012

Primary Failure Location: Tension Diagonal

S_R = 15.00 ksi (Effective Stress Range)

A_g = 2.85 in^2

U = 0.749

N = 271,111 cycles

AASHTO Fatigue Category: E′

Average Weld Size: Leg: 0.31″ **Throat:** 0.33″

Stiffness: **Initial:** 88.25 k/in **Final:** 82.37 k/in
6.67% loss of stiffness

Details:

- TxDOT Standard X-Type Cross Frame Detail
- Tension diagonal of cross frame positioned on the front side of the cross frame
- Compression diagonal angle-gusset plate weld intersected gusset-stiffener field weld

Crack Locations:

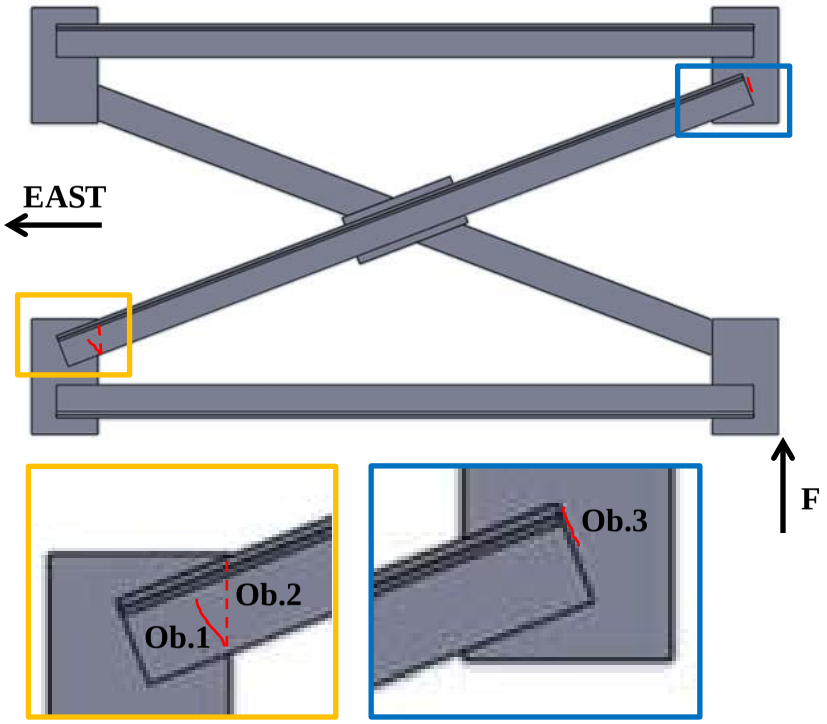

Observations:

1. First crack initiated at the forward edge of angle-gusset weld at angle toe and propagated into the angle
2. Crack eventually began propagating through throat of the back side angle-gusset weld
3. Crack also seen at failure at gusset toe of angle-gusset weld of the tension diagonal on the opposite end from failure

Test Specimen: XF2

First Observed Crack
C1: N = 271,111 cycles
C2: N = 271,111 cycles
C3: N = 271,111 cycles

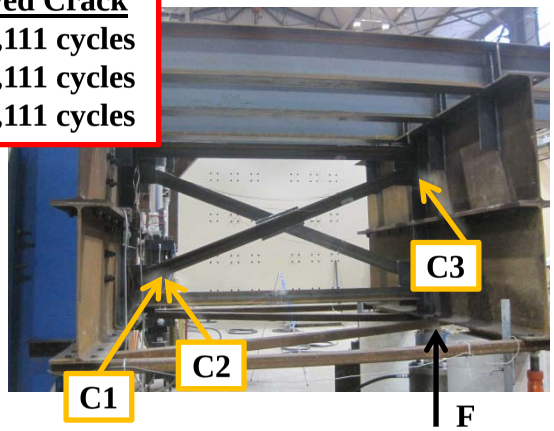

Crack 1:

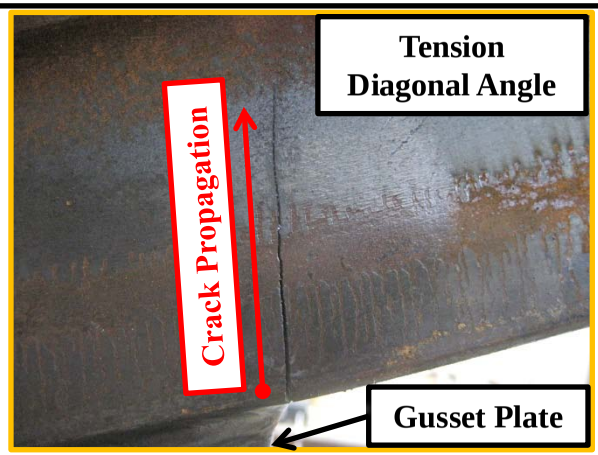

The first crack initiated at the forward edge of the fillet weld at the angle weld toe and propagated into angle.

Crack 2:

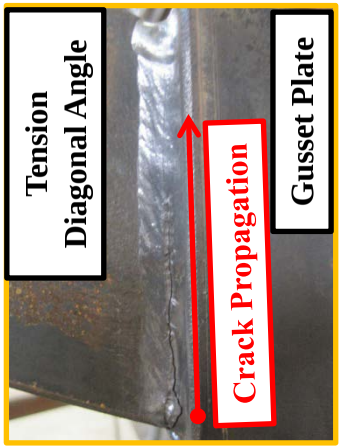

The crack also propagated through the weld throat on the angle back side fillet weld.

Crack 3:

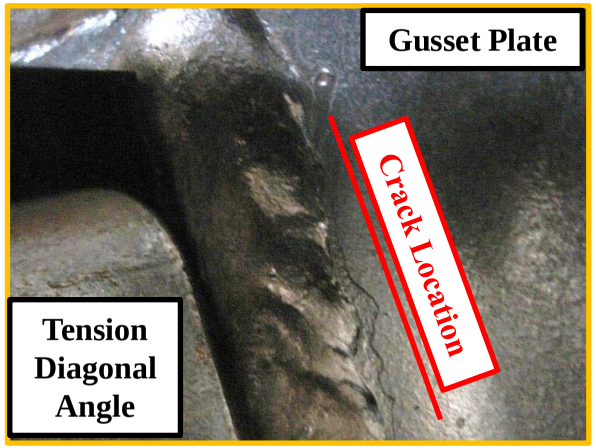

A small crack was also seen at failure at the gusset toe of the angle-gusset weld near the gusset stress concentration.

Test Specimen: XF3

Test Dates: 11/29/2012 – 12/3/2012

Primary Failure Location: Gusset Plate
S_R = 15 ksi (Tension Diagonal)
N = 99,120 cycles
AASHTO Fatigue Category: < E´

Average Weld Size: Leg: 0.31″ **Throat:** 0.29″

Stiffness: **Initial:** 87.65 k/in **Final:** 84.59 k/in
3.49% loss of stiffness

Details:
- TxDOT Standard X-Type Cross Frame Detail but tension diagonal length 1/2″ shorter to prevent weld intersection
- Tension diagonal of cross frame positioned on the back side of the cross frame
- Tension diagonal angle-gusset weld did not intersect gusset-stiffener weld but was separated by 3/16″ to 1/4″ at closest point

Crack Locations:

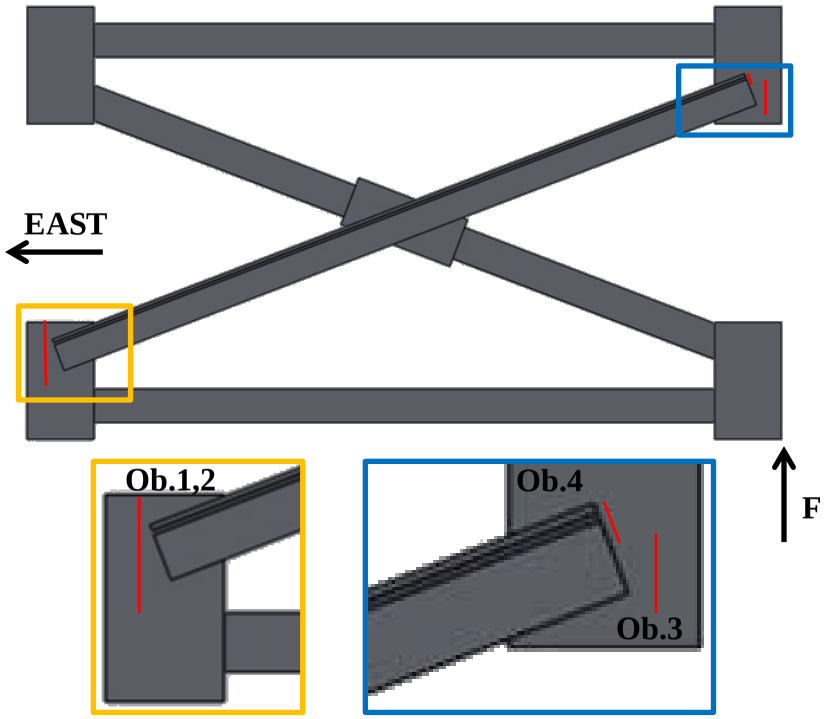

Observations:
1. Crack initiated along gusset toe of gusset-stiffener weld at bottom end of tension diagonal.
2. Although the welds did not intersect, the crack still initiated in the gusset plate.
3. A similar crack was seen at the top end of the tension diagonal. The crack was along the gusset toe of the gusset-stiffener weld. The crack did not extend to the top/bottom of gusset plate suggesting the initiation occurred where the welds are near intersection, then the crack propagates in both directions.
4. Another crack was observed in the gusset toe in the angle-gusset weld near the angle end stress concentration.

Test Specimen: XF3

First Observed Crack
C1: N = 77,648 cycles
C2: N = 77,648 cycles
C3: N = 77,648 cycles

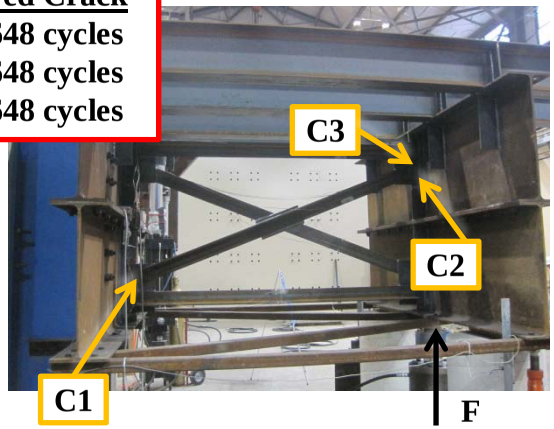

Crack 1: (Back)

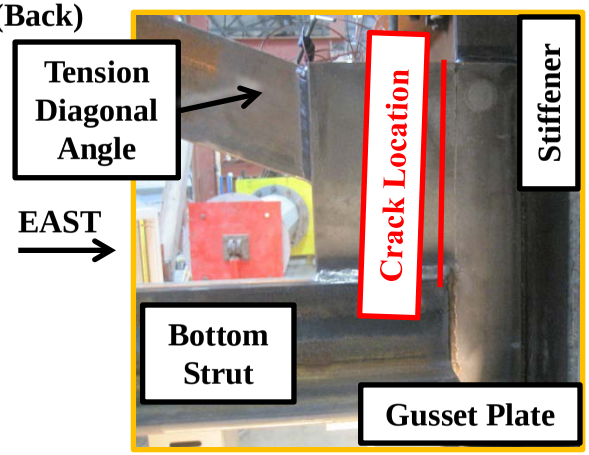

View of the crack on the back side of the gusset plate.

Crack 1: (Front)

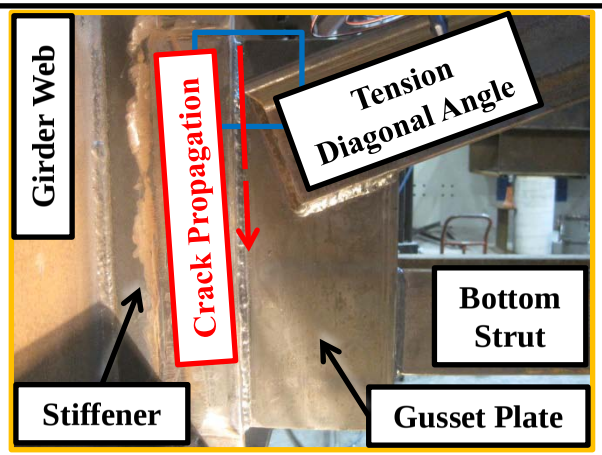

The first crack began near the weld intersection but had reached a length of 4″ from the top of the gusset plate along the gusset toe of the gusset to stiffener weld when first seen. It continued propagating downward.

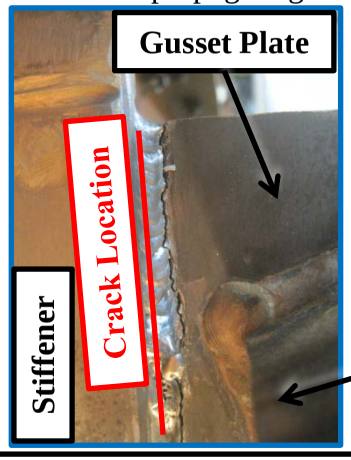

A close-up of the crack.

Test Specimen: XF3

Crack 2:

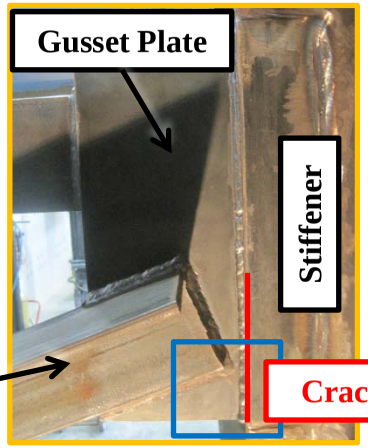

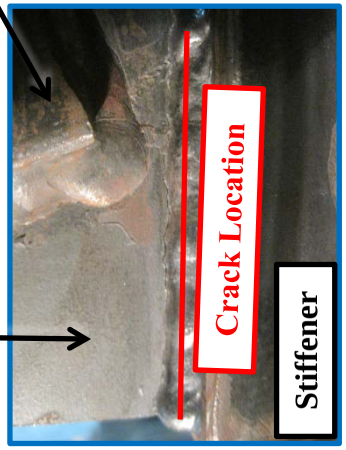

A similar crack formed at the other end of the tension diagonal along the gusset toe of the gusset-stiffener weld.

Crack 3:

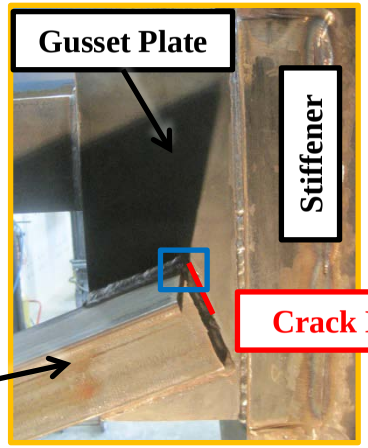

Another crack was observed on the gusset toe of the angle-gusset weld near the stress concentration associated with the angle end.

Test Specimen: XF4

Test Dates: 12/14/2012 – 12/18/2012

Primary Failure Location: Gusset Plate

S_R = 20.27 ksi

N = 19,078 cycles

AASHTO Fatigue Category: < E′

Average Weld Size: Leg: 0.32″ **Throat:** 0.31″

Stiffness: **Initial:** 88.75 k/in **Final:** 79.21 k/in
10.7% loss of stiffness

Details:

- TxDOT Standard X-Type Cross Frame Detail
- Tension diagonal of cross frame positioned on the back side of the cross frame
- Tension diagonal angle-gusset weld purposefully intersected with gusset-stiffener weld to be similar to XF1

Crack Locations:

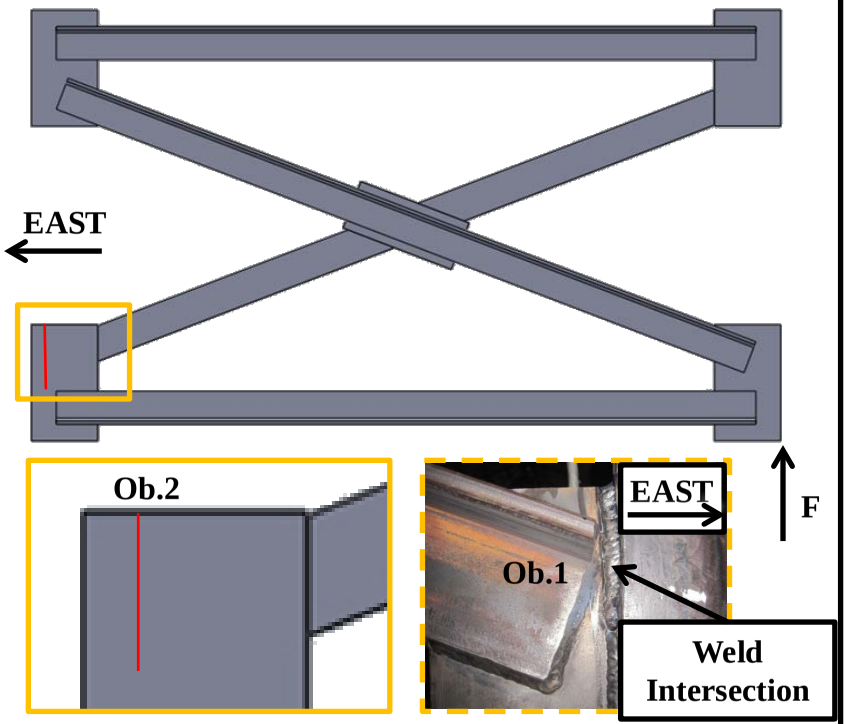

Observations:

1. Initial weld was undersized and did not intersect as welder attempted to avoid intersection. The weld was ground out from the top of the gusset to 2″ below the intersection point, and then welded again to intersect.
2. Crack initiated along gusset toe of gusset-stiffener weld at the location of weld intersection and then propagated upward to the edge of the gusset plate and downward along the gusset toe (N=2774 at first crack).
3. Cracks were discovered in the stiffener after the first sign of cracking in the gusset plate was observed. Ultimately it was a combination of the two cracks which led to the stopping of the test.

Test Specimen: XF4

First Observed Crack
C1: N = 2774 cycles
C2: N = 11,620 cycles

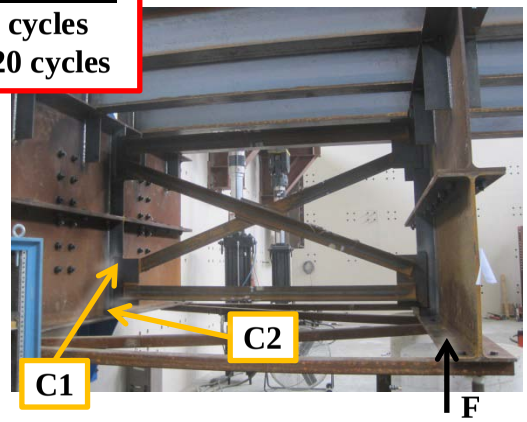

Crack 1: (Front)

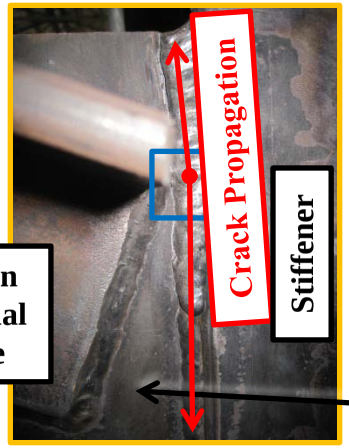

The first crack began at the weld intersection and extended upward to edge of gusset plate and downward along gusset toe.

Crack 1: (Back)

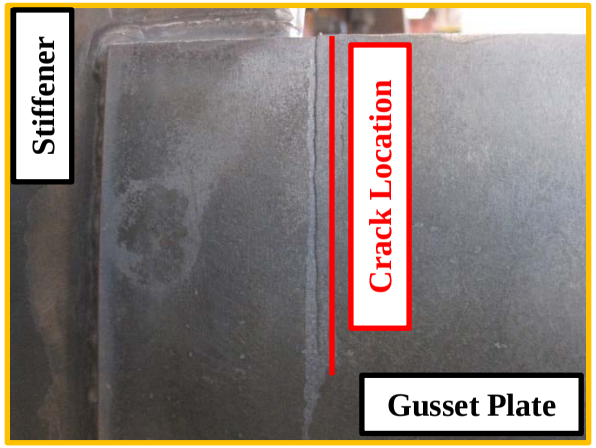

View of the crack on the back side of the gusset plate.

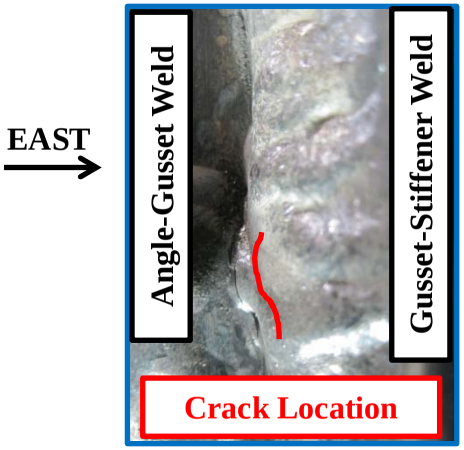

Test Specimen: XF4

Crack 2:

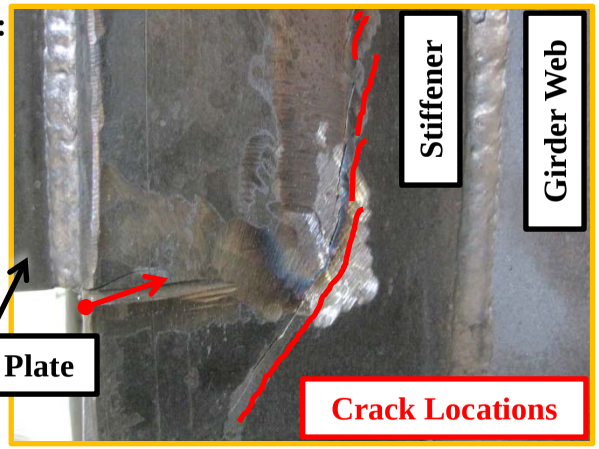

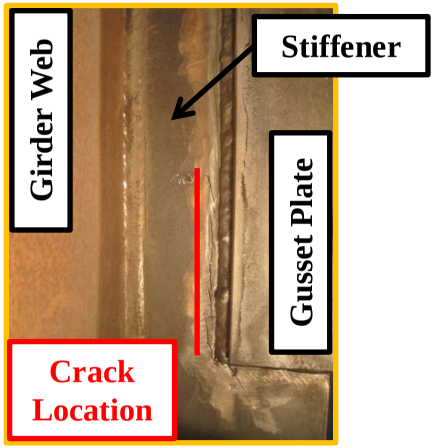

Cracks were observed in the stiffener due to the repeated grinding out and welding of multiple specimens.

Stiffness of cross frame was 83.30 k/in at the time stiffener cracks were noticed. (6.13% loss)

Test Specimen: XF5

Test Dates: 3/8/2013 – 3/14/2013

Primary Failure: Tension Diagonal	**Secondary Failure:** Tension Diagonal
S_R = 15.00 ksi (Effective Stress Range)	S_R = 15.00 ksi (Effective Stress Range)
A_g = 2.95 in^2 **U** = 0.734	A_g = 2.95 in^2 **U** = 0.734
N = 55,774 cycles	**N** = 179,907 cycles
AASHTO Fatigue Category: < E′	**AASHTO Fatigue Category: E′**
Stiffness: **Initial:** 89.12 k/in **Final:** 82.73 k/in 7.17% loss of stiffness	**Stiffness:** **Initial:** 89.49 k/in **Final:** 76.47 k/in 14.55% loss of stiffness

Average Weld Size: Leg: 0.32″ **Throat:** 0.31″

Details:

- TxDOT Standard X-Type Cross Frame Detail with members 1″ short prevent weld intersection
- The back of the angle was not welded to gusset
- Tension diagonal of cross frame positioned on the front side of the cross frame
- After tension diagonal cracked on one end, it was repaired to allow cracking at the other end

Crack Locations:

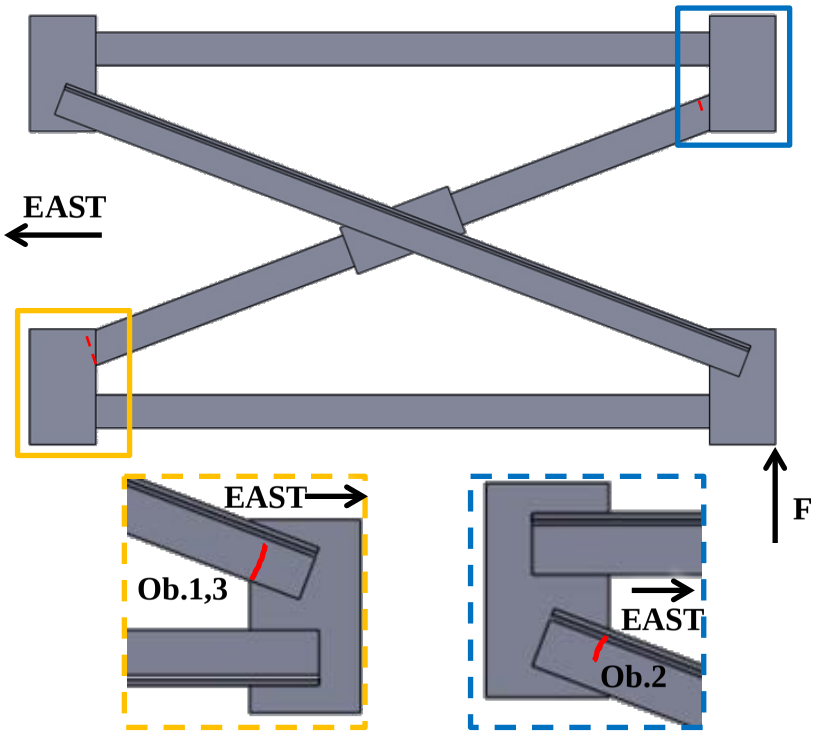

Observations:

1. First crack initiated at the forward edge of angle-gusset weld at angle toe and propagated into the angle
2. Second crack initiated at the forward edge of angle-gusset weld at angle heel and propagated into the angle
3. Repair of first crack resulted in system with similar stiffness as the original

Test Specimen: XF5

First Observed Crack
C1: N = 55,625 cycles
C2: N = 66,777 cycles

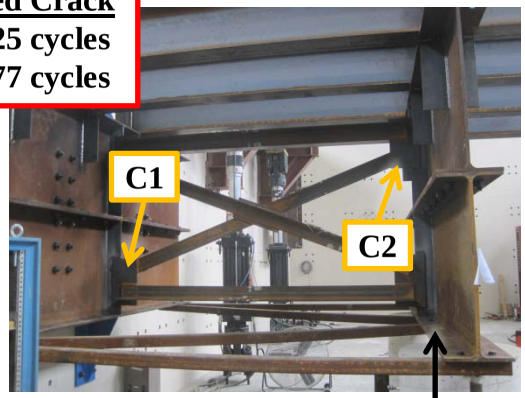

Crack 1: (Repair)
The repair resulted in a stiffness very close to the original.

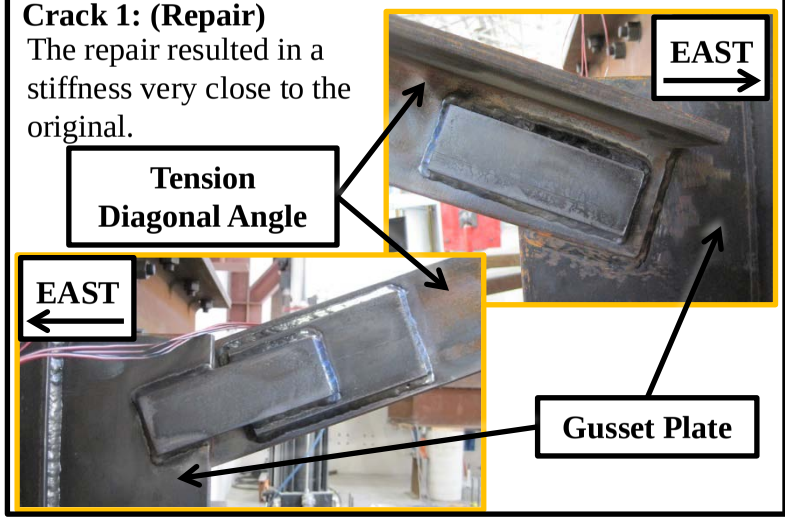

Crack 1: (Front)

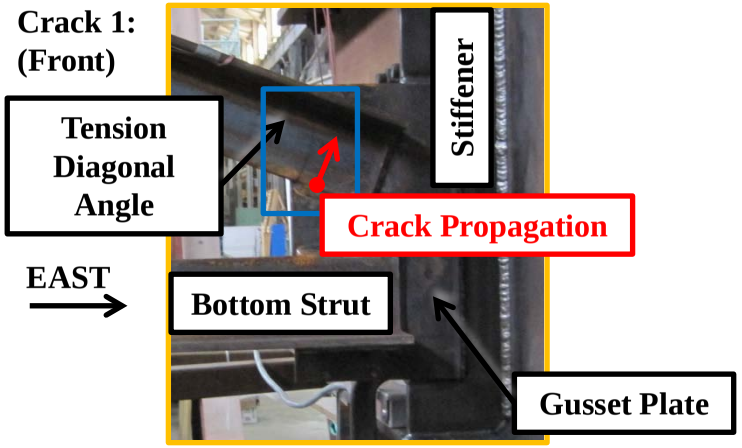

The first crack occurred at the forward edge of the angle-gusset connection initiating at the angle toe and propagating into the angle. A close up is shown below.

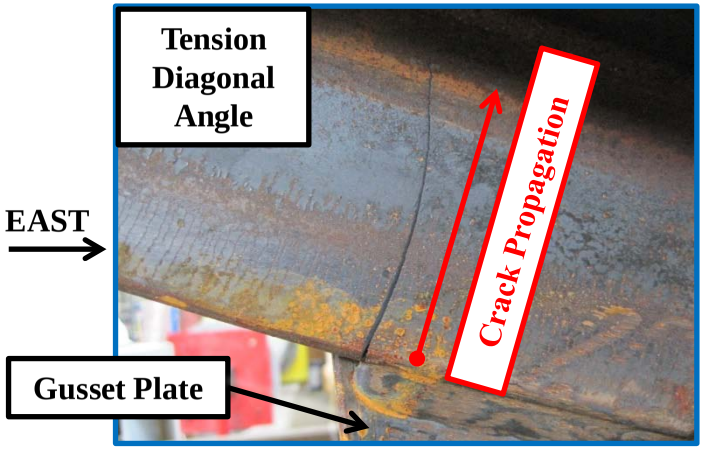

Test Specimen: XF5

Crack 2:

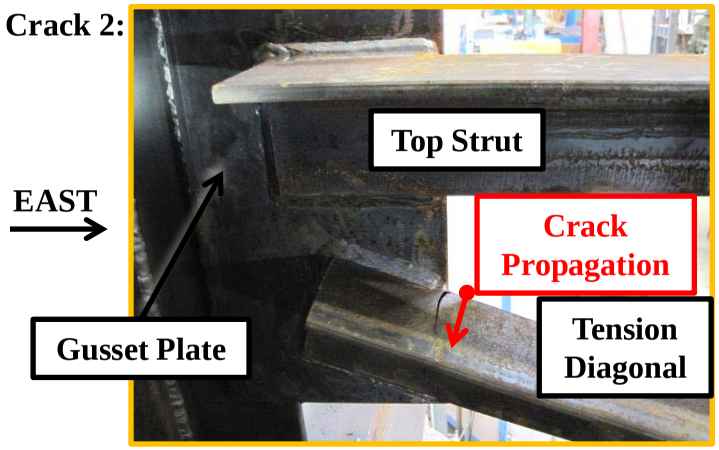

After the repair (N = 55,774 cycles), testing of the specimen continued. There was no sign of a crack at this location at the time of repair. At N = 66,777 cycles, a small crack was seen to initiate at the angle toe at the forward edge of angle-gusset connection and propagating into the heel of the angle (seen using magnifying glass). The crack propagated through the angle thickness and along both angle legs until failure.

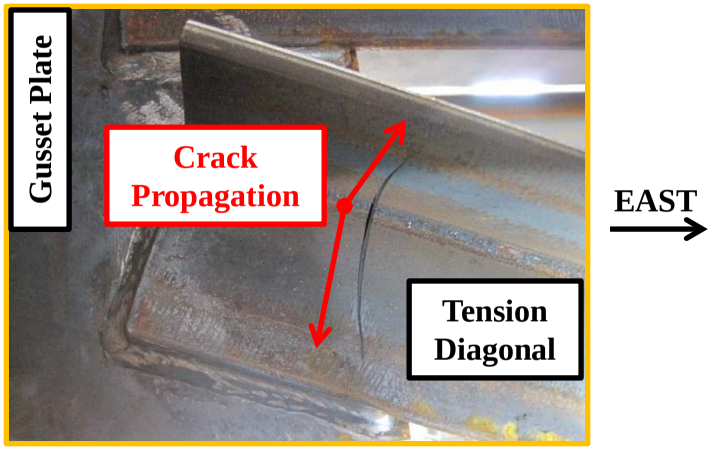

View of crack on the inside face of the angle.

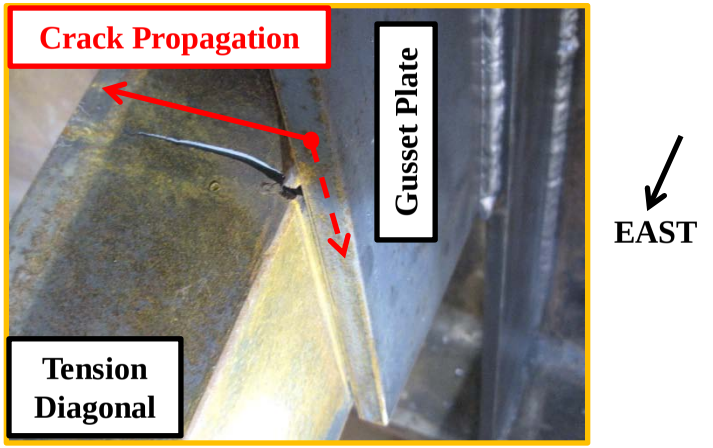

Top view of crack initiating at angle heel..

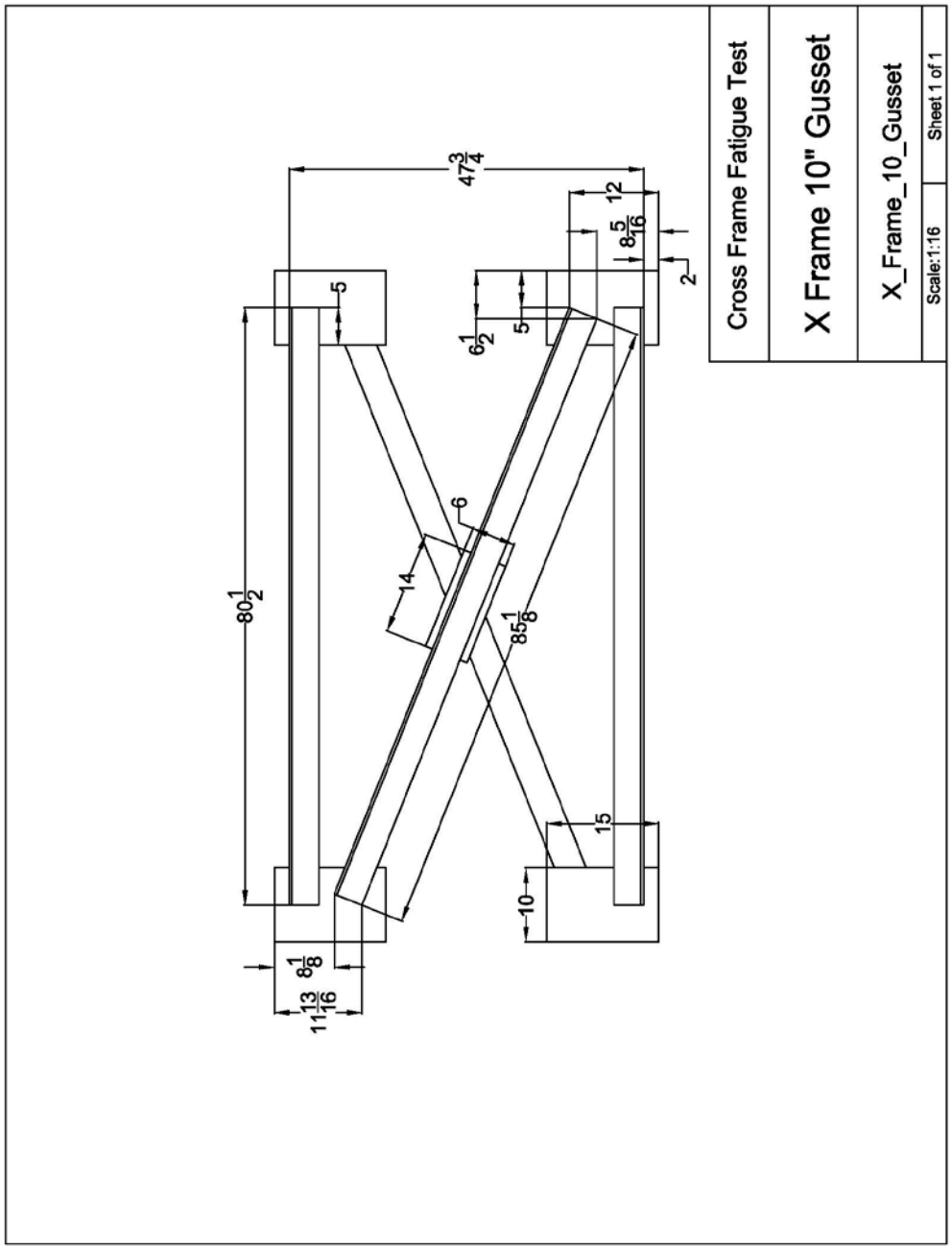
Cross Frame Fatigue Test
X Frame 10" Gusset
X_Frame_10_Gusset
Scale:1:16
Sheet 1 of 1
47 3/4
12
8 5/16
2
5
6 1/2
5
6
14
80 1/2
85 1/8
15
10
8 1/8
11 13/16

Test Specimen: XF6

Test Dates: 4/9/2013 – 4/19/2013

Primary Failure Location: Gusset Plate

S_R = 13.00 ksi (Tension Diagonal)

N = 683,364 cycles

AASHTO Fatigue Category: E

Stiffness: **Initial:** 97.97 k/in **Final:** 86.22 k/in
12.0% loss of stiffness

Average Weld Size: Leg: 0.31″ **Throat:** 0.34″

Details:

- TxDOT Standard X-Type Cross Frame Detail with members 4″ short prevent weld intersection
- The gusset plates were 2″ wider to maintain the same overlap as XF1-5 and the angle of the diagonals remained consistent
- Tension diagonal of cross frame positioned on the back side of the cross frame to see if increased space between angle-gusset weld and gusset-stiffener weld improves plate fatigue

Crack Locations:

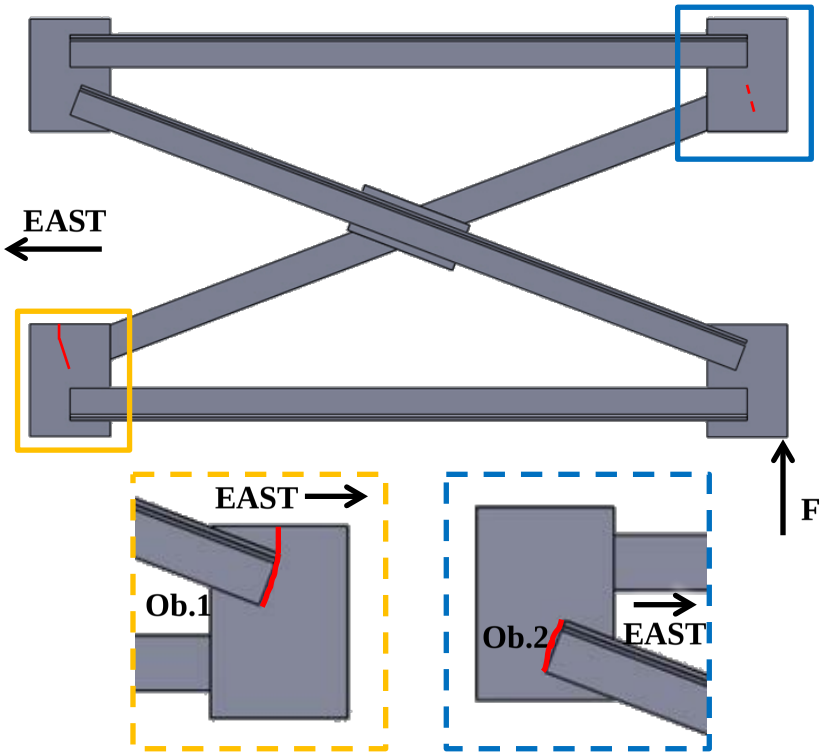

Observations:

1. First crack initiated at the back edge of angle-gusset weld at gusset toe and propagated into the gusset plate to the free edge
2. Second, similar crack found at opposite end of tension diagonal during final stiffness test

Test Specimen: XF6

First Observed Crack
C1: N = 369,836 cycles
C2: N = 683,364 cycles

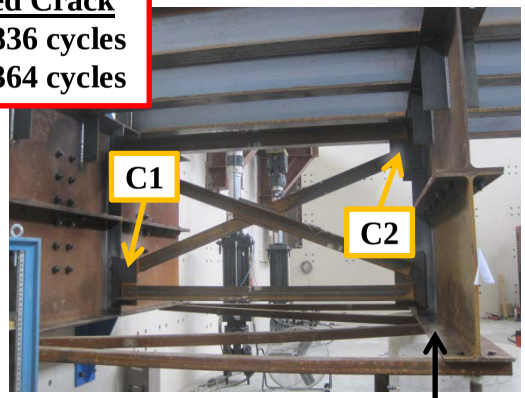

Crack 1: (Back)

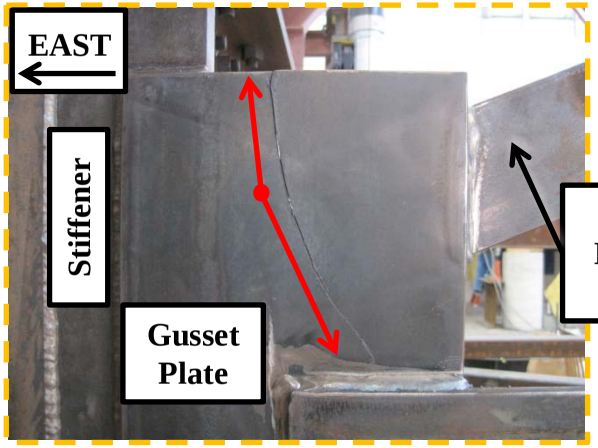

Crack 1: (Front)

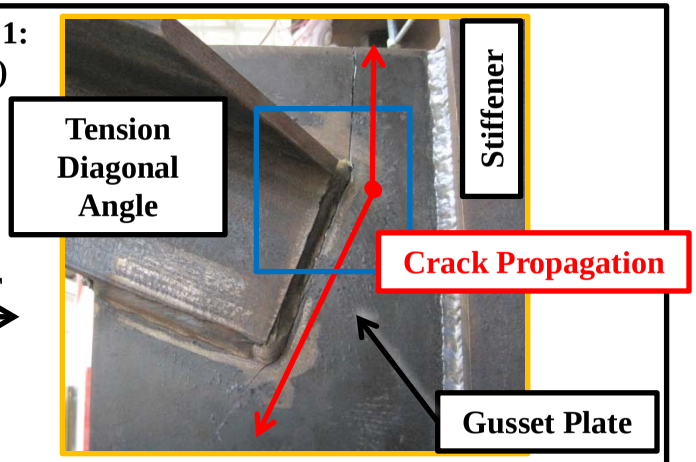

The first crack occurred at the back edge of the angle-gusset connection initiating at the gusset toe and propagating into the plate. A close up is shown below.

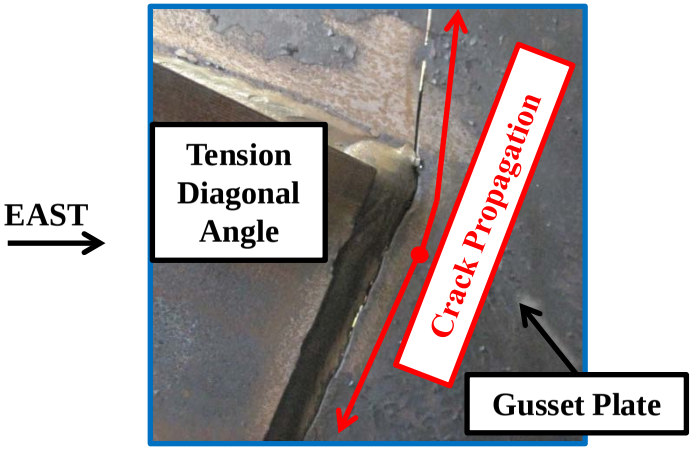

Test Specimen: XF6

Crack 2:
(Front)

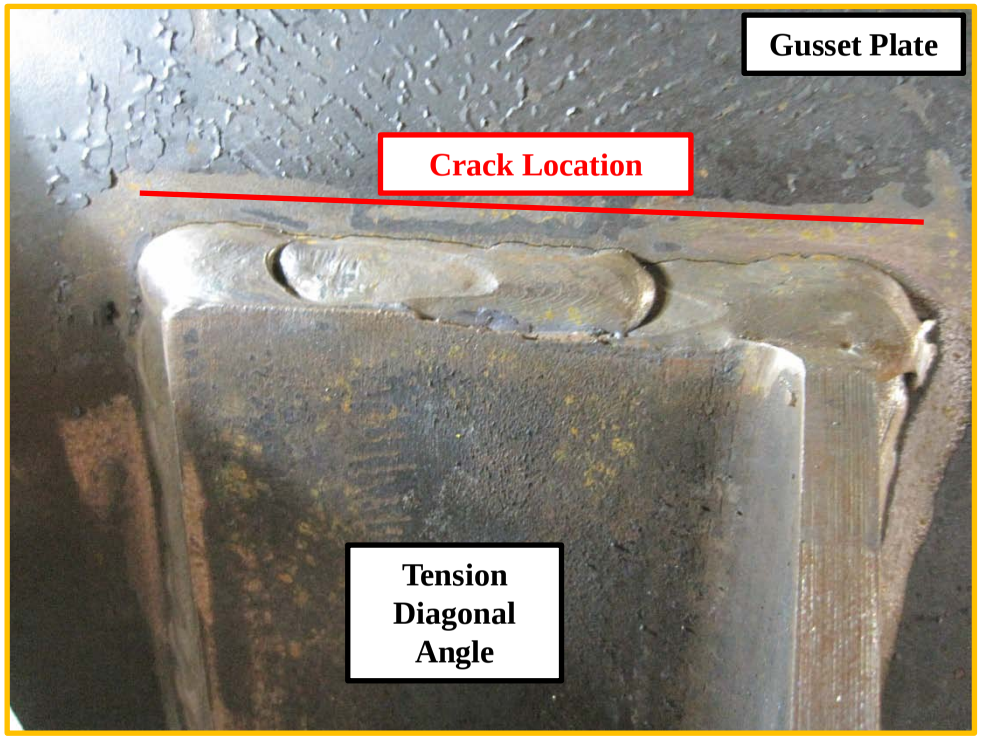

EAST

The second crack occurred at the opposite side of the tension diagonal along the back edge of the angle-gusset connection initiating at the gusset toe and propagating into the plate. The crack was first observed at failure.

There is also damage to the mill scale seen in this photo. It is possible some local yielding occurred by placing the angle further from the gusset-stiffener connection.

Test Specimen: XF7

Test Dates: 5/30/2013 – 6/4/2013

Primary Failure Location: Gusset Plate

S_R = 15.00 ksi (Tension Diagonal)

N = 300,001 cycles

AASHTO Fatigue Category: almost E

Stiffness: **Initial:** 98.12 k/in **Final:** 82.19 k/in
16.2% loss of stiffness

Average Weld Size: Leg: 0.31″ **Throat:** 0.32″

Details:

- TxDOT Standard X-Type Cross Frame Detail with members 4″ short prevent weld intersection
- The gusset plates were 2″ wider to maintain the same overlap as XF1-6 and the angle of the diagonals remained consistent
- Tension diagonal of cross frame positioned on the back side of the cross frame to validate results of XF_6 that increased space between angle-gusset weld and gusset-stiffener weld improves plate fatigue

Crack Locations:

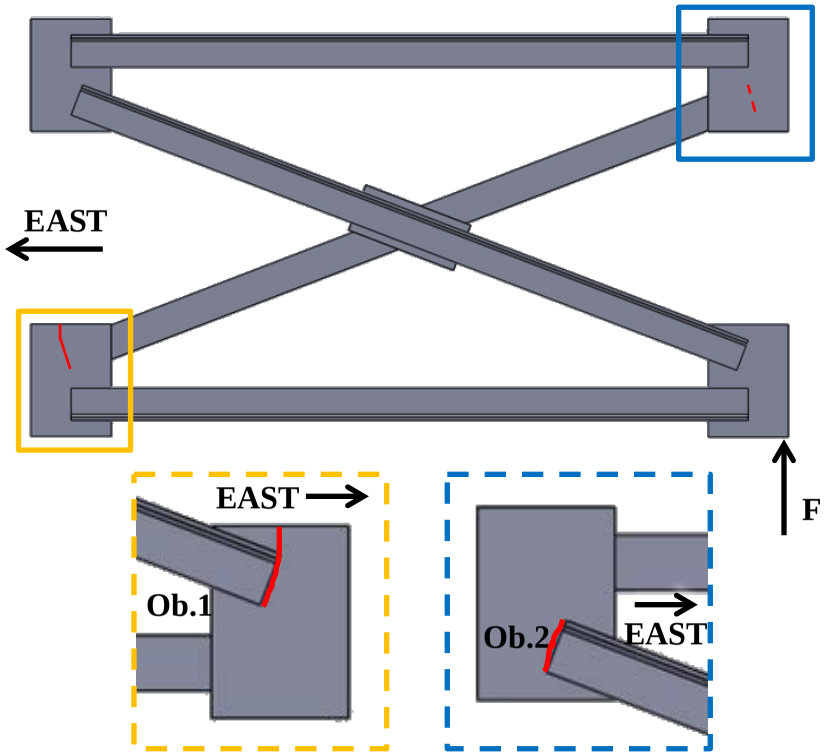

Observations:

1. First crack initiated at the back edge of angle-gusset weld at gusset toe and propagated into the gusset plate to the free edge
2. Second, similar crack found at opposite end of tension diagonal at the same time first crack was observed.

Test Specimen: XF7

First Observed Crack
C1: N = 175,700 cycles
C2: N = 175,700 cycles

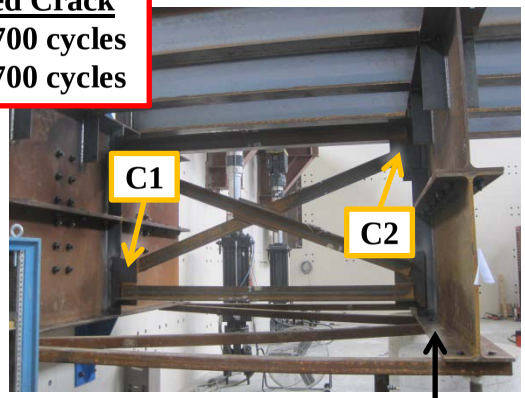

Crack 1: (Front)

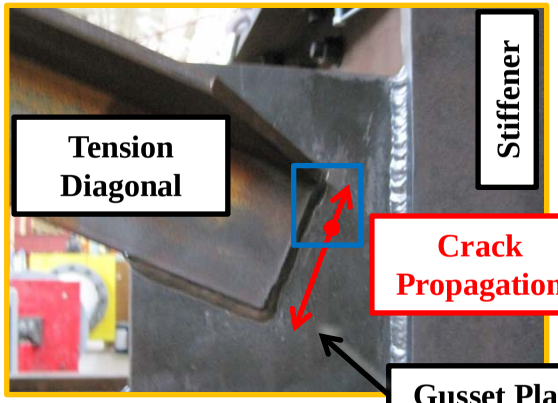

The first crack occurred at the back edge of the angle-gusset connection initiating at the gusset toe and propagating into the plate. Close ups are shown below. Note how the crack follows the weld toe. There is also minor undercut at this connection but it is within acceptable tolerances.

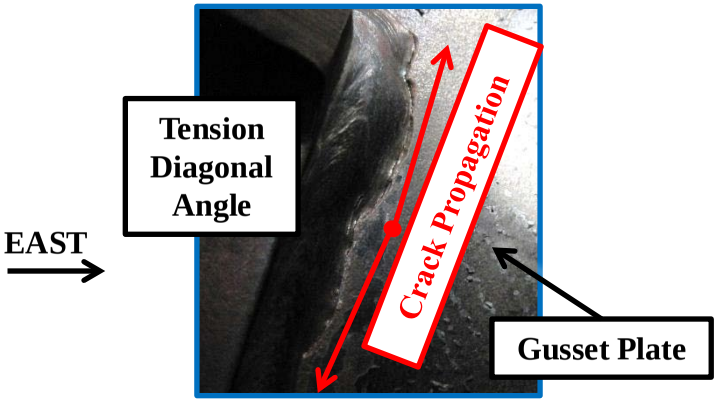

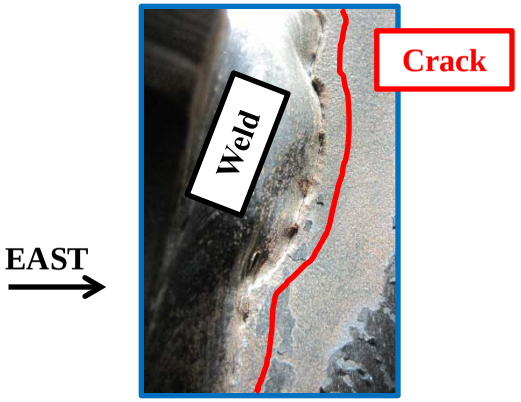

Test Specimen: XF7

Crack 1: (Failure- N=300,001)

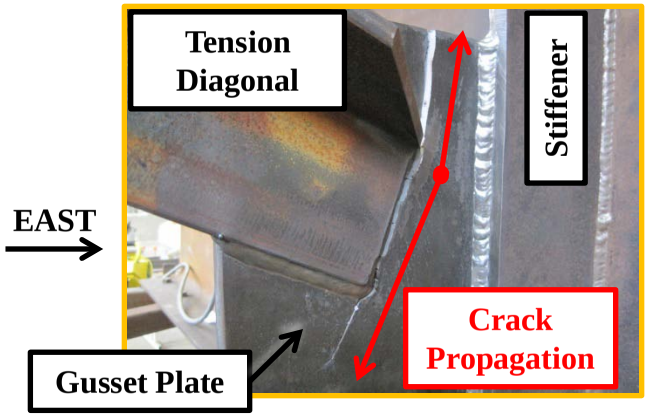

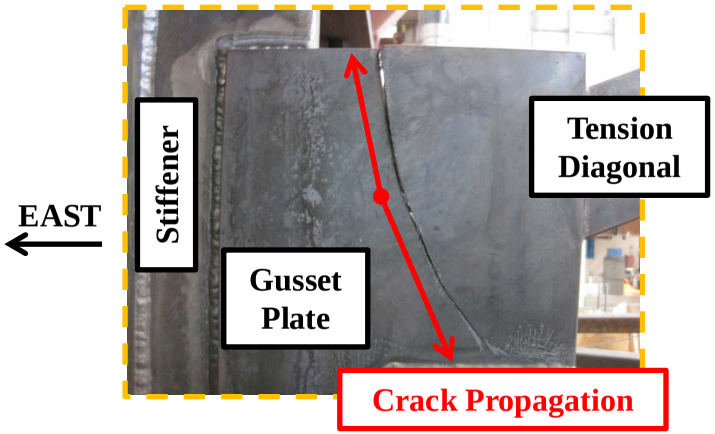

Crack 2: (Failure- N=300,001)

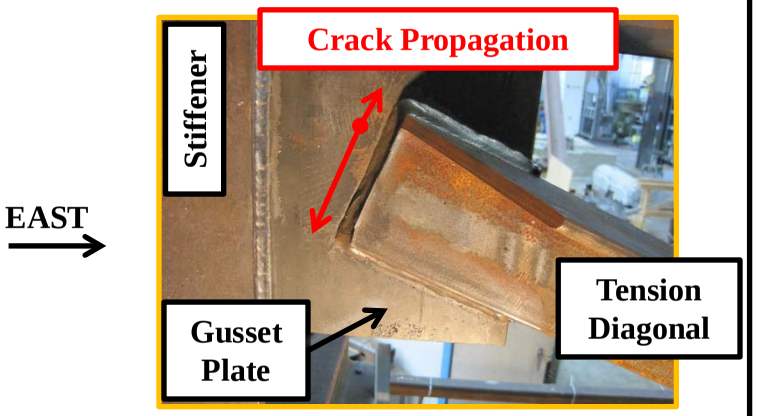

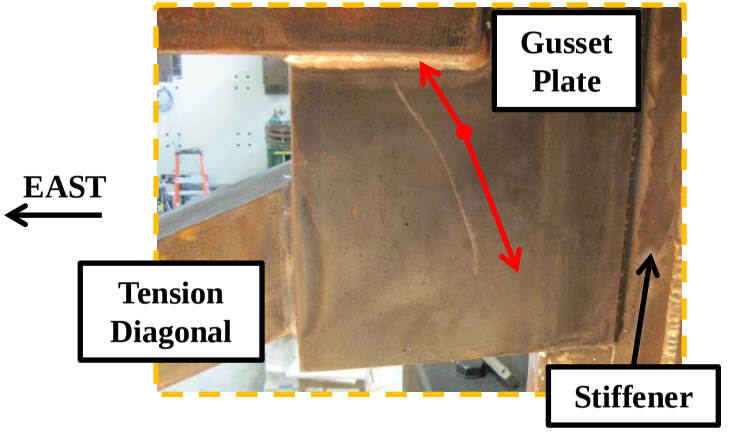

Test Specimen: XF8

Test Dates: 7/13/2013 – 7/16/2013

Primary Failure Location: Tension Diagonal

S_R = 15.00 ksi (Tension Diagonal)

N = 104, 924 cycles

AASHTO Fatigue Category: < E′

Nominal Weld Size: Leg: 5/16″

Details:

- TxDOT Standard X-Type Cross Frame Detail with members 4″ short prevent weld intersection
- The gusset plates were 2″ wider to maintain the same overlap as XF1-7 and the angle of the diagonals remained consistent
- Tension diagonal of cross frame positioned on the front side of the cross frame to validate results of XF_2,5
- Welds were not included on the back side of the angles to gusset plate

Crack Locations:

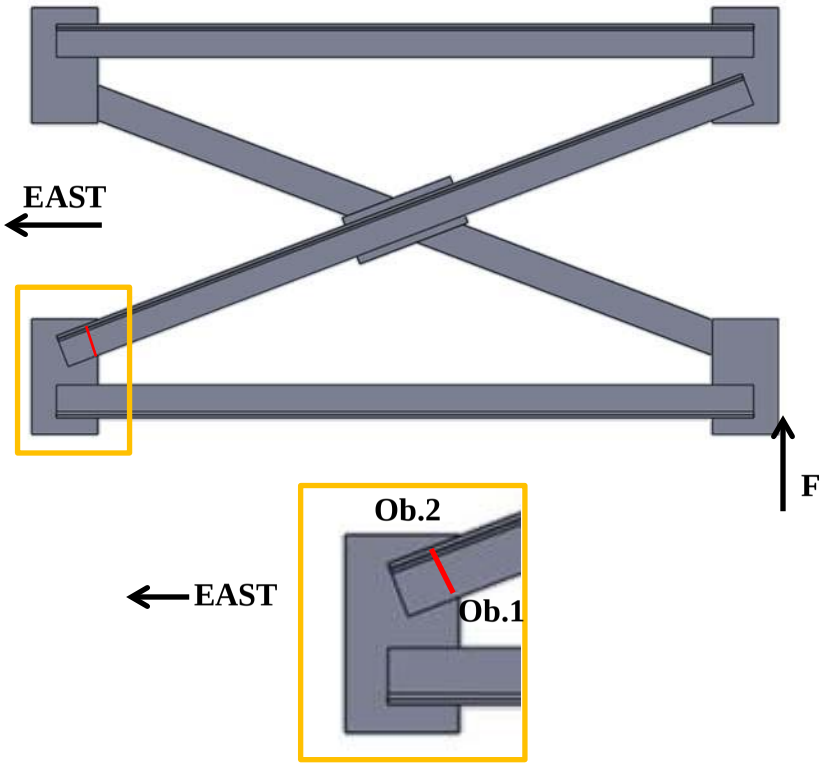

Observations:

1. First crack initiated at the forward edge of angle-gusset weld at angle toe and propagated into the angle through the horizontal leg
2. At failure, a crack was observed in the fillet weld at the forward edge of connection along the vertical angle leg

Test Specimen: XF8

First Observed Crack
C1: N = 88,548 cycles
C2: N = 104,924 cycles

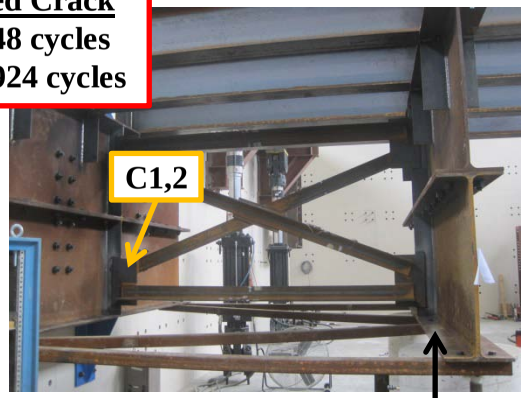

Crack 2:
(Failure- N = 104,924 cycles)

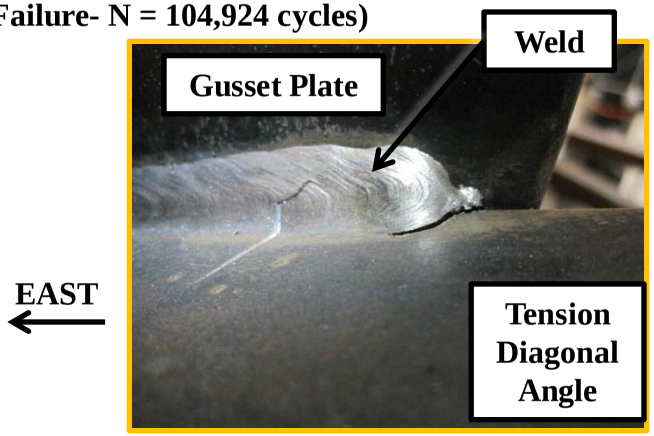

Crack 1: (Failure- N = 104,924 cycles)

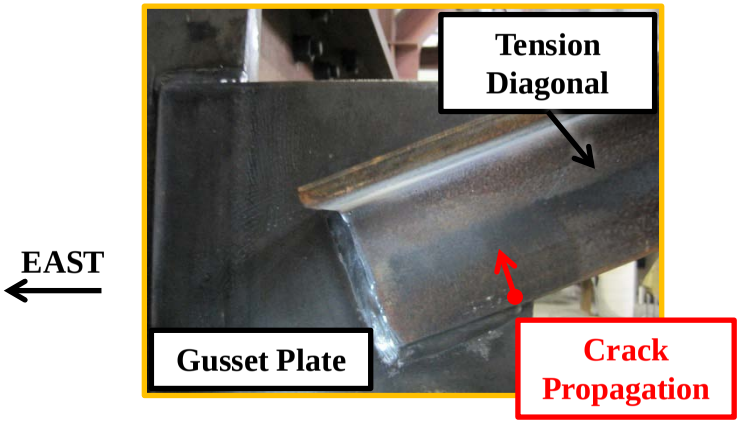

The first crack occurred at the forward edge of the angle-gusset connection propagating into the angle leg.

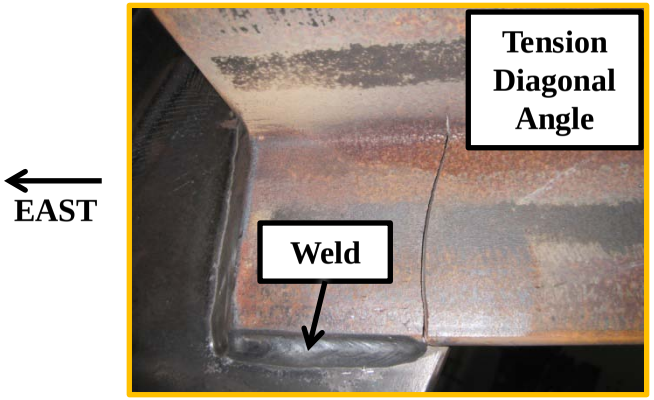

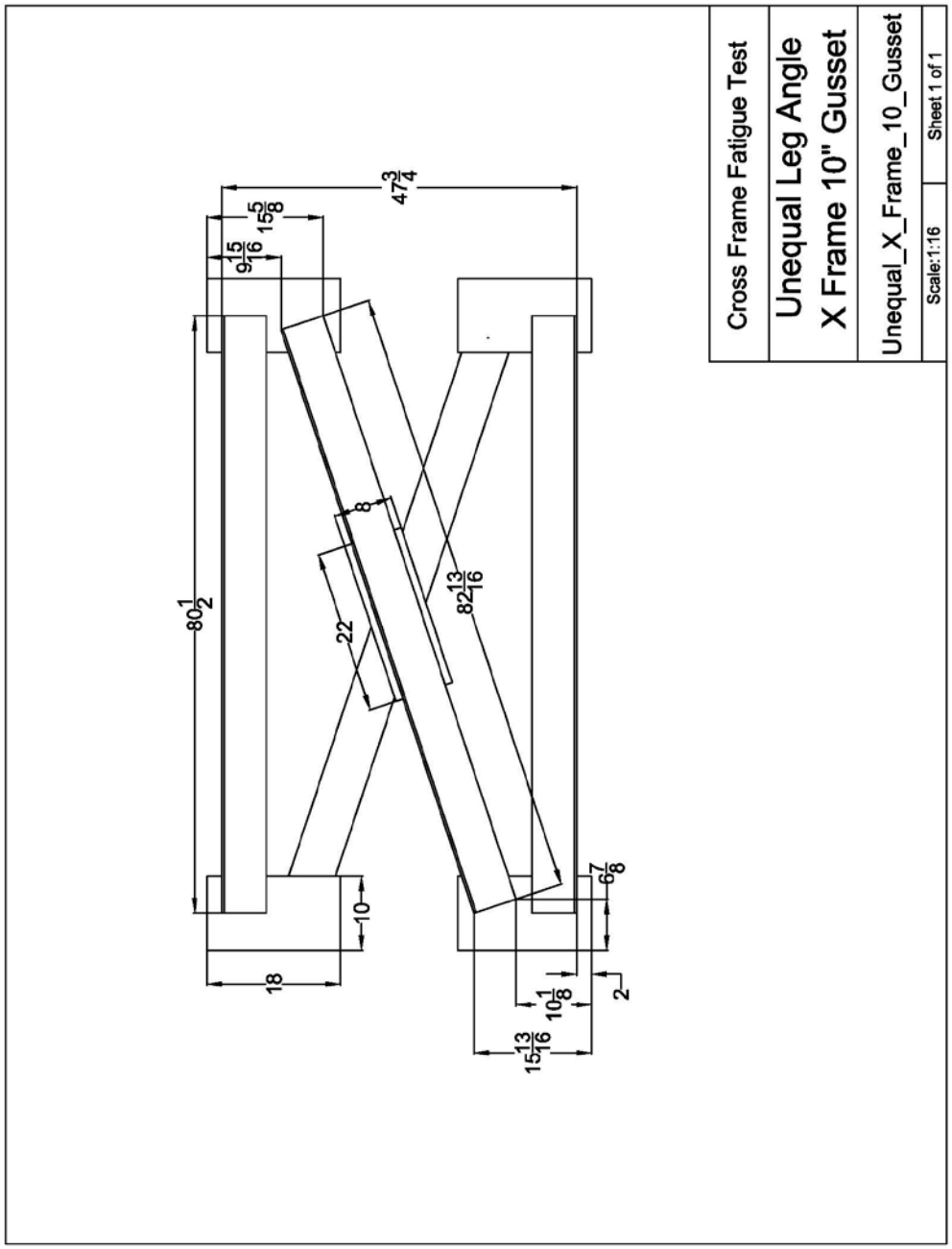
Cross Frame Fatigue Test
Unequal Leg Angle
X Frame 10" Gusset
Unequal_X_Frame_10_Gusset
Scale:1:16
Sheet 1 of 1
47 3/4
15 5/8
9 15/16
80 1/2
8
22
82 13/16
10
18
6 7/8
2
10 1/8
15 13/16

Test Specimen: XF_UL_1

Test Dates: 4/10/2013 – 4/12/2013

Primary Failure Location: Angle

S_R = 15.00 ksi

N = 86,970 cycles

AASHTO Fatigue Category: < E′

Stiffness: **Initial:** 94.32 k/in **Final:** 66.12 k/in
29.9% loss of stiffness

Average Weld Size: Leg: 0.31″ **Throat:** 0.31″

Details:

- Unequal leg L6 x 3.5 x 5/16 members
- TxDOT Standard X-Type Cross Frame Details for L4 x 4 x 3/8 followed for overlap
- TxDOT Standard X-Type Cross Frame Details for L6 x 6 x 9/16 followed for plate geometry
- Angles 1″ shorter to prevent weld intersection
- Tension diagonal of cross frame positioned on the front side of the cross frame to prevent interaction of angle-gusset weld and gusset-stiffener weld

Crack Locations:

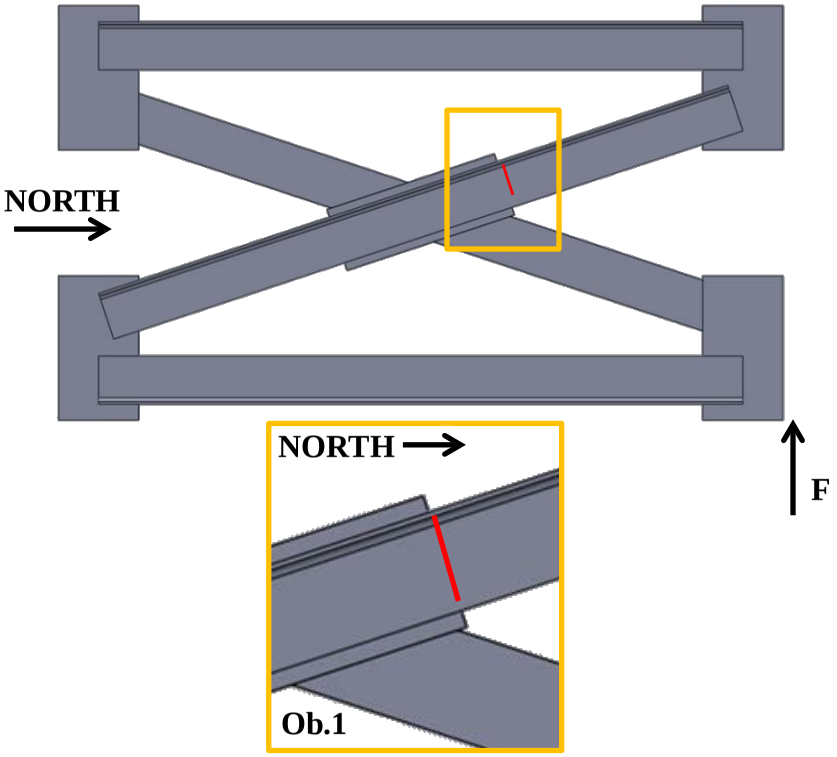

Observations:

1. First crack initiated at the angle toe of the angle-center plate weld at the heel of the angle and propagated along both legs of the angle

Test Specimen: XF_UL_1

First Observed Crack
C1: N = 83,373 cycles

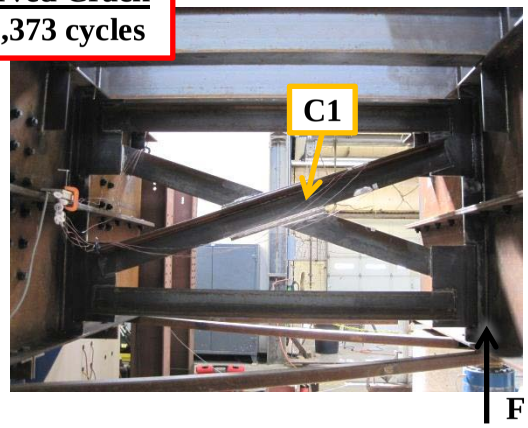

Crack 1: (Back- Horizontal Long Leg)

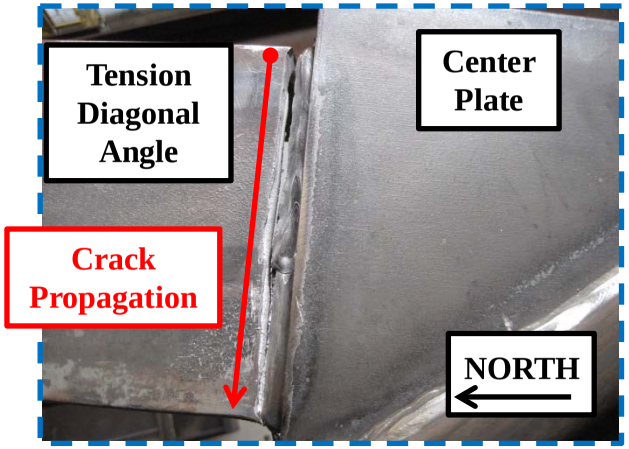

Crack 1: (Front)

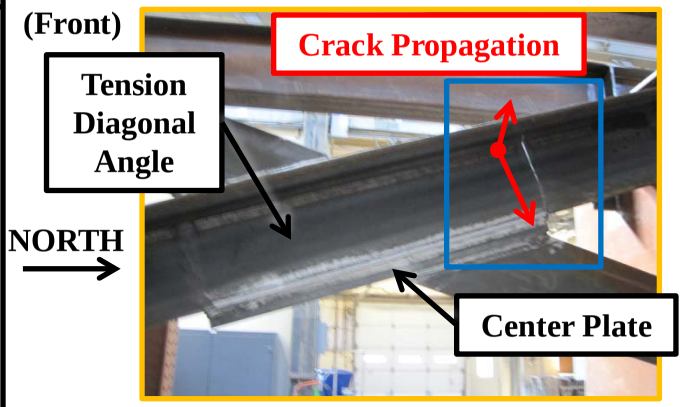

The crack occurred at the heel of the angle along the angle toe of the angle-center plate weld and propagating into the angle legs. The crack was not observed sooner as previous experiments did not lead researchers to monitor this location.

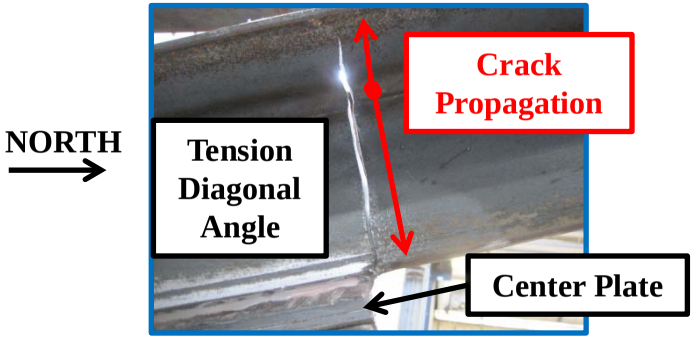

Test Specimen: XF_UL_1

Crack 1: (Top-Outstanding Short Leg)

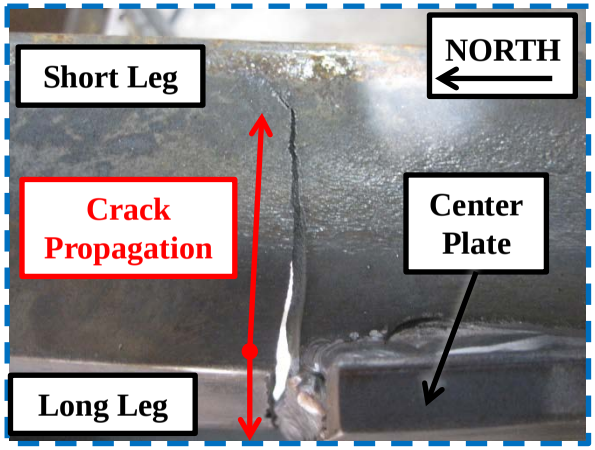

Test Specimen: XF_UL_2

Test Dates: 5/8/2013 – 5/20/2013

Primary Failure Location: Angle

S_R = 15.00 ksi

N = 620,464 cycles

AASHTO Fatigue Category: E′

Stiffness: **Initial:** 94.32 k/in **Final:** 74.5 k/in
21.0% loss of stiffness

Average Weld Size: Leg: 0.30″ **Throat:** 0.31″

Details:

- Unequal leg L6 x 3.5 x 5/16 members
- TxDOT Standard X-Type Cross Frame Details for L4 x 4 x 3/8 followed for overlap
- TxDOT Standard X-Type Cross Frame Details for L6 x 6 x 9/16 followed for plate geometry
- Angles 1″ shorter to prevent weld intersection
- Tension diagonal of cross frame positioned on the front side of the cross frame to prevent interaction of angle-gusset weld and gusset-stiffener weld

Crack Locations:

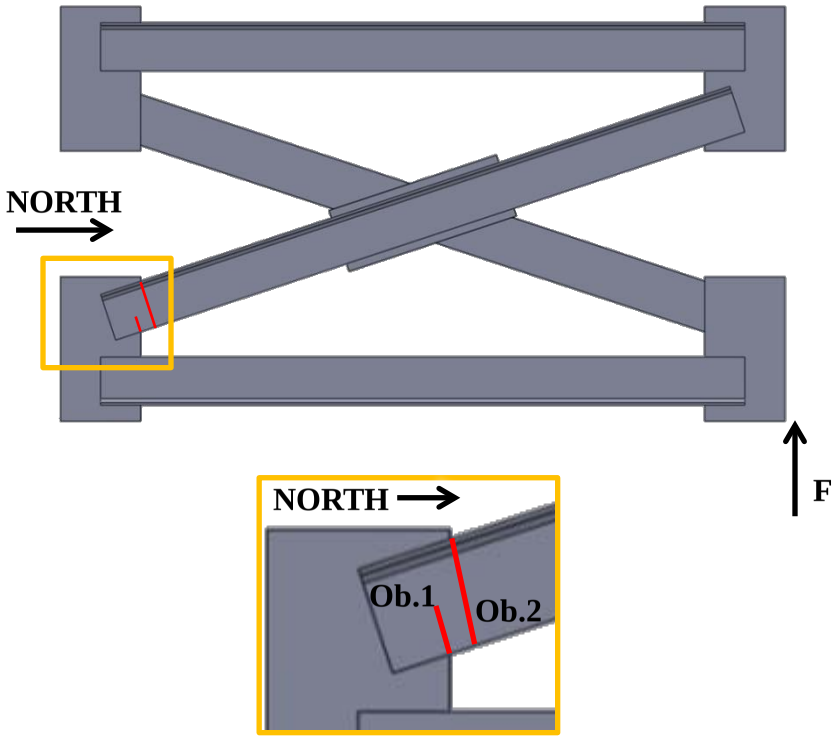

Observations:

1. First crack initiated at the forward toe of the angle-gusset plate weld at the toe of the angle and propagated into the angle.
2. A second crack formed in the member nearby, eventually propagating across the section.

Test Specimen: XF_UL_2

First Observed Crack
C1: N = 295,437 cycles
C2: N = 607,695 cycles

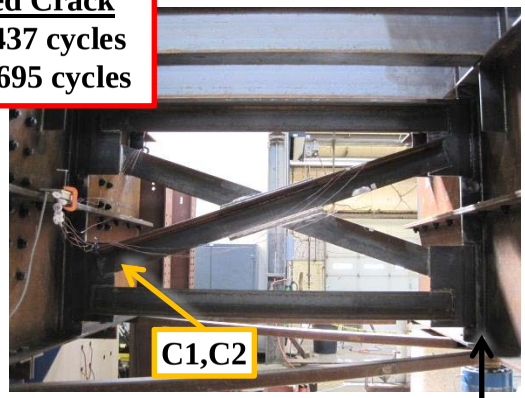

The first crack observed formed at the forward edge of the angle-gusset fillet weld, propagating into the angle toe and across the leg. The second crack was observed in the member, most likely originating at the toe of the backside weld and propagating through the thickness.

Crack 1,2:(N=607,695)

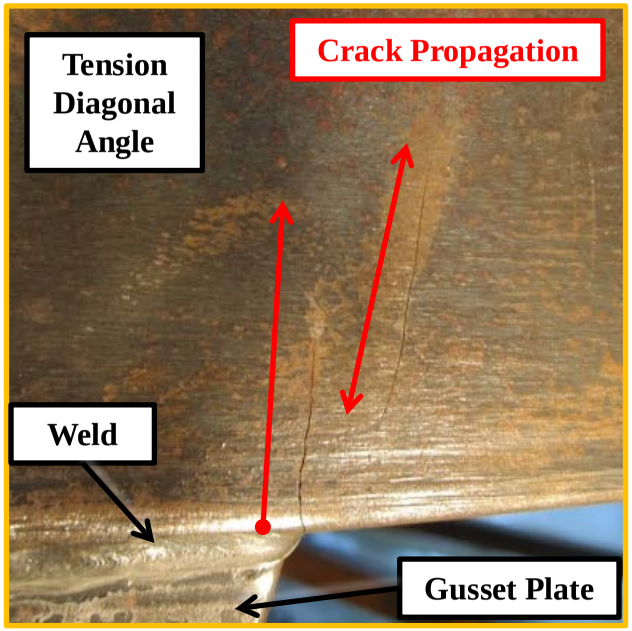

NORTH

Test Specimen: XF_UL_2

Crack 2: (Failure- N=620,464)

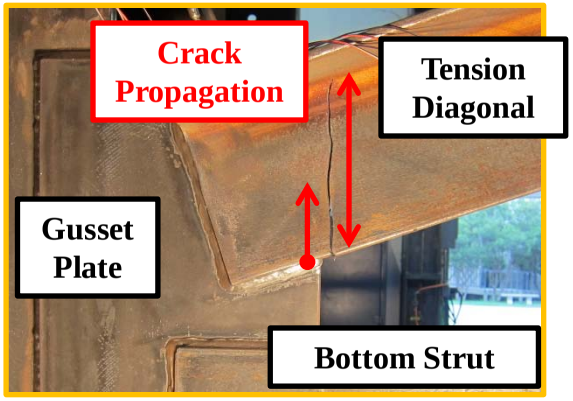

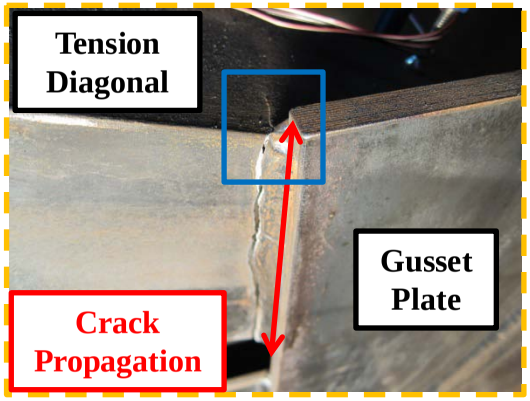

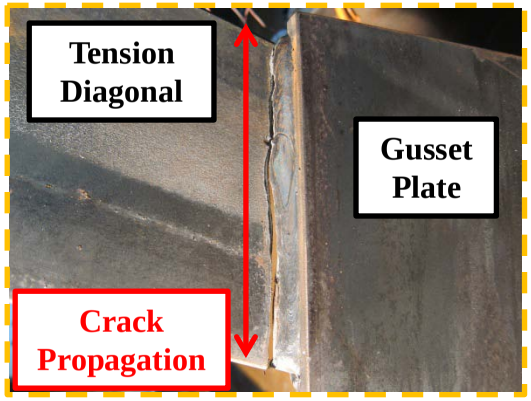

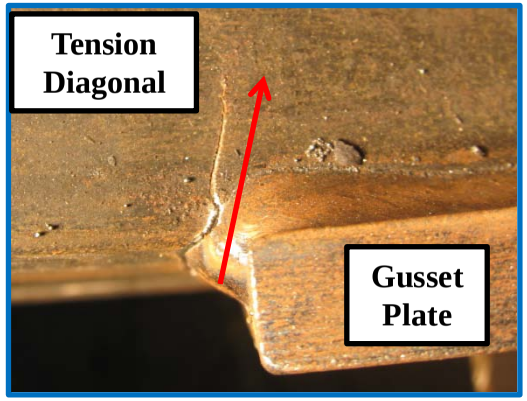

Test Specimen: XF_UL_3

Test Dates: 7/12/2013 – 7/15/2013

Primary Failure Location: Angle

S_R = 15.00 ksi

N = 103,050 cycles

AASHTO Fatigue Category: < E′

Nominal Weld Size: Leg: 5/16″

Details:

- Unequal leg L6 x 3.5 x 5/16 members
- TxDOT Standard X-Type Cross Frame Details for L4 x 4 x 3/8 followed for overlap
- TxDOT Standard X-Type Cross Frame Details for L6 x 6 x 9/16 followed for plate geometry
- Angles 1″ shorter to prevent weld intersection
- Gusset plates 2″ wider to prevent interaction of angle-gusset weld and gusset-stiffener weld
- No welds were provided on the back side of the angle

Crack Locations:

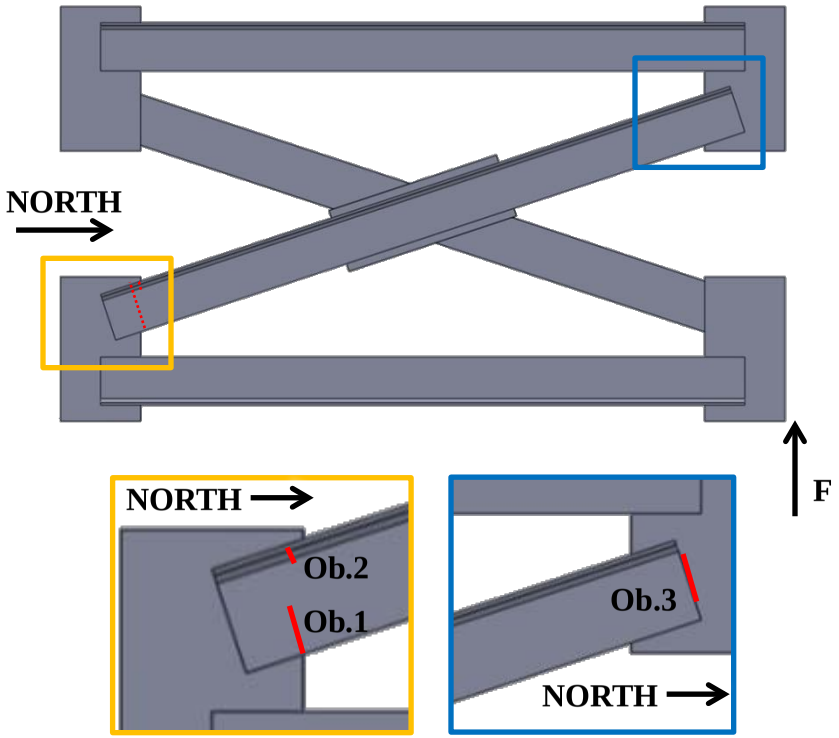

Observations:

1. First crack initiated at the forward toe of the angle-gusset plate weld at the toe of the angle and propagated into the angle.
2. A second crack formed in the member at the heel of the angle, propagating into the outstanding leg of the angle.
3. A third hairline crack was noticed on the other end of the angle at failure.

Test Specimen: XF_UL_3

First Observed Crack
C1: N = 103,050 cycles
C2: N = 103,050 cycles
C3: N = 103,050 cycles

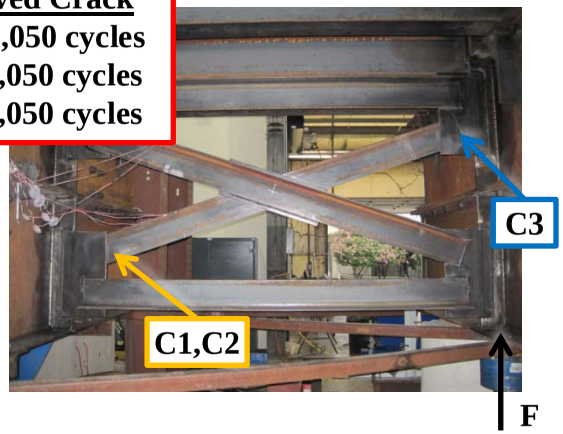

Crack 3:(N=103,050)

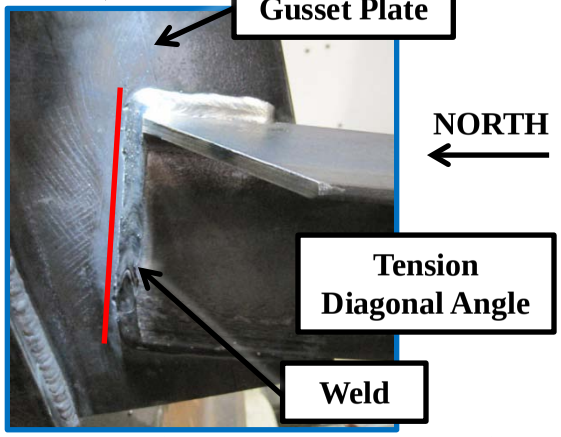

Hairline crack at end of angle along gusset toe of weld.

Crack 1,2:(N=103,050)

The first crack observed formed at the forward edge of the angle-gusset fillet weld, propagating into the angle toe and across the leg. The second crack was observed in the same location, forming at the angle toe at the forward edge of the angle-gusset fillet weld, propagating into the heel of the angle.

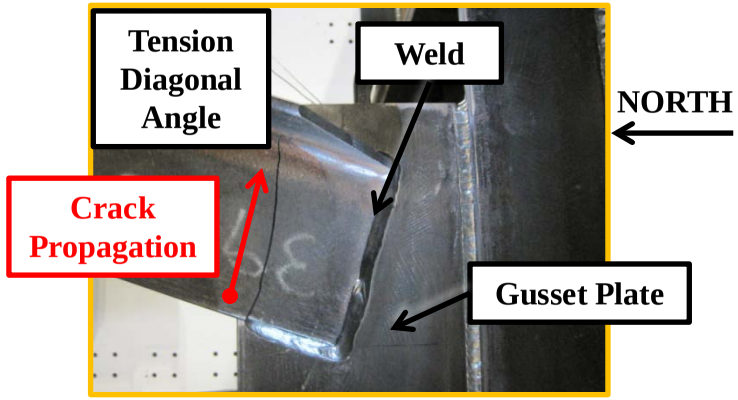

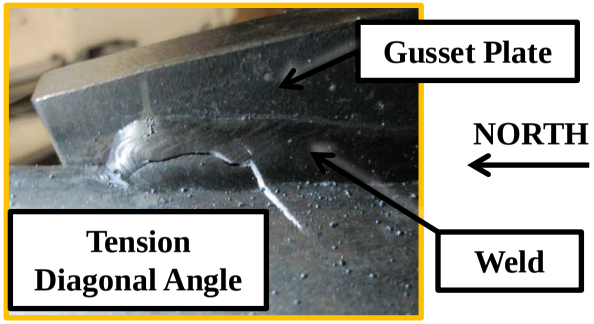

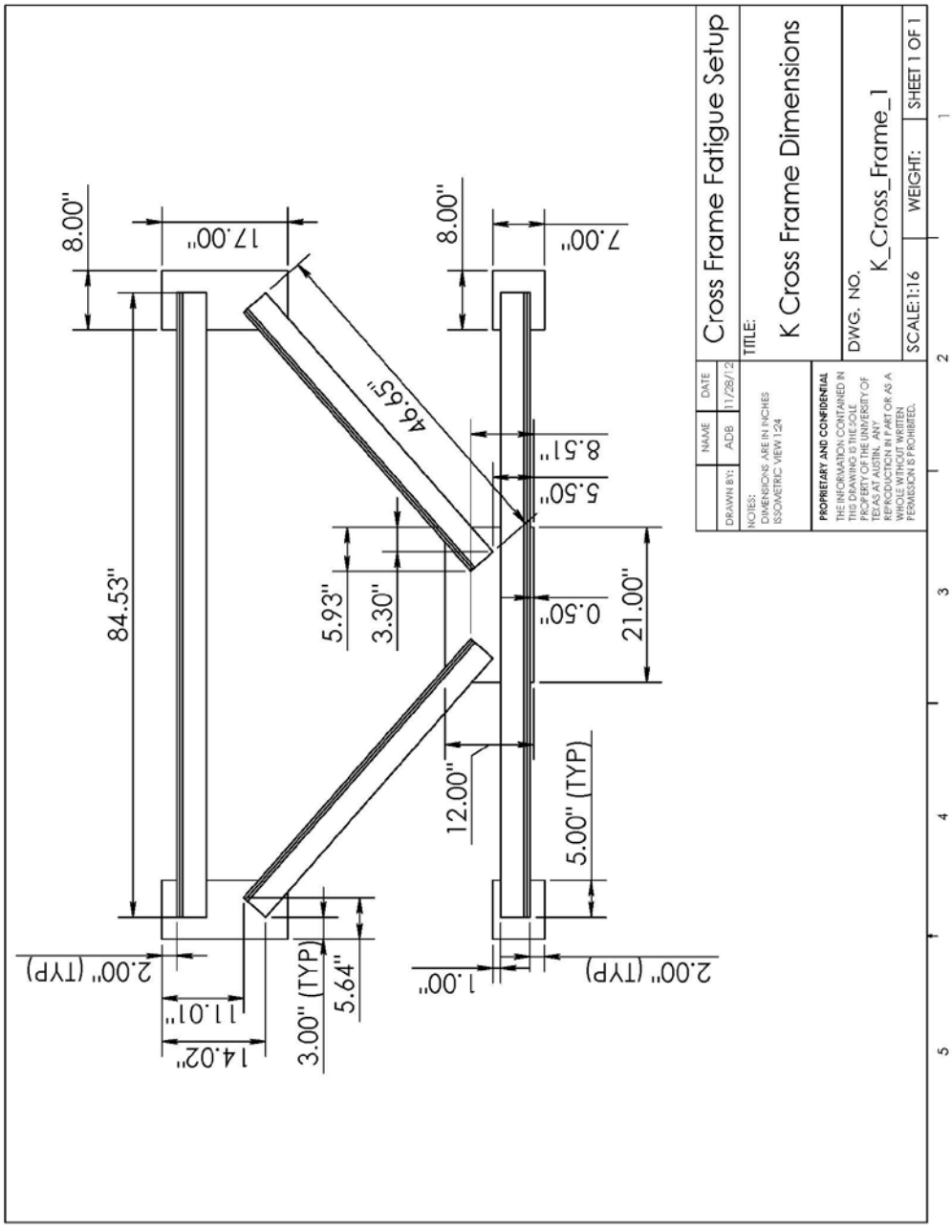
8.00"
17.00"
8.00"
7.00"
46.65"
84.53"
8.51"
5.50"
5.93"
3.30"
0.50"
21.00"
12.00"
5.00" (TYP)
2.00" (TYP)
1.00"
2.00" (TYP)
11.01"
14.02"
3.00" (TYP)
5.64"
NAME
DATE
DRAWN BY:
ADB
11/28/12
NOTES:
DIMENSIONS ARE IN INCHES
ISSOMETRIC VIEW 1:24
PROPRIETARY AND CONFIDENTIAL
THE INFORMATION CONTAINED IN THIS DRAWING IS THE SOLE PROPERTY OF THE UNIVERSITY OF TEXAS AT AUSTIN. ANY REPRODUCTION IN PART OR AS A WHOLE WITHOUT WRITTEN PERMISSION IS PROHIBITED.
Cross Frame Fatigue Setup
TITLE:
K Cross Frame Dimensions
DWG. NO.
K_Cross_Frame_1
SCALE:1:16
WEIGHT:
SHEET 1 OF 1

Test Specimen: KF_1

Test Dates: 1/22/2013 – 1/28/2013

Primary Failure Location: Tension Strut

S_R = 13.76 ksi

N = 186,732 cycles

AASHTO Fatigue Category: E′

Stiffness: **Initial:** 90.04 k/in **Final:** 67.30 k/in
25.3% loss of stiffness

Average Weld Size: Leg: 0.31″ **Throat:** 0.30″

Details:

- TxDOT Standard K-Type Cross Frame Details for L4 x 4 x 3/8
- Orientation of struts and diagonals were inverse of typical TxDOT layout (typical detail has center gusset plate attached to strut opposite loaded flange)

Crack Locations:

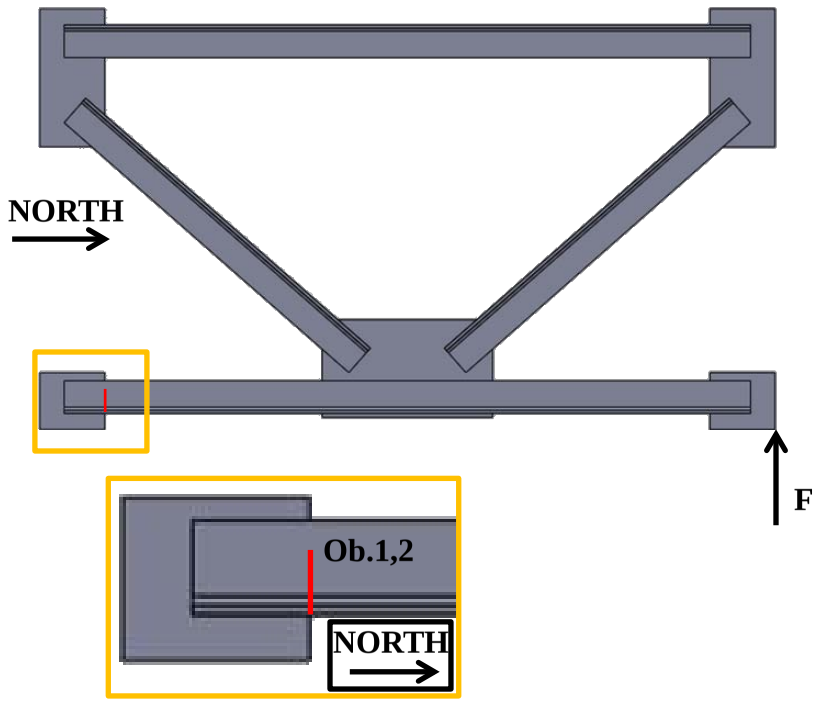

Observations:

1. First crack seen in the loaded strut, starting at the back side weld and propagating through the angle member.
2. The measured force was higher than that predicted by a truss analogy, and was close to the stress range of 15 ksi targeted in the tension diagonal.

Test Specimen: KF_1

First Observed Crack
C1: N = 182,825 cycles

Crack 1: (N=182,825)

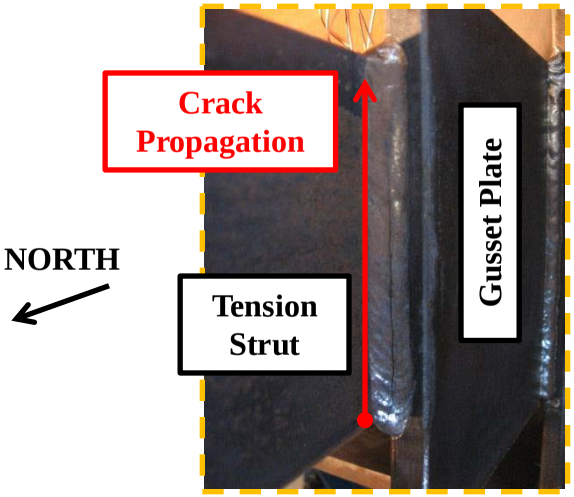

The crack began at the forward edge of the fillet weld near the transverse weld and propagated into the angle heel and through the weld throat.

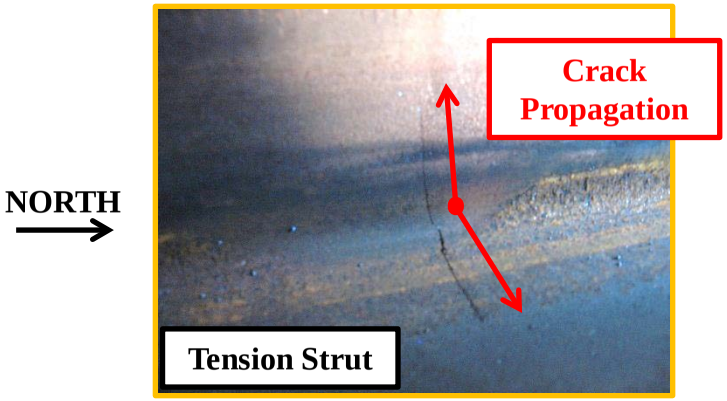

Test Specimen: KF_1

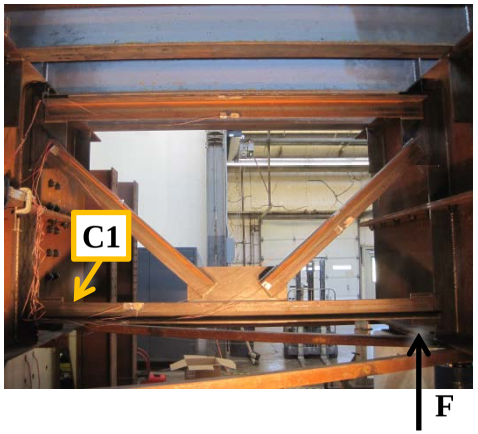

Crack 1: (Failure- N=186,732)

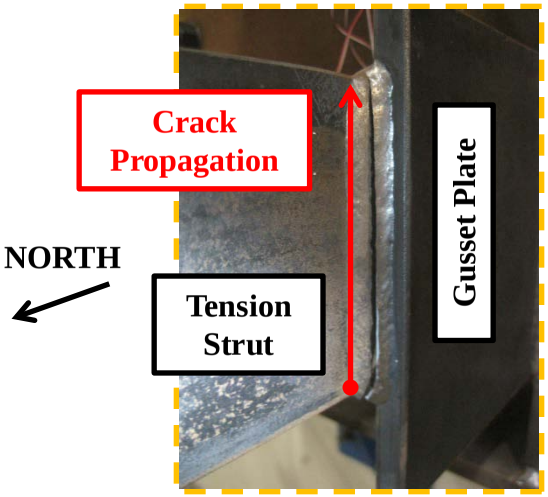

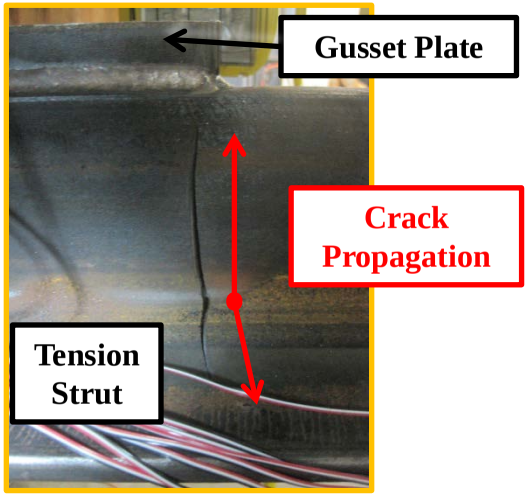

The crack continued to grow through both angle legs until the stress range could not be maintained.

Test Specimen: KF_2

Test Dates: 2/14/2013 – 3/1/2013

Primary Failure: Strut	**Secondary Failure:** Tension Diagonal
S_R = 9.51 ksi (Effective Stress Range)	S_R = 15.00 ksi (Effective Stress Range)
N =244,633 cycles	**N** = 437,412 cycles
AASHTO Fatigue Category: < E′	**AASHTO Fatigue Category: E**
Stiffness:	**Stiffness:**
Initial: 89.56 k/in	**Initial:** 91.57 k/in
Final: 75.08 k/in	**Final:** 45.54 k/in
16.2% loss of stiffness	50.3% loss of stiffness

Average Weld Size: Leg: 0.32″ **Throat:** 0.31″

Details:

- TxDOT Standard K-Type Cross Frame Details for L4 x 4 x 3/8
- Orientation of struts and diagonals follow TxDOT detail- strut near unloaded flange has outstanding leg on opposite side

Crack Locations:

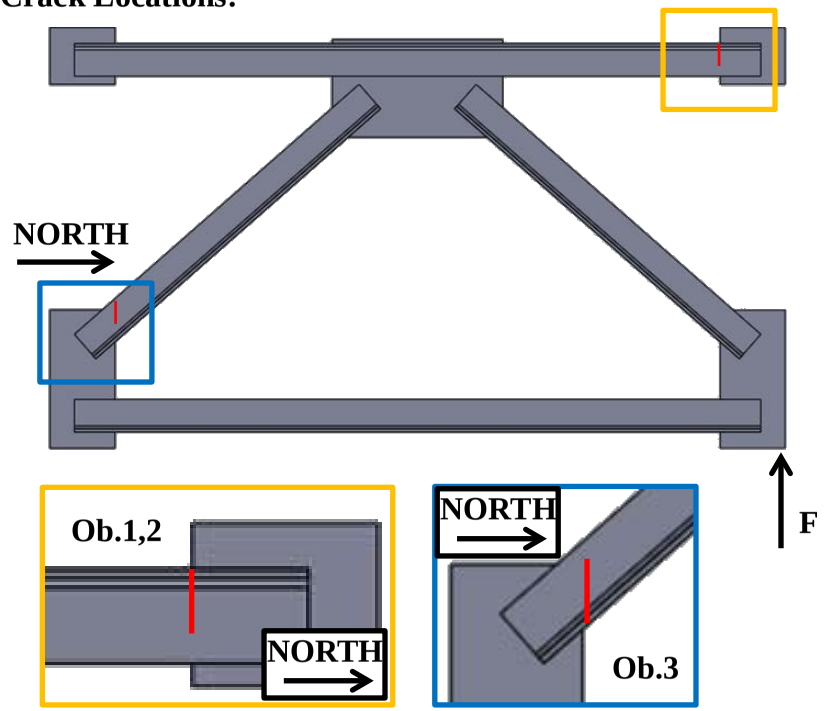

Observations:

1. First crack seen in the strut, starting at the toe of the back side weld and propagating through the angle member, most likely due to bending of the member (truss model indicates it is a zero force member).
2. The strut was repaired to continue testing the tension diagonal.
3. The tension diagonal cracked, originating at the angle toe of the backside angle-gusset weld.

Test Specimen: KF_2

First Observed Crack
C1: N = 244,633 cycles
C2: N = 410,567 cycles

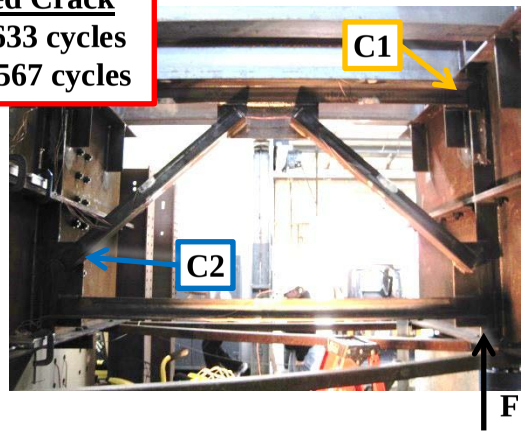

Crack 1: (N=244,633)

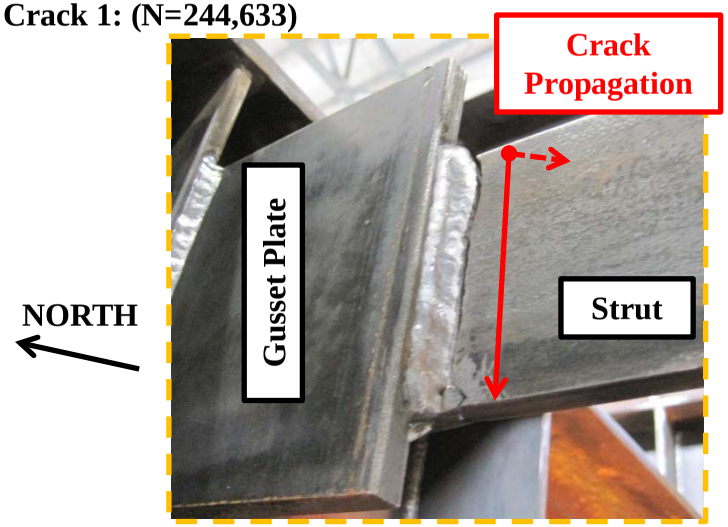

The crack began at the forward edge of the back side fillet weld and propagated into the angle heel along each leg.

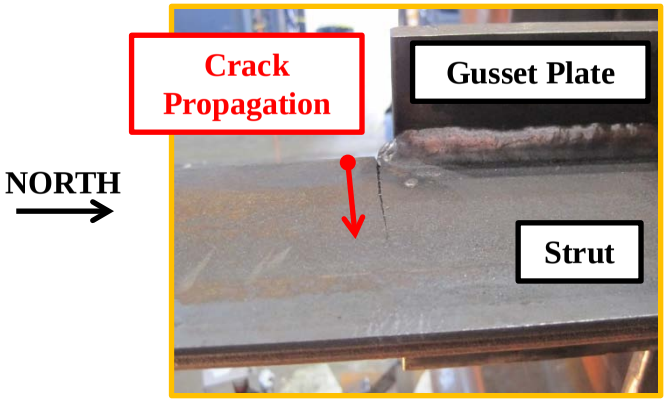

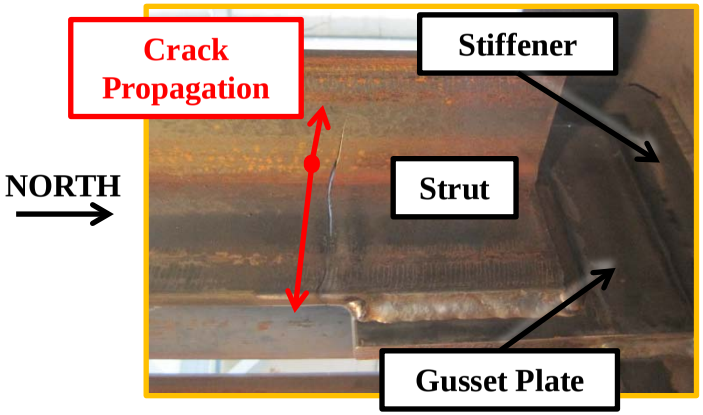

Test Specimen: KF_2

Crack 1: (Repair, N=244,633)

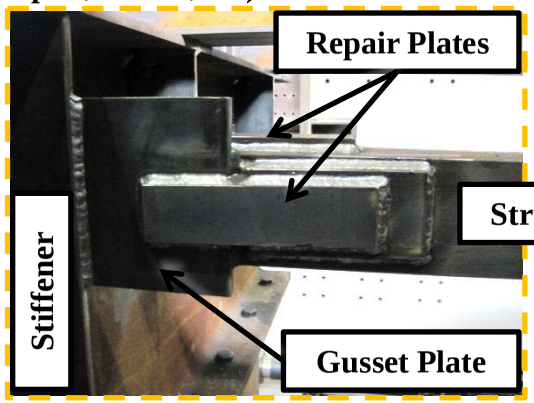

The first crack was repaired to further investigate the performance of the diagonal angle in tension. The stiffness post-repair (91.57 kip/in) was similar to the original stiffness of the specimen (89.56 kip/in).

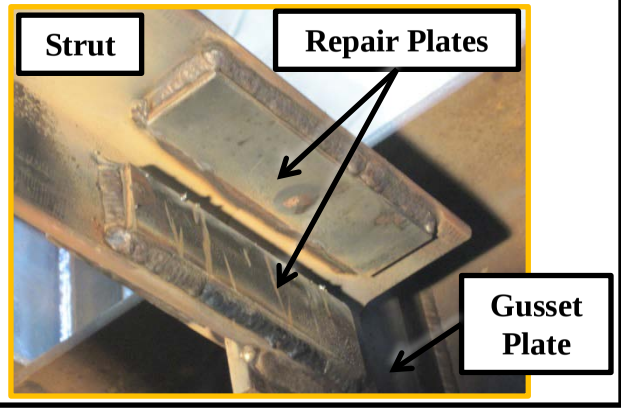

Crack 2: (N=437,412)

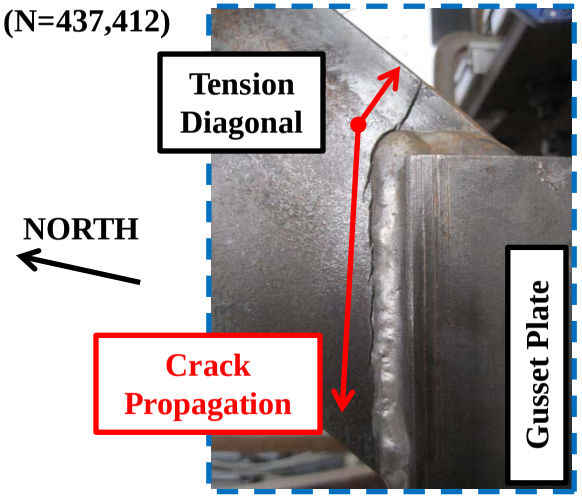

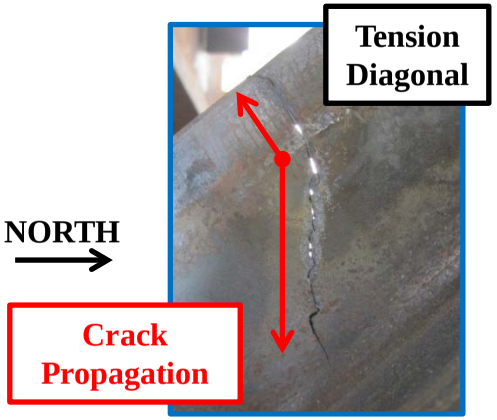

The second crack formed in the tension diagonal at the corner of the backside angle weld. The crack propagated along the weld toe into the angle.

Test Specimen: KF_3

Test Dates: 3/12/2013 – 3/21/2013

Primary Failure: Strut	**Secondary Failure:** Tension Diagonal
S_R = 9.27 ksi (Effective Stress Range)	S_R = 15.00 ksi (Effective Stress Range)
N =379,672 cycles **AASHTO Fatigue Category: < E′**	**N** = 379,672 cycles **AASHTO Fatigue Category: E**

Stiffness: **Initial:** 87.06 k/in **Final:** 59.17 k/in
32.0% loss of stiffness

Average Weld Size: Leg: 0.32″ **Throat:** 0.31″

Details:

- TxDOT Standard K-Type Cross Frame Details for L4 x 4 x 3/8
- Orientation of struts and diagonals follow TxDOT detail- strut near unloaded flange has outstanding leg on opposite side
- No backside welds were used

Crack Locations:

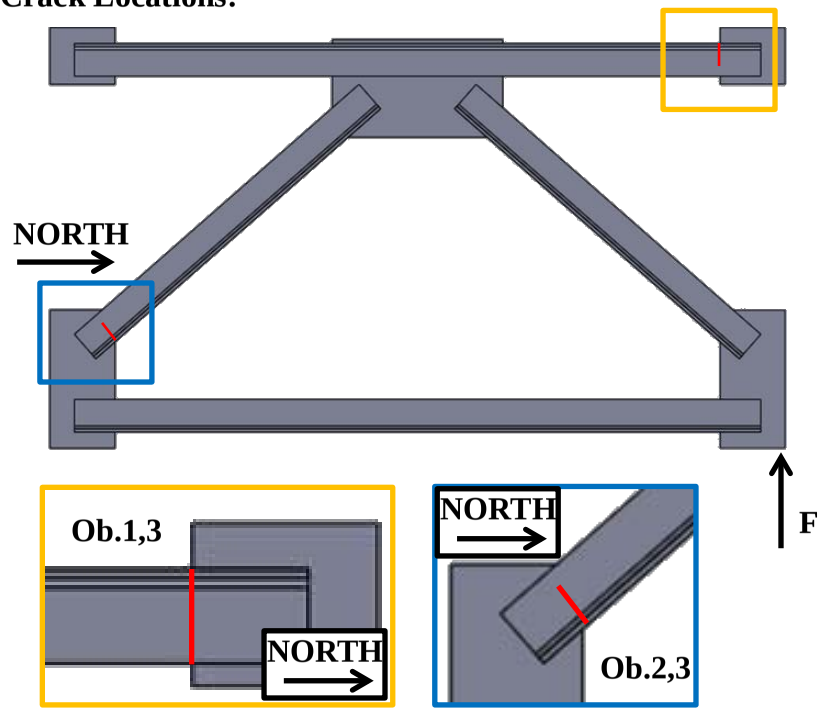

Observations:

1. First crack seen in the strut, starting at the toe of the forward edge of the angle-gusset fillet weld and propagating into the angle heel, most likely due to bending of the member.
2. A second crack developed shortly after in the tension diagonal member at the forward edge of the angle-gusset fillet weld and propagating into the angle heel.
3. The cracks grew somewhat simultaneously, and therefore a repair was not necessary.

Test Specimen: KF_3

First Observed Crack
C1: N = 220,538 cycles
C2: N = 270,363 cycles
C3: N = 379,672 cycles

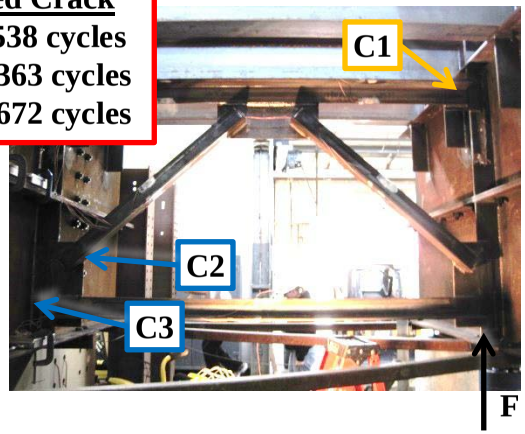

Crack 2: (N=270,363)

A second crack was observed in the tension diagonal at the forward edge of the fillet weld and propagated into the angle heel along each leg.

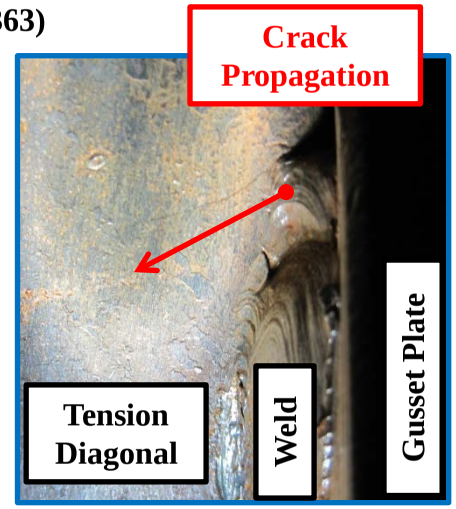

Crack 1: (N=220,538)

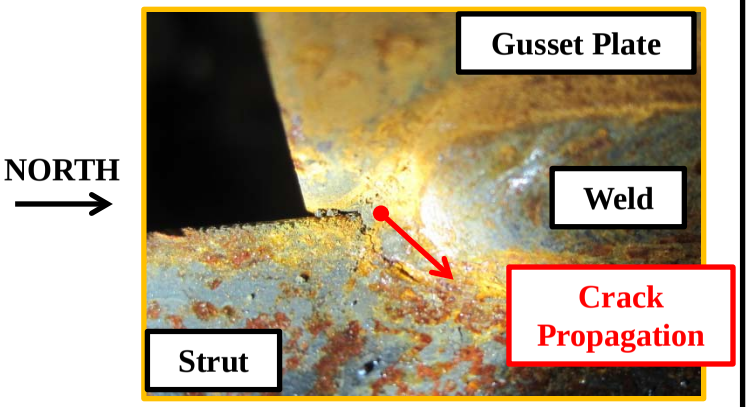

The strut crack at first observation.

Crack 1: (N=270,363)

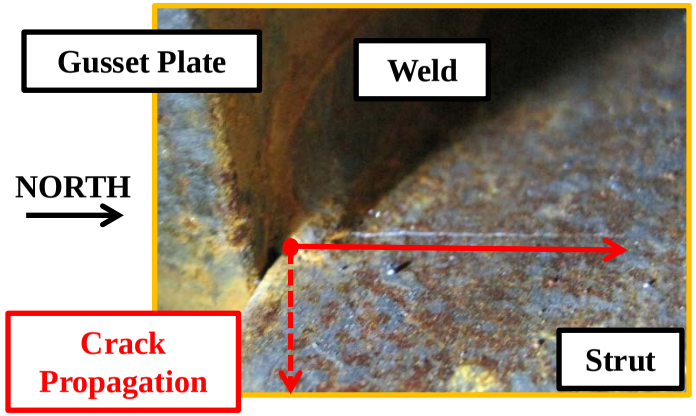

The crack began at the forward edge of the fillet weld and propagated into the angle heel along each leg.

Test Specimen: KF_3

Crack 2: (Failure, N=379,672)

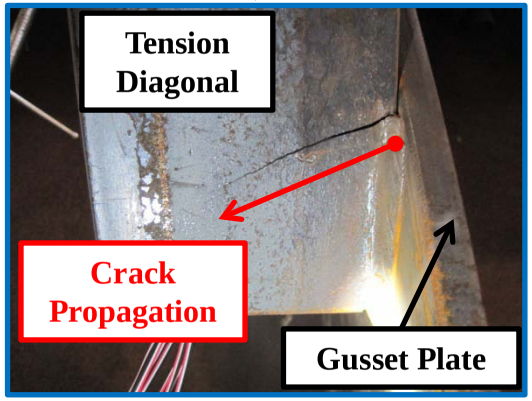

The second crack was quite large at complete fracture of crack 1.

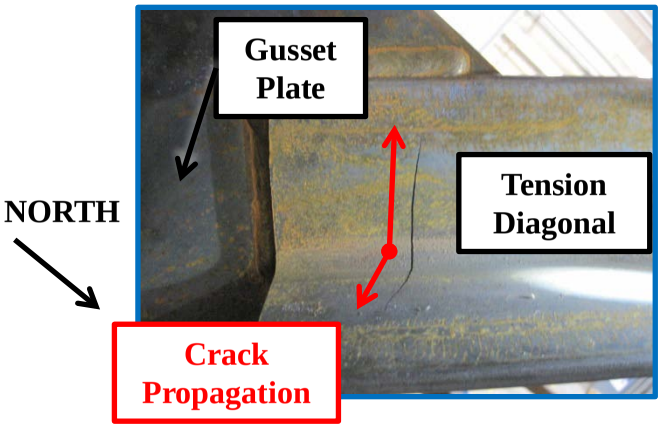

Crack 1: (Failure, N=379,672)

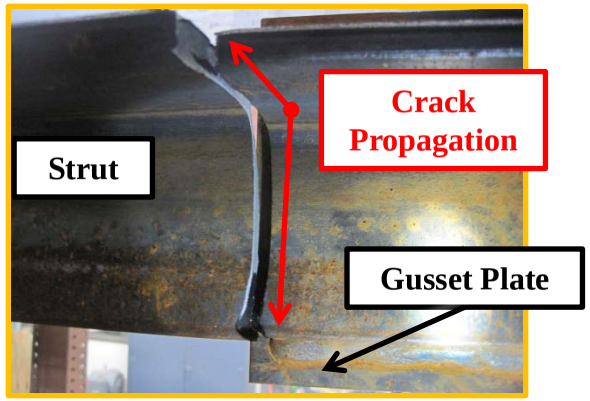

Crack 3: (Failure, N=379,672)

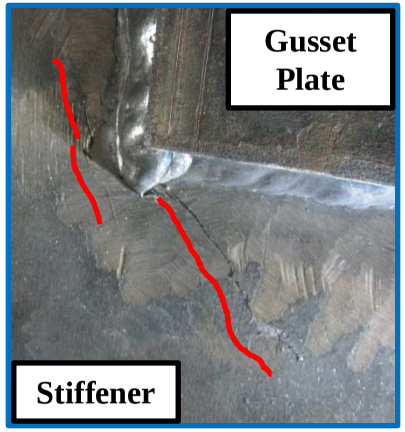

Small stiffener cracks were seen at the conclusion of the test. It was deemed not to be significant enough to affect the results.

Test Specimen: KF_4

Test Dates: 6/18/2013 – 6/27/2013

Primary Failure:	**Secondary Failure:**
Strut	Tension Diagonal
S_R = 13.14 ksi (Effective Stress Range)	S_R = 15.00 ksi (Effective Stress Range)
N =165,752 cycles **AASHTO Fatigue Category: < E′**	**N** = 217,373 cycles **AASHTO Fatigue Category: E′**

Stiffness: **Initial:** 85.92 k/in **Final:** 58.18 k/in
32.3% loss of stiffness

Nominal Weld Size: Leg: 5/16″

Details:

- TxDOT Standard K-Type Cross Frame Details for L4 x 4 x 3/8
- Orientation of struts and diagonals follow TxDOT detail- strut near unloaded flange has outstanding leg on opposite side of KF_2,3
- No backside welds were used

Crack Locations:

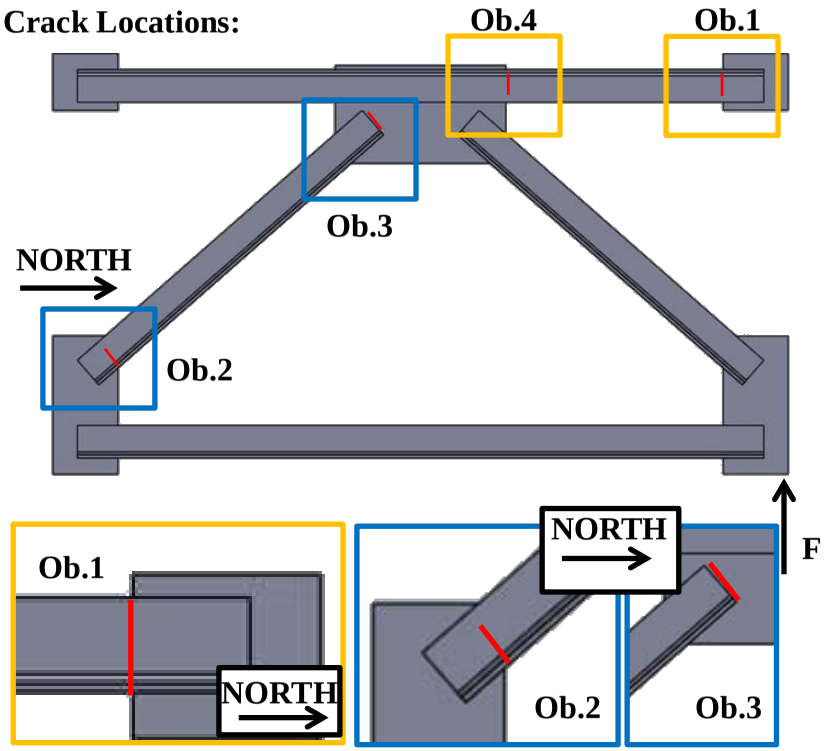

Observations:

1. First crack seen in the strut, starting at the toe of the forward edge of the angle-gusset fillet weld and propagating into the angle leg, most likely due to bending of the member.
2. The first crack was repaired and a second crack developed in the tension diagonal. At the forward edge of the angle-gusset fillet starting at the angle toe and propagating into the angle heel.
3. A crack was also observed at the other end of the tension diagonal along the gusset toe of the fillet weld.
4. A crack was also seen in the strut at failure.

Test Specimen: KF_4

First Observed Crack
C1: N = 115,343 cycles
C2: N = 209,074 cycles
C3: N = 209,074 cycles

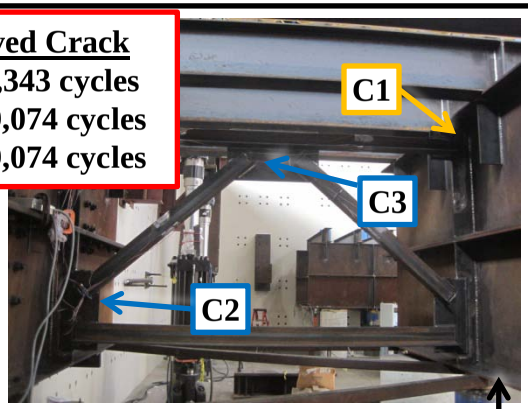

Crack 1: (Failure- N=165,752)

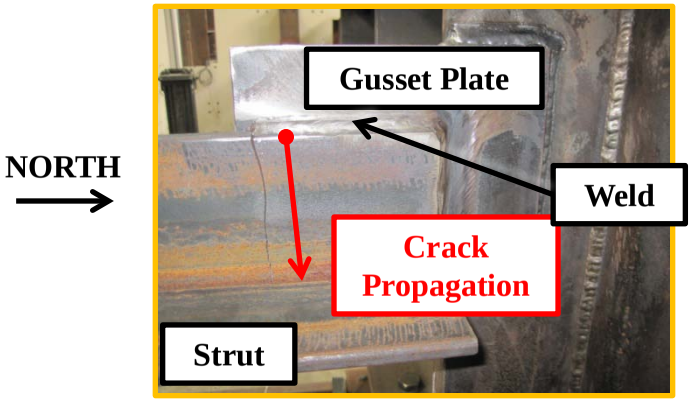

The strut crack at failure.

Crack 2: (Failure- N=217,373)

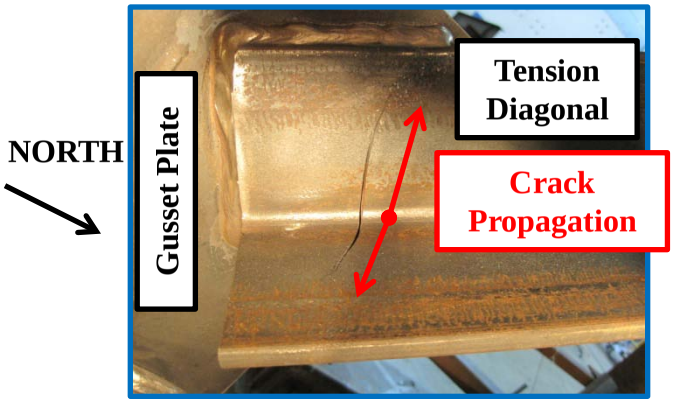

The second observed crack propagated into the heel of the angle at the forward edge of the connection.

Crack 3: (Failure- N=217,373)

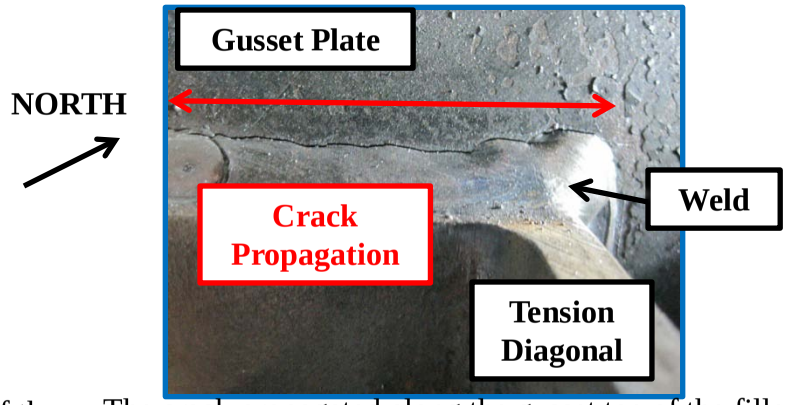

The crack propagated along the gusset toe of the fillet weld.

Test Specimen: KF_4

First Observed Crack
C4: N = 209,074 cycles

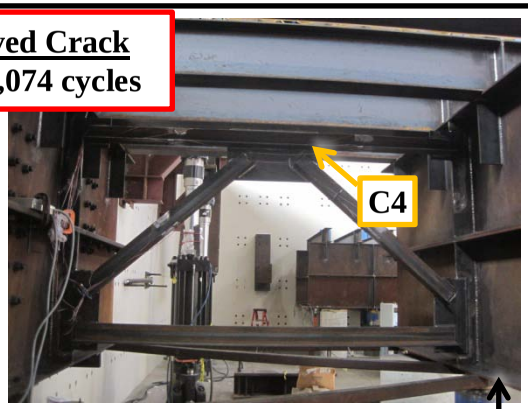

Crack 4: (Failure- N=217,373)

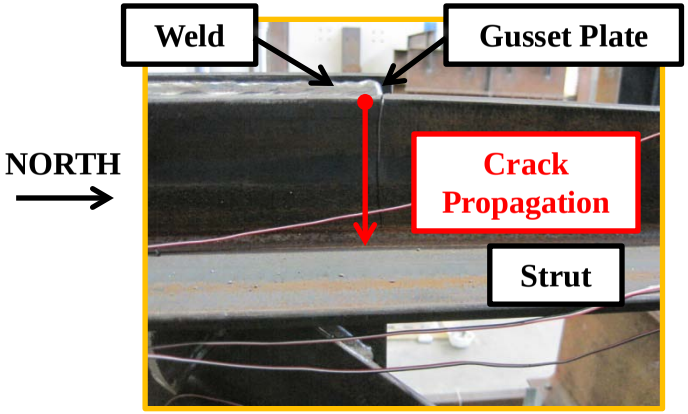

Another strut crack at failure.

Test Specimen: KF_5

Test Dates: 6/18/2013 – 7/1/2013

Primary Failure: Strut	**Secondary Failure:** Tension Diagonal
S_R = 12.61 ksi (Effective Stress Range)	S_R = 15.00 ksi (Effective Stress Range)
N =111,516 cycles **AASHTO Fatigue Category: < E′**	**N** = 227,563 cycles **AASHTO Fatigue Category: E′**
Stiffness: **Initial:** 88.69 k/in **Final:** 51.38 k/in 41.6% loss of stiffness	**Stiffness:** **Initial:** 90.02 k/in **Final:** 19.33 k/in 78.4% loss of stiffness

Nominal Weld Size: Leg: 5/16″

Details:
- Same as KF_1
- No backside welds were used

Crack Locations:

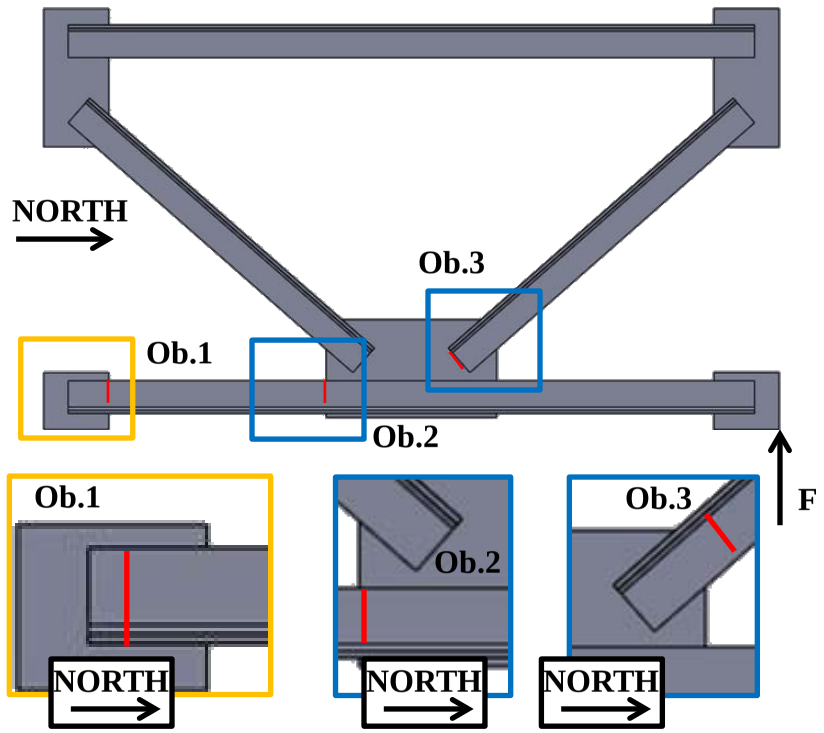

Observations:
1. First crack seen in the strut, starting at the toe of the forward edge of the angle-gusset fillet weld and propagating into the angle leg, most likely due to bending of the member.
2. The first crack was repaired and a second crack developed in the tension strut at the forward edge of the angle-gusset fillet starting at the angle toe and propagating into the angle leg near the center gusset plate.
3. A crack was also observed at the end of the tension diagonal along the gusset toe of the fillet weld.

Test Specimen: KF_5

First Observed Crack
C1: N = 76,925 cycles
C2: N = 148,082 cycles
C3: N = 168,115 cycles

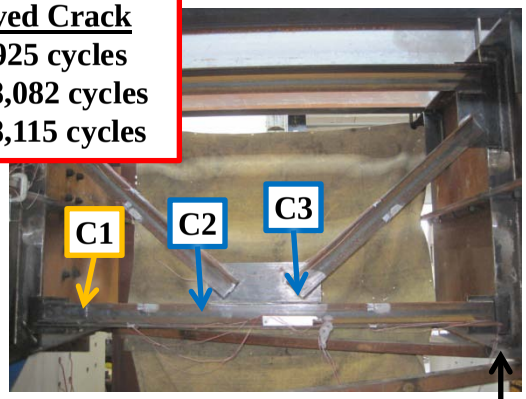

Crack 1: (Failure- N=111,516)

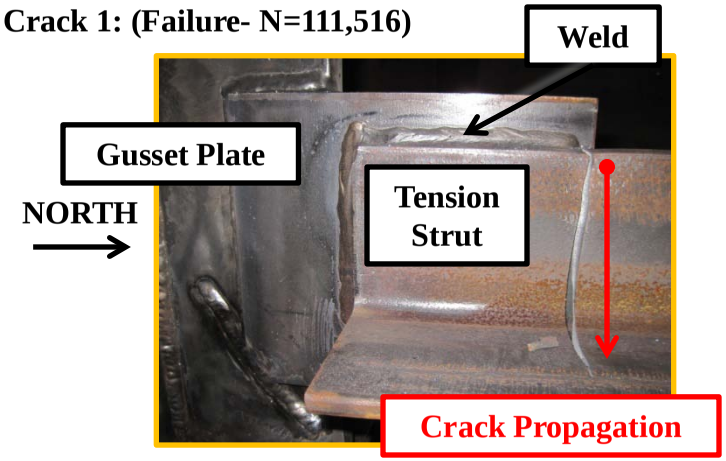

Crack 2: (Failure- N=227,563)

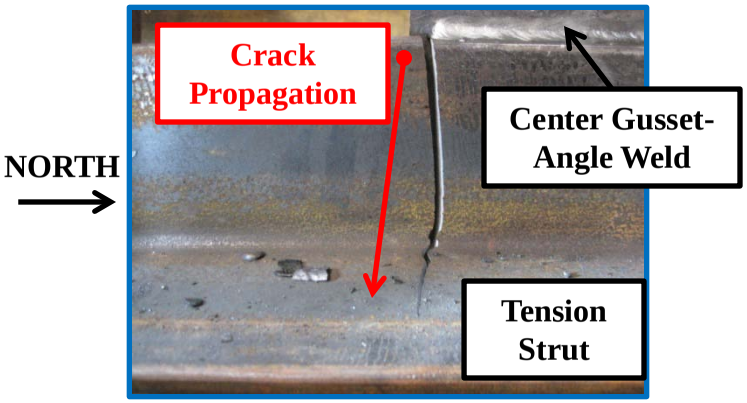

Crack 3: (Failure- N=227,563)

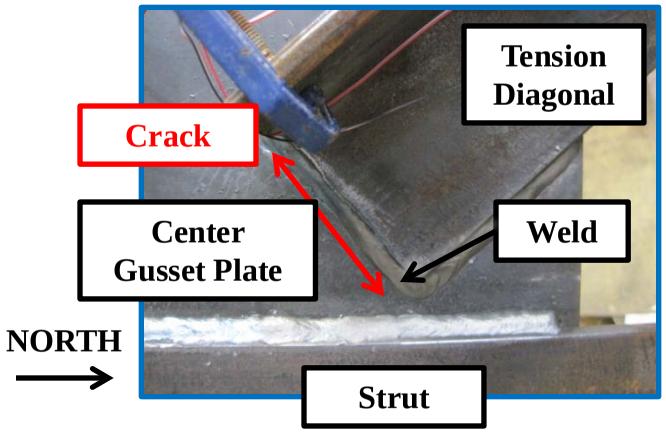

Test Specimen: KF_6

Test Dates: 8/2013

Primary Failure: Center Gusset Plate

S_R = 15.00 ksi

(Effective Stress Range)

N = 98,206 cycles

AASHTO Fatigue Category: < E′

Nominal Weld Size: Leg: 5/16″

Details:

- Same as KF_2,3
- Strut increased from L4x4x3/8 to L4x4x5/8
- No backside welds were used

Crack Locations:

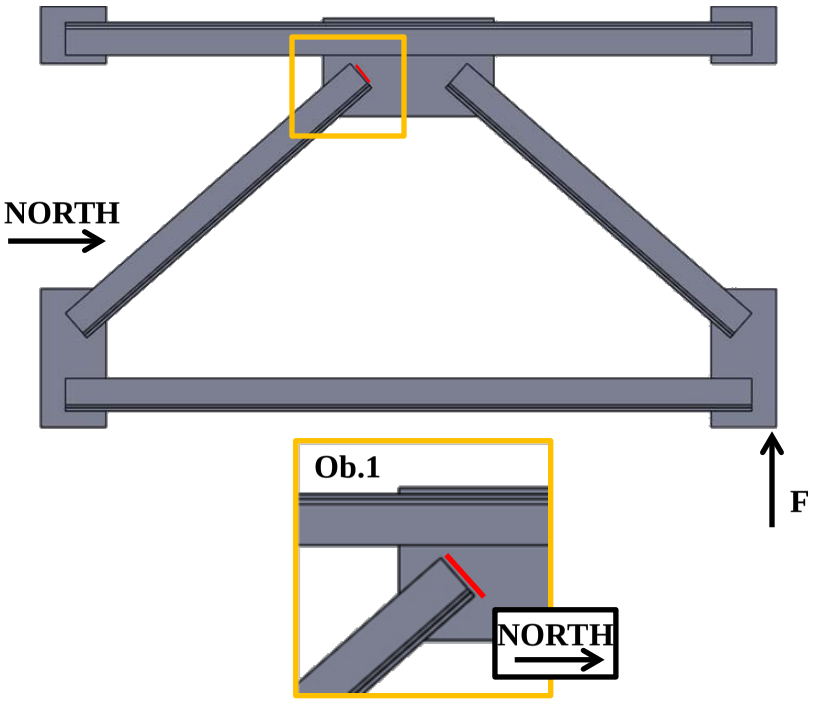

Observations:

1. Crack began at the gusset toe of the center gusset-angle weld propagating into the gusset plate.

Test Specimen: KF_6

First Observed Crack
C1: N = 98,206

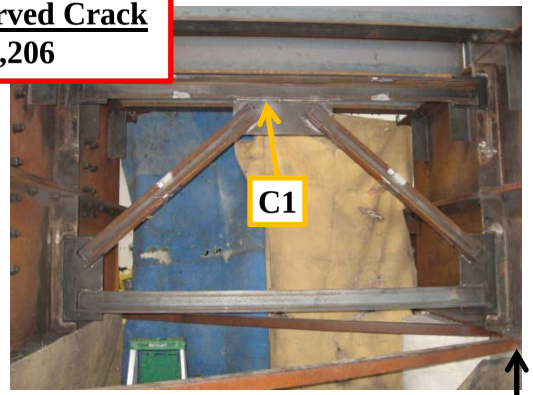

Crack 1: (Failure- N=98, 206)

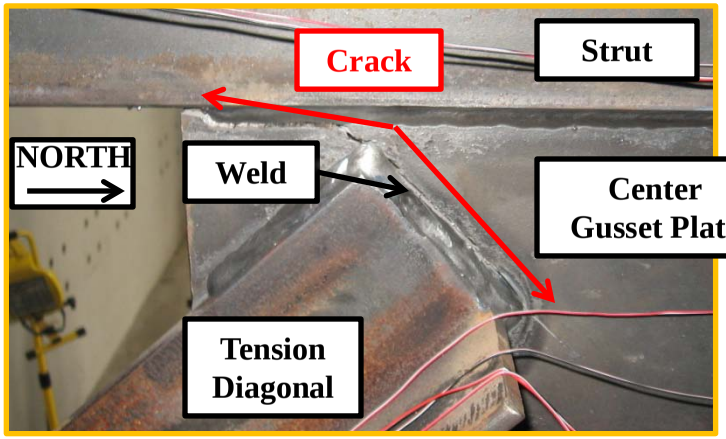

Test Specimen: KF_7

Test Dates: 8/2013

Primary Failure: Tension Diagonal

S_R = 15.00 ksi

(Effective Stress Range)

N = 158,005 cycles

AASHTO Fatigue Category: E′

Nominal Weld Size: Leg: 5/16″

Details:

- Same as KF_6
- Strut increased from L4x4x3/8 to L4x4x5/8 relative to TxDOT Standard Detail
- Center gusset plate thickness increased from 0.5″ to 0.75″
- No backside welds were used

Crack Locations:

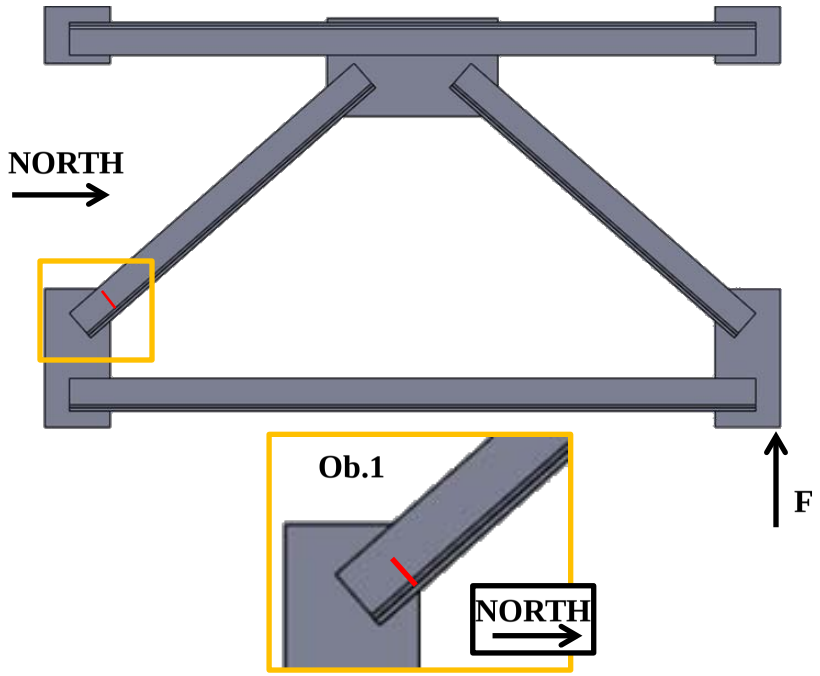

Observations:

1. Crack began at the angle toe at the forward edge of the angle-gusset weld connection; it propagated into the heel of the angle and then into each leg.

Test Specimen: KF_7

First Observed Crack
C1: N = 158,005

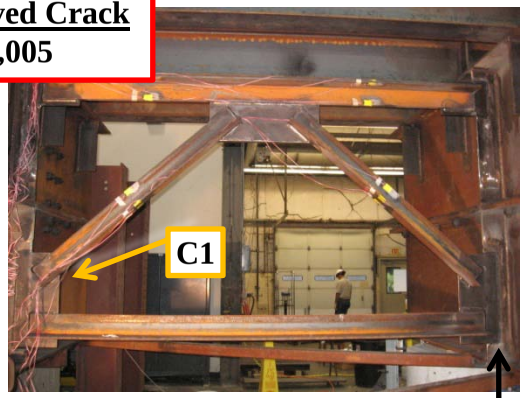

Crack 1: (Failure- N=98, 206)

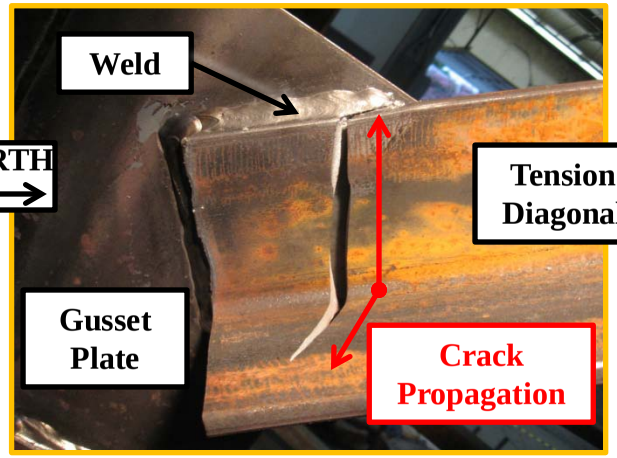

Test Specimen: KF_8

Test Dates: 9/2013

Primary Failure: Center Gusset Plate

S_R = 15.00 ksi

(Effective Stress Range)

N = 106,091 cycles

AASHTO Fatigue Category: < E′

Nominal Weld Size: Leg: 5/16″

Details:

- Same as KF_7
- Strut reduced from L4x4x3/8 to L3x3x1/2 relative to TxDOT Standard Detail
- Center gusset plate thickness increased from 0.5″ to 0.75″
- No backside welds were used

Crack Locations:

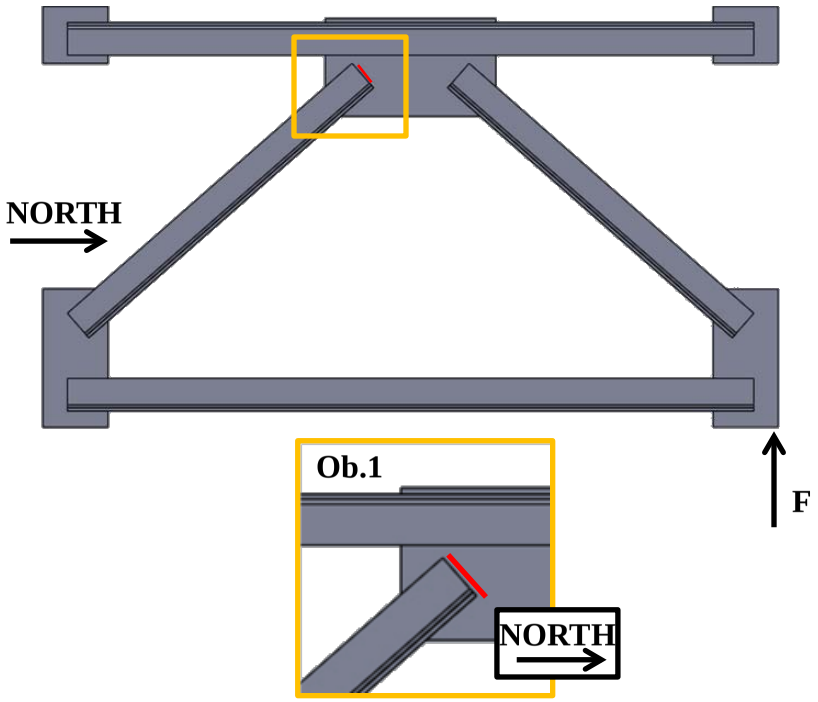

Observations:

1. Crack began at the gusset toe of the center gusset-angle weld propagating into the gusset plate.

Test Specimen: KF_8

First Observed Crack
C1: N = 79,110

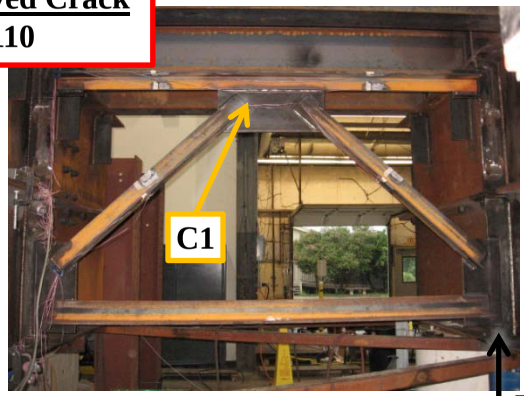

Crack 1: (N=79,110)

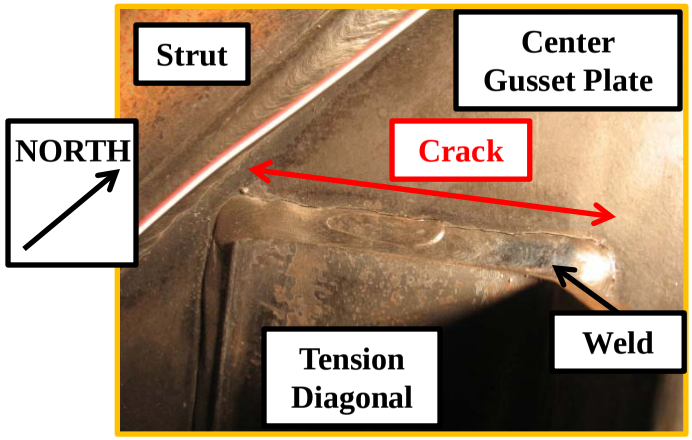

Crack 1: (Failure- N=106,091)

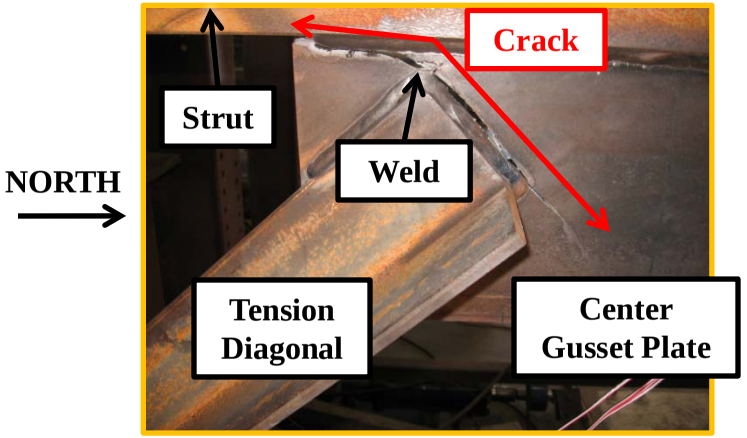

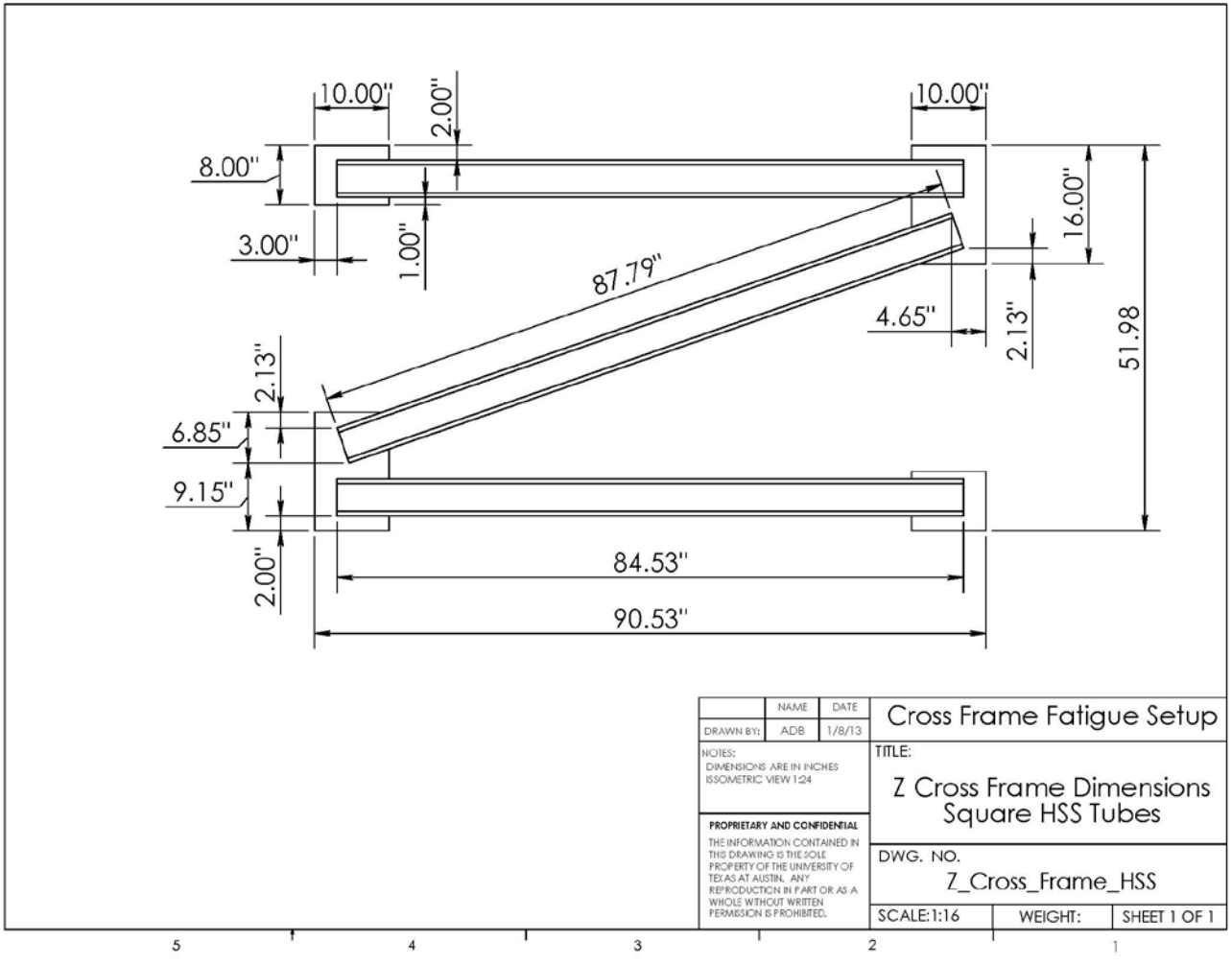
10.00"
2.00"
10.00"
8.00"
16.00"
3.00"
1.00"
87.79"
4.65"
2.13"
51.98
2.13"
6.85"
9.15"
2.00"
84.53"
90.53"
NAME
DATE
DRAWN BY:
ADB
1/8/13
NOTES:
DIMENSIONS ARE IN INCHES
ISSOMETRIC VIEW 1:24
PROPRIETARY AND CONFIDENTIAL
THE INFORMATION CONTAINED IN THIS DRAWING IS THE SOLE PROPERTY OF THE UNIVERSITY OF TEXAS AT AUSTIN. ANY REPRODUCTION IN PART OR AS A WHOLE WITHOUT WRITTEN PERMISSION IS PROHIBITED.
Cross Frame Fatigue Setup
TITLE:
Z Cross Frame Dimensions
Square HSS Tubes
DWG. NO.
Z_Cross_Frame_HSS
SCALE:1:16
WEIGHT:
SHEET 1 OF 1
5
4
3
2
1

Test Specimen: ZF_HSS_1

Test Dates: 1/22/2013 – 1/23/2013

Primary Failure Location: Weld

S_R = 20.00 ksi (Diagonal)

N = 25,179 cycles

AASHTO Fatigue Category: < E′

Stiffness: **Initial:** 96.65 k/in **Final:** 82.35 k/in
14.8% loss of stiffness

Average Weld Size: Leg: 0.31″ **Throat:** 0.29″

Details:

- TxDOT Standard X-Type Cross Frame Details for L5 x 5 x 1/2 followed for Z frame layout with HSS 5 x 5 x 3/8
- Stress relief hole of 1-5/8″ used at connection

Crack Locations:

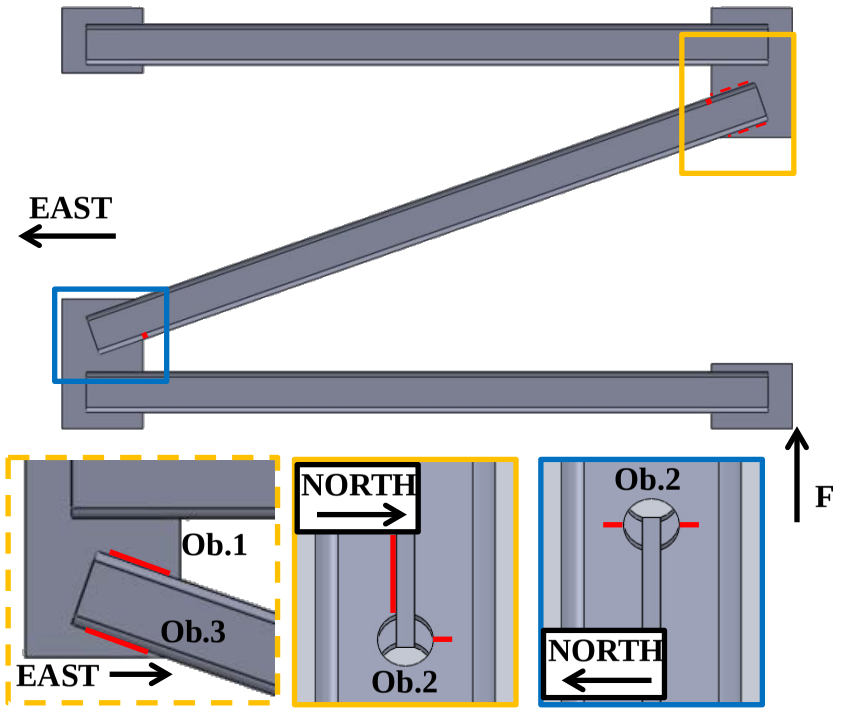

Observations:

1. First crack observation showed a full fracture through the throat of the tension diagonal fillet weld located at the top gusset plate on the top of the HSS on the SW side.
2. At the same time, cracks were also visible at the stress relief holes.
3. As the testing continued, the welds at the top gusset plate continued to crack. The top weld on the NW side cracked, originating at the back of the connection and moving forward through the weld throat. Shortly after the bottom weld on the SW side cracked ending the test.

Test Specimen: ZF_HSS_1

First Observed Crack
C1: N = 23,672 cycles
C2: N = 23,672 cycles
C3: N = 25,179 cycles

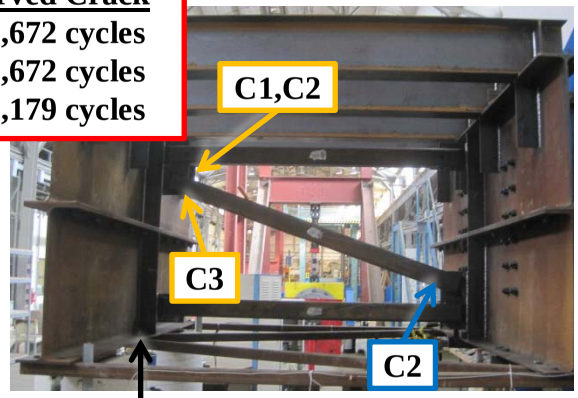

Crack 2: (Top West- Stress Relief Hole- N=23,672)

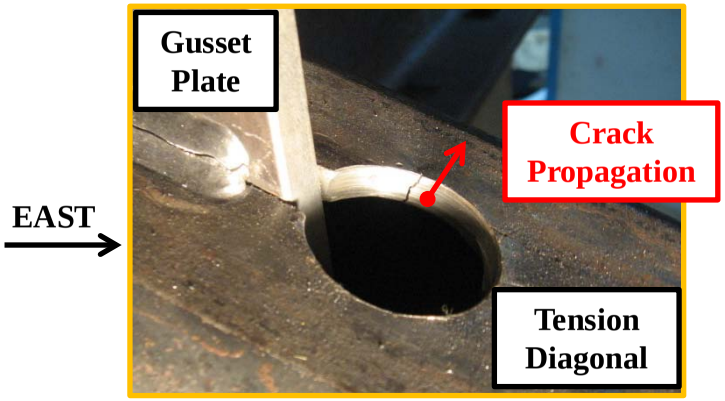

Crack 1:

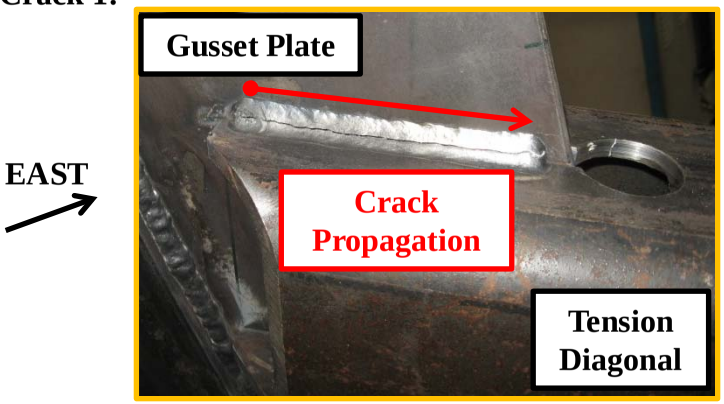

The crack began at the end of the connection and propagated towards the stress relief hole. The weld was later examined. The fillet weld was undersized at 3/16″ (supposed to be 5/16″) and the weld had significant voids and defects as shown below.

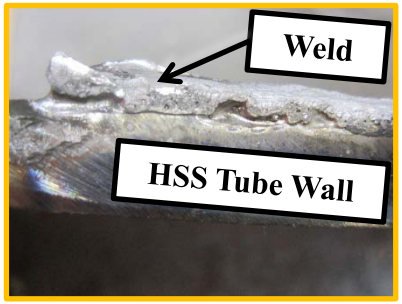

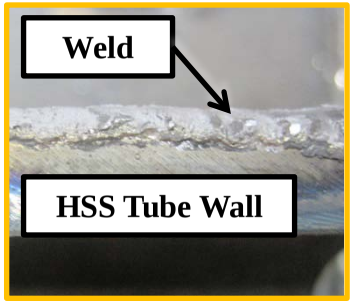

Test Specimen: ZF_HSS_1

Crack 2: (Bottom East- Stress Relief Hole)

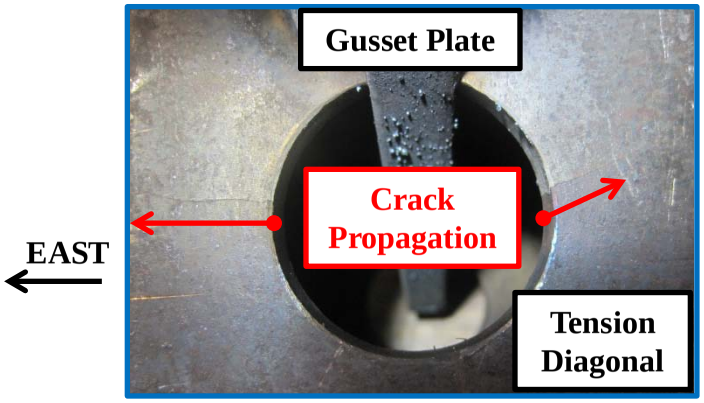

Crack 3: (Top West- Stress Relief Hole- N=25,179)

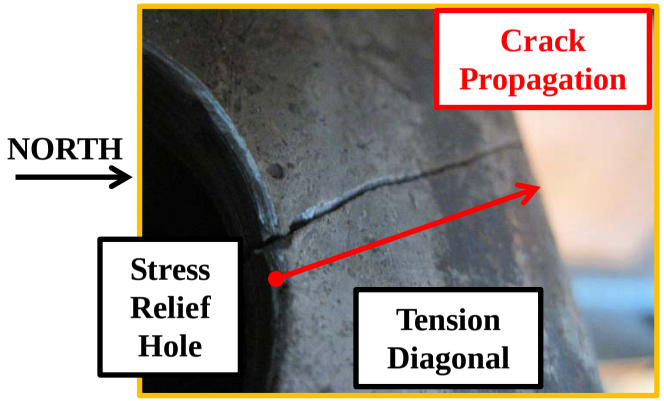

Crack 3: (NW Top Weld)

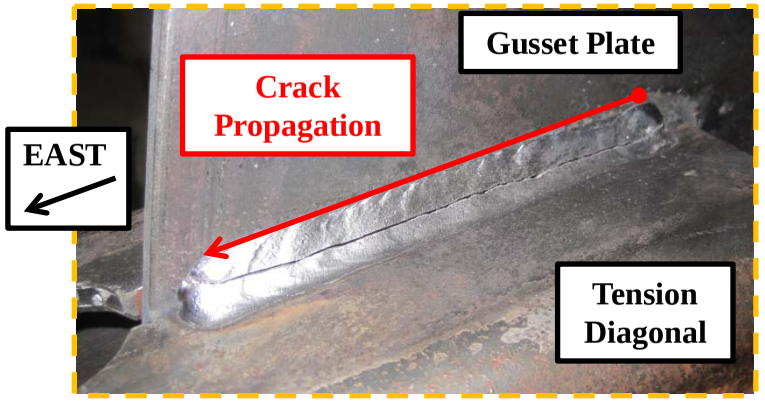

After crack 1 had completely fractured the weld, another crack began at the end of the top NW connection and propagated towards the stress relief hole (above). Once this fractured, the bottom SW connection fractured (below).

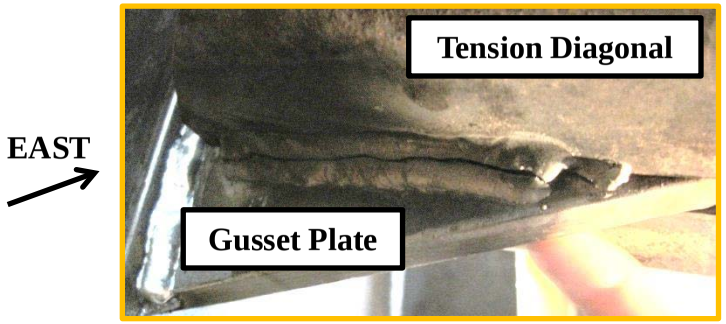

Test Specimen: ZF_HSS_2

Test Dates: 3/19/2013 – 3/22/2013

Primary Failure Location: Member

S_R = 15 ksi

A_{eff} = 4.03 in^2 **U** = 0.659

N = 104,747 cycles

AASHTO Fatigue Category: almost E′

Stiffness: **Initial:** 100.3 k/in **Final:** 77.81 k/in
22.4% loss of stiffness

Average Weld Size: Leg: 0.31″ **Throat:** 0.32″

Details:

- TxDOT Standard X-Type Cross Frame Details for L5 x 5 x 1/2 followed for Z frame layout with HSS 5 x 5 x 3/8
- Stress relief hole of 1-5/16″ used at connection

Crack Locations:

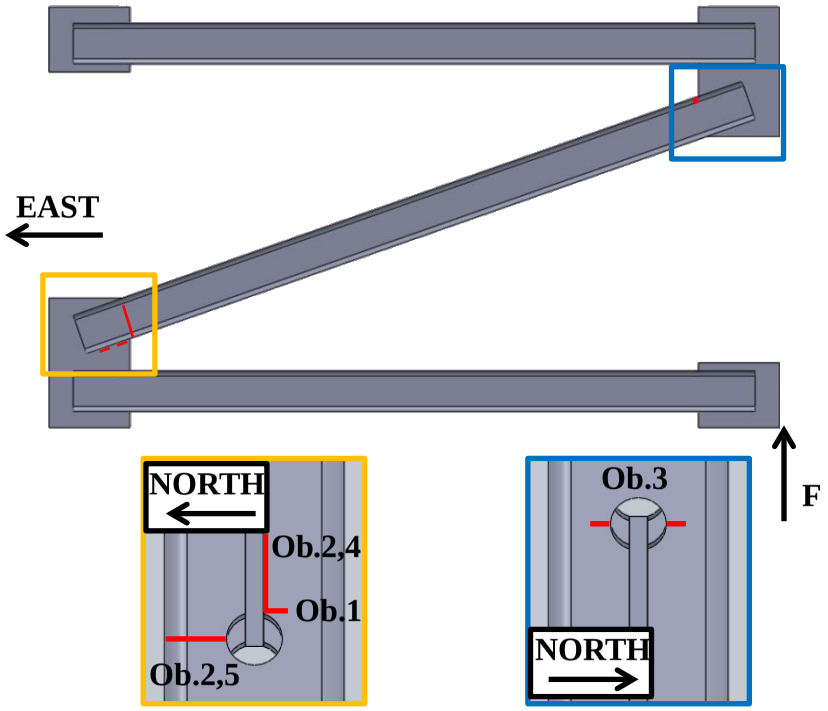

Observations:

1. First crack seen at the forward edge of the fillet weld on the south face of the bottom of the east connection.
2. A second crack was observed at the bottom stress relief hole at the east connection. A small crack was seen in the throat of the south facing weld on the bottom of the east connection.
3. Cracks were observed at the west connection on both sides of the top stress relief hole.
4. The throat weld fully propagated through the connection.
5. The crack from the stress relief hole continued to grow until the member fractured.

Test Specimen: ZF_HSS_2

First Observed Crack
C1: N = 32,100 cycles
C2: N = 50,881 cycles
C3: N = 58,252 cycles
C4: N = 63,284 cycles

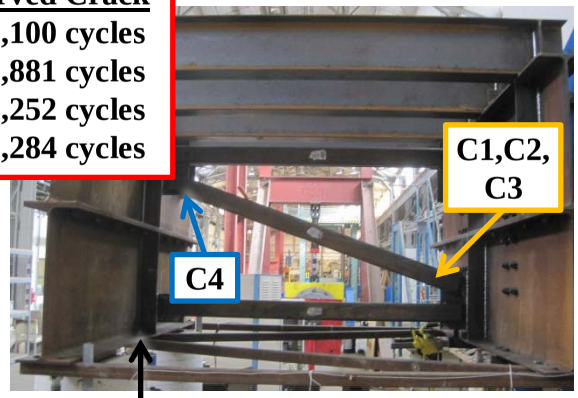

Crack 1: (Bottom East- N=32,100)

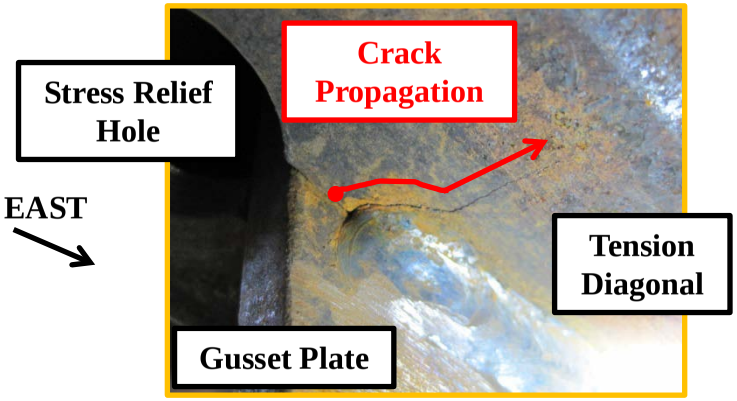

The crack began at the forward edge of the fillet weld and propagated into the HSS member.

Crack 2: (Bottom East- N=50,881)

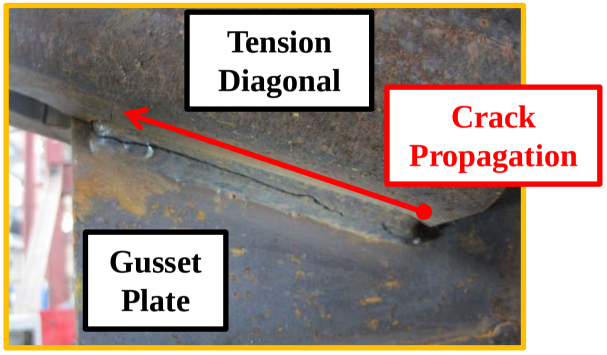

The second crack was observed in the throat of the weld at 50,881 cycles. It continued to grow until it completely fractured at 86,712 cycles.

Crack 3: (Bottom East- N=50,881)

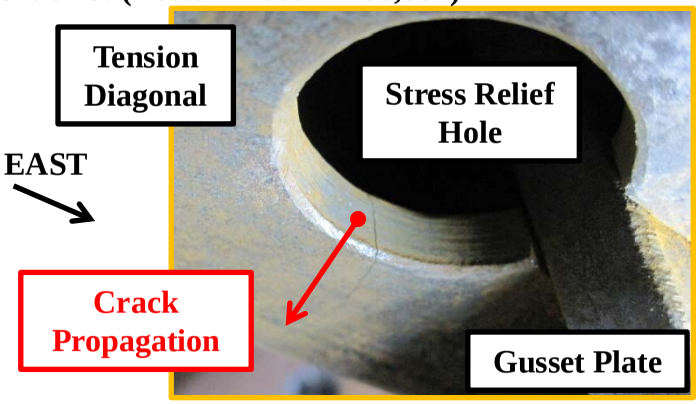

A crack was also observed at the stress relief hole, which would eventually grow into the failure crack.

Test Specimen: ZF_HSS_2

Crack 4: (Top West- N=63,284)

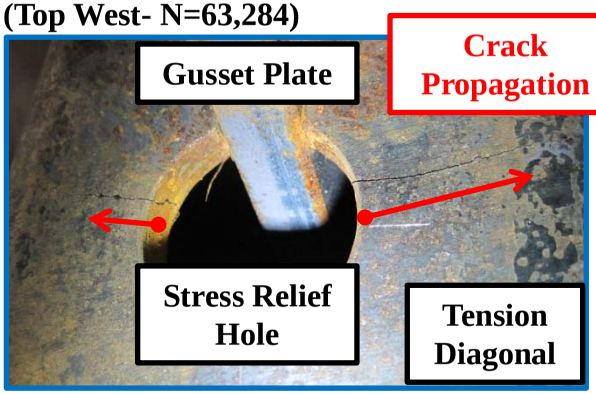

The fourth cracks were seen at the top stress relief hole at the west connection.

Crack 1, 2: (At Failure, N=104,747)

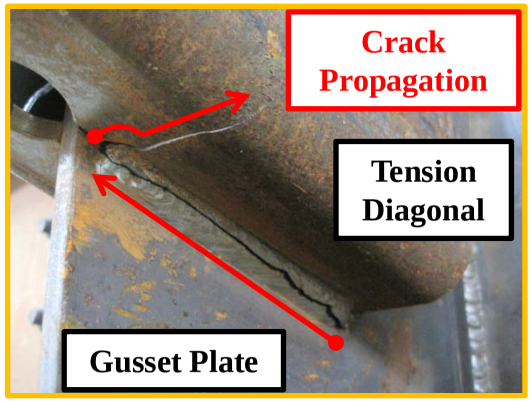

Crack 3: (At Failure- N=104,747)

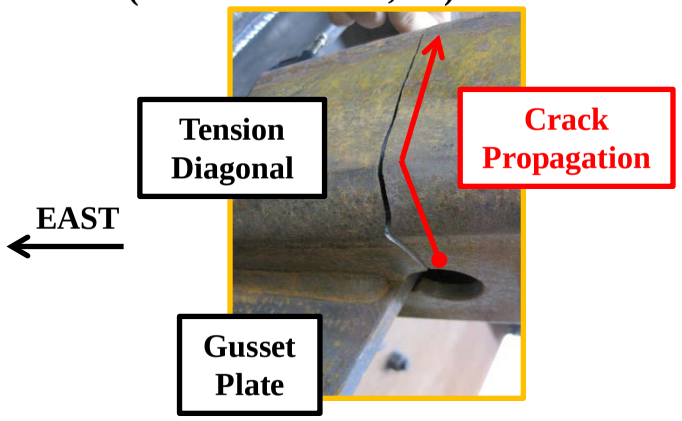

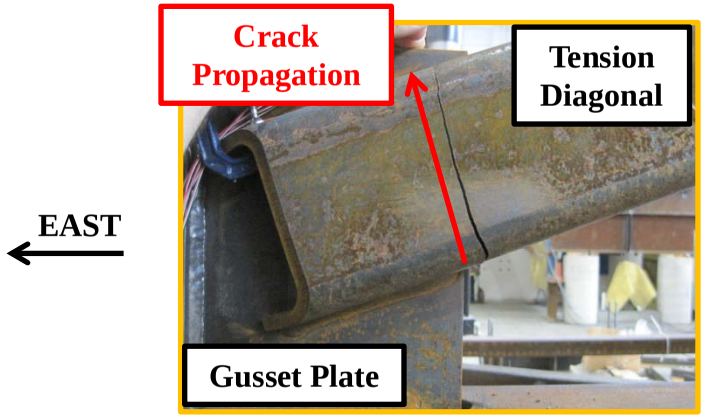

The crack observed earlier at the stress relief hole eventually propagated through North half of the tube resulting in fracture of the member.

Test Specimen: ZF_HSS_3

Test Dates: 5/30/2013 – 6/3/2013

Primary Failure Location: Member

S_R = 15 ksi (Diagonal)

N = 86,014 cycles

AASHTO Fatigue Category: < E′

Stiffness: **Initial:** 104.4 k/in **Final:** 65.55 k/in
37.2% loss of stiffness

Average Weld Size: Leg: 0.31″ **Throat:** 0.32″

Details:

- TxDOT Standard X-Type Cross Frame Details for L5 x 5 x 1/2 followed for Z frame layout with HSS 5 x 5 x 3/8
- Slots were cut using plasma torch; no stress relief hole

Crack Locations:

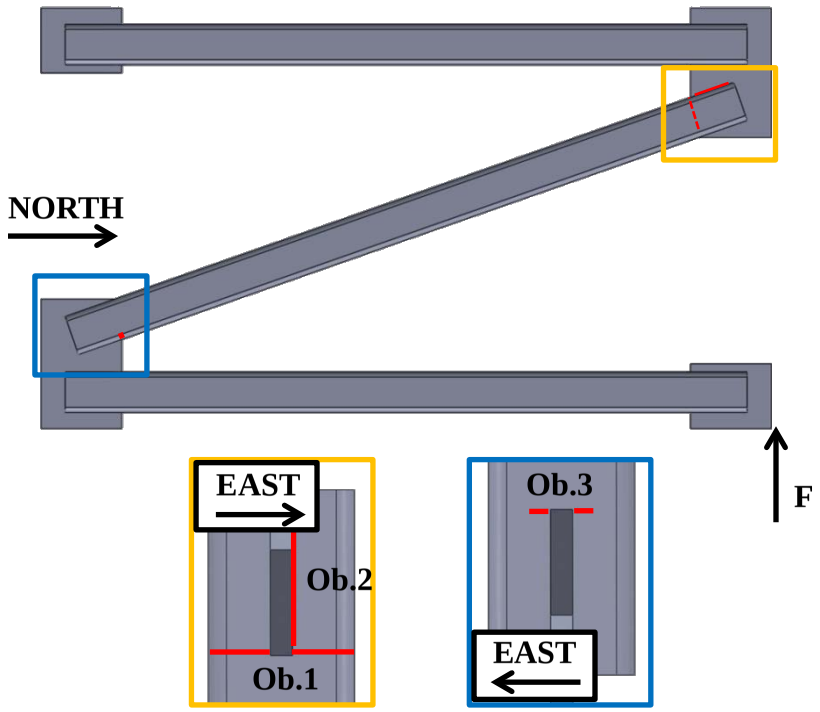

Observations:

1. First cracks seen at the forward edge of the fillet welds on the top face of the north connection propagating into the tube.
2. A second crack formed at the top northeast connection at the back of the fillet weld and propagated through the weld throat towards the forward edge of the connection.
3. Cracks were later observed at the forward edge of the fillet welds on the bottom face of the south connection propagating into the tube.

Test Specimen: ZF_HSS_3

First Observed Crack
C1: N = 19,892 cycles
C2: N = 41,419 cycles
C3: N = 45,960 cycles

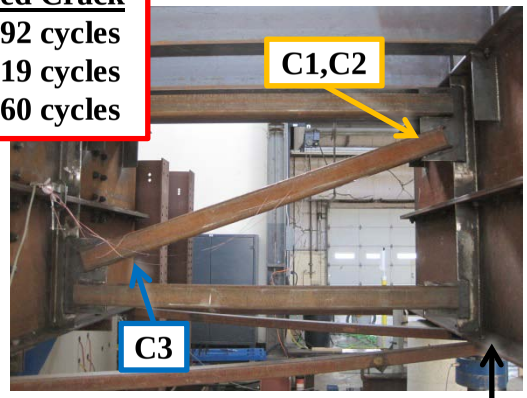

Crack 1,2: (Top North- N=86,014)

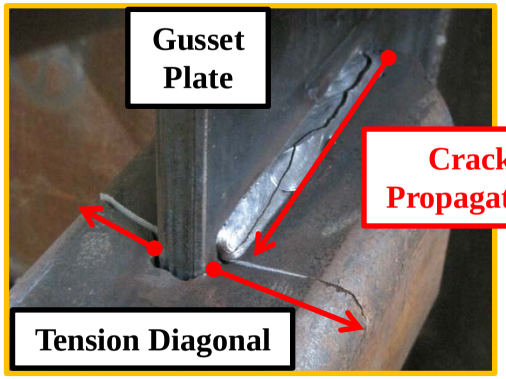

The second crack was observed in the throat of the weld at the back end of the connection at 41,419 cycles. It continued to grow until the tube fractured at 86,014 cycles.

Crack 1: (Top North- N=19,892)

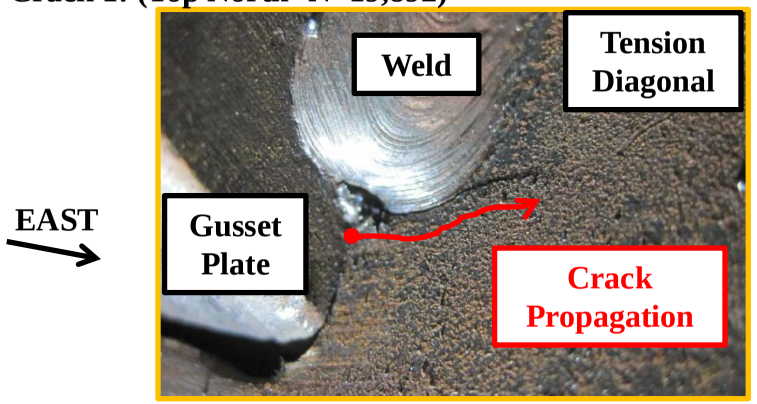

The crack began at the forward edge of the fillet welds and propagated into the HSS member.

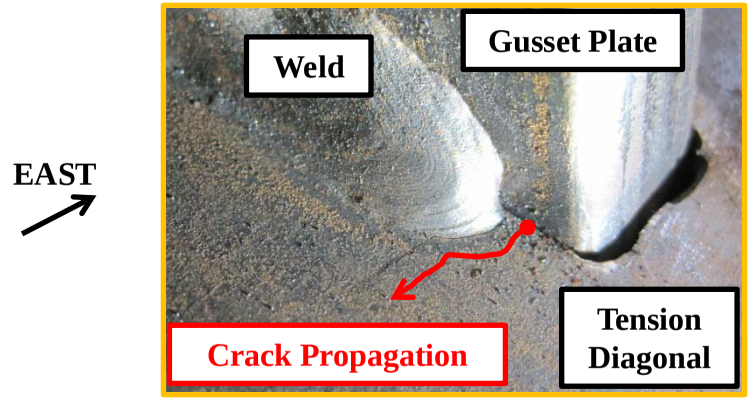

Test Specimen: ZF_HSS_3

Crack 1: (West Face- N=86,014)

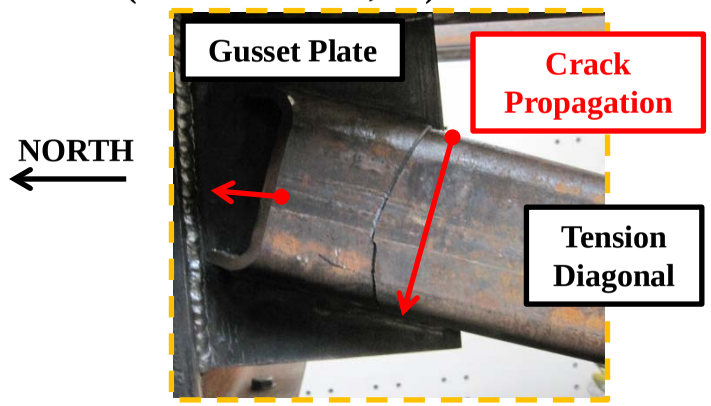

The first crack eventually propagated completely through the HSS tube. Near failure additional cracks formed at the forward toe of the fillet weld on the bottom face of the north connection.

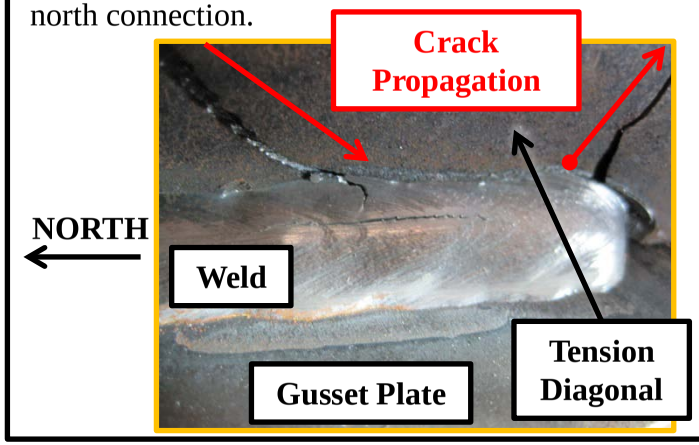

Crack 3: (Bottom South, N=86,014)

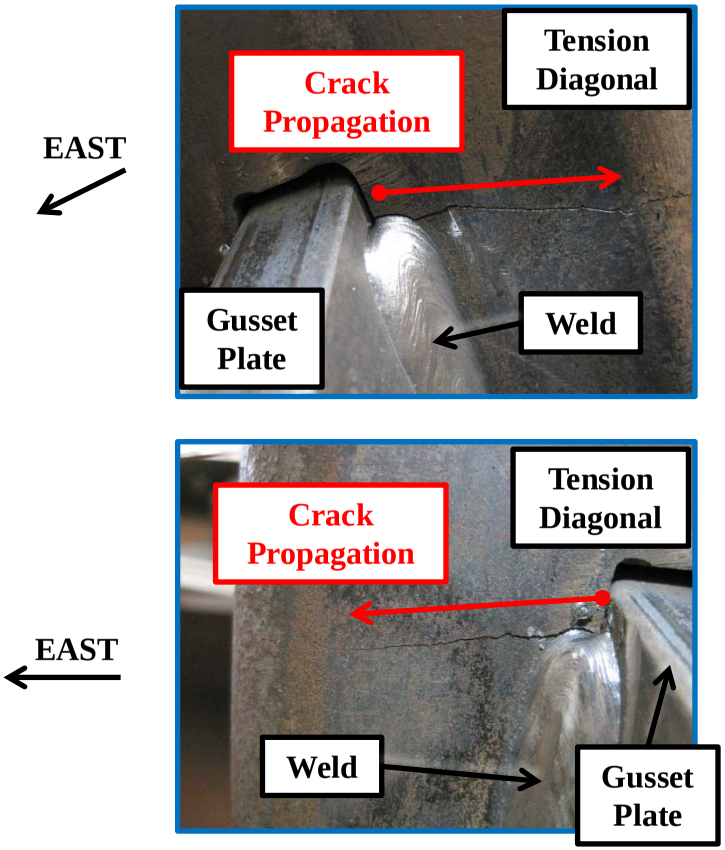

Cracks were also observed at the south connection on the bottom face originating at the forward edge of the fillet welds and propagating into the tube.

Test Specimen: ZF_HSS_4

Test Dates: 8/2013

Primary Failure Location: Member

S_R = 15 ksi (Diagonal)

N = 365, 114 cycles

AASHTO Fatigue Category: E

Nominal Weld Size: Leg: 5/16″

Details:

- Similar Z frame layout to ZF_HSS_1,2,3 but using HSS 6 x 3 x 5/16 with the slots cut in the short wall to minimize the bending stress at the weld
- Stress relief holes included

Crack Locations:

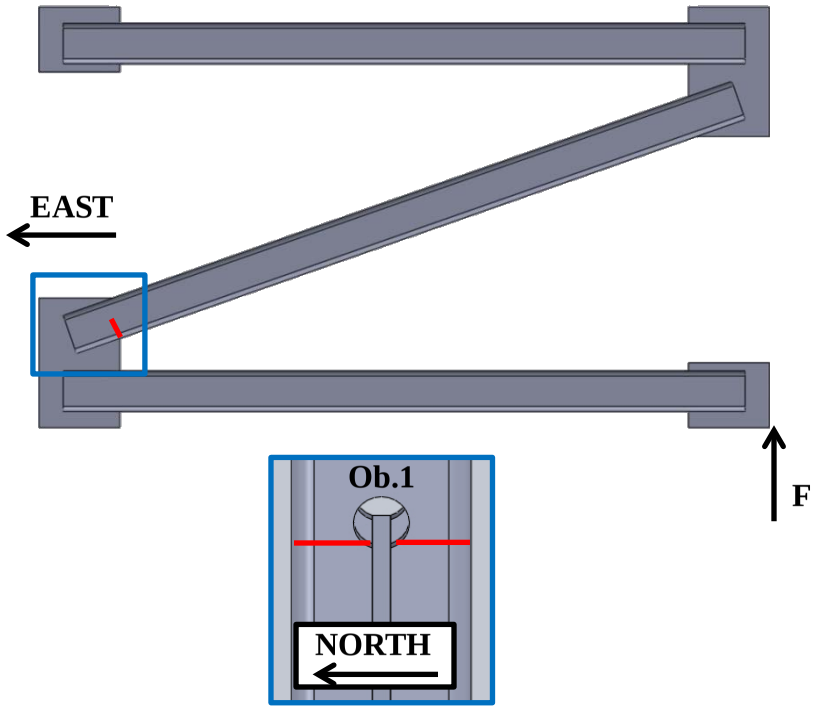

Observations:

1. Cracks formed at the forward edge of both fillet welds on the bottom face of the east connection propagating into the tube.

Test Specimen: ZF_HSS_4

First Observed Crack
C1: N = 365,114 cycles

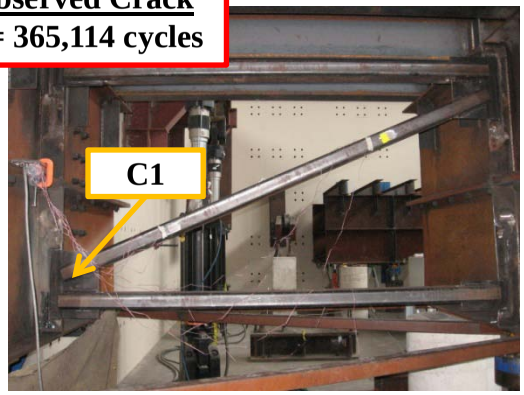

Crack 1: (Bottom East- N=365,114)

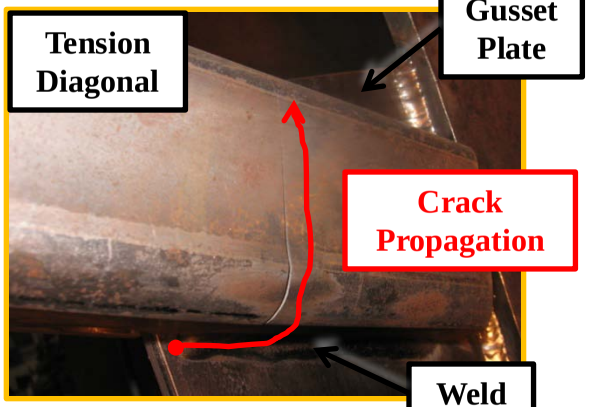

The crack began at the forward edge of the fillet welds and propagated into the HSS member.

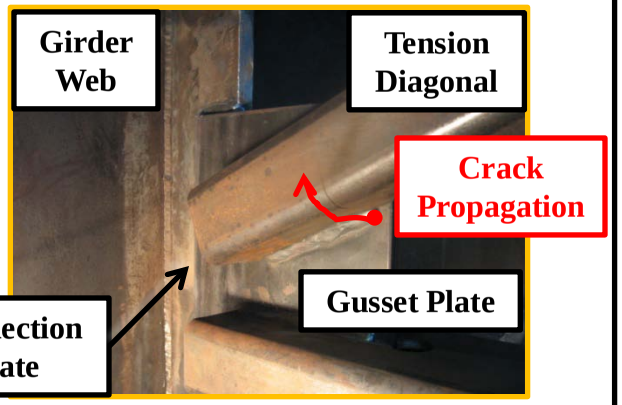

Test Specimen: ZF_HSS_5

Test Dates: 9/2013

Primary Failure Location: Member

S_R = 15 ksi (Diagonal)

N = 241, 113 cycles

AASHTO Fatigue Category: E′

Nominal Weld Size: Leg: 5/16″

Details:

- Same as ZF_HSS_4 using HSS 6 x 3 x 5/16 with the slots cut in the short wall to minimize the bending stress at the weld
- Stress relief holes included

Crack Locations:

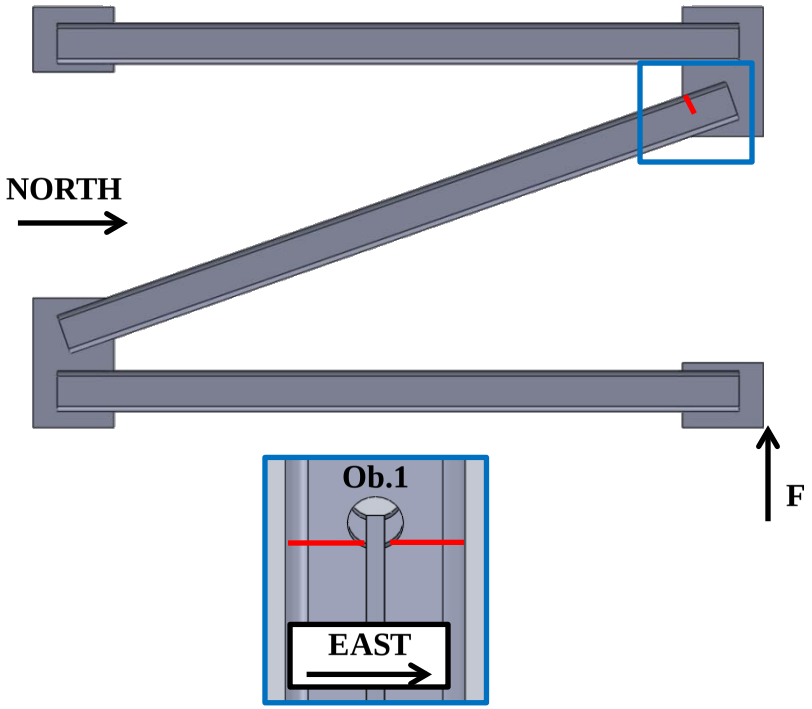

Observations:

1. Cracks formed at the forward edge of both fillet welds on the top face of the north connection propagating into the tube.

Test Specimen: ZF_HSS_5

First Observed Crack
C1: N = 241,113 cycles

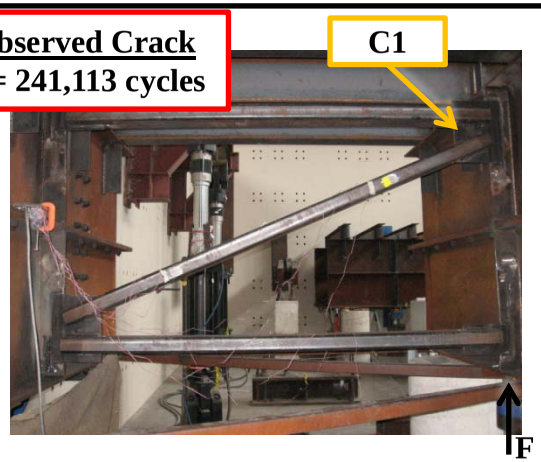

Crack 1: (Top North- N=241,113)

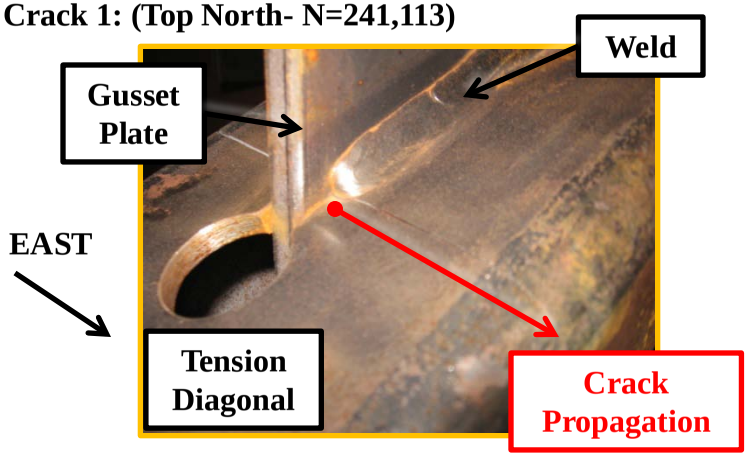

The crack began at the forward edge of the fillet welds and propagated into the HSS member.

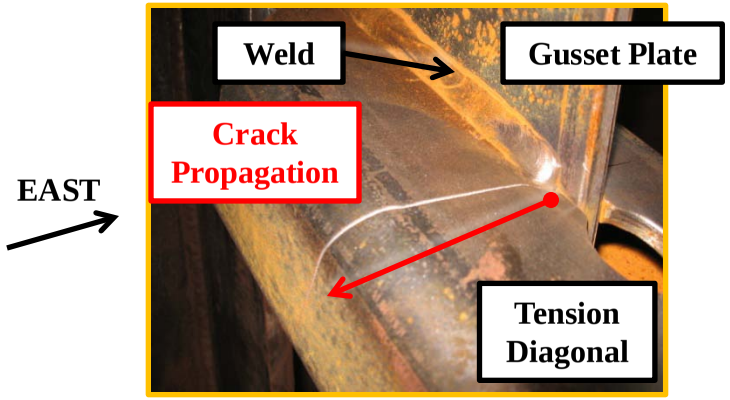

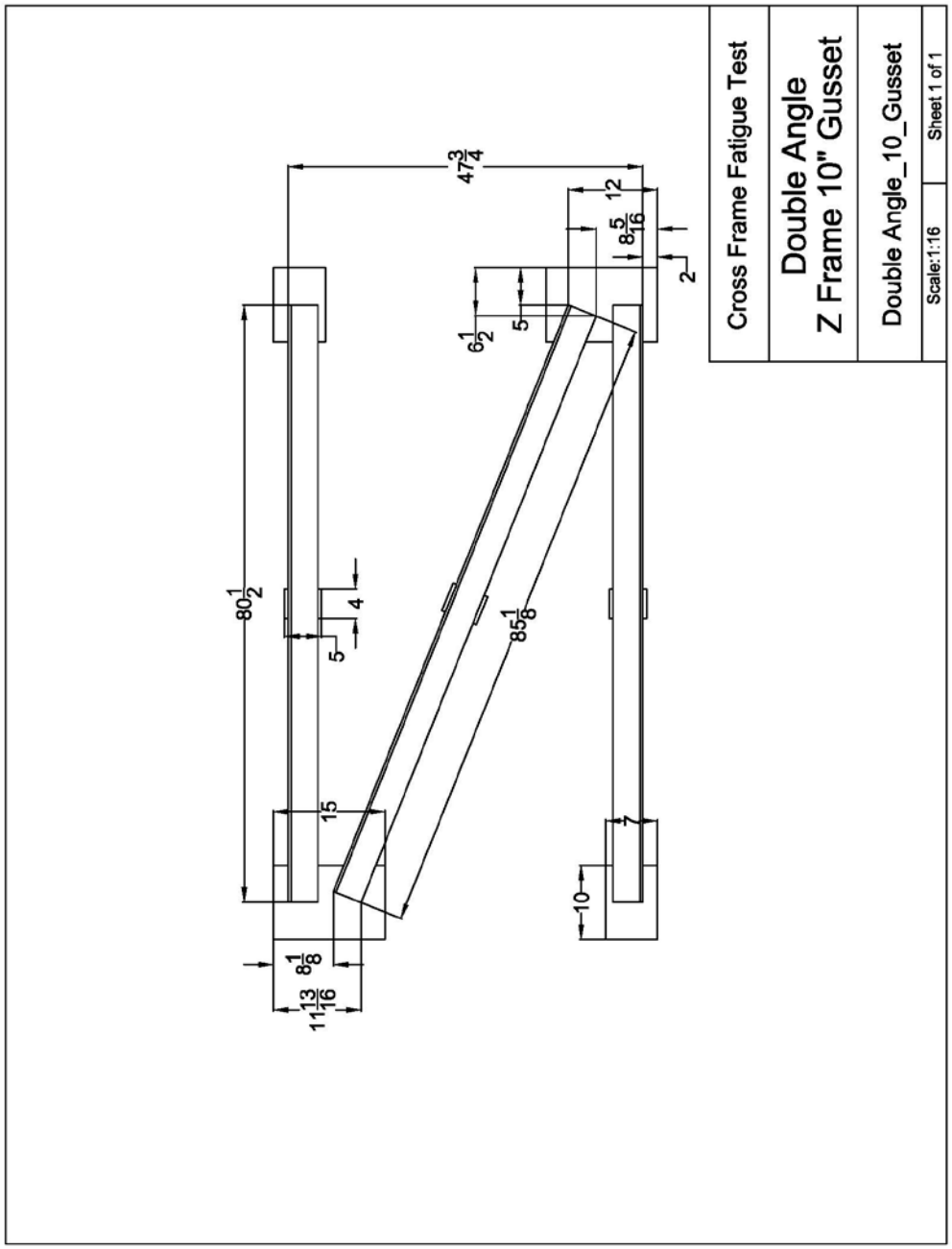
Cross Frame Fatigue Test
Double Angle
Z Frame 10" Gusset
Double Angle_10_Gusset
Scale:1:16
Sheet 1 of 1
47 3/4
12
8 5/16
2
6 1/2
5
80 1/2
4
5
85 1/8
15
10
8 1/8
11 13/16

Test Specimen: ZF_DA_1

Test Dates: 2/14/2013 – 2/18/2013

Primary Failure Location: Weld

S_R = 15.00 ksi (Diagonal)

N = 97,060 cycles

AASHTO Fatigue Category: < E′

Stiffness: **Initial:** 195.0 k/in **Final:** 123.9 k/in
36.4% loss of stiffness

Average Weld Size: Leg: 0.32″ **Throat:** 0.32″

Details:

- TxDOT Standard X-Type Cross Frame Details for L4 x 4 x 3/8 followed for Z frame layout
- Angles on back side of cross frame cut 1/2″ shorter to prevent weld intersection

Crack Locations:

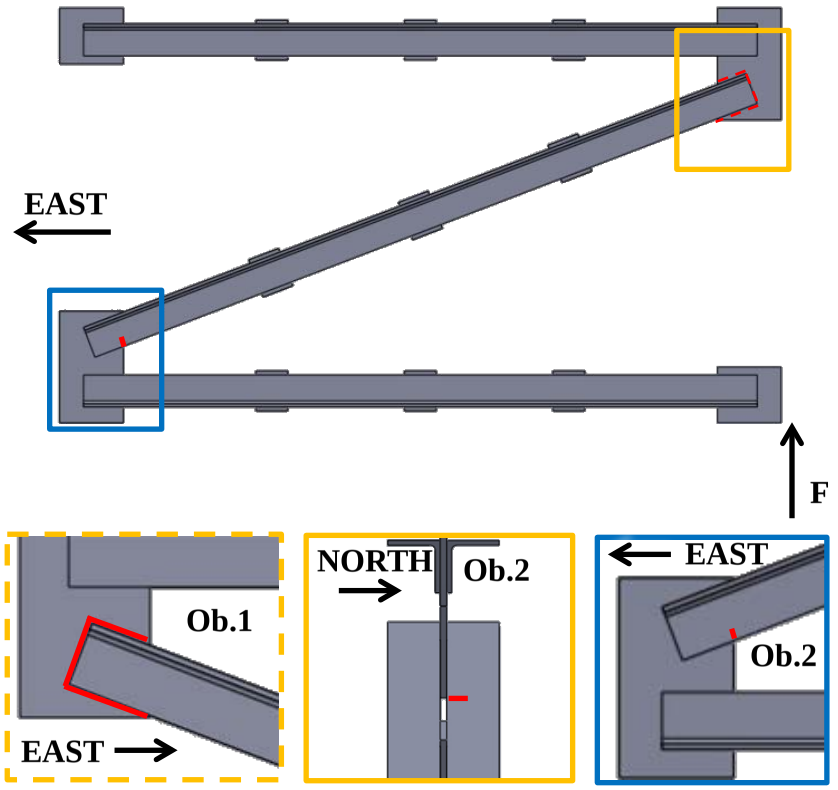

Observations:

1. First crack appeared to initiate at a tack weld at the angle-gusset weld at the heel of the SW angle and propagated along the weld through the throat
2. Secondary cracks formed in the NW angle heel and the SE and NE angle toes consistent with double curvature of member

Test Specimen: ZF_DA_1

First Observed Crack
C1: N = 90,862 cycles
C2: N = 94,058 cycles

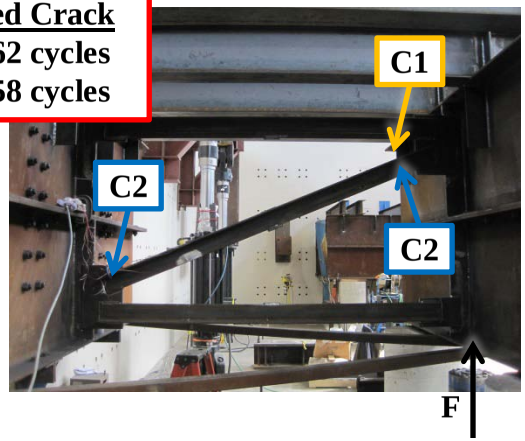

Crack 1: (Tack Weld)

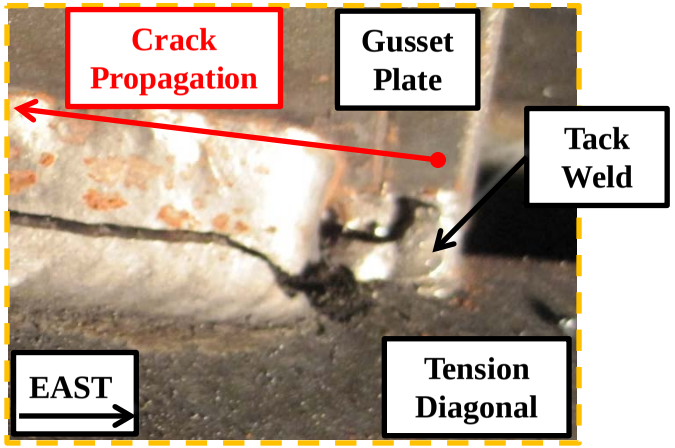

Crack 1:
(SW Angle)

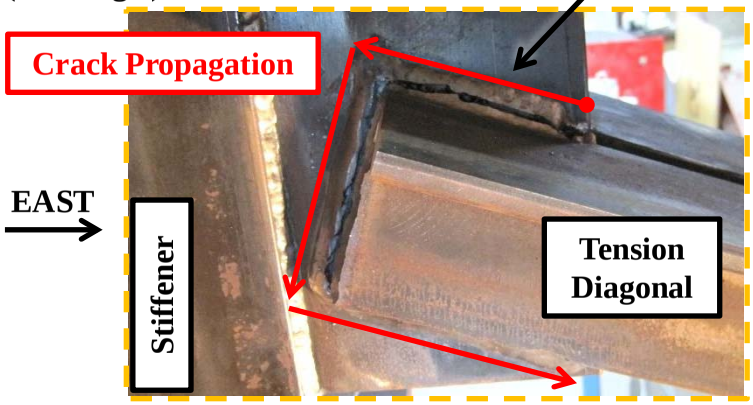

The crack began at a tack weld at the heel of the south angle of the diagonal at the west connection. The crack propagated through the throat of the weld around the connection.

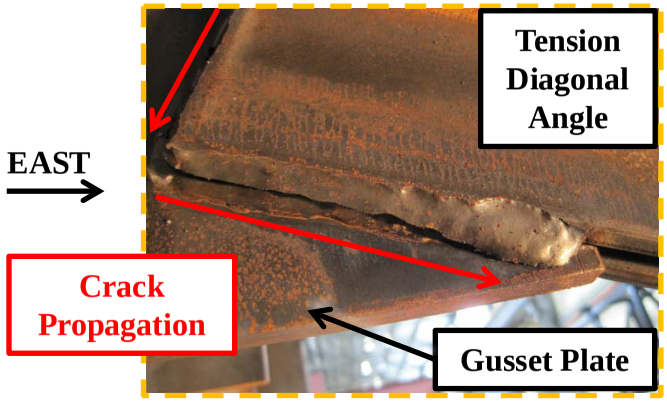

Test Specimen: ZF_DA_1

Crack 2: (NW Angle- Top)

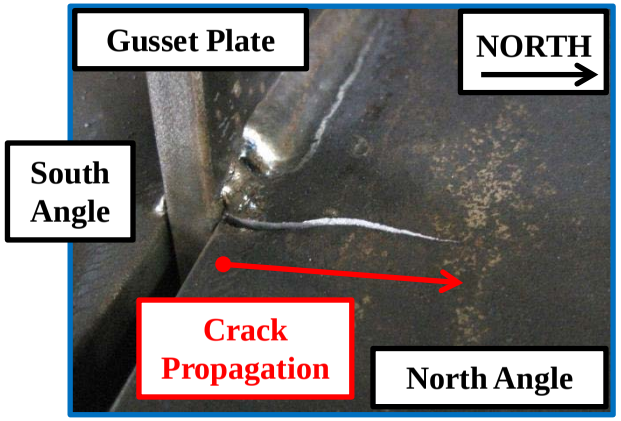

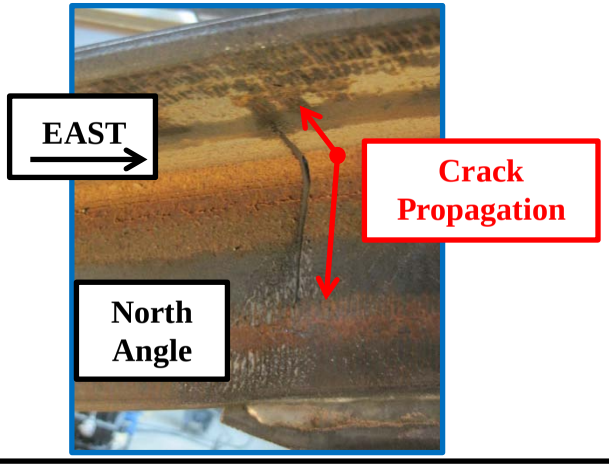

Crack 2: (SE Angle)

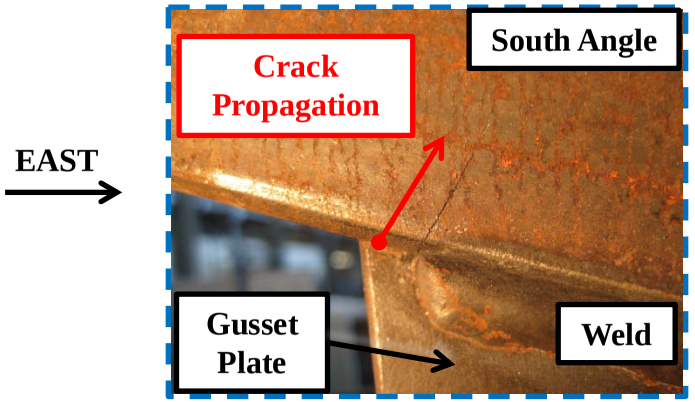

Crack 2: (NE Angle)

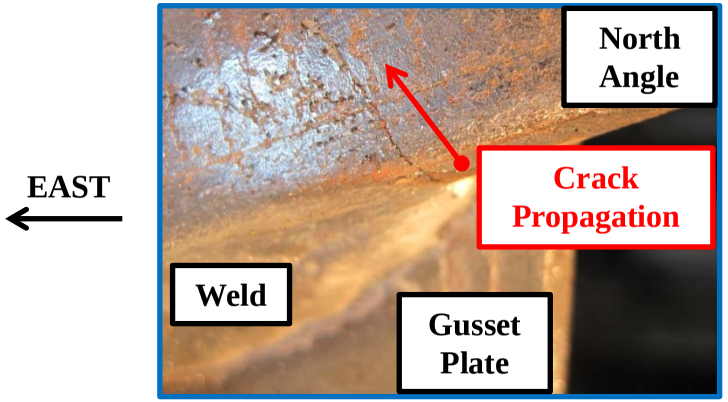

Test Specimen: ZF_DA_2

Test Dates: 2/22/2013 – 3/2/2013

Primary Failure:	**Secondary Failure:**
Gusset-Stiffener Weld	Angle-Gusset Weld
S_R = 15.00 ksi (Diagonal) (Effective Stress Range)	S_R = 15.00 ksi (Effective Stress Range)
N = 56,793 cycles **AASHTO Fatigue Category: < E′**	**N** = 134,638 cycles **AASHTO Fatigue Category: E′**
Stiffness: **Initial:** 193.4 k/in **Final:** 166.5 k/in 13.9% loss of stiffness	**Stiffness:** **Initial:** 191.5 k/in **Final:** 166.9 k/in 12.8% loss of stiffness

Average Weld Size: Leg: 0.32″ **Throat:** 0.32″

Details:

- TxDOT Standard X-Type Cross Frame Details for L4 x 4 x 3/8 followed for Z frame layout
- Angles on back side of cross frame cut 1/2″ shorter to prevent weld intersection
- Welded at Hirschfeld Industries

Crack Locations:

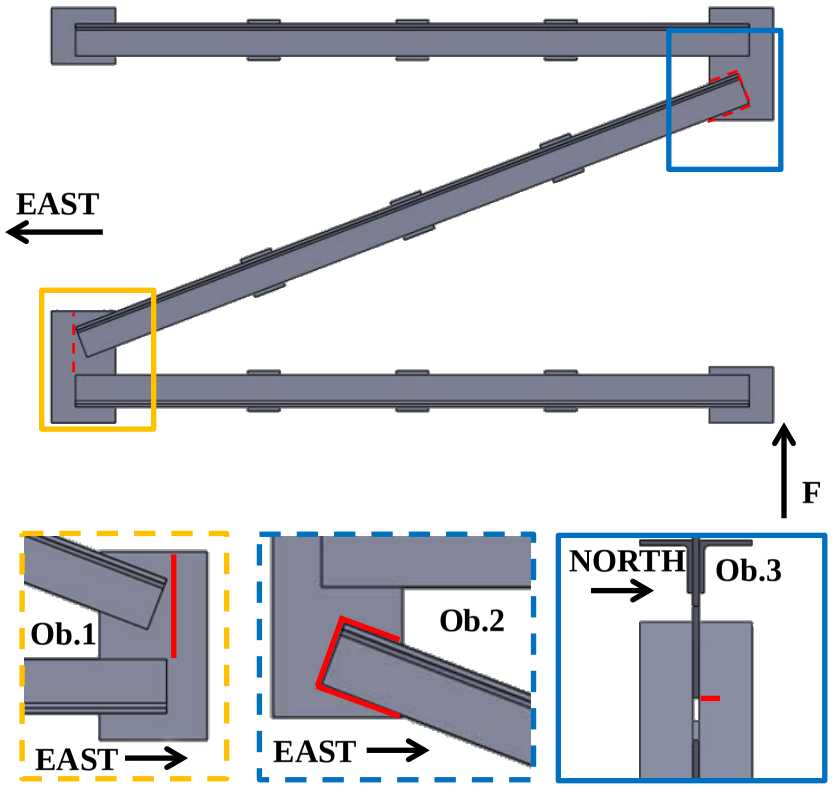

Observations:

1. First crack initiated at gusset toe of gusset-stiffener weld and propagated along the weld toe through the plate
2. A secondary crack formed at the SW angle heel at the forward weld toe propagating through the weld throat and around the connection consistent with a stress concentration caused by double curvature of the diagonal
3. An additional crack was seen at the NW angle heel originating at the angle toe and propagating into the angle

Test Specimen: ZF_DA_2

First Observed Crack
C1: N = 44,354 cycles
C2: N = 122,175 cycles
C3: N = 134,638 cycles

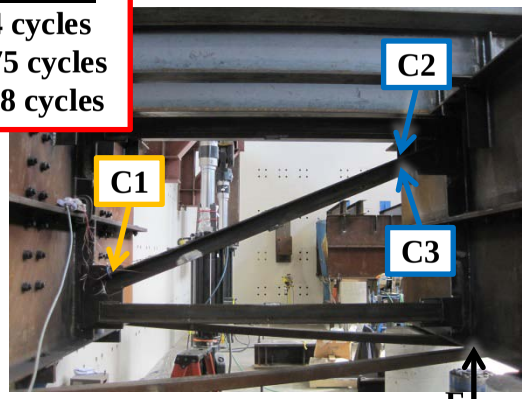

Crack 1: (Bottom East Gusset- North Face)

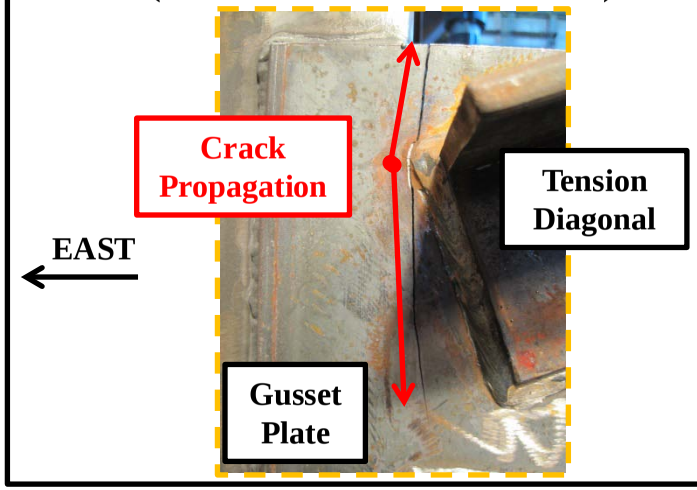

Crack 1: (Bottom East Gusset- South Face)

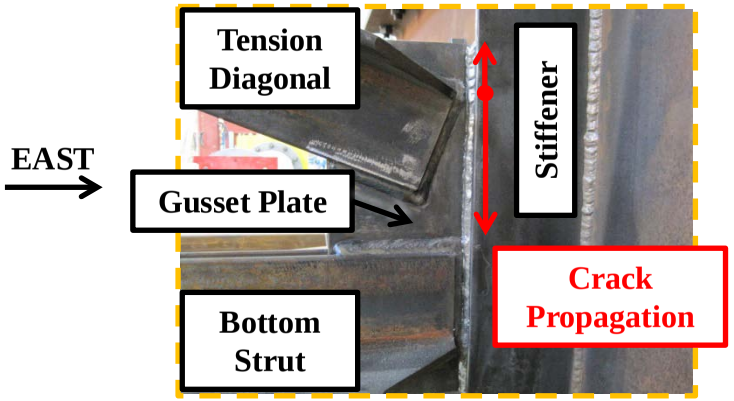

The crack began near the intersection of the angle-gusset weld and the gusset-stiffener weld. It began at the gusset toe of the gusset-stiffener weld and propagated up and down into the plate.

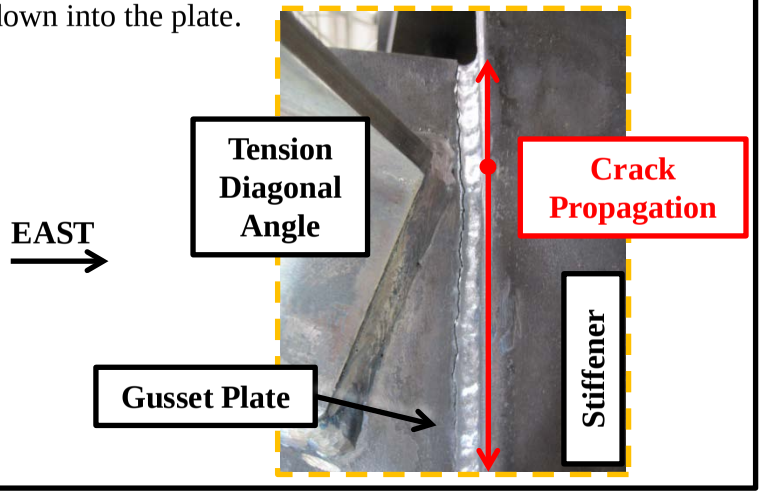

Test Specimen: ZF_DA_2

Repair: (Bottom East Gusset Plate)

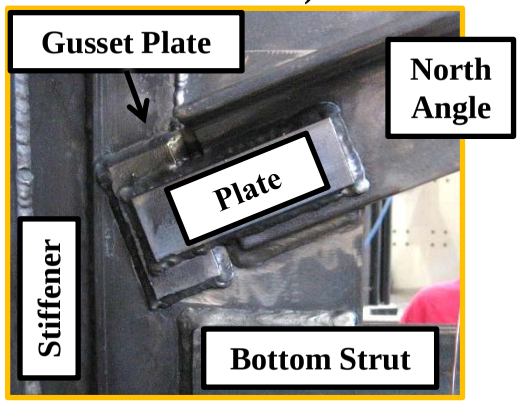

The crack was repaired by grinding out the crack and inserting a double groove weld. An additional plate and angle were used to bridge the crack. The repaired stiffness was very similar to the original stiffness.

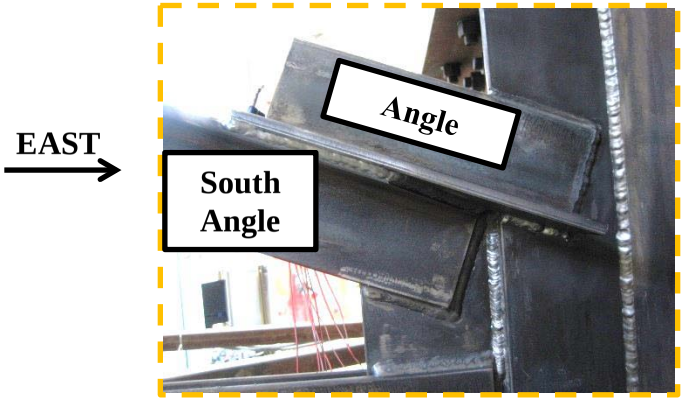

Crack 2: (SW Angle)

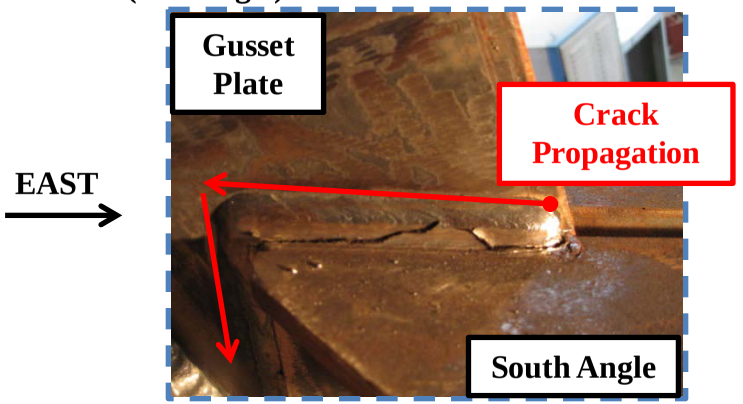

Very similar to ZF_DA_1, the crack began at the forward edge of the connection and worked its way around the weld through the throat.

Crack 3: (NW Angle)

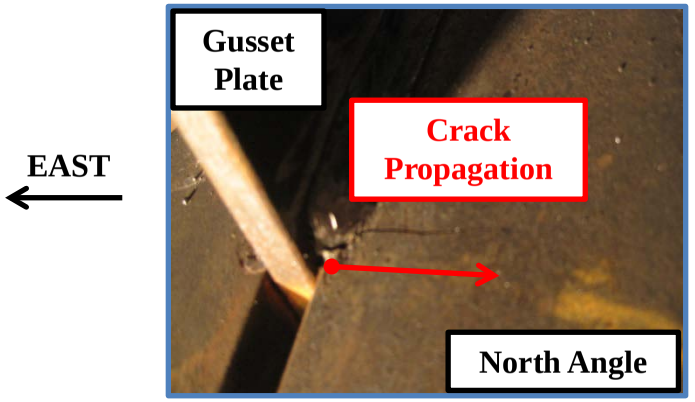

Test Specimen: ZF_DA_3

Test Dates: 5/7/2013 – 5/8/2013

Primary Failure Location: Weld

S_R = 15.00 ksi

N = 37,442 cycles

AASHTO Fatigue Category: < E′

Stiffness:

Initial: 212.7 k/in

Final: 164.2 k/in

22.8% loss of stiffness

Average Weld Size: Leg: 0.30″ **Throat:** 0.33″

Details:

- TxDOT Standard X-Type Cross Frame Detail with members 4″ short prevent weld intersection
- The gusset plates were 2″ wider to maintain the same overlap as XF1-6 and the angle of the diagonals remained consistent

Crack Locations:

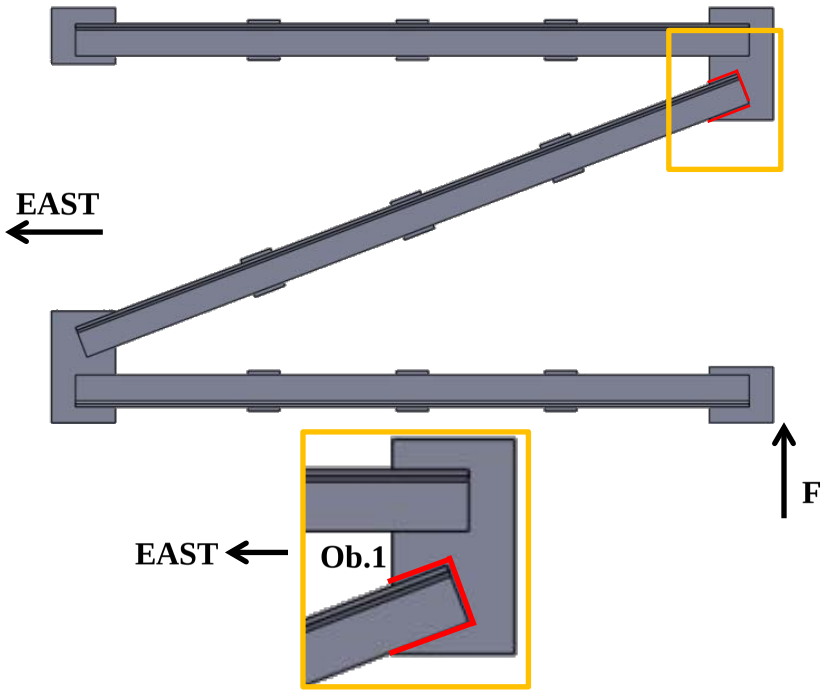

Observations:

1. First crack initiated at the NW angle heel at the forward weld toe propagating through the weld throat and around the connection consistent with a stress concentration caused by double curvature of the diagonal.

Test Specimen: ZF_DA_3

First Observed Crack
C1: N = 36,797 cycles

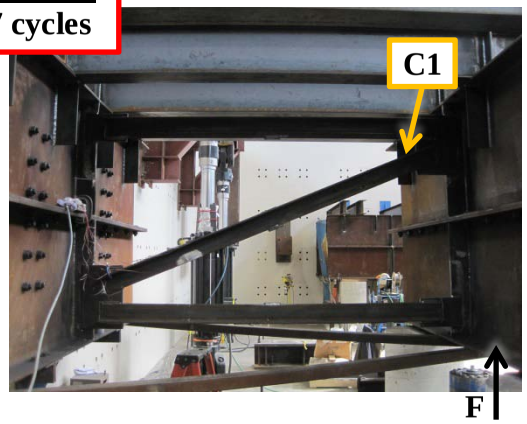

Crack 1: (Top West Gusset- North Face- At Failure)

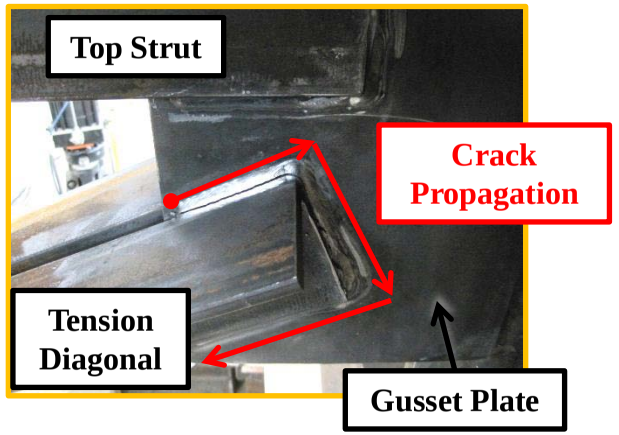

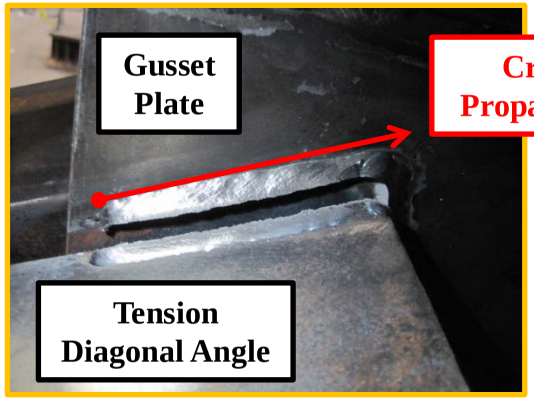

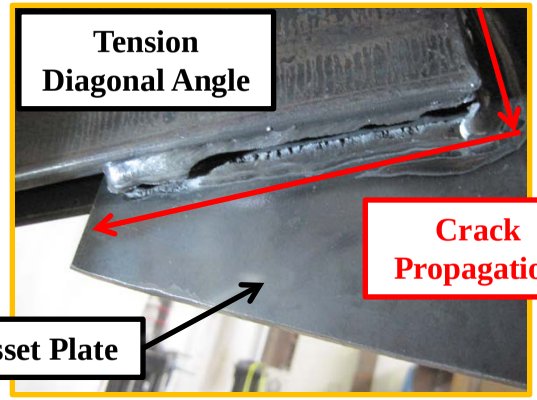

The crack began at the forward edge of the fillet weld at the heel of the angle and continued around connection.

References

Adan, S., and Gibb, W. (2008). "Inelastic Cyclic Testing of the Kaiser Bolted Bracket Moment Connection." *ASCE Structures Congress Conference Proceedings*.

American Institute of Steel Construction (AISC). (2005). *Steel Construction Manual, 13th Edition*.

American Institute of Steel Construction (AISC). (2010). *Steel Construction Manual, 14th Edition*.

American Association of State Highway and Transportation Officials, *AASHTO LRFD Bridge Design Specifications, 4th Edition*, 2007.

American Association of State Highway and Transportation Officials, *AASHTO LRFD Bridge Design Specifications, 6th Edition*, 2012.

American Society for Testing and Materials (ASTM) Standards.

American Welding Society. (2012). *AWS D1.1/D1.1M: 2012 Structural Welding Code-Steel*. American Welding Society, Miami, FL.

ANSYS Inc. (2011). "Elements Reference." *Release 11.0 Documentation for ANSYS*.

Battistini, Anthony. "Skewed Cross Frame Connection Stiffness." *Master's Thesis presented to The University of Texas.* Austin, TX, December 2009.

Brannon, S., McElrath, M., Reddy, R., and Counselor, S. (2001, October). "Navigating the Ripples of Flow Coating." *Modern Casting*, 29-31.

Connor, L., editor. (1987). *Welding Handbook,8th Edition*. Volume 1, American Welding Society. Miami, FL.

de Oliveira, Juan-Carlos. "Cast Steel Connector for Tubular Braces in Seismic Building Applications." *Master's Thesis presented to The University of Toronto.* Toronto, Ontario, Canada, 2006.

de Oliveira, J.C., Packer, J., and Christopoulos, C. (2008, March) "Cast Steel Connectors for Circular Hollow Section Braces under Inelastic Cyclic Loading." *Journal of Structural Engineering, 134 (3),* 374-383.

de Oliveira, C., and Stine, T. (2008, July). "Convenient Connections." *Modern Steel Construction*.

Det Norske Veritas (DNV). (2010, April). "Fatigue Design of Offshore Structures." *Recommended Practice, DNV-RP-C203*.

Dowswell, B. and Barber, S. (2005). "Shear Lag in Rectangular Hollow Structural Sections Tension Members: Comparison of Design Equations to Test Data." *Practice Periodical on Structural Design and Construction 10 (3),* 195-199.

Fasl, Jeremiah. "Estimating the Remaining Fatigue Life of Steel Bridges Using Field Measurements." *Dissertation presented to The University of Texas.* Austin, TX, May 2013.

Federal Highway Administration. (2001, March) "Steel Bridge Fabrication Technologies in Europe and Japan." Report No. FHWA-PL-01-018.

Fisher, J.W., Kulak, G.L., and Smith, I.F.C. (1998). "A Fatigue Primer for Structural Engineers." National Steel Bridge Alliance.

Frank, K.H. (2008). "CE 383D: Steel Bridge Design" Class Notes. The University of Texas at Austin.

Frank, K.H. (2010). Chief Engineer at Hirschfeld Industries. Discussion.

Frank, K.H and Fisher, J.W. (1979). "Fatigue Strength of Fillet Welded Cruciform Joints." *Journal of the Structural Division, 105 (ST9),* 1727-1740.

Haldimann-Sturm, S.C., and Nussbaumer, A. (2008). "Fatigue Design of Cast Steel Nodes in Tubular Bridge Structures." *International Journal of Fatigue, 30,* 528-537.

Helwig, T. and Fan, Z. (2000). "Field and Computational Studies of Steel Trapezoidal Box Girder Bridges", TxDOT Research Report 1395-3, The University of Houston.

Kaufmann, E. J.; Viscomi, B. V.; and Lu, L. (1995). "Beam-to-column Connections Using High Strength Steel Castings with Improved Weldability." *Structures Congress- Proceedings v. 1, Restructuring America and Beyond*, ASCE, 405-418.

Lincoln Electric. (2013 July). Ultracore 71A85- C3126 Product Information. Retrieved July 2013:
http://www.lincolnelectric.com/assets/global/Products/Consumable_Flux-CoredWires-Gas-Shielded-UltraCore-UltraCore71A85/c3126.pdf

http://www.lincolnelectric.com/assets/en_us/Products/Consumable_Flux-CoredWires-Gas-Shielded-UltraCore-UltraCore70C/c3122.pdf

http://www.lincolnelectric.com/assets/en_us/Products/Consumable_Flux-CoredWires-Gas-Shielded-Outershield-Outershield70/c3105.pdf

Liu, Y., Dawe, J.L., and Li, L. (2006). "Experimental Study of Gusset Plate Connections for Tubular Bracing." *Journal of Constructional Steel Research*, *62*, 132-143.

Lye, P. F. (1971). *Metalwork Theory, Metric Edition*. Thomas Nelson and Sons Ltd, 1985.

Maddox, S.J. (2008). "Status Review on Fatigue Performance of Fillet Welds." *Journal of Offshore Mechanics and Arctic Engineering*, *130*, 031006-1 – 031006-10.

Martinez-Saucedo, G., and Packer, J.A. (2009). "Static Design Recommendations for Slotted End HSS Connections in Tension." *Journal of Structural Engineering*, *135 (7)*, 797-805.

MASTAN2, v3.3.1. Ziemian, R.D., and McGuire, W. (2013). Downloaded from Internet: http://www.mastan2.com/

McDonald, G. and Frank, K. (2009, December). "The Fatigue Performance of Angle Cross-Frame Members in Bridges." Report FSEL No: 09-1 at the University of Texas at Austin.

MDX Software. (2013, July). User Manual, NetHelp, and FAQ. Retrieved July 8, 2013, from MDX: http://www.mdxsoftware.com/NetHelp/default.htm#!Documents/Girder_System_Analysis.htm

http://www.mdxsoftware.com/pdf/MDXV65.pdf

http://www.mdxsoftware.com/8.htm

http://www.mdxsoftware.com/12.htm

Mori, T.; Kainuma, S.; and Ichimiya, M. (2000). "A Study of Fatigue Crack Initiation Points in Load-Carrying Type Fillet Welded Joints." *IIW Document No. XIII-1832-2000*.

Munse, W.H. (1964). *Fatigue of Welded Structures*. New York: Welding Research Council.

Ningbo Yinzhou KST Machinery Co. Ltd (2010). "Investment Casting." Retrieved August 29, 2010: http://www.casting-investment.com/investment-casting-process.htm

Quadrato, Craig. "Stability of Skewed I-shaped Girder Bridges Using Bent Plate Connections." *Dissertation presented to The University of Texas.* Austin, TX, May 2010.

Soderberg, E. (2010, March). "Colossal Cranes." *2010 STEER Conference*, Ferguson Structural Engineering Laboratory at the University of Texas at Austin, Presentation

SolidWorks. (2010).

Steel Founders' Society of America. (2009). "SFSA: Overview of the Casting Process." Retrieved December 17, 2009: http://www.sfsa.org/sfsa/cstintcp.php#prcint2.4

SSRC. (2010). *Stability Design Criteria for Metal Structures* (Six ed.). (R. Ziemian, Ed.) New York: Wiley & Sons.

Stith, Jason. "Predicting the Behavior of Horizontally Curved I-Girders During Construction." *Dissertation presented to The University of Texas.* Austin, TX, August 2010.

Taylor, A. and Ojalvo, M. (1966, April). "Torsional Restraint of Lateral Buckling." *Journal of the Structural Division*, 115-129.

Texas Department of Transportation. (2006, April). Miscellaneous Details Steel Girders and Beams. Retrieved December 14, 2009, from Texas Department of Transportation: ftp://ftp.dot.state.tx.us/pub/txdot-info/cmd/cserve/standard/bridge/spgdste1.pdf

Timoshenko, Stephen P., and James M. Gere. *Theory of Elastic Stability.* New York: McGraw-Hill, 1961.

Topkaya, C., and Williamson, E.B. (2003). "Development of computational software for analysis of curved girders under construction loads." *Computers and Structures*, *81*, 2087-2098.

Totten, G.E., Funatani, K., and Xie, L. (2004). *Handbook of Metallurgical Process Design*. New York: Marcel Dekker, Inc., 353-356.

Turco, G. (2009, November). "Wichita Falls Ramp 'T': Torsional Bracing Retrofit To 3-Span Steel Plate Girder Units." *2009 World Steel Bridge Symposium*, National Steel Bridge Alliance, Presentation.

Wang, Weihua. "Stiffness of Steel Bridge Cross Frames of Various Designs and Connections." *Dissertation presented to The University of Texas.* Austin, TX, August 2013.

Willibald, S., Packer, J.A., and Martinez-Saucedo, G. (2006). "Behaviour of Gusset Plate Connections to Ends of Round and Elliptical Hollow Structural Section Members." *Canadian Journal of Civil Engineering, 33*, 373-383.

Winter, G. (1958). Lateral Bracing of Columns and Beams. *Journal of the Structural Divsion Proceedings of the American Society of Civil Engineers , 84* (ST2), 1561-1 - 1561-22.

Yura, J. (2001). "Fundamentals of Beam Bracing." *Engineering Journal*, First Quarter, 11-26.

VITA

Anthony David Battistini was born and raised in South Jersey. Son of David and Susanne Battistini, he attended St. Mary Magdalen Elementary School, and then went on to Sacred Heart High School, graduating as Valedictorian in June 2003. From there he studied at Lehigh University in Bethlehem, Pennsylvania, earning a Bachelor of Science in Civil Engineering in May 2007 and graduating with Highest Honors. Anthony began graduate school in August 2007 at The University of Texas at Austin working as a graduate research assistant at the Phil M. Ferguson Structural Engineering Laboratory, where he fell in love with steel. He completed his Master of Science degree in December 2009, and continued on to pursue his doctorate degree. In 2013-2014, Anthony began his career in academia at Washington State University. Beginning in Fall 2014, Anthony will be an assistant professor at George Mason University. In his spare time, Anthony and his lovely wife Liz enjoy traveling, friends, and life.

Permanent Address: anthony.battistini@utexas.edu

This dissertation was typed by the author.